Spring 5-15-2023

The Role of NS1 in Flavivirus Immunity and Pathogenesis

Alex W. Wessel

WASHINGTON UNIVERSITY IN ST. LOUIS

Division of Biology and Biomedical Sciences
Immunology

Dissertation Examination Committee:
Michael Diamond, Chair
Adrianus Boon
Daved Fremont
Michael Gross
Robyn Klein
Deborah Lenschow
Jonathan Miner

The Role of NS1 in Flavivirus Immunity and Pathogenesis

by
Alex W. Wessel

A dissertation presented to
Washington University in St. Louis
in partial fulfillment of the
requirements for the degree
of Doctor of Philosophy

May 2023
St. Louis, Missouri

Table of Contents

List of Figures

List of Tables

Acknowledgements

I have many people to thank for helping me reach this point in my career. I first became interested in scientific research as an undergraduate at the University of Wisconsin after enrolling in the Biology Core Curriculum ("Biocore") program. This was a rigorous three-year biology program with an emphasis on learning by the scientific method, giving students first-hand experience in the development, execution, and analysis of research questions. The enthusiasm of the program directors and professors in the program instilled a sense of curiosity for the process by which we do science in practice and come to learn new information. My experiences in the program led me to apply for a fellowship to complete a senior thesis research project. This was a very straightforward project; however, even early on I was challenged by science and had to troubleshoot experimental methods and deal with negative or uncertain data. I owe immense gratitude to my first mentor, Dr. Jyoti Watters, in helping me to setup and execute this small project. Indeed, her excitement for science was inspiring and convinced me to stick with science.

The next step of my career in science was at the National Institutes of Health, where I did a two-year postbaccalaureate program under the mentorship of Dr. Eric Hanson. This experience was completely new to me, both scientifically and personally. I was able to shadow Dr. Hanson not only in the lab, but also in the pediatric rheumatology clinic where he bridged science and clinic to study inborn errors of immunity. Dr. Hanson, Dr. John O'Shea, and many others at the NIH fueled my excitement not only for basic science questions in immunology but also for translational work. Dr. Hanson, in particular, instilled in me the importance of hard work in science as well as a sense of excitement for data generation. Though work in the lab was challenging and grueling at times, and though sometimes I felt incapable, Dr. Hanson constantly pushed me to learn new techniques in the lab and to grow as a scientist. Thanks to his mentorship, I was able to give

talks at two national conferences.

Above all, I need to thank Dr. Diamond for his mentorship over the past five years of my PhD. He has served as a role model to me both scientifically and personally and in ways that I am sure he does not even realize. First, his immutable enthusiasm and dedication to science is inspiring and enabled me to get through challenging periods of my PhD. At certain points, I felt lost in negative data and incapable of keeping a positive attitude or of figuring out what question or experiment to next address. Without fail, every meeting I had with Dr. Diamond revitalized my enthusiasm for my projects and kept me moving forward. I owe immense gratitude to him for helping me to finish projects that I didn't think would ever come to fruition. He challenged me to keep a positive attitude and to just follow the science. Although I still struggle with this at times, I will continue trying to improve as I move forward in my career and in life. His ability to maintain a cheerful and collaborative, scientifically engaging, and productive lab environment also helped to create a wonderful PhD experience. Dr. Diamond's mentorship surely has helped me to grow scientifically and has made me more confident in my ability to cope with challenges both in and out of the lab.

I also would like to thank all current and past Diamond Lab members for creating an overwhelmingly positive and uplifting lab environment and PhD experience. The scientific advice of everyone has been incredibly useful in my development as a scientist, and the camaraderie has helped me to make it through. I need to thank Jen Govero, Julie Fox, Matt Gorman, and Jenny Hyde for helping me to start up in the lab and learn new techniques, and for always taking the time to help others around them. Likewise, I owe great gratitude to Bradley Whitener for his intense dedication to helping others in the lab so that it could do such exciting science. I need to thank Yael Alippe, Jonathan Miner, Ahmed Hassan, Sharmila Nair, Ofer Zimmerman, Hamid Salimi,

and Zhenlu Chong not only for our scientific discussions but also for our personal communications and for your support. I also would like to thank Larissa Thackray, Adam Bailey, Chris Nelson, Prisesh Desai, Laura VanBlargan, Roseanne Zhao, Melissa Edeling, Brett Case, Brett Jagger, Liz Caine, Hongming Ma, and Rong Zhang for serving as incredible scientific mentors in the lab. Nia Fernandez, Rita Chen, Natasha Kafai, Arthur Kim, and Emma Winkler have been incredibly inspiration peers who I admire both as scientists and for their ability to uplift others around them and create a positive environment. Of course, I need to thank my lab bench bay-mate, James Earnest, for all of the great conversations and for the light-hearted, comedic relief when it was most needed.

My experiences at Washington University have been immensely rewarding, and I would like to thank the directors and staff of the MSTP and the Immunology Program for helping me to further develop as a scientist and as an aspiring MD/PhD. The members of my committee have also been incredibly useful mentors that I need to thank, namely Daved Fremont, Robyn Klein, Deborah Lenschow, Jacco Boon, Jonathan Miner, and Ali Ellebedy.

As a first-generation college graduate, I never expected to go this far in academia. I could not have done it without the guidance of my mentors and also the support of my family and friends. My mother has always supported my academic endeavors and deserves a great deal of credit for enabling me to get to this point. I also am eternally grateful for the love and support from Andrew Metzger, Geoffrey Alexander, Kalyan Tripathy, Hueylie Lin, Mark Suthoff, Brett Tortelli, John Gram, Rita Chen, and Natasha Kafai throughout this experience. Thank you!

Alex W. Wessel

Washington University in St. Louis

May 2023

ABSTRACT OF THE DISSERTATION

The Role of NS1 in Flavivirus Immunity and Pathogenesis

by

Alex W. Wessel

Doctor of Philosophy in Biology and Biomedical Sciences

Immunology

Washington University in St. Louis, 2023

Professor Michael Diamond, Chair

Flaviviruses are a genus of enveloped, arthropod-transmitted RNA viruses that include clinically relevant pathogens such as yellow fever, dengue, Zika, and West Nile viruses. These viruses cause a spectrum of potentially life-threatening diseases including hepatitis, vascular shock, congenital abnormalities, and encephalitis. Dengue virus, alone, infects up to 390 million individuals in any given year, and its endemic regions continue to expand along with the geographical spread of its mosquito vectors. Flaviviruses also have a history of emergence and re-emergence, such as the recent dissemination of Zika virus (ZIKV) to Oceania and the Americas in 2015. During this epidemic, the virus caused an estimated 1.5 million infections in Brazil, drawing global attention due to new clinical manifestations of microcephaly and other congenital malformations. The dissemination of West Nile virus (WNV) to North America in 1999 also resulted in thousands of infections, along with considerable morbidity and mortality due to neuroinvasive disease. Notwithstanding this epidemiology, no approved vaccine or antiviral therapeutic exists for many flaviviruses such as ZIKV and WNV.

The approved vaccines for dengue, Japanese encephalitis, and yellow fever viruses have demonstrated efficacy by targeting the flavivirus envelope protein, generating neutralizing

antibody responses. However, cross-reactive, sub-neutralizing antibodies reportedly can enhance infection of homologous and heterologous flaviviruses, particularly for dengue virus and ZIKV. This phenomenon, termed antibody-dependent enhancement (ADE), remains a concern for envelope-targeted vaccines and antibody therapeutics. An alternative approach in the field has been to target the flavivirus nonstructural protein 1 (NS1), a membrane-associated and secreted glycoprotein also involved in virus replication. Prior reports indicate that anti-NS1 monoclonal antibodies (mAbs) can confer protection against certain flaviviruses, but the mechanisms and epitopes associated with protection are poorly characterized.

Herein, I describe correlates of protection by anti-NS1 monoclonal antibodies (mAbs) for ZIKV and WNV. Panels of anti-ZIKV and anti-WNV NS1 human and murine mAbs were generated to study their efficacy *in vivo*. Administration of anti-ZIKV NS1 human and murine mAbs to non-pregnant mice conferred protection against lethal ZIKV challenge. Additionally, several mAbs conferred protection to the developing fetus upon infection of pregnant mice by limiting viral burden in the fetal head and placenta. Protection correlated with the avidity of mAb binding to cell-surface-expressed NS1 and with Fc effector function engagement, suggesting that anti-NS1 mAbs may protect through clearance of virus-infected cells. The protective mAbs mapped to exposed epitopes on the cell-surface form of NS1, including the outer, electrostatic surface of the wing domain and loop face of the β-platform domain. Administration of anti-WNV NS1 human mAbs protected mice against lethal WNV challenge. For most mAbs, protection also correlated with binding to cell-surface-expressed NS1. Epitope mapping through mutagenesis revealed most of the protective mAbs to bind the outer surface of the wing domain or loop face of the β-platform. Unlike the anti-ZIKV NS1 mAbs, however, one protective mAb was identified that mapped to the flexible loop of the wing domain. Additionally, one mAb conferred protection

against WNV despite lacking binding to cell-surface NS1 and mapping to a poorly exposed epitope on cell-surface NS1. These data suggest that NS1-specific mAbs likely protect through Fc-mediated clearance of infected cells expressing NS1 on the surface. However, other mechanisms potentially exist through binding to secreted NS1 and blocking its pathogenic functions. The protective epitopes defined in these studies can be informative for the design of NS1-targeted vaccine immunogens and antibody therapeutics that avoid ADE.

Cell-surface-expressed and secreted NS1 are thought to contribute to viral pathogenesis through interaction with host factors such as complement, toll-like receptors, and endothelial cells. Despite these ascribed functions, their relevance during *in vivo* infection has not been clearly established for many flaviviruses, such as WNV. Mutagenesis studies are often complicated by the inability to uncouple the role of NS1 in replication from its accessory roles in pathogenesis. A proline to lysine substitution at residue 101 (P101K) of WNV NS1 did not affect WNV replication yet resulted in decreased lethality in mice, accompanied by lower levels of virus spreading to the brain. The NS1-P101K substitution led to lower levels of secreted NS1 in circulation in mice, and exogenous reconstitution of the NS1 levels restored virus levels in the brain. These studies suggest that the levels of NS1 in circulation during infection can contribute to WNV dissemination to the brain, and support the general notion that NS1 contributes to flavivirus disease.

Chapter 1

Introduction to Flavivirus NS1

1.1 Overview of Flaviviruses

Flaviviruses are enveloped, positive-sense RNA viruses belonging to the Flavivirus genus of the *Flaviviridae* family. They are transmitted by arthropod vectors and include numerous human pathogens such as yellow fever (YFV), dengue serotypes 1 to 4 (DENV1-4), Zika (ZIKV), West Nile (WNV), Japanese encephalitis (JEV), Murray Valley encephalitis (MVEV), St. Louis encephalitis (SLEV), and tick-borne encephalitis (TBEV) viruses. Flavivirus-endemic regions are geographically expansive (**Figure 1.1**) and continue to grow with changes in vector habitats, climate, and urbanization[1]. Nearly a quarter of the world's population live in DENV-endemic regions, leading to an estimated 390 million infections every year[2,3]. Additionally, YFV, WNV, and JEV cause thousands to hundreds of thousands of infections annually[2,4]. The dissemination of flaviviruses to new geographic areas also has caused epidemics in recent decades, such as the spread of WNV to North America in 1999 and the ZIKV epidemic in 2015.

Flavivirus infections are often asymptomatic or subclinical but can present with diverse clinical symptoms ranging from mild febrile syndromes to liver failure, hypotensive shock, congenital malformations, and encephalitis (**Figure 1.2**). For example, patients with severe DENV infection develop a vascular leakage syndrome resulting in hypotensive shock. A subset of patients with WNV or JEV infection develops neuroinvasive disease that can cause life-threatening meningitis, encephalitis, and acute flaccid paralysis. Notably, the incidence of WNV neuroinvasive disease in the United States has increased by over 25% in recent years compared to the preceding decade[5]. ZIKV infection of pregnant women can lead to serious fetal complications such as intrauterine growth restriction and microcephaly. Despite the history of epidemics and severity of disease outcomes, many flaviviruses lack vaccines or therapeutic countermeasures. WNV and ZIKV, in particular, lack approved antiviral therapies yet pose threats to public health as recently

re-emerged flaviviruses.

1.1.1 ZIKV epidemiology and disease

The first isolate of ZIKV was recovered in 1947 from a rhesus monkey in the Zika Forest of Uganda[6]. For decades, reported cases of ZIKV were sporadic and confined to Africa and Asia. The first evidence of transmission beyond these continents occurred in 2007 on Yap Island of the Federated States of Micronesia, where over 70% of the population became infected[7]. A larger outbreak encompassing nearly 30,000 cases occurred in 2013 in French Polynesia, demonstrating further dissemination of the virus in the Pacific islands[8]. ZIKV was then identified in South American and the Caribbean in 2015 and caused an estimated 1.5 million infections in Brazil, alone[9]. From 2015-2016, transmission occurred throughout numerous countries of the Americas, the Caribbean, and the Pacific and included additional travel-related cases.

Human transmission of ZIKV primarily occurs through *Aedes aegypti* and *Aedes albopictus* mosquitos. Although humans are the principal amplifying host for ZIKV during epidemics, sylvatic cycles involving *Aedes* mosquitos and non-human primates likely serve as reservoirs. Human-to-human sexual transmission of ZIKV also has been reported, as ZIKV can replicate in testes and persist in the seminal fluid of infected individuals[10,11]. Notably, fetuses acquire ZIKV through vertical transmission, which can leads to serious fetal complications[12]. First trimester intrauterine transmission, rather than late-stage pregnancy or intrapartum transmission, seems to be the most detrimental to fetal development[13].

Approximately 80% of ZIKV infections are asymptomatic, whereas the remainder usually manifest as a mild febrile illness accompanied by rash, arthralgia, and conjunctivitis. In rare cases, adult patients develop neurologic complications including acute myelitis, meningoencephalitis, and Guillain-Barré Syndrome[9,14]. Notably, ZIKV also can cause microcephaly and other fetal

malformations upon infection of pregnant women[15-17]. From 2015-2017 in Brazil, over 2,500 cases of microcephaly were attributed to ZIKV infection[18]. No approved vaccine or therapeutic countermeasure exists for ZIKV.

1.1.2 WNV epidemiology and disease

WNV was first isolated in 1937 from a febrile patient in Uganda[19]. For decades, WNV epidemics occurred sporadically in the Nile Delta region and Mediterranean basin, reportedly causing mostly mild, self-limiting illness[20]. However, in the 1960s and 1970s, more severe neurologic complications were recognized during outbreak in Europe and South Africa[20]. WNV transmitted to North America in 1999 and caused numerous cases of encephalitis in the New York City region[20]. From 1999 to 2019, over 50,000 infections, 25,000 cases of neuroinvasive disease, and 2,000 deaths have been reported in the United States[5]. The virus is now widely established across North America, Africa, Europe, and Asia[20].

Transmission of WNV to humans predominately occurs through *Culex* species mosquitoes. In nature, WNV mainly cycles between mosquitoes and birds, which sustain viremias that support transmission to mosquito vectors[21]. In contrast, humans are considered dead-end hosts due to transient, low-level viremias[21].

An estimated 80% of WNV infections are asymptomatic or subclinical, whereas most other infections present with mild, self-limiting symptoms including fever, headache, myalgias, and rash[22]. Approximately 1 in 150 infections progress to neuroinvasive disease, characterized by neurological symptoms such as stupor, disorientation, numbness, and muscle weakness[22]. A subset of patients with neuroinvasive disease develop acute flaccid paralysis or life-threatening encephalitis and meningitis, with 10% fatality. The risk for neuroinvasive disease and death becomes higher in elderly and immunocompromised individuals[23]. Patients who recover from

WNV infection often report sequelae consisting of fatigue, muscle weakness, and cognitive impairment lasting weeks to months[24,25]. No approved vaccine or antiviral therapeutic exists for WNV.

1.1.3 Flavivirus replication and NS1

The flavivirus positive-sense RNA genome is ~11 kilobases in length and encodes three structural proteins (capsid, C; pre-membrane, prM; and envelope, E) and seven nonstructural (NS) proteins (NS1, NS2A/B, NS3, NS4A/B, and NS5) (**Figure 1.3**). Following virus entry and uncoating, the viral genome is translated into a single polypeptide at rough endoplasmic reticulum (ER) membranes[26]. Viral and host machinery processes the polypeptide into its constituent viral proteins prior to RNA replication and virion assembly. The mature virus particle is comprised of C, prM/M, and E proteins. The C protein packages viral RNA to form a nucleocapsid core, which becomes enveloped by ER membrane[27]. The prM and E proteins insert into the membrane to form the outer surface of the immature virus particle[27]. The host protease furin partially cleaves prM into membrane protein (M) in the Golgi, generating mature, infectious virus particles (**Figure 1.3**) which egress through exocytosis.

The nonstructural proteins perform roles in virus replication, associating at the ER within vesicle packets to form the viral replicase complex (**Figure 1.4**). NS3 and NS2B together constitute the viral protease and also exhibit helicase and nucleoside triphosphatase activity[28], whereas NS5 serves as the RNA-dependent RNA polymerase. The functions of NS2A, NS4A, and NS4B are essential for viral RNA accumulation and virus assembly, although their precise functions are not entirely understood[28,29]. Flavivirus NS1 is a glycoprotein that is also essential for replication, acting as a scaffold to associate the necessary viral and host proteins at the ER membrane[30-33]. In addition, NS1 localizes to the cell surface as a dimer and is secreted from cells

as a soluble hexamer that can be found in circulation of infected animals and humans[34-42]. Extracellular forms of NS1 reportedly play roles in immune evasion and activation and dysregulation of endothelial blood-tissue barriers[43-48]. However, the relative importance of NS1 in mediating viral pathogenesis *in vivo* is not entirely understood. NS1 also serves as an immunogen, eliciting adaptive immune responses which can mediate protection against disease but also potentially contribute to autoimmunity[49-54]. How antibodies contribute to either protection or disease, particularly in terms of the epitopes they bind, remains to be fully elucidated. Recent structural characterizations of flavivirus NS1 proteins have aided in understanding structure-function relationships, including how NS1 associates with membranes, contributes to pathogenesis, and engages antibodies[55-59].

1.2 NS1 expression, post-translational processing, and localization

During translation of the flavivirus genome, NS1 translocates into the lumen of the ER via a signal sequence corresponding to the last 24 amino acids of E[60]. An ER-resident host peptidase then cleaves E from the N-terminus of NS1 in the elongating polypeptide[26]. At the C-terminus of NS1, an unidentified protease (likely ER-resident) cleaves NS1 from NS2A via a motif corresponding to the last eight amino acids of NS1[61-64]. Fully cleaved NS1 is a hydrophilic monomer consisting of 352 amino acids with six disulfide bonds, which are important for proper folding and dimerization[65,66]. Pulse-chase studies indicate that NS1 rapidly homodimerizes (20 to 40 minutes) in the ER[36], after which it becomes partially hydrophobic and associates with membrane fractions[37,67,68]. NS1 also is glycosylated in the ER[36,69]; however, glycosylation is dispensable for dimerization and membrane association[37,69]. The dimeric form of NS1 is stable and resistant to dissociation by ionic and non-ionic detergents[36]. It can be visualized by non-heated, non-reduced SDS-PAGE for virtually all flaviviruses such as YFV, JEV, and DENV[36,67,70]. Heat

treatment dissociates dimeric NS1 into its monomeric form, which migrates at ~46-55 kDa depending on N-linked glycosylation[35,36]. For flaviviruses within the Japanese encephalitis (JE) serocomplex (*e.g.*, JEV, WNV, and MVEV), a higher molecular weight NS1, termed NS1', also can be observed at ~52-53 kDa[67,71,72]. Mutational studies indicate that NS1' is the product of a -1 ribosomal frameshift[73], resulting from a conserved heptanucleotide frameshift motif followed by an RNA pseudoknot in the NS2A gene of the JE serocomplex[74]. Notwithstanding the additional C-terminal amino acids, NS1' displays similar glycosylation and cellular trafficking patterns as NS1[67,75], and can trans-complement the function of NS1 in replication[75].

Intracellular NS1 predominately localizes to vesicle packets of the ER membrane, associating with other viral nonstructural proteins and dsRNA in the replicase complex[76,77]. However, a fraction of NS1 is also trafficked to the infected cell surface[37,39,78,79] where it becomes a target of antibodies[78,80] (**Figure 1.5**). Cross-linking studies of the YFV NS1 protein suggest that cell surface NS1 predominately exists as a homodimer[78], consistent with structural analyses suggesting that membrane association occurs through hydrophobic interactions with domains present on one surface of the NS1 dimer[55-57] (detailed in **Section 1.3**). However, at least DENV and JEV NS1 also can be found in association with detergent-resistant membrane fractions characteristic of lipid rafts[81]. DENV NS1 also can acquire a glycosylphosphatidylinositol (GPI) membrane anchor through a GPI addition motif corresponding to a hydrophobic sequence at the N-terminus of NS2A[82]. The addition motif leads to the incorporation of GPI moiety-specific components (*e.g.*, ethanolamine and inositol) into NS1[82]. Furthermore, binding of NS1-specific antibodies to cell surface NS1 reportedly induces tyrosine phosphorylation of cellular proteins, suggesting that surface NS1 may mediate GPI-linked signal transduction[82]. Notably, treatment of cells with phospholipase C releases only a portion of surface NS1 into the supernatant[82], suggesting

that NS1 does not require GPI linkage for membrane association.

A fraction of cellular NS1 is trafficked through the secretory pathway of the Golgi apparatus, as evidenced by the acquisition of Golgi-specific glycan modifications prior to secretion[34]. Secretion is at least partially glycosylation-dependent, as abolishing the N-linked glycosylation sites or treatment with inhibitors of Golgi-specific glycosylation enzymes reduces levels of NS1 in the supernatant of infected cells[34,79]. Secreted NS1 consists predominately of hexamers formed by trimerization of dimer protomers[34,35,83,84], although tetramers and other aggregates may form[34]. Unlike the dimer, the hexamer dissociates in the presence of detergent[34,85]. Triton X-114 partitioning experiments reveal the amphipathic nature of secreted NS1: whereas detergent phases contain NS1 dimers, aqueous phases contain hexamers[85]. Electron microscopy (EM) of the DENV hexamer reveals an open barrel-like organization, and a central hydrophobic core packed with lipid cargo[84,85]. Separation of the lipid core contents by thin-layer chromatography and subsequent NMR analysis indicate the presence of various membrane-associated lipids, such as triglycerides, cholesteryl esters, and phospholipids[85]. Inhibitors of lipid synthesis (*e.g.,* niacin) reduce NS1 secretion without affecting levels of cell-associated NS1[85]. Given these findings, it has been suggested that the formation of hexameric NS1 possibly requires the interaction of dimeric NS1 with membrane lipids so that they may be dragged into the core of the hexamer[85]. This idea is consistent with evidence that NS1 can interact with lipids to remodel liposomes[56] and ER membranes to form vesicle packets[33,86,87]. A T164S substitution that leads to enhanced secretion of DENV NS1 alters the lipid classes carried in the core of hexameric NS1[88], further suggesting that differential interactions with lipids possibly regulate NS1 secretion[88].

NS1 glycosylation occurs at two or three asparagine residues (Asn130, Asn207, +/- Asn175), depending on the virus. Almost all flavivirus NS1 proteins contain the conserved N-

linked glycans at Asn130 and Asn207[68,69,89-91]. For the JE serocomplex (*e.g.,* WNV, MVEV, and SLEV), NS1 acquires additional glycans at Asn175[65,92]. Glycan analysis of YFV NS1 indicates that cell-associated NS1 contains predominately high-mannose moieties, whereas secreted NS1 acquires complex carbohydrates that are resistant to digestion by endoglycosidase H[91]. This data supports the notion that NS1 transits through the Golgi prior to secretion, undergoing trimming and processing of mannose residues. For DENV2 NS1, the glycan at Asn130 undergoes processing to acquire complex carbohydrates, whereas Asn207 retains high-mannose glycans[69]. Glycosylation is not absolutely critical for dimerization of NS1[37] or expression on the cell surface[37,79], though it can affect dimer stability[69] and appears to regulate secretion and virus replication[34,69,93-96]. This is consistent with lack of NS1 secretion from insect cells, which possess different glycosidases in the Golgi compared to mammalian cells[67]. However, the precise role of N-linked glycans in hexamer stability and secretion remains ambiguous[95,96]. In some studies, removal of the glycan at Asn130 leads to instability of the hexamer, whereas removal of the glycan at Asn207 leads to decreased secretion[69,95]. Another study suggests that the glycan at Asn130 is required for protein secretion whereas the glycan at Asn207 is dispensable for secretion and hexamer stability[96]. These conflicting results potentially stem from differences in the cell type used for NS1 expression (BHK-21 versus 293F cells) or the method of NS1 purification[95,96]. While the presence of N-linked glycans may impact secretion, modification of the high-mannose glycans is not critical, as secretion still occurs in the presence of deoxymannojirimycin (an inhibitor of N-linked glycan modification in the Golgi)[79].

Soluble flavivirus NS1 can be detected in circulation in infected animals and humans[41,42,97-99], reaching particularly high levels during DENV infection (~1 to 10 ug/mL)[40,100-102]. Notably, flaviviruses secrete variable levels of NS1 which may contribute to differences in NS1

antigenemia. Compared to WNV-infected cells, DENV-infected cells secrete higher levels of NS1 and reciprocally express lower levels of cell surface-associated NS1[79]. This finding is consistent with clinical data suggesting that levels of soluble NS1 in circulation are higher in DENV-infected relative to WNV-infected patients[40,42,101]. For WNV and DENV NS1, amino acid variation at positions 10 and 11 affect the retention of NS1 in the ER, leading to an inverse correlation between the amount of cell surface expression and secretion[79]. Other amino acid variations also are associated with differences in NS1 secretion. For example, the substitutions T164S in DENV[88] and A188V in ZIKV[103] NS1 lead to enhanced secretion *in vitro* and elevated NS1 antigenemia in infected mice. However, the mechanism by which these variations affect NS1 secretion is not determined.

Following secretion, soluble NS1 can bind back to the surface of infected or uninfected cells[48,104,105] via surface glycosaminoglycans (GAGs), such as heparan sulfate or chondroitin sulfate[104]. Surface binding by flavivirus NS1 proteins also displays cell type specificity that varies by flavivirus[48,104]. Remarkably, binding to tissue-specific vascular endothelial cells *in vitro* and *in vivo* correlates with flavivirus disease tropism[48]. The mechanism underlying this specificity is not known; however, cell type differences in expression of GAGs or proteoglycans possibly contribute[106,107]. Following surface binding, NS1 is endocytosed in a dynamin- and clathrin-dependent manner that requires the N-liked glycosylation site, Asn207[96]. DENV NS1 internalized by hepatocytes accumulates in late endosomes, potentiating subsequent virus infection[105]. Endocytosis by endothelial cells mediates disruptions in blood-tissue barrier integrity (outlined in Section 1.4.3)[47,48,96,108,109]. Binding by secreted NS1 can be blocked by inhibiting surface GAG expression with sodium chlorate treatment of cells, though notably this does not prevent expression of surface NS1 from intracellular pools of infected cells[104]. Moreover, reportedly cell surface NS1

stems predominately from intracellular pools rather than binding back of secreted NS1[104].

1.3 NS1 protein structure

The NS1 dimer crystal structure has been solved for DENV2[56,58], WNV[56,58], and ZIKV[55,57,110]. Additionally, the C-terminal domain structures for JEV[111] and YFV[112] NS1 have been solved. Despite considerable amino acid variation in NS1 between flaviviruses (*e.g.,* ~50-55% identity between DENV2, WNV, and ZIKV NS1), the available NS1 structures retain virtually identical folding and domain arrangements[55,56,111,112]. Each protomer of the dimer comprises three domains: the N-terminal β-roll domain (residues 1-29), the wing domain (residues 30-180), and the C-terminal 'β-platform' or 'β-ladder' domain (residues 181-352)[55,56] (**Figure 1.6**). The overall structure consists of a cross-shaped dimer, in which the β-platform domains are aligned end-to-end and flanked by the protruding wing domains[55,56]. Dimerization occurs via intertwining β-hairpins that curve into the roll-like shape of the β-roll domains[55,56]. Adjacent to the β-roll, a discontinuous connector subdomain (residues 30-37 and 152-180) links the wing to the β-platform through a disulfide bond (Cys179 to Cys223)[55-58]. Each β-platform consists of anti-parallel β-strands that arrange into β-sheets[55,56,58]. The interstrand loop between β13 and β14, termed the 'spaghetti loop' (residues 219-272), is particularly long and covers one face of the β-sheets[55,56,58]. Lacking in secondary structure, the spaghetti loop achieves order through hydrogen bonds[56]. The 'inner' face of the NS1 dimer is hydrophobic and thought to mediate interactions with lipid membranes[55-57] and other nonstructural proteins[30,33]. The 'outer' face is polar and contains the conserved N-linked glycosylation sites (Asn130, Asn207, +/- Asn175). The outer face displays the most sequence diversity between flaviviruses, particularly in the outer face of the wing domain[57]. Electrostatic potentials in this region can be markedly variably; for example, ZIKV NS1 displays positively charged residues whereas DENV2 and WNV display negative or neutral

residues[55-57]. The outer face of the β-platform domain corresponds to the loop face, with the underlying anti-parallel β-sheets making up the inner face of the β-platform. Notably, the C-terminal 'distal tip' (residues 278-352) of the β-platform displays considerable sequence conservation between flaviviruses[55,56] as well as peptide sequences (residues 305-330) with homology to human proteins[51,52,113].

The inner face of the NS1 dimer contains the putative membrane-interacting surface, formed by hydrophobic contributions of three distinct regions: the β-roll, the 'greasy finger' (residues 159-163), and the 'flexible loop' (residues 108-129) of the wing domain[55,57]. The greasy finger protrudes toward the inner surface and consists of invariably hydrophobic amino acids (usually with two phenylalanine residues) that are likely candidates for membrane association. The β-roll and flexible loop contribute three conserved tryptophan residues (Trp28, Trp115, and Trp118) that also are putative anchor points for hydrophobic membrane interaction. In addition, the flexible loop contributes a dipeptide (123-124) that is invariably hydrophobic in flavivirus NS1 sequences and often contains phenylalanine[55,57]. Notably, the flexible loop is disordered in the crystal structures for DENV2 and WNV NS1[56], but is relatively stabilized in ZIKV NS1[55,57]. The ZIKV NS1 structure reveals the flexible loop oriented toward the inner face of the dimer, forming a hydrophobic 'spike' which possibly mediates interactions with membranes[55,57]. Notwithstanding this orientation, the flexible loop displays a considerable amount of conformational flexibility[55-57] and possibly adopts alternative orientations in the context of membrane association and NS1 oligomerization. Mutational analysis suggests that residues in this region (W115, W118, and G119) facilitate the initial attachment of secreted soluble NS1 to the cell surface[59].

DENV2, WNV, and ZIKV NS1 also arrange similarly in the hexamer (**Figure 1.6**), which appears in the absence of detergent and is visualized by negative-stain electron microscopy (EM)

or cryo-EM[55,56,84,85]. Three dimers assemble into an open barrel-shaped hexamer, with the outer polar faces oriented outward and the inner hydrophobic faces oriented toward the inner channel[55,56], which carries lipid cargo (as described in Section 1.2)[85]. Superposition of the dimer structure on the hexamer reveals the spaghetti loops and polar faces of the wing domains to be on the exposed outer surface of the hexamer, whereas the hydrophobic inner faces of the dimer are oriented toward the inner channel[55,56]. Notably, the flexible loop extends from one dimer subunit toward the β-platform of the adjacent dimer subunit, suggesting that it possibly plays a role in hexamer stability[55,57].

1.4 NS1 functions

1.4.1 Virus replication and assembly

Confocal and cryoelectron microscopy reveal that NS1 and dsRNA predominately co-localize within 'vesicle packets' of the ER membrane, the site of flavivirus genome replication[76,114,115]. Reportedly, NS1 is required for remodeling ER membranes into vesicle packet structures, potentially through its interactions with negatively charged lipids[86,87]. Protein-liposome co-floating assays suggest that NS1 preferentially binds negatively charged lipids commonly found in ER membranes, such as PI4P[87]. On the inner face of the NS1 dimer, positively charged residues adjacent to the hydrophobic protrusions (*e.g.,* greasy finger and flexible loop) likely facilitate these interactions[55,87]. Indeed, charge-reversal at these positively charged residues or downregulation of PI4P (through Sac1 overexpression) disrupt the ability of NS1 to remodel ER membranes and attenuate virus replication[87]. More studies are required to elucidate the mechanism of NS1-dependent membrane remodeling.

Trans-complementation and mutagenesis studies indicate that NS1 is required for flavivirus replication, serving as a scaffold for assembly of other necessary viral and host factors[30-

[33,77,116]. Indeed, NS1 co-localizes in vesicle packets with other nonstructural proteins such as NS2B and NS3[114]. NS1 also reportedly interacts with NS4A[77,115] and NS4B[30], at least for some flaviviruses (**Figure 1.5**). WNV NS1 physically associates with NS4B, potentially via the β-roll as substitutions in this domain (residues 10 and 11) disrupt virus replication but can be rescued by escape mutations in NS4B[30]. In contrast, DENV NS1 reportedly does not interact with NS4A or NS4B; rather, it directly interacts with the NS4A-2K-NS4B cleavage intermediate via the greasy finger[33]. Due to the proximal locations of the greasy finger and β-roll[56], it is possible that both regions are involved in interactions with the other nonstructural proteins. Indeed, substituting with charged amino acids in the otherwise hydrophobic greasy finger leads to defective RNA synthesis by DENV2[56]. Despite acting as a scaffold, the precise function of NS1 in genome replication is not entirely understood. Glycosylation at Asn130 is required for efficient virus replication[93], though it is not clear how the glycans are involved in this process.

Apart from its role in the replicase complex, NS1 appears to be involved in virion assembly and/or release from infected cells. Study of a WNV-DENV chimeric flavivirus reveals that adaptive mutations in the ribosomal frameshift motif in NS2A, which regulates the production of NS1'[117], affect viral genome packaging[117]. Specifically, abolishing the frameshift motif and thus NS1' with synonymous mutations leads to more efficient encapsidation of particles during virion assembly[117]. Co-immunoprecipitation and co-localization studies indicate that NS1 dimers also interact with the flavivirus structural proteins C, prM, and E at sites of virion assembly[118,119]. Residues within the wing flexible loop (S114 and W115) and wing/β-platform domains (D180 and T301) of DENV NS1 mediate these interactions[118]. Reportedly, substitutions at these sites disproportionately impair infectious virion production despite only minor effects on virus replication[118]. A variant of DENV NS1 containing a threonine to serine substitution at position

164 (T164S) leads to impaired infectious virus production without affecting viral RNA replication[88]. Possibly, this substitution disrupts interactions between NS1 and the viral structural proteins without affecting interactions or function in the replicase complex. The precise role of NS1 in virion assembly and/or egress is not clear, though it potentially serves another scaffolding function for the structural proteins.

Reportedly, soluble DENV NS1 in circulation is endocytosed by hepatocytes, leading to enhanced hepatocyte infection and virus production[105]. Endocytosis of soluble DENV NS1 by dendritic cells also potentiates subsequent infection and virus production[120]. The mechanism by which NS1 mediates these effects is not evident; however, one possibly is that elevated intracellular levels of NS1 enhance genome replication and/or virus assembly.

1.4.2 Immune modulation

Initially, NS1 was identified as a soluble complement-fixing antigen in the blood of DENV-infected humans and mice[121-123] following reports that complement consumption and dysregulation were associated with severe DENV disease [124,125]. NS1 proteins display interactions with various complement proteins, some of which are flavivirus-specific whereas others are more general (**Figure 1.7**). For instance, WNV but not JEV NS1 binds to factor H, promoting factor I-mediated cleavage of C3b and thus evading deposition of C3b and the C5b-9 membrane attack complex (MAC) on infected cells[44,126]. At least DENV NS1 binds to clusterin to evade MAC deposition on infected cells[127] and to mannose-binding lectin (MBL) to evade MBL-mediated neutralization of virus[128]. DENV, WNV, and ZIKV NS1 bind vitronectin or C9 to inhibit MAC formation by yet another mechanism[129]. DENV, WNV, and YFV NS1 all bind to C4, recruiting C1s and leading to accelerated cleavage of C4 into C4b[43]. NS1 proteins from these three flaviviruses also directly associate with C4b binding protein, recruiting factor I and attenuating

complement pathways via inactivation of C4b in solution or on the plasma membrane[130]. Additionally, soluble DENV NS1 can directly activate complement, consistent with the elevated levels of the C5a anaphylatoxin and C5b-9 detected in the blood of patients with severe DENV[131]. NS1 possibly contributes to the systemic inflammation and vascular leakage syndrome in severe DENV through release of these vasoactive and pro-inflammatory complement factors.

The mechanism of NS1 binding to complement factors is not known, though experimental data and structural analysis provide some insight. Dimeric NS1 or NS1 lacking N-linked glycosylation at Asn130 show less binding to complement factors (C4, C4b, and C1s) compared to hexameric or fully glycosylated NS1[95]. NS1 lacking the Asn130-linked glycan, however, predominately forms higher-order aggregates over hexamers[95], suggesting that perhaps binding to complement depends more on the oligomeric state of NS1 than its glycosylation status. Typically, complement factors like factor H, C4, C4b, and C1s interact with pathogens through repeats of the complement control protein (CCP) motif, or 'sushi domain'. For several known pathogen proteins[132-134], interaction with CCP motifs occurs through domains containing anti-parallel β-sheets that resemble the β-roll or β-platform domains of NS1[135].

DENV NS1 activates platelets and immune cells via Toll-like receptor 4 (TLR4), inducing platelet aggregation and expression of vasoactive and pro-inflammatory cytokines, and perhaps contributing to severe DENV disease involving capillary leakge[45,46,136]. Indeed, severe DENV infection is associated with thrombocytopenia and the release of vasoactive and pro-inflammatory cytokines from activated T cells and monocytes[137]. Local DENV NS1-dependent production of cytokines and chemokines such as CCL2 also potentially promote the recruitment of additional virus-permissive immune cells such as monocytes, leading to greater infection[120]. WNV NS1 reportedly can inhibit TLR3-mediated gene expression[138]; however, this finding is disputed and

the mechanism is not clear[139]. Aside from complement and TLRs, NS1 interacts with additional host factors to evade or modulate the immune response. For example, NS1 from some ZIKV strains interacts with TBK1 to antagonize antiviral type I interferon (IFN) production[140], and this interaction is dependent on a valine to alanine substitution at position 188[141]. Residue 188 is buried within the β-platform structure, suggesting that perhaps this substitution affects the interaction with TBK1 via allosteric rather than direct binding effects. Additional reports suggest a role for JEV and WNV NS1 in antagonizing the type I IFN pathway through respective inhibition of MAVs[142] or RIG-I and MDA5[143]. Other reports indicate that DENV NS1 interacts with thrombin[144], human ribonucleoprotein C1/C2[145], and human STAT3β[146], though the significance of these interactions is not apparent.

Circulating soluble NS1 in mammalian hosts enhances the infectivity of mosquito vectors upon blood feeding[147,148]. Spiking recombinant DENV NS1 into DENV-infected human blood enhances virus acquisition by *Aedes aegypti* mosquitos in membrane blood feeding experiments[148]. Addition of anti-NS1 antibodies attenuates mosquito infectivity for both DENV- and JEV-infected blood[148]. A naturally occurring ZIKV strain with elevated NS1 antigenemia also facilitates enhanced mosquito infectivity[147]. In this case, an alanine to valine substitution at position 188 in NS1 leads to enhanced secretion of NS1 and elevated antigenemia in mice without significantly affecting viremia[147]. Mechanistically, DENV2 NS1 suppresses the expression of immune-related genes in the mosquito gut, leading to enhanced virus propagation[148]. Thus, soluble NS1 modulates immunity in both the mammalian host and mosquito vector.

1.4.3 Endothelial dysfunction

In the context of DENV, NS1-mediated expression of vasoactive cytokines (*e.g.*, through TLR4, anaphylatoxins, etc.) is thought to contribute to the pathogenesis of vascular leak[45,46,136].

However, soluble flavivirus NS1 also mediates TLR4-independent, endothelial intrinsic effects *in vitro* and *in vivo*[47,149]. Following binding to the surface of pulmonary endothelial cells through sulfated GAGs[104,149] (and possibly other unidentified protein receptors), DENV NS1 induces the expression of sialidases, heparanase, and cathepsin L[109] (**Figure 1.8**). Together, these enzymes mediate the degradation of sialic acid and shedding of heparan sulfate proteoglycans (*e.g.*, syndecan-1), thereby disrupting the endothelial glycocalyx (EGL) and triggering endothelial hyperpermeability[47]. Indeed, serum levels of syndecan-1 and chondroitin sulfate are positively associated with plasma leakage in patients with severe DENV[150]. These effects require dynamin- and clathrin-mediated endocytosis of NS1 and are abolished by substitution at the N-linked glycosylation site Asn207[96]. The mechanism by which NS1 mediates subsequent enzyme expression and activation for EGL disruption remains unknown, although one report suggests that NS1-dependent vascular permeability requires autophagy[151,152]. Residues at the tip of the β-platform domain (T301, A303, E326, and D327) are critical for NS1-mediated endothelial hyperpermeability but not cell binding[59]. Possibly, the β-platform tip and/or the N-linked glycan at Asn207 recruit host factors for cell signaling.

NS1 proteins from DENV[47,48,96], ZIKV[48,96,108], WNV[48,96], and other flaviviruses[48] can mediate disruptions to the EGL. Remarkably, flavivirus NS1 triggers vascular dysfunction in a tissue-specific manner that reflects disease tropism and depends on tissue-specific cell binding[48]. For example, NS1 from WNV or JEV binds to brain microvasculature but not pulmonary endothelial cells, consistent with the neurotropism of these flaviviruses[48]. The mechanism underlying this tissue specificity is not known, but likely reflects local differences in surface expression of glycocalyx components such as GAGs and proteoglycans[48,104,153] or possibly of unidentified protein receptors for NS1. Mutational analysis suggests that initial attachment of NS1

to cells requires hydrophobic residues in the wing flexible loop (*e.g.*, W115 , W118, and G119)[59]. Given that these residues are highly conserved amongst flaviviruses, other residues or regions of NS1 likely determine the cell-type specificity of binding.

Flavivirus NS1-dependent endothelial hyperpermeability also can be observed *in vivo*, and is triggered in an organ-specific manner in mice[47] (**Figure 1.8**). These findings are consistent with the vascular leakage syndrome observed in severe DENV infection; however, the relevance of these findings to the pathogenesis of other flaviviruses is not readily apparent. A role for NS1-dependent permeability in virus entry and tropism has been suggested[47,96], although it is not clear whether flaviviruses cross blood-tissue barrier through a paracellular route or other mechanisms[154]. As discussed above, NS1 is internalized after binding to the cell surface[96,105] and accumulates in endosomes[105]. Possibly, NS1 facilitates simultaneous endocytosis of infectious virions in circulation through its interactions with the structural proteins[118,119]. Indeed, flaviviruses such as DENV can gain entry into cells through clathrin-mediated endocytosis[155,156]. More studies will be required to elucidate potential mechanisms of flavivirus migration across blood-tissue barriers, through the paracellular route, transcytosis, or other mechanisms.

1.5 NS1-targeted antibodies and vaccines

1.5.1 NS1-specific antibodies

Passive administration of NS1-specific antibodies confers protection in animal models for several different flaviviruses, including YFV[50,157], DENV[59,109,158-163], ZIKV[164,165], WNV[49], and JEV[166,167]. Many studies measure protection against lethal flavivirus challenge[49,164-166] or other disease processes such as bleeding time and vascular permeability, particularly for DENV challenge[109,158,163]. Several studies demonstrate protection following prophylactic antibody administration[50,59,109,157,159-167], though some NS1-specific monoclonal antibodies (mAbs) confer

protection when administered up to one[158] or four days[49] post-infection. One mode of protection depends on Fc effector functions that promote the clearance of infected cells expressing NS1 on the surface. Natural human mAbs targeting ZIKV NS1 protect mice against lethal ZIKV challenge only in the context of an intact Fc, losing protection with Fc variants (*e.g.*, LALA-PG) that lack binding to Fcγ receptors and complement[164]. Murine mAbs generated by immunizing mice with soluble WNV NS1 protein protect against WNV mostly through Fc-dependent mechanisms, as they lose protection in mice deficient in complement or Fcγ receptors[49]. Specific IgG subclasses (*e.g.*, IgG2a) also are associated with protection by anti-WNV NS1 murine mAbs, indicating a role for subclass-specific effector functions[49]. Anti-NS1 mAbs indeed can engage complement[126,158,161,168] and Fcγ receptors[80,164] to promote lysis or phagocytosis of infected cells. For example, anti-NS1 mAbs can sensitize YFV-infected cells to complement-dependent cytotoxicity, but this effect is lost upon isotype switching to non-complement fixing IgG subclasses[168]. Anti-NS1 mAbs also can act as opsonins, promoting phagocytosis of WNV-infected cells by Fc receptor-expressing macrophages[80]. In concept, anti-NS1 mAbs might facilitate natural killer cell-mediated antibody-dependent cellular cytotoxicity through binding to cell surface NS1. However, murine mAbs against WNV NS1 retain full protection in mice deficient in Fcγ receptor III or depleted of NK cells[80]. The relative importance of different Fc effector functions remains to be explored using larger panels of anti-NS1 mAbs, and possibly varies between flaviviruses.

Fc-independent mechanisms also contribute to protection, at least for two NS1-specific antibodies (2B7[59] and 1G5.3[160]) in the context of DENV infection. The single-chain variable fragment (scFv) of 2B7 and Fab fragment of 1G5.3 retain protection against lethal DENV2 infection in mice without the ability to clear infected cells through Fc effector functions[59]. The mAbs also prevent soluble NS1 from inducing endothelial hyperpermeability *in vitro* and in

mice[59,109,160], suggesting that blocking soluble NS1 may be an alternative mode of protection by NS1-specific antibodies. Notably, both mAbs map to the distal tip of the β-platform domain[59,160]. 2B7 is speculated to block endothelial hyperpermeability through two mechanisms: i) steric hindrance of the wing flexible loop to block binding of NS1 to cells; and ii) direct binding to the β-platform tip region known to facilitate permeability[59]. Notably, the scFv and Fab fragments of 2B7 and 1G5.3 did not retain full protection compared to their respective IgG counterparts[59,160], suggesting that Fc engagement may provide additional benefit (or that intact Fc simply improves antibody half-life *in vivo*). Indeed, some antibodies against pathogen toxins require Fc engagement to efficiently clear toxin from circulation[169]. Alternatively, Fc-dependent clearance of infected cells and Fc-independent inhibition of soluble NS1 may work in concert to confer protection. The role of Fc-independent protection for flaviviruses other than DENV is unknown, although one anti-WNV NS1 mAb (14NS1) retains considerable protection in mice lacking Fcγ receptors or complement[49]. Potentially, the role of Fc may vary between flaviviruses depending on the relative expression of cell surface and secreted NS1[79].

Currently, few epitopes have been mapped for protective flavivirus NS1-specific mAbs. At least for DENV NS1, the immunodominant B cell epitopes following infection map to the wing flexible loop and tip of the β-platform[170]. Indeed, one protective anti-DENV NS1 mAb (33D2)[161] and one protective anti-WNV NS1 mAb (16NS1)[166] map to the wing flexible loop. Two other protective anti-DENV NS1 mAbs respectively map to the β-platform (2E8)[158] and β-roll (1H7.4)[109,171]. Three structures of NS1-antibody complexes help to visualize how mAbs engage particular epitopes[58,59,160]. One such structure indicates that a protective murine mAb against WNV NS1 (22NS1) binds the spaghetti loop of the β-platform domain[58]. Two other structures of protective mAbs against DENV NS1 (2B7 and IG5.3) show binding to the distal tip of the β-

platform[59,160]. Notably, 2B7 and IG5.3 display broad cross-reactivity with heterologous flavivirus NS1 proteins[59,160], consistent with sequence conservation at the tip of the β-platform[57]. However, the epitope for both mAbs corresponds to a region of DENV NS1 that reportedly generates autoreactive and potentially pathogenic mAbs (detailed below)[51,52,113,172-174]. Currently, no NS1-antibody complex structure exists for human mAbs or for mAbs binding other epitopes associated with protection such as the wing flexible loop. Of the few known epitopes, most are for mAbs against DENV NS1. Protective epitopes for other flaviviruses may vary depending on the expression pattern of cell surface and secreted NS1[79], variations in epitope accessibility, or differences in electrostatic potentials (*e.g.*, in the outer surface of the wing domain)[55-57]. Additionally, little is known about the types of epitopes targeted by protective human mAbs generated by natural flavivirus infection. To fully discern protective, non-protective, and pathogenic epitopes, more rigorous mapping studies will be required.

Some anti-DENV NS1 antibodies cross-react with host factors and contribute to pathogenesis in animal models[159,175,176]. Sera from DENV-infected patients or mice immunized against NS1 bind platelets[53,177] and plasminogen[51], dysregulating coagulation when administered to mice. DENV NS1-immune human or murine sera also bind to endothelial cells[175,178-180], inducing NF-kB activation[181], caspase-dependent apoptosis[180], or complement-mediated lysis *in vitro*[178]. Reportedly, immunization of mice against DENV NS1 also can lead to NS1-specific antibody deposition on the liver vascular endothelium and induce liver tissue damage[182]. The above findings suggest that NS1-induced autoantibodies may represent another mechanism by which DENV causes vascular dysfunction.

Mice immunized against DENV2 NS1 indeed generate mAbs that cross-react with epitopes of human plasminogen, platelets, and endothelial cells[51,113,175]. Autoreactive mAbs can induce

hemorrhaging in some mouse models as well[175]. Proteomic analysis suggests that some mAbs may target the C-terminal tip of the β-platform (particularly residues 305 to 330), which possesses homologous sequences to host platelet and endothelial cell proteins[52]. Indeed, immunizing mice with DENV NS1 that lacks this C-terminal region (amino acids 271-352) generates antibodies that do not induce platelet aggregation or increase bleeding time, in contrast with antibodies against full-length DENV NS1[183]. The platelet-expressed protein disulfide isomerase is one such autoimmune target of mAbs elicited by the 311-330 peptide of DENV NS1[113]. Another mAb target is plasminogen, elicited by the cross-reactive peptide 305-311 of NS1[51]. These autoreactive mAbs can induce plasminogen activation and conversion into plasmin[51]. Another study finds that some anti-DENV NS1 mAbs cross-react with the host protein LYRIC, via a homologous peptide in the wing flexible loop (amino acids 116-119)[54]. These mAbs bind endothelial cells and induce apoptosis or complement-dependent cytotoxicity[54]. Altogether, these data suggest that at least DENV NS1 elicits autoreactive antibodies, some of which confer pathogenic consequences *in vivo*. The design of therapeutic mAbs against flavivirus NS1 will require careful testing for possible autoreactivity, especially mAbs against DENV NS1 and those mapping to particular epitope regions.

1.5.2 NS1-targeted vaccines

NS1-targeted vaccines exhibit immunogenicity and confer protection in animal models. For example, recombinant NS1 protein vaccines confer protection against subsequent YFV[168,184,185] or DENV[170,186,187] challenge in mice[168,170,185-187] and monkeys[184]. Other vaccine platforms also elicit protective immune responses, such as: i) vaccinia vectors for YFV[188], DENV[189], and MVEV[190]; ii) replication-defective adenovirus vectors for DENV[191] and TBEV[192-194] NS1; iii) DNA vaccines for DENV[195], ZIKV[164,196], and JEV[197]; and iv) Modified Vaccinia

Ankara vectors for ZIKV[198]. Passive transfer of serum from NS1-immunized mice can confer protection against flavivirus challenge[165,168,189], suggesting that humoral immunity may be sufficient in some cases. However, cellular immunity plays a role for some NS1-targeted vaccines[192,196]. An adenovirus vector vaccine for TBEV NS1[192-194] confers both protective humoral and cellular immunity, as transfer of antibodies, B cells, or T cells from vaccinated mice protects recipient mice against lethal TBEV challenge[192]. One DNA vaccine encoding ZIKV NS1 protects more efficiently in the presence of $CD8^+$ T cells, again suggesting a role for cellular immunity[196]. Indeed, cytotoxic T lymphocytes recognize NS1-derived peptides for DENV[191], ZIKV[196], and JEV[191,199] and can kill infected cells[199].

Other vaccine strategies target both the structural proteins and NS1[200,201]. An attenuated recombinant vesicular stomatitis virus-based vaccine expressing ZIKV prM-E-NS1 polyprotein elicits superior responses compared to an NS1-only vaccine[200]. Additionally, an adenovirus-vectored vaccine expressing prM-E-NS1 conferred superior protection compared to both prM-E-only and NS1-only vaccines[201].

One study performed epitope mapping of DENV-immune murine and human sera using a microarray of overlapping NS1 peptides for DENV1-3[170]. Following natural infection with DENV in mice and humans, immunodominant epitopes mapped largely to the wing flexible loop and tip of the β-platform domain[170]. However, the immunodominant epitopes in mice varied between natural DENV infection and adjuvanted DENV NS1 protein immunization[170]. These findings suggest that recombinant protein vaccination elicits responses to additional epitopes in NS1, particularly to the β-roll and greasy finger regions on the inner face of the NS1 dimer[170]. Given that some antibodies protect against DENV by blocking binding of soluble NS1 to cells[59], vaccine immunogens designed to target the inner face of NS1 possibly provide a means to confer protection

while avoiding the autoreactive C-terminal region of NS1 (*i.e.*, the tip of the β-platform)[51]. Some vaccine designs indeed demonstrate protection while avoiding these cross-reactive epitopes. For example, a chimeric DENV NS1 vaccine that swaps the C-terminal domain (residues 271 to 352) of DENV2 for that of JEV retains immunogenicity and generates antibodies that confer protection against DENV challenge[161,163]. A peptide vaccine corresponding to only amino acids 37 to 55 of TBEV NS1 also protects against lethal challenge, as does adoptive transfer of immune sera to naïve mice[202]. Extensive epitope mapping of protective NS1-specific mAbs may provide insight for the design of vaccine immunogens that focus the immune response on particular epitopes. In particular, NS1 immunogens could be designed to exclude the conserved C-terminal region or possibly to mask this epitope by attaching N-linked glycans in a site-specific manner[203-206].

1.6 Conclusions

No approved vaccines or antibody therapeutics exist for many clinically relevant flaviviruses including WNV and ZIKV. Currently, approved flavivirus vaccines target the structural proteins of YFV, JEV, TBEV, or DENV1-4. Antibody-dependent enhancement (ADE) of infection and disease, however, remains a concern for anti-E antibodies that cross-react with heterologous flaviviruses (or across serotypes in the case of DENV). NS1 represents an alternative target for vaccines and antibody therapeutics to avoid ADE[207,208]. While NS1-specific antibodies have been shown to confer protection in animal models, few epitopes have been mapped, and thus the breadth of epitopes that confer protection against flaviviruses is not known. Knowledge of epitopes also is critical for identifying therapeutic antibodies that avoid potentially pathogenic, autoreactive epitopes. Furthermore, the role of human antibodies against NS1 in protection is not known for many flaviviruses, including WNV. An extensive understanding of protective and non-protective epitopes, especially for human antibodies, will be important for the design of therapeutic

antibodies and vaccine antigens targeting flavivirus NS1. The studies herein begin to identify the breadth of epitopes in NS1 for two clinically relevant flaviviruses, ZIKV and WNV, and provide insight for the development of therapeutics.

Multiple functions have been ascribed to NS1 that suggest it plays a role in viral pathogenesis through immune evasion, immune activation, or dysregulation of blood-tissue endothelial barriers. Secreted NS1 can be detected in sera from infected animals and humans for virtually all flaviviruses[40,42,97-101], and the levels of NS1 in circulation correlate with disease severity, at least for DENV[102,131]. Still, the relative contribution of secreted NS1 to disease is not entirely understood for all flaviviruses. Studies herein contribute to the understanding of soluble WNV NS1 as a driver of flavivirus pathogenesis and raise interesting questions regarding its mechanisms.

1.7 References

1 Young, P. R. Arboviruses: A Family on the Move. *Adv Exp Med Biol* **1062**, 1-10, doi:10.1007/978-981-10-8727-1_1 (2018).

2 Daep, C. A., Muñoz-Jordán, J. L. & Eugenin, E. A. Flaviviruses, an expanding threat in public health: focus on dengue, West Nile, and Japanese encephalitis virus. *J Neurovirol* **20**, 539-560, doi:10.1007/s13365-014-0285-z (2014).

3 Bhatt, S. *et al.* The global distribution and burden of dengue. *Nature* **496**, 504-507, doi:10.1038/nature12060 (2013).

4 Faria, N. R. *et al.* Genomic and epidemiological monitoring of yellow fever virus transmission potential. *Science* **361**, 894-899, doi:10.1126/science.aat7115 (2018).

5 CDC. *West Nile virus: Final Cumulative Maps & Data for 1999-2019*, <https://www.cdc.gov/westnile/statsmaps/cumMapsData.html> (2020).

6 Simpson, D. I. ZIKA VIRUS INFECTION IN MAN. *Trans R Soc Trop Med Hyg* **58**, 335-338 (1964).

7 Duffy, M. R. *et al.* Zika virus outbreak on Yap Island, Federated States of Micronesia. *N Engl J Med* **360**, 2536-2543, doi:10.1056/NEJMoa0805715 (2009).

8 Kucharski, A. J. *et al.* Transmission Dynamics of Zika Virus in Island Populations: A Modelling Analysis of the 2013-14 French Polynesia Outbreak. *PLoS Negl Trop Dis* **10**, e0004726, doi:10.1371/journal.pntd.0004726 (2016).

9 Petersen, L. R., Jamieson, D. J., Powers, A. M. & Honein, M. A. Zika Virus. *New England Journal of Medicine* **374**, 1552-1563, doi:10.1056/NEJMra1602113 (2016).

10 Matheron, S. *et al.* Long-Lasting Persistence of Zika Virus in Semen. *Clin Infect Dis* **63**, 1264, doi:10.1093/cid/ciw509 (2016).

11 Lazear, H. M. *et al.* A Mouse Model of Zika Virus Pathogenesis. *Cell Host Microbe* **19**, 720-730, doi:10.1016/j.chom.2016.03.010 (2016).

12 Coyne, C. B. & Lazear, H. M. Zika virus — reigniting the TORCH. *Nature Reviews Microbiology* **14**, 707-715, doi:10.1038/nrmicro.2016.125 (2016).

13 Chibueze, E. C. *et al.* Zika virus infection in pregnancy: a systematic review of disease course and complications. *Reprod Health* **14**, 28, doi:10.1186/s12978-017-0285-6 (2017).

14 Cao-Lormeau, V. M. *et al.* Guillain-Barré Syndrome outbreak associated with Zika virus infection in French Polynesia: a case-control study. *Lancet* **387**, 1531-1539, doi:10.1016/s0140-6736(16)00562-6 (2016).

15 Mlakar, J. *et al.* Zika Virus Associated with Microcephaly. *New England Journal of Medicine* **374**, 951-958, doi:10.1056/NEJMoa1600651 (2016).

16 Rasmussen, S. A., Jamieson, D. J., Honein, M. A. & Petersen, L. R. Zika Virus and Birth Defects — Reviewing the Evidence for Causality. *New England Journal of Medicine* **374**, 1981-1987, doi:10.1056/NEJMsr1604338 (2016).

17 Miner, J. J. *et al.* Zika Virus Infection during Pregnancy in Mice Causes Placental Damage and Fetal Demise. *Cell* **165**, 1081-1091, doi:10.1016/j.cell.2016.05.008 (2016).

18 Peiter, P. C. *et al.* Zika epidemic and microcephaly in Brazil: Challenges for access to health care and promotion in three epidemic areas. *PLOS ONE* **15**, e0235010, doi:10.1371/journal.pone.0235010 (2020).

19 Suthar, M. S., Diamond, M. S. & Gale, M., Jr. West Nile virus infection and immunity. *Nat Rev Microbiol* **11**, 115-128, doi:10.1038/nrmicro2950 (2013).

20 Sejvar, J. J. West nile virus: an historical overview. *Ochsner J* **5**, 6-10 (2003).

21 Kramer, L. D., Styer, L. M. & Ebel, G. D. A Global Perspective on the Epidemiology of West Nile Virus. *Annual Review of Entomology* **53**, 61-81, doi:10.1146/annurev.ento.53.103106.093258 (2008).
22 Sejvar, J. J. *et al.* Neurologic Manifestations and Outcome of West Nile Virus Infection. *JAMA* **290**, 511-515, doi:10.1001/jama.290.4.511 (2003).
23 Fischer, S. A. Emerging Viruses in Transplantation: There Is More to Infection After Transplant Than CMV and EBV. *Transplantation* **86**, 1327-1339, doi:10.1097/TP.0b013e31818b6548 (2008).
24 Patel, H., Sander, B. & Nelder, M. P. Long-term sequelae of West Nile virus-related illness: a systematic review. *Lancet Infect Dis* **15**, 951-959, doi:10.1016/s1473-3099(15)00134-6 (2015).
25 Murray, K. O. *et al.* Survival Analysis, Long-Term Outcomes, and Percentage of Recovery up to 8 Years Post-Infection among the Houston West Nile Virus Cohort. *PLOS ONE* **9**, e102953, doi:10.1371/journal.pone.0102953 (2014).
26 Nowak, T., Färber, P. M., Wengler, G. & Wengler, G. Analyses of the terminal sequences of west nile virus structural proteins and of the in vitro translation of these proteins allow the proposal of a complete scheme of the proteolytic cleavages involved in their synthesis. *Virology* **169**, 365-376, doi:https://doi.org/10.1016/0042-6822(89)90162-1 (1989).
27 Mukhopadhyay, S., Kuhn, R. J. & Rossmann, M. G. A structural perspective of the flavivirus life cycle. *Nat Rev Microbiol* **3**, 13-22, doi:10.1038/nrmicro1067 (2005).
28 Murray, C. L., Jones, C. T. & Rice, C. M. Architects of assembly: roles of Flaviviridae non-structural proteins in virion morphogenesis. *Nat Rev Microbiol* **6**, 699-708, doi:10.1038/nrmicro1928 (2008).
29 Leung, J. Y. *et al.* Role of Nonstructural Protein NS2A in Flavivirus Assembly. *Journal of Virology* **82**, 4731-4741, doi:doi:10.1128/JVI.00002-08 (2008).
30 Youn, S. *et al.* Evidence for a genetic and physical interaction between nonstructural proteins NS1 and NS4B that modulates replication of West Nile virus. *J Virol* **86**, 7360-7371, doi:10.1128/jvi.00157-12 (2012).
31 Lindenbach, B. D. & Rice, C. M. trans-Complementation of yellow fever virus NS1 reveals a role in early RNA replication. *J Virol* **71**, 9608-9617 (1997).
32 Youn, S., Ambrose, R. L., Mackenzie, J. M. & Diamond, M. S. Non-structural protein-1 is required for West Nile virus replication complex formation and viral RNA synthesis. *Virology Journal* **10**, 339, doi:10.1186/1743-422X-10-339 (2013).
33 Plaszczyca, A. *et al.* A novel interaction between dengue virus nonstructural protein 1 and the NS4A-2K-4B precursor is required for viral RNA replication but not for formation of the membranous replication organelle. *PLoS Pathog* **15**, e1007736, doi:10.1371/journal.ppat.1007736 (2019).
34 Flamand, M. *et al.* Dengue virus type 1 nonstructural glycoprotein NS1 is secreted from mammalian cells as a soluble hexamer in a glycosylation-dependent fashion. *J Virol* **73**, 6104-6110, doi:10.1128/jvi.73.7.6104-6110.1999 (1999).
35 Crooks, A. J., Lee, J. M., Easterbrook, L. M., Timofeev, A. V. & Stephenson, J. R. The NS1 protein of tick-borne encephalitis virus forms multimeric species upon secretion from the host cell. *J Gen Virol* **75 (Pt 12)**, 3453-3460, doi:10.1099/0022-1317-75-12-3453 (1994).

36 Winkler, G., Randolph, V. B., Cleaves, G. R., Ryan, T. E. & Stollar, V. Evidence that the mature form of the flavivirus nonstructural protein NS1 is a dimer. *Virology* **162**, 187-196, doi:10.1016/0042-6822(88)90408-4 (1988).
37 Winkler, G., Maxwell, S. E., Ruemmler, C. & Stollar, V. Newly synthesized dengue-2 virus nonstructural protein NS1 is a soluble protein but becomes partially hydrophobic and membrane-associated after dimerization. *Virology* **171**, 302-305, doi:10.1016/0042-6822(89)90544-8 (1989).
38 Noisakran, S. *et al.* Association of dengue virus NS1 protein with lipid rafts. *J Gen Virol* **89**, 2492-2500, doi:10.1099/vir.0.83620-0 (2008).
39 Fan, W. F. & Mason, P. W. Membrane association and secretion of the Japanese encephalitis virus NS1 protein from cells expressing NS1 cDNA. *Virology* **177**, 470-476, doi:10.1016/0042-6822(90)90511-o (1990).
40 Young, P. R., Hilditch, P. A., Bletchly, C. & Halloran, W. An Antigen Capture Enzyme-Linked Immunosorbent Assay Reveals High Levels of the Dengue Virus Protein NS1 in the Sera of Infected Patients. *Journal of Clinical Microbiology* **38**, 1053-1057 (2000).
41 Bosch, I. *et al.* Rapid antigen tests for dengue virus serotypes and Zika virus in patient serum. *Science Translational Medicine* **9**, eaan1589, doi:10.1126/scitranslmed.aan1589 (2017).
42 Macdonald, J. *et al.* NS1 Protein Secretion during the Acute Phase of West Nile Virus Infection. *Journal of Virology* **79**, 13924-13933, doi:10.1128/jvi.79.22.13924-13933.2005 (2005).
43 Avirutnan, P. *et al.* Antagonism of the complement component C4 by flavivirus nonstructural protein NS1. *J Exp Med* **207**, 793-806, doi:10.1084/jem.20092545 (2010).
44 Chung, K. M. *et al.* West Nile virus nonstructural protein NS1 inhibits complement activation by binding the regulatory protein factor H. *Proc Natl Acad Sci U S A* **103**, 19111-19116, doi:10.1073/pnas.0605668103 (2006).
45 Modhiran, N. *et al.* Dengue virus NS1 protein activates immune cells via TLR4 but not TLR2 or TLR6. *Immunol Cell Biol* **95**, 491-495, doi:10.1038/icb.2017.5 (2017).
46 Chao, C. H. *et al.* Dengue virus nonstructural protein 1 activates platelets via Toll-like receptor 4, leading to thrombocytopenia and hemorrhage. *PLoS Pathog* **15**, e1007625, doi:10.1371/journal.ppat.1007625 (2019).
47 Puerta-Guardo, H., Glasner, D. R. & Harris, E. Dengue Virus NS1 Disrupts the Endothelial Glycocalyx, Leading to Hyperpermeability. *PLOS Pathogens* **12**, e1005738, doi:10.1371/journal.ppat.1005738 (2016).
48 Puerta-Guardo, H. *et al.* Flavivirus NS1 Triggers Tissue-Specific Vascular Endothelial Dysfunction Reflecting Disease Tropism. *Cell Rep* **26**, 1598-1613.e1598, doi:10.1016/j.celrep.2019.01.036 (2019).
49 Chung, K. M. *et al.* Antibodies against West Nile Virus nonstructural protein NS1 prevent lethal infection through Fc gamma receptor-dependent and -independent mechanisms. *J Virol* **80**, 1340-1351, doi:10.1128/jvi.80.3.1340-1351.2006 (2006).
50 Schlesinger, J. J., Brandriss, M. W. & Walsh, E. E. Protection against 17D yellow fever encephalitis in mice by passive transfer of monoclonal antibodies to the nonstructural glycoprotein gp48 and by active immunization with gp48. *J Immunol* **135**, 2805-2809 (1985).

51 Chuang, Y. C., Lin, J., Lin, Y. S., Wang, S. & Yeh, T. M. Dengue Virus Nonstructural Protein 1-Induced Antibodies Cross-React with Human Plasminogen and Enhance Its Activation. *J Immunol* **196**, 1218-1226, doi:10.4049/jimmunol.1500057 (2016).
52 Cheng, H. J. *et al.* Proteomic analysis of endothelial cell autoantigens recognized by anti-dengue virus nonstructural protein 1 antibodies. *Exp Biol Med (Maywood)* **234**, 63-73, doi:10.3181/0805-rm-147 (2009).
53 Sun, D. S. *et al.* Antiplatelet autoantibodies elicited by dengue virus non-structural protein 1 cause thrombocytopenia and mortality in mice. *J Thromb Haemost* **5**, 2291-2299, doi:10.1111/j.1538-7836.2007.02754.x (2007).
54 Liu, I. J., Chiu, C. Y., Chen, Y. C. & Wu, H. C. Molecular mimicry of human endothelial cell antigen by autoantibodies to nonstructural protein 1 of dengue virus. *J Biol Chem* **286**, 9726-9736, doi:10.1074/jbc.M110.170993 (2011).
55 Brown, W. C. *et al.* Extended surface for membrane association in Zika virus NS1 structure. *Nat Struct Mol Biol* **23**, 865-867, doi:10.1038/nsmb.3268 (2016).
56 Akey, D. L. *et al.* Flavivirus NS1 structures reveal surfaces for associations with membranes and the immune system. *Science* **343**, 881-885, doi:10.1126/science.1247749 (2014).
57 Xu, X. *et al.* Contribution of intertwined loop to membrane association revealed by Zika virus full-length NS1 structure. *Embo j* **35**, 2170-2178, doi:10.15252/embj.201695290 (2016).
58 Edeling, M. A., Diamond, M. S. & Fremont, D. H. Structural basis of Flavivirus NS1 assembly and antibody recognition. *Proc Natl Acad Sci U S A* **111**, 4285-4290, doi:10.1073/pnas.1322036111 (2014).
59 Biering, S. B. *et al.* Structural basis for antibody inhibition of flavivirus NS1–triggered endothelial dysfunction. *Science* **371**, 194-200, doi:10.1126/science.abc0476 (2021).
60 Falgout, B., Chanock, R. & Lai, C. J. Proper processing of dengue virus nonstructural glycoprotein NS1 requires the N-terminal hydrophobic signal sequence and the downstream nonstructural protein NS2a. *J Virol* **63**, 1852-1860 (1989).
61 Falgout, B. & Markoff, L. Evidence that flavivirus NS1-NS2A cleavage is mediated by a membrane-bound host protease in the endoplasmic reticulum. *Journal of Virology* **69**, 7232-7243, doi:doi:10.1128/jvi.69.11.7232-7243.1995 (1995).
62 Hori, H. & Lai, C. J. Cleavage of dengue virus NS1-NS2A requires an octapeptide sequence at the C terminus of NS1. *Journal of Virology* **64**, 4573-4577, doi:doi:10.1128/jvi.64.9.4573-4577.1990 (1990).
63 Addis, S. N., Lee, E., Bettadapura, J. & Lobigs, M. Proteolytic cleavage analysis at the Murray Valley encephalitis virus NS1-2A junction. *Virol J* **12**, 144, doi:10.1186/s12985-015-0375-4 (2015).
64 Pethel, M., Falgout, B. & Lai, C. J. Mutational analysis of the octapeptide sequence motif at the NS1-NS2A cleavage junction of dengue type 4 virus. *J Virol* **66**, 7225-7231, doi:10.1128/jvi.66.12.7225-7231.1992 (1992).
65 Blitvich, B. J. *et al.* Determination of the intramolecular disulfide bond arrangement and biochemical identification of the glycosylation sites of the nonstructural protein NS1 of Murray Valley encephalitis virus. *Journal of General Virology* **82**, 2251-2256, doi:https://doi.org/10.1099/0022-1317-82-9-2251 (2001).

66 Wallis, T. P., Huang, C.-Y., Nimkar, S. B., Young, P. R. & Gorman, J. J. Determination of the Disulfide Bond Arrangement of Dengue Virus NS1 Protein*. *Journal of Biological Chemistry* **279**, 20729-20741, doi:https://doi.org/10.1074/jbc.M312907200 (2004).
67 Mason, P. W. Maturation of Japanese encephalitis virus glycoproteins produced by infected mammalian and mosquito cells. *Virology* **169**, 354-364, doi:10.1016/0042-6822(89)90161-x (1989).
68 Flamand, M., Deubel, V. & Girard, M. Expression and secretion of japanese encephalitis virus nonstructural protein NS1 by insect cells using a recombinant baculovirus. *Virology* **191**, 826-836, doi:https://doi.org/10.1016/0042-6822(92)90258-Q (1992).
69 Pryor, M. J. & Wright, P. J. Glycosylation Mutants of Dengue Virus NS1 Protein. *Journal of General Virology* **75**, 1183-1187, doi:https://doi.org/10.1099/0022-1317-75-5-1183 (1994).
70 Chambers, T. J., McCourt, D. W. & Rice, C. M. Yellow fever virus proteins NS2A, NS213, and NS4B: Identification and partial N-terminal amino acid sequence analysis. *Virology* **169**, 100-109, doi:https://doi.org/10.1016/0042-6822(89)90045-7 (1989).
71 Blitvich, B. J., Scanlon, D., Shiell, B. J., Mackenzie, J. S. & Hall, R. A. Identification and analysis of truncated and elongated species of the flavivirus NS1 protein. *Virus Res* **60**, 67-79, doi:10.1016/s0168-1702(99)00003-9 (1999).
72 Chen, L. K. *et al.* Persistence of Japanese encephalitis virus is associated with abnormal expression of the nonstructural protein NS1 in host cells. *Virology* **217**, 220-229, doi:10.1006/viro.1996.0109 (1996).
73 Melian, E. B. *et al.* NS1′ of Flaviviruses in the Japanese Encephalitis Virus Serogroup Is a Product of Ribosomal Frameshifting and Plays a Role in Viral Neuroinvasiveness. *Journal of Virology* **84**, 1641-1647, doi:doi:10.1128/JVI.01979-09 (2010).
74 Firth, A. E. & Atkins, J. F. A conserved predicted pseudoknot in the NS2A-encoding sequence of West Nile and Japanese encephalitis flaviviruses suggests NS1' may derive from ribosomal frameshifting. *Virol J* **6**, 14, doi:10.1186/1743-422x-6-14 (2009).
75 Young, L. B., Melian, E. B. & Khromykh, A. A. NS1' colocalizes with NS1 and can substitute for NS1 in West Nile virus replication. *J Virol* **87**, 9384-9390, doi:10.1128/jvi.01101-13 (2013).
76 Mackenzie, J. M., Jones, M. K. & Young, P. R. Immunolocalization of the Dengue Virus Nonstructural Glycoprotein NS1 Suggests a Role in Viral RNA Replication. *Virology* **220**, 232-240, doi:https://doi.org/10.1006/viro.1996.0307 (1996).
77 Lindenbach, B. D. & Rice, C. M. Genetic Interaction of Flavivirus Nonstructural Proteins NS1 and NS4A as a Determinant of Replicase Function. *Journal of Virology* **73**, 4611-4621, doi:doi:10.1128/JVI.73.6.4611-4621.1999 (1999).
78 Schlesinger, J. J., Brandriss, M. W., Putnak, J. R. & Walsh, E. E. Cell surface expression of yellow fever virus non-structural glycoprotein NS1: consequences of interaction with antibody. *J Gen Virol* **71 (Pt 3)**, 593-599, doi:10.1099/0022-1317-71-3-593 (1990).
79 Youn, S., Cho, H., Fremont, D. H. & Diamond, M. S. A Short N-Terminal Peptide Motif on Flavivirus Nonstructural Protein NS1 Modulates Cellular Targeting and Immune Recognition. *Journal of Virology* **84**, 9516-9532, doi:10.1128/jvi.00775-10 (2010).
80 Chung, K. M., Thompson, B. S., Fremont, D. H. & Diamond, M. S. Antibody Recognition of Cell Surface-Associated NS1 Triggers Fc-γ Receptor-Mediated Phagocytosis and

Clearance of West Nile Virus-Infected Cells. *Journal of Virology* **81**, 9551-9555, doi:10.1128/jvi.00879-07 (2007).
81 Lee, C.-J., Lin, H.-R., Liao, C.-L. & Lin, Y.-L. Cholesterol Effectively Blocks Entry of Flavivirus. *Journal of Virology* **82**, 6470-6480, doi:doi:10.1128/JVI.00117-08 (2008).
82 Jacobs, M. G., Robinson, P. J., Bletchly, C., Mackenzie, J. M. & Young, P. R. Dengue virus nonstructural protein 1 is expressed in a glycosyl-phosphatidylinositol-linked form that is capable of signal transduction. *The FASEB Journal* **14**, 1603-1610, doi:https://doi.org/10.1096/fj.99-0829com (2000).
83 Crooks, A. J., Lee, J. M., Dowsett, A. B. & Stephenson, J. R. Purification and analysis of infectious virions and native non-structural antigens from cells infected with tick-borne encephalitis virus. *Journal of Chromatography A* **502**, 59-68, doi:https://doi.org/10.1016/S0021-9673(01)89563-7 (1990).
84 Muller, D. A. *et al.* Structure of the dengue virus glycoprotein non-structural protein 1 by electron microscopy and single-particle analysis. *Journal of General Virology* **93**, 771-779, doi:https://doi.org/10.1099/vir.0.039321-0 (2012).
85 Gutsche, I. *et al.* Secreted dengue virus nonstructural protein NS1 is an atypical barrel-shaped high-density lipoprotein. *Proc Natl Acad Sci U S A* **108**, 8003-8008, doi:10.1073/pnas.1017338108 (2011).
86 Ci, Y. *et al.* Zika NS1-induced ER remodeling is essential for viral replication. *J Cell Biol* **219**, doi:10.1083/jcb.201903062 (2020).
87 Ci, Y., Yang, Y., Xu, C., Qin, C. F. & Shi, L. Electrostatic Interaction Between NS1 and Negatively Charged Lipids Contributes to Flavivirus Replication Organelles Formation. *Front Microbiol* **12**, 641059, doi:10.3389/fmicb.2021.641059 (2021).
88 Chan, K. W. K. *et al.* A T164S mutation in the dengue virus NS1 protein is associated with greater disease severity in mice. *Science Translational Medicine* **11**, eaat7726, doi:10.1126/scitranslmed.aat7726 (2019).
89 Smith, G. W. & Wright, P. J. Synthesis of Proteins and Glycoproteins in Dengue Type 2 Virus-infected Vero and Aedes albopictus Cells. *Journal of General Virology* **66**, 559-571, doi:https://doi.org/10.1099/0022-1317-66-3-559 (1985).
90 Zhao, B. T. *et al.* Expression of dengue virus structural proteins and nonstructural protein NS1 by a recombinant vaccinia virus. *Journal of Virology* **61**, 4019-4022, doi:doi:10.1128/jvi.61.12.4019-4022.1987 (1987).
91 Post, P. R., Carvalho, R. & Galler, R. Glycosylation and secretion of yellow fever virus nonstmctural protein NS1. *Virus Research* **18**, 291-302, doi:https://doi.org/10.1016/0168-1702(91)90025-Q (1991).
92 Trent, D. W. *et al.* Partial nucleotide sequence of St. Louis encephalitis virus RNA: Structural proteins, NS1, ns2a, and ns2b. *Virology* **156**, 293-304, doi:https://doi.org/10.1016/0042-6822(87)90409-0 (1987).
93 Muylaert, I. R., Chambers, T. J., Galler, R. & Rice, C. M. Mutagenesis of the N-Linked Glycosylation Sites of the Yellow Fever Virus NS1 Protein: Effects on Virus Replication and Mouse Neurovirulence. *Virology* **222**, 159-168, doi:https://doi.org/10.1006/viro.1996.0406 (1996).
94 Tajima, S., Takasaki, T. & Kurane, I. Characterization of Asn130-to-Ala mutant of dengue type 1 virus NS1 protein. *Virus Genes* **36**, 323-329, doi:10.1007/s11262-008-0211-7 (2008).

95 Somnuke, P., Hauhart, R. E., Atkinson, J. P., Diamond, M. S. & Avirutnan, P. N-linked glycosylation of dengue virus NS1 protein modulates secretion, cell-surface expression, hexamer stability, and interactions with human complement. *Virology* **413**, 253-264, doi:https://doi.org/10.1016/j.virol.2011.02.022 (2011).
96 Wang, C. *et al.* Endocytosis of flavivirus NS1 is required for NS1-mediated endothelial hyperpermeability and is abolished by a single N-glycosylation site mutation. *PLoS Pathog* **15**, e1007938, doi:10.1371/journal.ppat.1007938 (2019).
97 Chung, K. M. & Diamond, M. S. Defining the levels of secreted non-structural protein NS1 after West Nile virus infection in cell culture and mice. *J Med Virol* **80**, 547-556, doi:10.1002/jmv.21091 (2008).
98 Li, Y. Z. *et al.* A specific and sensitive antigen capture assay for NS1 protein quantitation in Japanese encephalitis virus infection. *J Virol Methods* **179**, 8-16, doi:10.1016/j.jviromet.2011.06.008 (2012).
99 Yap T.L., H. S. Y., Soh J.H., Ravichandraprabhu L., Lim V.W.X., Chan H., Ong T.Z., Chua Y.P., Koh S.E., Wang H., Leo Y.S., Ying J.Y., and Sun W. Engineered NS1 for Sensitive, Specific Zika Virus Diagnosis from Patient Serology. *Emerg Infect Dis* **27**, 1427-1437, doi:https://doi.org/10.3201/eid2705.190121 (2021).
100 Alcon-LePoder, S. *et al.* Secretion of flaviviral non-structural protein NS1: from diagnosis to pathogenesis. *Novartis Found Symp* **277**, 233-247; discussion 247-253, doi:10.1002/0470058005.ch17 (2006).
101 Alcon, S. *et al.* Enzyme-linked immunosorbent assay specific to Dengue virus type 1 nonstructural protein NS1 reveals circulation of the antigen in the blood during the acute phase of disease in patients experiencing primary or secondary infections. *J Clin Microbiol* **40**, 376-381, doi:10.1128/jcm.40.02.376-381.2002 (2002).
102 Libraty, D. H. *et al.* High Circulating Levels of the Dengue Virus Nonstructural Protein NS1 Early in Dengue Illness Correlate with the Development of Dengue Hemorrhagic Fever. *The Journal of Infectious Diseases* **186**, 1165-1168, doi:10.1086/343813 (2002).
103 Han, G.-Z. A Single Substitution Changes Zika Virus Infectivity in Mosquitoes. *Trends in Microbiology* **25**, 603-605, doi:10.1016/j.tim.2017.05.014 (2017).
104 Avirutnan, P. *et al.* Secreted NS1 of dengue virus attaches to the surface of cells via interactions with heparan sulfate and chondroitin sulfate E. *PLoS Pathog* **3**, e183, doi:10.1371/journal.ppat.0030183 (2007).
105 Alcon-LePoder, S. *et al.* The secreted form of dengue virus nonstructural protein NS1 is endocytosed by hepatocytes and accumulates in late endosomes: implications for viral infectivity. *J Virol* **79**, 11403-11411, doi:10.1128/jvi.79.17.11403-11411.2005 (2005).
106 Safaiyan, F., Lindahl, U. & Salmivirta, M. Structural Diversity of N-Sulfated Heparan Sulfate Domains: Distinct Modes of Glucuronyl C5 Epimerization, Iduronic Acid 2-O-Sulfation, and Glucosamine 6-O-Sulfation. *Biochemistry* **39**, 10823-10830, doi:10.1021/bi000411s (2000).
107 Hoffman, M. P. *et al.* Cell Type-specific Differences in Glycosaminoglycans Modulate the Biological Activity of a Heparin-binding Peptide (RKRLQVQLSIRT) from the G Domain of the Laminin α1 Chain *. *Journal of Biological Chemistry* **276**, 22077-22085, doi:10.1074/jbc.M100774200 (2001).
108 Puerta-Guardo, H. *et al.* Zika Virus Nonstructural Protein 1 Disrupts Glycosaminoglycans and Causes Permeability in Developing Human Placentas. *J Infect Dis* **221**, 313-324, doi:10.1093/infdis/jiz331 (2020).

109 Beatty, P. R. *et al.* Dengue virus NS1 triggers endothelial permeability and vascular leak that is prevented by NS1 vaccination. *Science Translational Medicine* **7**, 304ra141-304ra141, doi:10.1126/scitranslmed.aaa3787 (2015).
110 Song, H., Qi, J., Haywood, J., Shi, Y. & Gao, G. F. Zika virus NS1 structure reveals diversity of electrostatic surfaces among flaviviruses. *Nat Struct Mol Biol* **23**, 456-458, doi:10.1038/nsmb.3213 (2016).
111 Poonsiri, T. *et al.* Structural Study of the C-Terminal Domain of Nonstructural Protein 1 from Japanese Encephalitis Virus. *J Virol* **92**, doi:10.1128/jvi.01868-17 (2018).
112 Wang, H. *et al.* Crystal structure of the C-terminal fragment of NS1 protein from yellow fever virus. *Sci China Life Sci* **60**, 1403-1406, doi:10.1007/s11427-017-9238-8 (2017).
113 Cheng, H. J. *et al.* Anti-dengue virus nonstructural protein 1 antibodies recognize protein disulfide isomerase on platelets and inhibit platelet aggregation. *Mol Immunol* **47**, 398-406, doi:10.1016/j.molimm.2009.08.033 (2009).
114 Westaway, E. G., Mackenzie, J. M., Kenney, M. T., Jones, M. K. & Khromykh, A. A. Ultrastructure of Kunjin virus-infected cells: colocalization of NS1 and NS3 with double-stranded RNA, and of NS2B with NS3, in virus-induced membrane structures. *Journal of Virology* **71**, 6650-6661, doi:doi:10.1128/jvi.71.9.6650-6661.1997 (1997).
115 Welsch, S. *et al.* Composition and Three-Dimensional Architecture of the Dengue Virus Replication and Assembly Sites. *Cell Host & Microbe* **5**, 365-375, doi:https://doi.org/10.1016/j.chom.2009.03.007 (2009).
116 Khromykh, A. A., Sedlak, P. L. & Westaway, E. G. cis- and trans-acting elements in flavivirus RNA replication. *J Virol* **74**, 3253-3263, doi:10.1128/jvi.74.7.3253-3263.2000 (2000).
117 Winkelmann, E. R., Widman, D. G., Suzuki, R. & Mason, P. W. Analyses of mutations selected by passaging a chimeric flavivirus identify mutations that alter infectivity and reveal an interaction between the structural proteins and the nonstructural glycoprotein NS1. *Virology* **421**, 96-104, doi:10.1016/j.virol.2011.09.007 (2011).
118 Scaturro, P., Cortese, M., Chatel-Chaix, L., Fischl, W. & Bartenschlager, R. Dengue Virus Non-structural Protein 1 Modulates Infectious Particle Production via Interaction with the Structural Proteins. *PLOS Pathogens* **11**, e1005277, doi:10.1371/journal.ppat.1005277 (2015).
119 Blitvich, B. J., Mackenzie, J. S., Coelen, R. J., Howard, M. J. & Hall, R. A. A novel complex formed between the flavivirus E and NS1 proteins: analysis of its structure and function. *Arch Virol* **140**, 145-156, doi:10.1007/bf01309729 (1995).
120 Alayli, F. & Scholle, F. Dengue virus NS1 enhances viral replication and pro-inflammatory cytokine production in human dendritic cells. *Virology* **496**, 227-236, doi:10.1016/j.virol.2016.06.008 (2016).
121 Russell, P. K., Chiewsilp, D. & Brandt, W. E. Immunoprecipitation analysis of soluble complement-fixing antigens of dengue viruses. *J Immunol* **105**, 838-845 (1970).
122 Brandt, W. E., Chiewslip, D., Harris, D. L. & Russell, P. K. Partial purification and characterization of a dengue virus soluble complement-fixing antigen. *J Immunol* **105**, 1565-1568 (1970).
123 Brandt, W. E., Cardiff, R. D. & Russell, P. K. Dengue virions and antigens in brain and serum of infected mice. *J Virol* **6**, 500-506 (1970).

124 Bokisch, V. A., Top, F. H., Russell, P. K., Dixon, F. J. & Müller-Eberhard, H. J. The Potential Pathogenic Role of Complement in Dengue Hemorrhagic Shock Syndrome. *New England Journal of Medicine* **289**, 996-1000, doi:10.1056/nejm197311082891902 (1973).
125 Russell, P. K., Intavivat, A. & Kanchanapilant, S. Anti-dengue immunoglobulins and serum beta 1 c-a globulin levels in dengue shock syndrome. *J Immunol* **102**, 412-420 (1969).
126 Krishna, V. D., Rangappa, M. & Satchidanandam, V. Virus-Specific Cytolytic Antibodies to Nonstructural Protein 1 of Japanese Encephalitis Virus Effect Reduction of Virus Output from Infected Cells. *Journal of Virology* **83**, 4766-4777, doi:10.1128/jvi.01850-08 (2009).
127 Kurosu, T., Chaichana, P., Yamate, M., Anantapreecha, S. & Ikuta, K. Secreted complement regulatory protein clusterin interacts with dengue virus nonstructural protein 1. *Biochemical and Biophysical Research Communications* **362**, 1051-1056, doi:https://doi.org/10.1016/j.bbrc.2007.08.137 (2007).
128 Thiemmeca, S. *et al.* Secreted NS1 Protects Dengue Virus from Mannose-Binding Lectin-Mediated Neutralization. *J Immunol* **197**, 4053-4065, doi:10.4049/jimmunol.1600323 (2016).
129 Conde, J. N. *et al.* Inhibition of the Membrane Attack Complex by Dengue Virus NS1 through Interaction with Vitronectin and Terminal Complement Proteins. *J Virol* **90**, 9570-9581, doi:10.1128/jvi.00912-16 (2016).
130 Avirutnan, P. *et al.* Binding of flavivirus nonstructural protein NS1 to C4b binding protein modulates complement activation. *J Immunol* **187**, 424-433, doi:10.4049/jimmunol.1100750 (2011).
131 Avirutnan, P. *et al.* Vascular leakage in severe dengue virus infections: a potential role for the nonstructural viral protein NS1 and complement. *J Infect Dis* **193**, 1078-1088, doi:10.1086/500949 (2006).
132 Persson, B. D. *et al.* Adenovirus type 11 binding alters the conformation of its receptor CD46. *Nat Struct Mol Biol* **14**, 164-166, doi:10.1038/nsmb1190 (2007).
133 Schneider, M. C. *et al.* Neisseria meningitidis recruits factor H using protein mimicry of host carbohydrates. *Nature* **458**, 890-893, doi:10.1038/nature07769 (2009).
134 Bhattacharjee, A. *et al.* Structural basis for complement evasion by Lyme disease pathogen Borrelia burgdorferi. *J Biol Chem* **288**, 18685-18695, doi:10.1074/jbc.M113.459040 (2013).
135 Akey, D. L., Brown, W. C., Jose, J., Kuhn, R. J. & Smith, J. L. Structure-guided insights on the role of NS1 in flavivirus infection. *Bioessays* **37**, 489-494, doi:10.1002/bies.201400182 (2015).
136 Modhiran, N. *et al.* Dengue virus NS1 protein activates cells via Toll-like receptor 4 and disrupts endothelial cell monolayer integrity. *Sci Transl Med* **7**, 304ra142, doi:10.1126/scitranslmed.aaa3863 (2015).
137 Kurane, I. *et al.* Immunopathologic mechanisms of dengue hemorrhagic fever and dengue shock syndrome. *Arch Virol Suppl* **9**, 59-64, doi:10.1007/978-3-7091-9326-6_7 (1994).
138 Wilson, J. R., de Sessions, P. F., Leon, M. A. & Scholle, F. West Nile virus nonstructural protein 1 inhibits TLR3 signal transduction. *J Virol* **82**, 8262-8271, doi:10.1128/jvi.00226-08 (2008).
139 Baronti, C., Sire, J., de Lamballerie, X. & Quérat, G. Nonstructural NS1 proteins of several mosquito-borne Flavivirus do not inhibit TLR3 signaling. *Virology* **404**, 319-330, doi:https://doi.org/10.1016/j.virol.2010.05.020 (2010).

140 Wu, Y. *et al.* Zika virus evades interferon-mediated antiviral response through the co-operation of multiple nonstructural proteins in vitro. *Cell Discovery* **3**, 17006, doi:10.1038/celldisc.2017.6 (2017).
141 Xia, H. *et al.* An evolutionary NS1 mutation enhances Zika virus evasion of host interferon induction. *Nature Communications* **9**, 414, doi:10.1038/s41467-017-02816-2 (2018).
142 Zhou, D. *et al.* The Japanese Encephalitis Virus NS1' Protein Inhibits Type I IFN Production by Targeting MAVS. *J Immunol* **204**, 1287-1298, doi:10.4049/jimmunol.1900946 (2020).
143 Zhang, H. L. *et al.* West Nile Virus NS1 Antagonizes Interferon Beta Production by Targeting RIG-I and MDA5. *J Virol* **91**, doi:10.1128/jvi.02396-16 (2017).
144 Lin, S.-W. *et al.* Dengue virus nonstructural protein NS1 binds to prothrombin/thrombin and inhibits prothrombin activation. *Journal of Infection* **64**, 325-334, doi:https://doi.org/10.1016/j.jinf.2011.11.023 (2012).
145 Noisakran, S. *et al.* Identification of human hnRNP C1/C2 as a dengue virus NS1-interacting protein. *Biochemical and Biophysical Research Communications* **372**, 67-72, doi:https://doi.org/10.1016/j.bbrc.2008.04.165 (2008).
146 Chua, J. J.-E., Bhuvanakantham, R., Chow, V. T.-K. & Ng, M.-L. Recombinant non-structural 1 (NS1) protein of dengue-2 virus interacts with human STAT3β protein. *Virus Research* **112**, 85-94, doi:https://doi.org/10.1016/j.virusres.2005.03.025 (2005).
147 Liu, Y. *et al.* Evolutionary enhancement of Zika virus infectivity in Aedes aegypti mosquitoes. *Nature* **545**, 482-486, doi:10.1038/nature22365 (2017).
148 Liu, J. *et al.* Flavivirus NS1 protein in infected host sera enhances viral acquisition by mosquitoes. *Nature microbiology* **1**, 16087-16087, doi:10.1038/nmicrobiol.2016.87 (2016).
149 Glasner, D. R. *et al.* Dengue virus NS1 cytokine-independent vascular leak is dependent on endothelial glycocalyx components. *PLoS Pathog* **13**, e1006673, doi:10.1371/journal.ppat.1006673 (2017).
150 Suwarto, S., Sasmono, R. T., Sinto, R., Ibrahim, E. & Suryamin, M. Association of Endothelial Glycocalyx and Tight and Adherens Junctions With Severity of Plasma Leakage in Dengue Infection. *J Infect Dis* **215**, 992-999, doi:10.1093/infdis/jix041 (2017).
151 Chen, H.-R. *et al.* Dengue Virus Nonstructural Protein 1 Induces Vascular Leakage through Macrophage Migration Inhibitory Factor and Autophagy. *PLOS Neglected Tropical Diseases* **10**, e0004828, doi:10.1371/journal.pntd.0004828 (2016).
152 Chen, H.-R. *et al.* Macrophage migration inhibitory factor is critical for dengue NS1-induced endothelial glycocalyx degradation and hyperpermeability. *PLOS Pathogens* **14**, e1007033, doi:10.1371/journal.ppat.1007033 (2018).
153 Modhiran, N. *et al.* Dual targeting of dengue virus virions and NS1 protein with the heparan sulfate mimic PG545. *Antiviral Res* **168**, 121-127, doi:10.1016/j.antiviral.2019.05.004 (2019).
154 Mustafá, Y. M., Meuren, L. M., Coelho, S. V. A. & de Arruda, L. B. Pathways Exploited by Flaviviruses to Counteract the Blood-Brain Barrier and Invade the Central Nervous System. *Frontiers in Microbiology* **10**, doi:10.3389/fmicb.2019.00525 (2019).
155 Cruz-Oliveira, C. *et al.* Receptors and routes of dengue virus entry into the host cells. *FEMS Microbiol Rev* **39**, 155-170, doi:10.1093/femsre/fuu004 (2015).

156 Ho, M. R. *et al.* Blockade of dengue virus infection and viral cytotoxicity in neuronal cells in vitro and in vivo by targeting endocytic pathways. *Sci Rep* **7**, 6910, doi:10.1038/s41598-017-07023-z (2017).
157 Gould, E. A., Buckley, A., Barrett, A. D. & Cammack, N. Neutralizing (54K) and non-neutralizing (54K and 48K) monoclonal antibodies against structural and non-structural yellow fever virus proteins confer immunity in mice. *J Gen Virol* **67 (Pt 3)**, 591-595, doi:10.1099/0022-1317-67-3-591 (1986).
158 Wan, S. W. *et al.* Therapeutic Effects of Monoclonal Antibody against Dengue Virus NS1 in a STAT1 Knockout Mouse Model of Dengue Infection. *J Immunol* **199**, 2834-2844, doi:10.4049/jimmunol.1601523 (2017).
159 Henchal, E. A., Henchal, L. S. & Schlesinger, J. J. Synergistic interactions of anti-NS1 monoclonal antibodies protect passively immunized mice from lethal challenge with dengue 2 virus. *J Gen Virol* **69 (Pt 8)**, 2101-2107, doi:10.1099/0022-1317-69-8-2101 (1988).
160 Modhiran, N. *et al.* A broadly protective antibody that targets the flavivirus NS1 protein. *Science* **371**, 190-194, doi:10.1126/science.abb9425 (2021).
161 Lai, Y. C. *et al.* Antibodies Against Modified NS1 Wing Domain Peptide Protect Against Dengue Virus Infection. *Sci Rep* **7**, 6975, doi:10.1038/s41598-017-07308-3 (2017).
162 Wong, M. P. *et al.* Characterization of a protective antibody against dengue virus non-structural protein 1 (NS1) reveals critical domains required for NS1-triggered pathogenesis. *The Journal of Immunology* **204**, 167.123-167.123 (2020).
163 Wan, S. W. *et al.* Protection against dengue virus infection in mice by administration of antibodies against modified nonstructural protein 1. *PLoS One* **9**, e92495, doi:10.1371/journal.pone.0092495 (2014).
164 Bailey, M. J. *et al.* Human antibodies targeting Zika virus NS1 provide protection against disease in a mouse model. *Nat Commun* **9**, 4560, doi:10.1038/s41467-018-07008-0 (2018).
165 Bailey, M. J. *et al.* Antibodies Elicited by an NS1-Based Vaccine Protect Mice against Zika Virus. *mBio* **10**, doi:10.1128/mBio.02861-18 (2019).
166 Lee, T. H. *et al.* A cross-protective mAb recognizes a novel epitope within the flavivirus NS1 protein. *Journal of General Virology* **93**, 20-26, doi:https://doi.org/10.1099/vir.0.036640-0 (2012).
167 Li, Y. *et al.* Protective immunity to Japanese encephalitis virus associated with anti-NS1 antibodies in a mouse model. *Virology Journal* **9**, 135, doi:10.1186/1743-422X-9-135 (2012).
168 Schlesinger, J. J., Foltzer, M. & Chapman, S. The Fc portion of antibody to yellow fever virus NS1 is a determinant of protection against YF encephalitis in mice. *Virology* **192**, 132-141, doi:10.1006/viro.1993.1015 (1993).
169 Abboud, N. *et al.* A requirement for FcgammaR in antibody-mediated bacterial toxin neutralization. *J Exp Med* **207**, 2395-2405, doi:10.1084/jem.20100995 (2010).
170 Hertz, T. *et al.* Antibody Epitopes Identified in Critical Regions of Dengue Virus Nonstructural 1 Protein in Mouse Vaccination and Natural Human Infections. *J Immunol* **198**, 4025-4035, doi:10.4049/jimmunol.1700029 (2017).
171 Falconar, A. K., Young, P. R. & Miles, M. A. Precise location of sequential dengue virus subcomplex and complex B cell epitopes on the nonstructural-1 glycoprotein. *Arch Virol* **137**, 315-326, doi:10.1007/bf01309478 (1994).

172 Chuang, Y. C., Lin, Y. S., Liu, H. S. & Yeh, T. M. Molecular mimicry between dengue virus and coagulation factors induces antibodies to inhibit thrombin activity and enhance fibrinolysis. *J Virol* **88**, 13759-13768, doi:10.1128/jvi.02166-14 (2014).
173 Chang, H. H. *et al.* Facilitation of cell adhesion by immobilized dengue viral nonstructural protein 1 (NS1): arginine-glycine-aspartic acid structural mimicry within the dengue viral NS1 antigen. *J Infect Dis* **186**, 743-751, doi:10.1086/342600 (2002).
174 Cheng, H. J. *et al.* Correlation between serum levels of anti-endothelial cell autoantigen and anti-dengue virus nonstructural protein 1 antibodies in dengue patients. *Am J Trop Med Hyg* **92**, 989-995, doi:10.4269/ajtmh.14-0162 (2015).
175 Falconar, A. K. The dengue virus nonstructural-1 protein (NS1) generates antibodies to common epitopes on human blood clotting, integrin/adhesin proteins and binds to human endothelial cells: potential implications in haemorrhagic fever pathogenesis. *Arch Virol* **142**, 897-916, doi:10.1007/s007050050127 (1997).
176 Falconar, A. K. Monoclonal antibodies that bind to common epitopes on the dengue virus type 2 nonstructural-1 and envelope glycoproteins display weak neutralizing activity and differentiated responses to virulent strains: implications for pathogenesis and vaccines. *Clin Vaccine Immunol* **15**, 549-561, doi:10.1128/cvi.00351-07 (2008).
177 Lin, C. F. *et al.* Generation of IgM anti-platelet autoantibody in dengue patients. *J Med Virol* **63**, 143-149 (2001).
178 Lin, C. F. *et al.* Antibodies from dengue patient sera cross-react with endothelial cells and induce damage. *J Med Virol* **69**, 82-90, doi:10.1002/jmv.10261 (2003).
179 Immenschuh, S. *et al.* Antibodies against dengue virus nonstructural protein-1 induce heme oxygenase-1 via a redox-dependent pathway in human endothelial cells. *Free Radic Biol Med* **54**, 85-92, doi:10.1016/j.freeradbiomed.2012.10.551 (2013).
180 Lin, C. F. *et al.* Endothelial cell apoptosis induced by antibodies against dengue virus nonstructural protein 1 via production of nitric oxide. *J Immunol* **169**, 657-664, doi:10.4049/jimmunol.169.2.657 (2002).
181 Lin, C.-F. *et al.* Expression of Cytokine, Chemokine, and Adhesion Molecules during Endothelial Cell Activation Induced by Antibodies against Dengue Virus Nonstructural Protein 1. *The Journal of Immunology* **174**, 395-403, doi:10.4049/jimmunol.174.1.395 (2005).
182 Lin, C.-F. *et al.* Liver injury caused by antibodies against dengue virus nonstructural protein 1 in a murine model. *Laboratory Investigation* **88**, 1079-1089, doi:10.1038/labinvest.2008.70 (2008).
183 Chen, M.-C. *et al.* Deletion of the C-Terminal Region of Dengue Virus Nonstructural Protein 1 (NS1) Abolishes Anti-NS1-Mediated Platelet Dysfunction and Bleeding Tendency. *The Journal of Immunology* **183**, 1797-1803, doi:10.4049/jimmunol.0800672 (2009).
184 Schlesinger, J. J., Brandriss, M. W., Cropp, C. B. & Monath, T. P. Protection against yellow fever in monkeys by immunization with yellow fever virus nonstructural protein NS1. *J Virol* **60**, 1153-1155 (1986).
185 Cane, P. A. & Gould, E. A. Reduction of yellow fever virus mouse neurovirulence by immunization with a bacterially synthesized non-structural protein (NS1) fragment. *J Gen Virol* **69 (Pt 6)**, 1241-1246, doi:10.1099/0022-1317-69-6-1241 (1988).

186 Schlesinger, J. J., Brandriss, M. W. & Walsh, E. E. Protection of mice against dengue 2 virus encephalitis by immunization with the dengue 2 virus non-structural glycoprotein NS1. *J Gen Virol* **68 (Pt 3)**, 853-857, doi:10.1099/0022-1317-68-3-853 (1987).
187 Calvert, A. E., Huang, C. Y.-H., Kinney, R. M. & Roehrig, J. T. Non-structural proteins of dengue 2 virus offer limited protection to interferon-deficient mice after dengue 2 virus challenge. *Journal of General Virology* **87**, 339-346, doi:https://doi.org/10.1099/vir.0.81256-0 (2006).
188 Putnak, J. R. & Schlesinger, J. J. Protection of mice against yellow fever virus encephalitis by immunization with a vaccinia virus recombinant encoding the yellow fever virus non-structural proteins, NS1, NS2a and NS2b. *J Gen Virol* **71 (Pt 8)**, 1697-1702, doi:10.1099/0022-1317-71-8-1697 (1990).
189 Falgout, B., Bray, M., Schlesinger, J. J. & Lai, C. J. Immunization of mice with recombinant vaccinia virus expressing authentic dengue virus nonstructural protein NS1 protects against lethal dengue virus encephalitis. *J Virol* **64**, 4356-4363 (1990).
190 Hall, R. A. *et al.* Protective immune responses to the E and NS1 proteins of Murray Valley encephalitis virus in hybrids of flavivirus-resistant mice. *Journal of General Virology* **77**, 1287-1294, doi:https://doi.org/10.1099/0022-1317-77-6-1287 (1996).
191 Gao, G. *et al.* Adenovirus-based vaccines generate cytotoxic T lymphocytes to epitopes of NS1 from dengue virus that are present in all major serotypes. *Hum Gene Ther* **19**, 927-936, doi:10.1089/hum.2008.011 (2008).
192 Timofeev, A. V. *et al.* Immunological basis for protection in a murine model of tick-borne encephalitis by a recombinant adenovirus carrying the gene encoding the NS1 non-structural protein. *Journal of General Virology* **79**, 689-695, doi:https://doi.org/10.1099/0022-1317-79-4-689 (1998).
193 Jacobs, S. C., Stephenson, J. R. & Wilkinson, G. W. G. Protection elicited by a replication-defective adenovirus vector expressing the tick-borne encephalitis virus non-structural glycoprotein NS1. *Journal of General Virology* **75**, 2399-2402, doi:https://doi.org/10.1099/0022-1317-75-9-2399 (1994).
194 Jacobs, S. C., Stephenson, J. R. & Wilkinson, G. W. High-level expression of the tick-borne encephalitis virus NS1 protein by using an adenovirus-based vector: protection elicited in a murine model. *Journal of Virology* **66**, 2086-2095 (1992).
195 Wu, S.-F. *et al.* Evaluation of protective efficacy and immune mechanisms of using a non-structural protein NS1 in DNA vaccine against dengue 2 virus in mice. *Vaccine* **21**, 3919-3929, doi:https://doi.org/10.1016/S0264-410X(03)00310-4 (2003).
196 Grubor-Bauk, B. *et al.* NS1 DNA vaccination protects against Zika infection through T cell-mediated immunity in immunocompetent mice. *Sci Adv* **5**, eaax2388, doi:10.1126/sciadv.aax2388 (2019).
197 Lin, Y.-L. *et al.* DNA Immunization with Japanese Encephalitis Virus Nonstructural Protein NS1 Elicits Protective Immunity in Mice. *Journal of Virology* **72**, 191-200, doi:doi:10.1128/JVI.72.1.191-200.1998 (1998).
198 Brault, A. C. *et al.* A Zika Vaccine Targeting NS1 Protein Protects Immunocompetent Adult Mice in a Lethal Challenge Model. *Scientific Reports* **7**, 14769, doi:10.1038/s41598-017-15039-8 (2017).
199 Murali-Krishna, K., Ramireddy, B., Ravi, V. & Manjunath, R. Recognition of Nonstructural Protein Peptides by Cytotoxic T Lymphocytes Raised against Japanese

Encephalitis Virus. *Microbiology and Immunology* **39**, 1021-1024, doi:https://doi.org/10.1111/j.1348-0421.1995.tb03294.x (1995).

200 Li, A. *et al.* A Zika virus vaccine expressing premembrane-envelope-NS1 polyprotein. *Nature Communications* **9**, 3067, doi:10.1038/s41467-018-05276-4 (2018).

201 Liu, X. *et al.* Incorporation of NS1 and prM/M are important to confer effective protection of adenovirus-vectored Zika virus vaccine carrying E protein. *npj Vaccines* **3**, 29, doi:10.1038/s41541-018-0072-6 (2018).

202 Volpina, O. M. *et al.* A synthetic peptide based on the NS1 non-structural protein of tick-borne encephalitis virus induces a protective immune response against fatal encephalitis in an experimental animal model. *Virus Research* **112**, 95-99, doi:https://doi.org/10.1016/j.virusres.2005.03.026 (2005).

203 Duan, H. *et al.* Glycan Masking Focuses Immune Responses to the HIV-1 CD4-Binding Site and Enhances Elicitation of VRC01-Class Precursor Antibodies. *Immunity* **49**, 301-311.e305, doi:10.1016/j.immuni.2018.07.005 (2018).

204 Hariharan, V. & Kane, R. S. Glycosylation as a tool for rational vaccine design. *Biotechnology and Bioengineering* **117**, 2556-2570, doi:https://doi.org/10.1002/bit.27361 (2020).

205 Bajic, G. *et al.* Influenza Antigen Engineering Focuses Immune Responses to a Subdominant but Broadly Protective Viral Epitope. *Cell Host Microbe* **25**, 827-835.e826, doi:10.1016/j.chom.2019.04.003 (2019).

206 Eggink, D., Goff, P. H. & Palese, P. Guiding the Immune Response against Influenza Virus Hemagglutinin toward the Conserved Stalk Domain by Hyperglycosylation of the Globular Head Domain. *Journal of Virology* **88**, 699-704, doi:doi:10.1128/JVI.02608-13 (2014).

207 Gibson, C. A., Schlesinger, J. J. & Barrett, A. D. T. Prospects for a virus non-structural protein as a subunit vaccine. *Vaccine* **6**, 7-9, doi:https://doi.org/10.1016/0264-410X(88)90004-7 (1988).

208 Miller, N. Recent progress in dengue vaccine research and development. *Curr Opin Mol Ther* **12**, 31-38 (2010).

209 Pierson, T. C. & Diamond, M. S. The continued threat of emerging flaviviruses. *Nature Microbiology* **5**, 796-812, doi:10.1038/s41564-020-0714-0 (2020).

210 Muller, D. A. & Young, P. R. The flavivirus NS1 protein: molecular and structural biology, immunology, role in pathogenesis and application as a diagnostic biomarker. *Antiviral Res* **98**, 192-208, doi:10.1016/j.antiviral.2013.03.008 (2013).

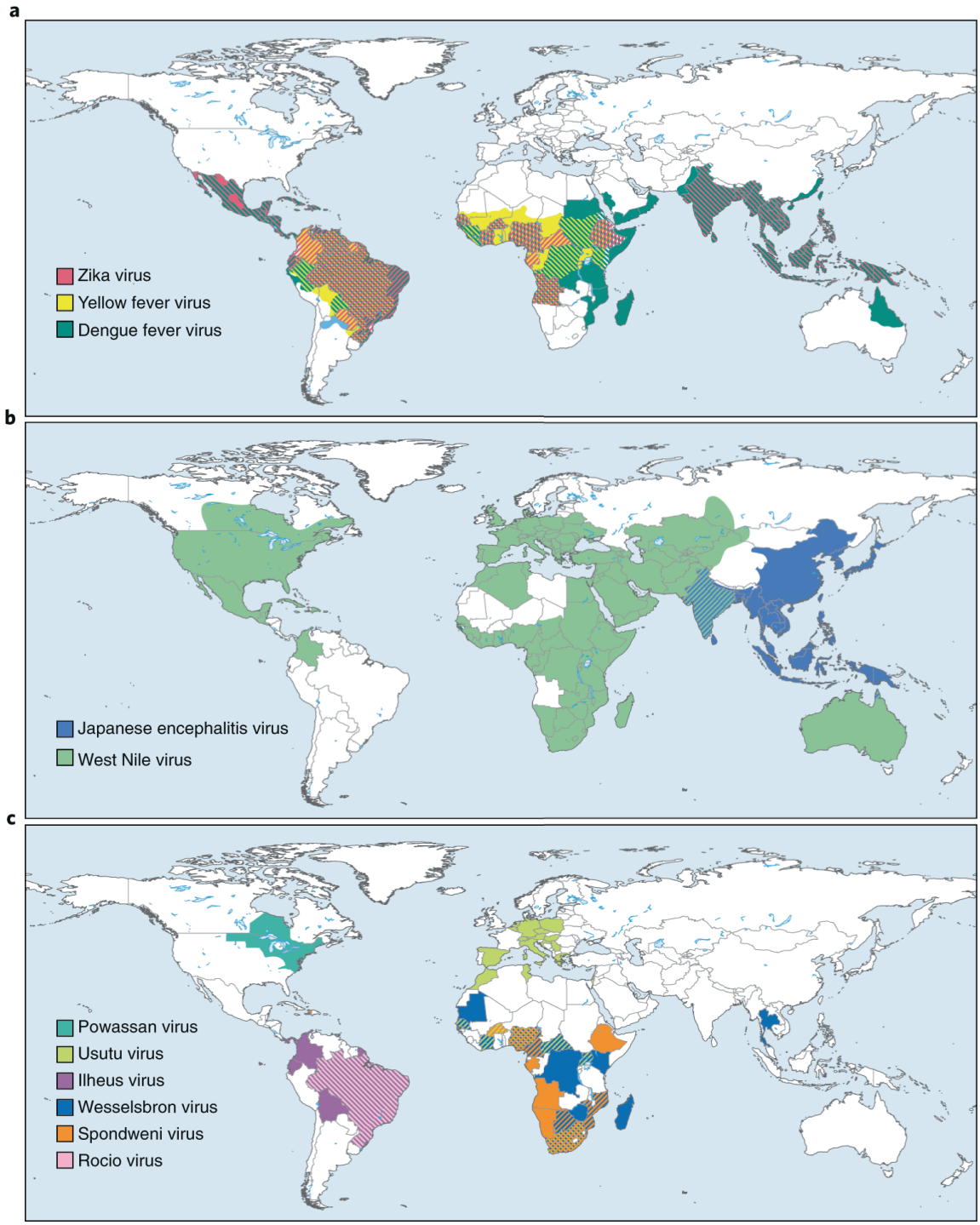

Figure 1.1. Geographical distribution of mosquito-transmitted flaviviruses, including (**a**) ZIKV, YFV, and DENV; (**b**) JEV and WNV; and (**c**) other less common flaviviruses. Figure adapted from Pierson & Diamond, 2020[209].

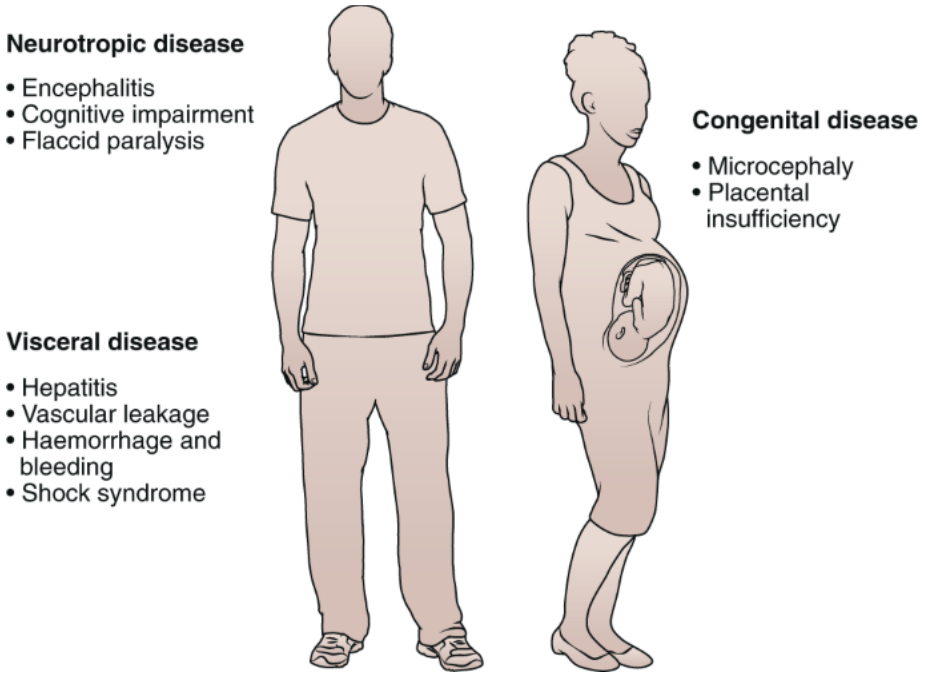

Figure 1.2. Clinical manifestations of flavivirus infection in humans. Neurotropic flaviviruses (*e.g.*, WNV, JEV, ZIKV, MVEV, and TBEV) can infect the brain and spinal cord, causing encephalitis, meningitis, and acute flaccid paralysis. Other flaviviruses (*e.g.*, YFV and DENV) can cause systemic disease resulting in liver failure and vascular shock. ZIKV infection of pregnant women can cause congenital complications, including microcephaly and intrauterine growth restriction. Figure adapted from Pierson & Diamond, 2020[209].

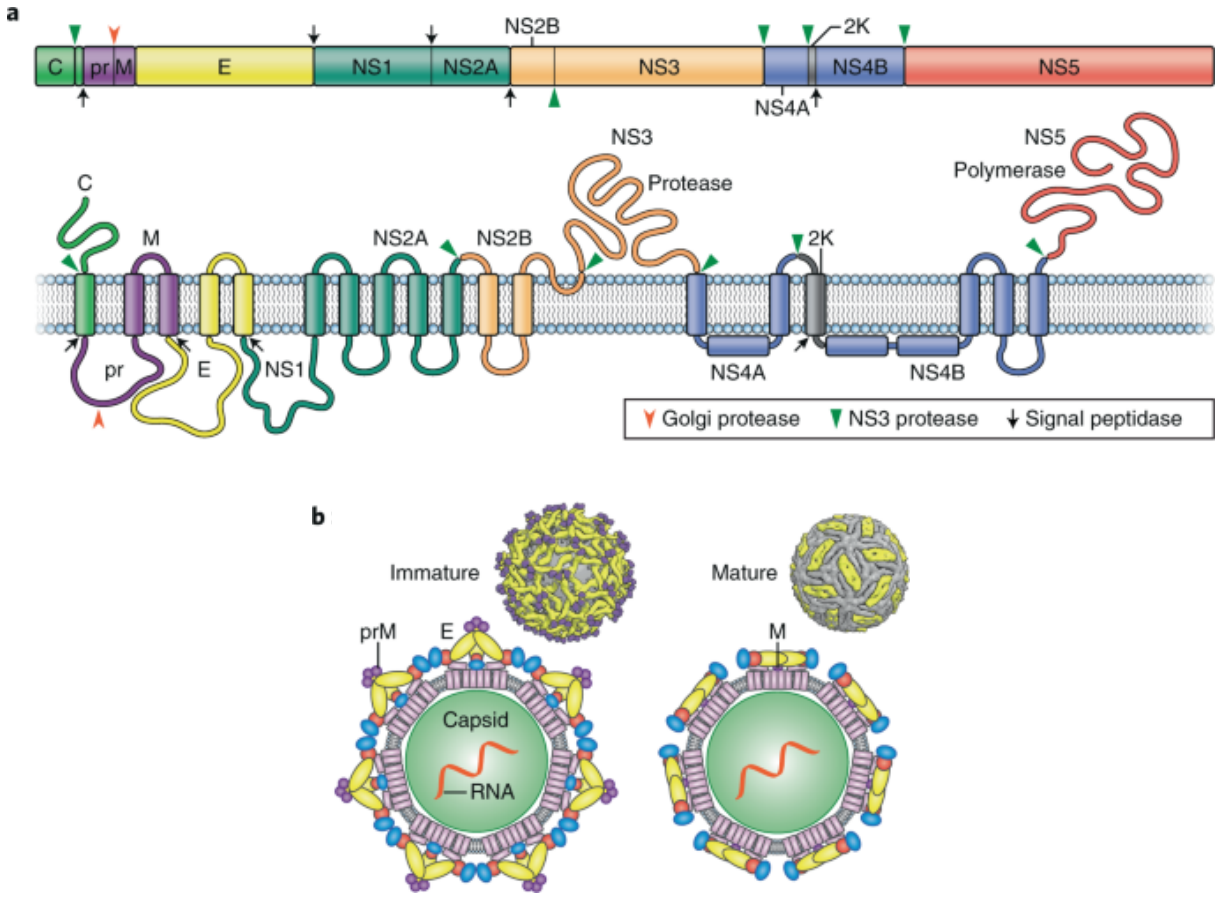

Figure 1.3. Flavivirus genome organization and virion structure. (**a**) The flavivirus genome encodes three structural (C, prM, E) and seven nonstructural (NS1, NS2A/B, NS3, NS4A/B, NS5) proteins (*top*) that are translated at ER membranes (*bottom*). Arrows indicate polyprotein cleavage sites by host or viral factors. (**b**) Mature flavivirus particles are formed by the cleavage of prM protein into M protein on the virion surface. Figure adapted from Pierson & Diamond, 2020[209].

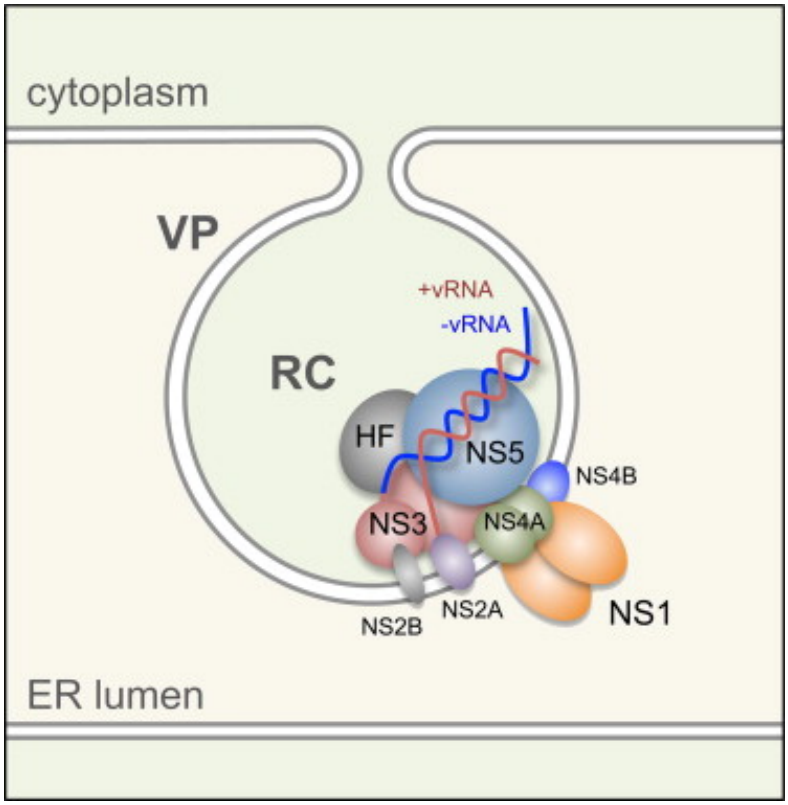

Figure 1.4. Schematic of the flavivirus replicase complex (RC) within vesicle packets (VP) of ER membrane. All seven nonstructural proteins (NS1, NS2A/B, NS3, NS4A/B, NS5) co-localize to the RC with dsRNA, along with host factors (HF). NS1 resides at the luminal membrane, providing a requires scaffold function during viral genome replication. NS1 indirectly or directly interacts with NS4A, NS4B, and/or NS4A-2K-NS4B. Figure adapted from Muller & Young, 2013[210].

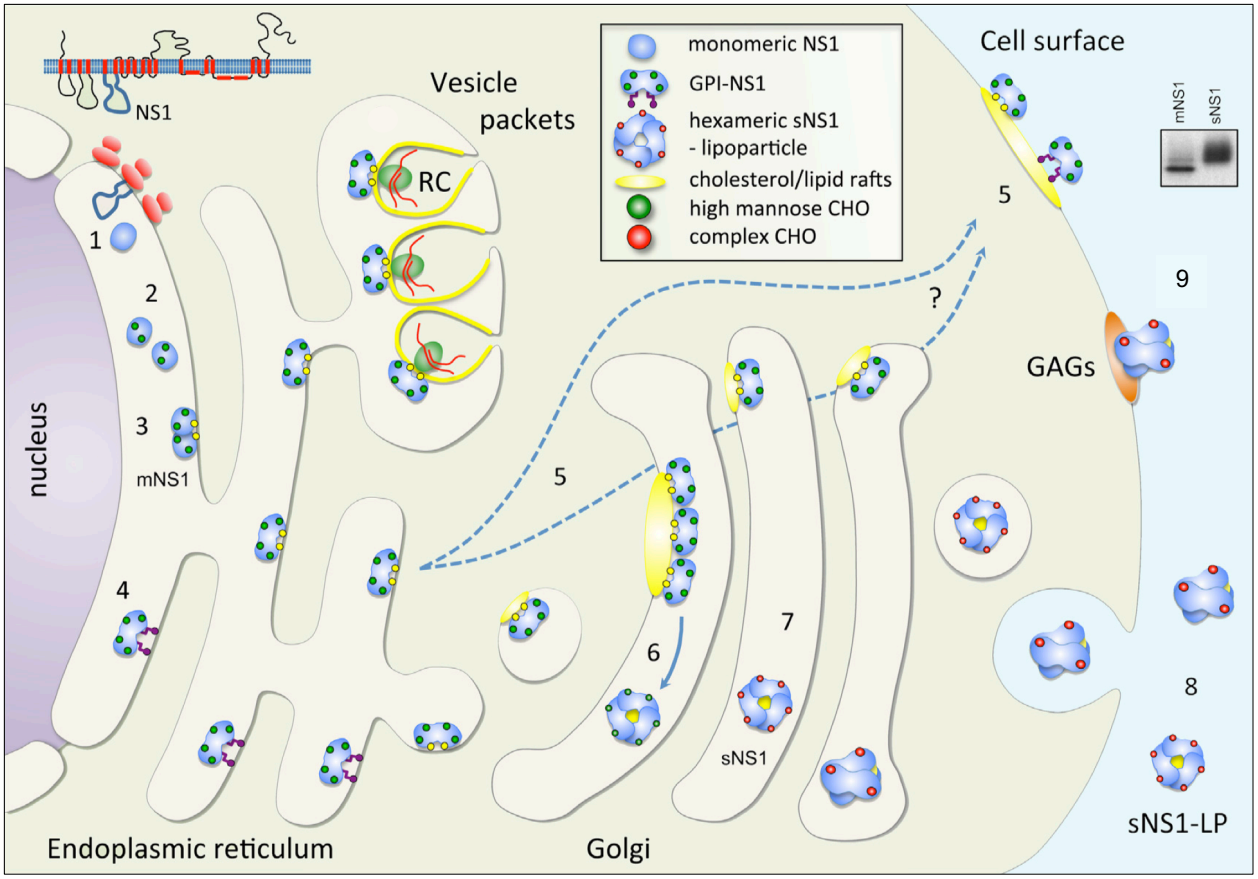

Figure 1.5. Schematic of NS1 cellular trafficking in infected cells. (**1**) NS1 is translocated into the ER via a signal sequence corresponding to the last 24 amino acids of E. Within the ER, NS1 (**2**) acquires high-mannose N-linked glycans (Asn130, Asn207, +/- Asn175), (**3**) dimerizes, and (**4**) associates with membranes (mNS1). (**5**) A fraction of cell associated dimeric NS1 traffics to the plasma membrane, where sometimes it can be found in associated with lipid rafts and/or GPI anchors. Another fraction of NS1 (**6**) hexamerizes, (**7**) undergoes glycan processing in the Golgi, and (**8**) is secreted from infected cells. Secreted NS1 (sNS1) carries lipid cargo in its hollow core (sNS1-LP) and (**9**) can bind back to infected or non-infected cells via glycosaminoglycans (GAGs) or possibly unidentified protein receptors. Figure adapted from Muller & Young, 2013[210].

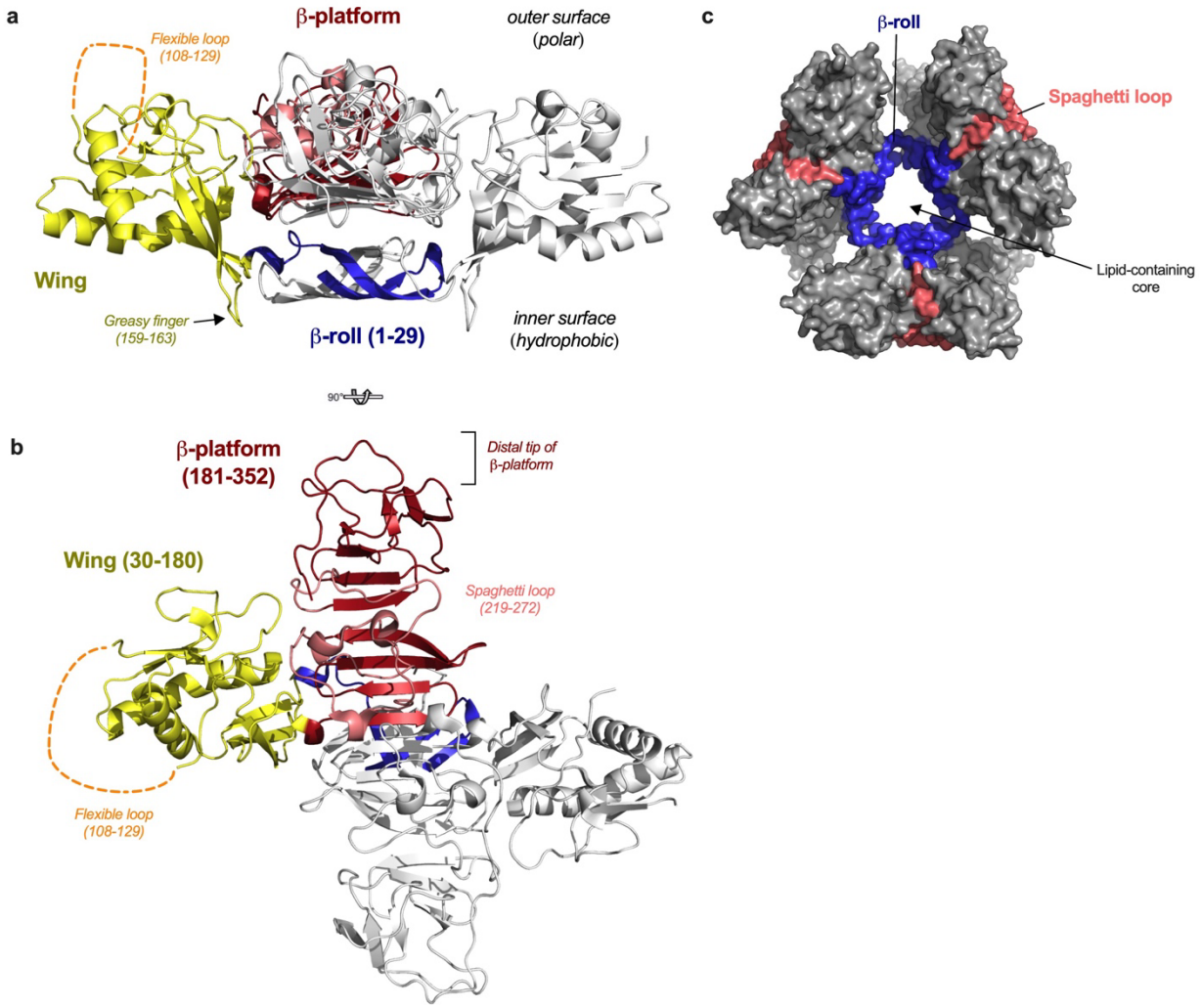

Figure 1.6. Protein structure of dimeric and hexameric NS1. (**a**-**b**) Structure of dimeric WNV NS1 (PDB 4O6D) from side (**a**) and top (**b**) views. In each structure, one monomer is gray and one is color-coded by domain (blue, β-roll; yellow, wing; red, β-platform; and salmon, spaghetti loop). The disordered flexible loop is indicated with orange dashed lines. Amino acid residues corresponding to each particular domain are indicated in parentheses. (**c**) Surface representation of the DENV2 NS1 hexamer (PDB 4O6B). The hexamer core contains the inner hydrophobic surfaces (β-rolls colored in blue). The exposed surfaces include the polar outer surfaces of the wing domains and the spaghetti loops (colored in salmon). Figure generated using PyMOL version 2.0 (Schrödinger, LLC).

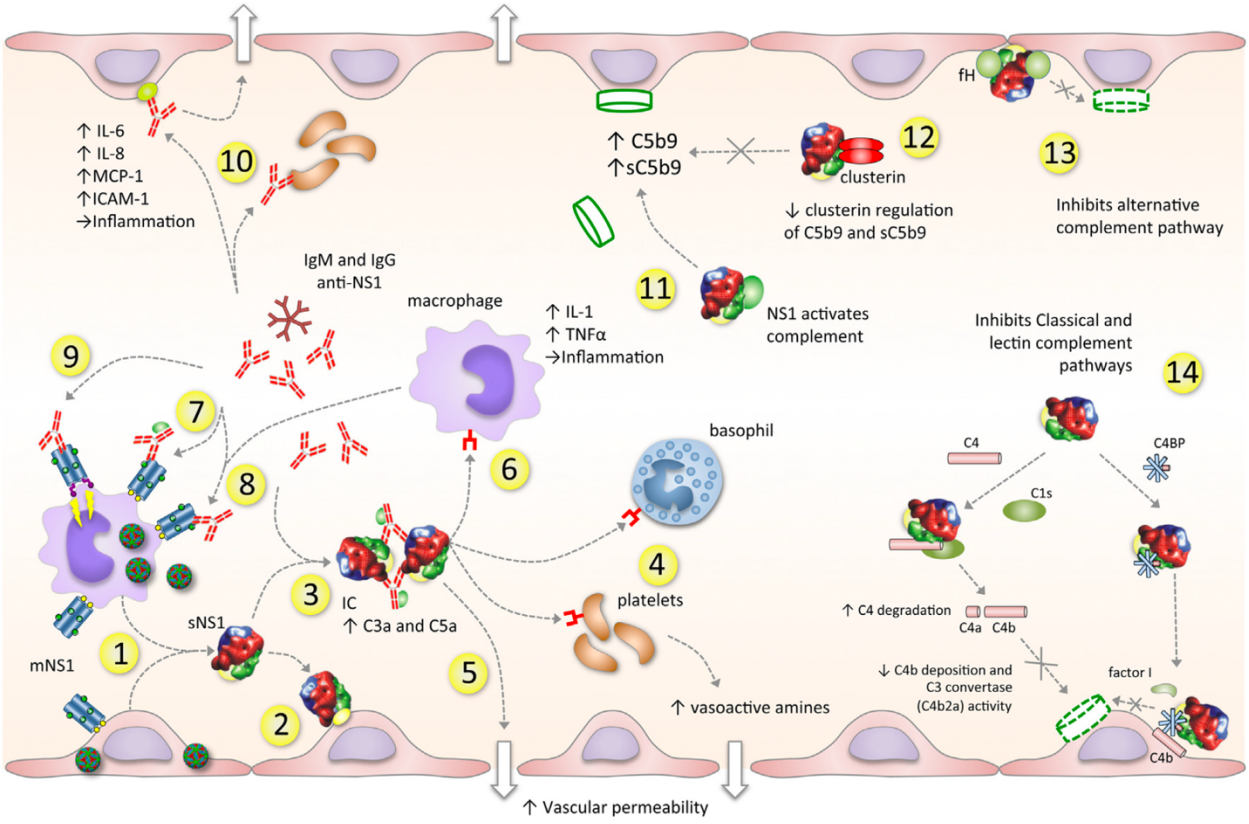

Figure 1.7. Schematic of NS1 interactions with host factors in the vasculature related to immune evasion, activation, and modulation. (**1**) Secreted, soluble NS1 (sNS1) can bind to the surface of endothelial cells via GAGs or possibly other unidentified receptors. (**2**) During acute DENV infection, anti-NS1 antibodies can form immune complexes that (**3**) can activate complement, releasing anaphylatoxins C3a and C5a to mediate inflammation. (**4**) DENV NS1 can activate platelets via TLR4, mediating aggregation and thrombocytopenia. (**5**) NS1-induced inflammation and platelet aggregation potentially contribute to enhanced vascular permeability seen during DENV infection. (**6**) DENV NS1 can bind TLR4 on monocytes, leading to expression of pro-inflammatory and vasoactive cytokines contributing to pathogenesis. Cell surface NS1 (mNS1) expressed on infected cells can engage anti-NS1 antibodies that mediate (**7**) complement-dependent lysis or (**8**) phagocytosis. (**9**) Antibodies binding to NS1 linked to GPI anchors may possibly mediate intracellular signaling. (**10**) Some DENV NS1-specific antibodies are autoreactive with host factors such as platelets and endothelial cells, potentially contributing to inflammation and pathogenesis. (**11**) DENV NS1 can directly activate complement in solution, releasing anaphylatoxin C5a and soluble C5b9 complexes (sC5b9). (**12**) Interaction of DENV NS1 with clusterin leads to increased formation of sC5b9 complexes during infection. (**13**) WNV NS1 binds factor H of the alternative complement pathway to evade immunity. (**14**) At least DENV, YFV, and WNV NS1 interact with components of the classical complement pathway such as C4, recruiting C1s to promote cleavage of C4 to C4b and thus attenuate C4b deposition and C3 convertase activity. NS1 also interacts with C4 binding protein (C4BP), recruiting factor I to inactivate C4b on cell surfaces. Figure adapted from Muller & Young, 2013[210].

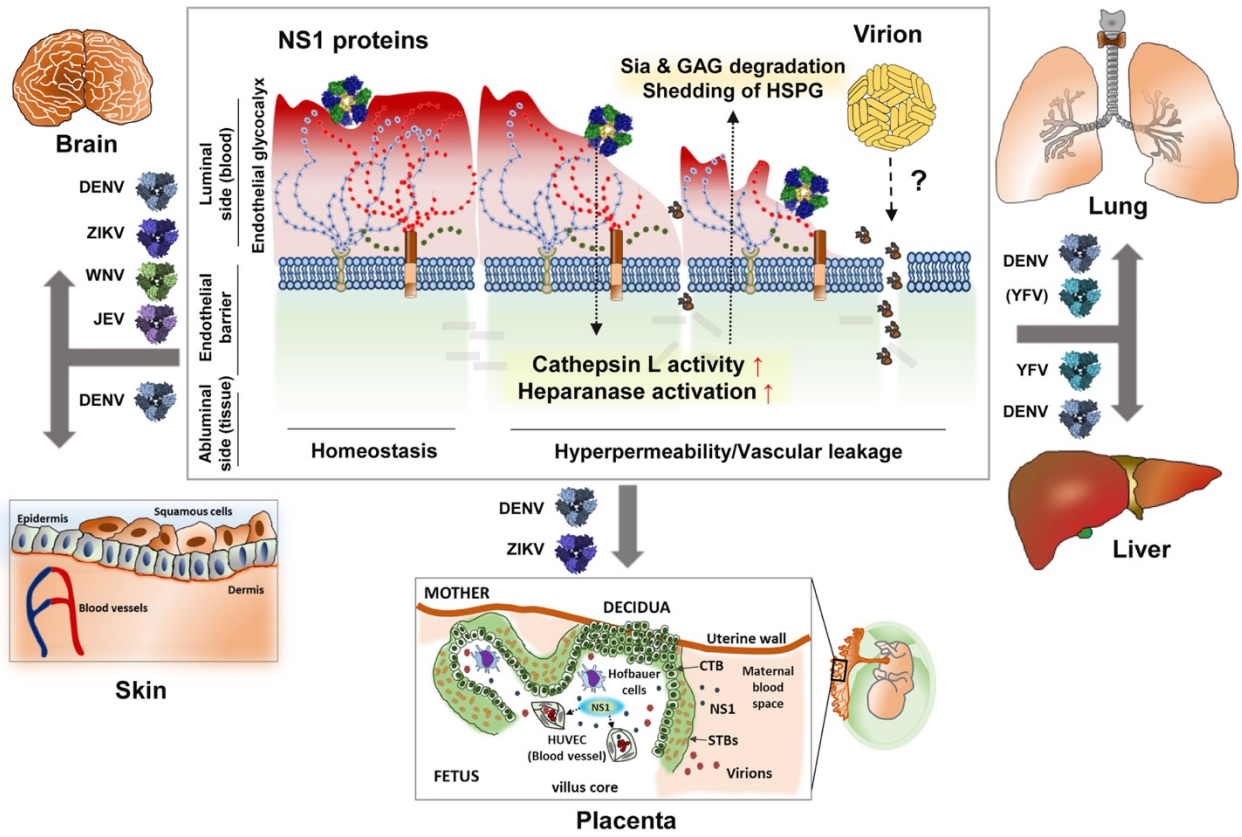

Figure 1.8. Schematic of NS1-mediated endothelial hyperpermeability. Soluble NS1 binds to the surface of endothelial cells via glycosaminoglycans (GAGs) or unidentified receptors. Binding induces the expression and activation of enzymes such as cathepsin L and heparanase, leading to sialic acid (Sia) and GAG degradation and shedding of heparan sulfate proteoglycans (HSPG) such as syndecan-1. This degradation of the endothelial glycocalyx (EGL) is associated with endothelial hyperpermeability. Notably, flaviviruses trigger vascular permeability in a tissue-specific manner that correlates with disease tropism. Possibly, increased permeability across blood-tissue barriers facilitates virion entry into tissues, although this is not known. Figure adapted from Puerta-Guardo *et al.*, 2019[48].

Chapter 2

Antibodies targeting epitopes on the cell-surface form of NS1 protect against Zika virus infection during pregnancy

This chapter is adapted from a manuscript published in *Nature Communications*:

Wessel AW, Kose N, Bombardi RG, Roy V, Chantima W, Mongkolsapaya J, Edeling MA, Nelson CA, Bosch I, Alter G, Screaton GR, Fremont DH, Crowe JE Jr, Diamond MS. (2020) Antibodies targeting epitopes on the cell-surface form of NS1 protect against Zika virus infection during pregnancy. *Nat Commun*. 11(1):5278.

A.W.W. performed all ELISA and flow cytometry studies, antibody sequencing, and infection studies with ZIKV. A.W.W. and M.S.D. generated the murine anti-NS1 mAbs. N.K., R.G.B., W.C., and J.M. generated the human anti-NS1 mAbs. V.R. performed in vitro antibody effector function studies. M.A.E. generated the expression vectors for full-length and DII/III ZIKV NS1, and purified DII/III NS1 protein used in ELISA. I.B. provided murine anti-NS1 mAb 130.99. A.W.W. performed data analysis. C.A.N. aided in structural analysis. G.A., J.E.C., D.H.F., G.R.S., and M.S.D. acquired resources and directed the project. A.W.W. and M.S.D. wrote the initial manuscript draft. All other authors provided editorial comments.

2.1 Summary

There are no licensed therapeutics or vaccines available against Zika virus (ZIKV) to counteract its potential for congenital disease. Furthermore, antibody-based countermeasures targeting the ZIKV envelope protein have been hampered by concerns for cross-reactive responses that induce antibody-dependent enhancement (ADE) of heterologous flavivirus infection. Nonstructural protein 1 (NS1) is a membrane-associated and secreted glycoprotein that functions in flavivirus replication and immune evasion but is absent from the virion. Although some studies suggest that antibodies against ZIKV NS1 are protective, their activity during congenital infection is unknown. Here we develop mouse and human anti-NS1 monoclonal antibodies that protect against ZIKV in both non-pregnant and pregnant mice. Avidity of antibody binding to cell-surface NS1 along with Fc effector functions engagement correlate with protection *in vivo*. Furthermore, protective mAbs map to exposed epitopes in the wing domain and loop face of the β-platform. Anti-NS1 antibodies provide an alternative strategy for protection against congenital ZIKV infection without causing ADE.

2.2 Introduction

Zika virus (ZIKV) is an arthropod-transmitted flavivirus that historically caused sporadic human infections in Africa and Asia after its discovery in 1947 [1]. However, its recent dissemination to Oceania and the Americas drew global attention due to its association with new and severe clinical manifestations [2]. Whereas most ZIKV infections are asymptomatic or present as a mild febrile illness, the epidemic in French Polynesia established a linkage to severe neurological complications including Guillain-Barré syndrome [3-5]. In Brazil and other countries of the Americas, infection during pregnancy caused microcephaly and other congenital malformations [6,7]. Although the epidemic has waned, the potential for re-emergence of ZIKV poses a significant threat to public health. Nonetheless, there are no approved vaccine or therapeutic countermeasures.

ZIKV is related closely to other pathogenic flaviviruses, including the four serotypes of dengue (DENV), West Nile (WNV), Japanese encephalitis (JEV), yellow fever (YFV), and tick-borne encephalitis (TBEV) viruses. Flavivirus NS1 is a highly conserved 48-kDa glycoprotein that dimerizes upon translocation into the endoplasmic reticulum, where it fulfills a scaffolding function in viral RNA replication [8-10]. NS1 also is expressed on the plasma membrane of infected cells as a dimer [11,12] and secreted into the extracellular space as a soluble hexamer [13]. The cell-surface and soluble forms of NS1 modulate host immunity through interaction with complement proteins [14-17] and possibly Toll-like receptors (TLRs) [18,19]. Soluble NS1 accumulates in the serum of flavivirus-infected human subjects [20-22], which reportedly enhances infectivity of virus transmitted to mosquito vectors during a blood meal [23,24]. Soluble NS1 also can bind back to the surface of uninfected or infected cells, and this activity may impact endothelial integrity and permeability at blood-tissue barriers [25-28]. The significance of these findings to pathogenesis, however, remains uncertain [13].

NS1 is comprised of three distinct domains: an N-terminal β-roll domain (residues 1-29), a wing domain (residues 30-180), and a β-platform domain (residues 181-352), which has two faces, one of β-strands and a second largely composed of an extended loop, termed the spaghetti loop (residues 219-272) [29,30]. Following translation in the ER, NS1 dimerizes via intertwining of the β-roll domains from two protomers. The dimer creates a surface for membrane interaction via conserved hydrophobic residues within the β-roll domain and flexible loop (residues 108-129) and 'greasy finger' (residues 159-163) regions of the wing domain [29,31,32]. This hydrophobic surface also facilitates trimerization of dimers into the NS1 hexamer, which contains an inner hydrophobic channel that is rich in lipids [33]. Other regions of the wing and β-platform domains contribute to forming the electrostatic exterior surface of the hexamer and the membrane-distal surface of the dimer.

Monoclonal antibodies (mAbs) against NS1 can confer protection against WNV, JEV, and YFV in animal models [34-36]. Passive transfer of a single NS1-specific human mAb or polyclonal antibodies elicited by an NS1 DNA vaccine protected against lethal ZIKV challenge in *Stat2*$^{-/-}$ mice [37,38]. Although anti-NS1 mAbs have been developed against multiple flaviviruses, few studies have mapped the epitopes involved in protection, and the epitope location or mechanism of action has not been determined for any anti-ZIKV NS1 mAb. Here, we generate murine and human mAbs against ZIKV NS1 and assess their efficacy *in vivo* in immunocompetent human STAT2 knock-in (hSTAT2 KI) mice [39]. Four murine mAbs (Z11, Z15, Z17, and Z18) and three human mAbs (749-A4, ZIKV-231, and ZIKV-292) confer protection against ZIKV in non-pregnant mice by limiting viral infection. A subset of these mAbs also confer protection to the developing fetus following virus inoculation of pregnant mice. Protection *in vivo* by anti-NS1 mAbs correlates with strength and density of binding to NS1 on the cell surface and depends on Fc interactions, as a variant

antibody that cannot engage Fc-γ receptors or complement loses protective activity. Mapping analyses reveals that the protective mAbs bind to one of two epitopes: (i) the exposed hydrophilic surface of the wing domain or (ii) the C-terminal tip of the loop face of the β-platform domain. Our findings suggest that antibodies recognizing epitopes that are accessible on cell-surface forms of NS1 confer protection against ZIKV *in vivo*, including during pregnancy.

2.3 Results

Generation of anti-ZIKV NS1 mAbs. To generate murine mAbs against NS1, we inoculated and boosted BALB/c mice with a mouse-adapted variant of ZIKV Dakar 41525 (Senegal, 1984) [39]. To focus the humoral response on NS1, we also boosted mice two additional times with adjuvanted recombinant full-length ZIKV NS1 protein. We isolated 42 hybridomas that secreted NS1-binding mAbs as determined by ELISA with recombinant NS1 protein and flow cytometry of ZIKV-infected cells (**Table 2.1**). Ten antibodies of the IgG2a subclass were prioritized given prior evidence of the protective activity of anti-WNV NS1 mAbs of this isotype [35]. One IgG2a mAb, Z21, displayed weak binding to ZIKV NS1 and was not studied further.

We separately generated human mAbs against ZIKV NS1 from B cells of subjects who had been infected with ZIKV [40]. We isolated 22 human mAbs that bound to ZIKV NS1 protein by ELISA. Initially, we tested the human mAbs in a stringent, lethal challenge model of ZIKV in immunocompromised mice [41]. Two of the 22 human mAbs, ZIKV-231 and ZIKV-292, conferred some protection against lethality (12 and 40% survival, respectively, compared to 0% of controls) and were prioritized for further testing. One additional human IgG1, 749-A4, was isolated from a DENV-immune subject and was prioritized because it cross-reacted with ZIKV NS1.

We evaluated 10 murine IgG2a and all 23 human IgG mAbs for more extensive cross-reactivity with NS1 proteins of ZIKV, DENV serotype 2 (DENV2), WNV, JEV, TBEV, and YFV

(**Table 2.2**). All of the murine IgG2a and 20 of the 23 human IgG mAbs were ZIKV-specific, whereas human mAbs ZIKV-240 and ZIKV-315 demonstrated weak reactivity with JEV and DENV2, respectively. However, human mAb 749-A4 bound to ZIKV, DENV2, WNV, and JEV NS1, but not TBEV or YFV NS1. In comparison, 9NS1, a previously generated mouse IgG1 mAb against WNV NS1 [35], recognized all six flavivirus NS1 proteins tested.

We performed an ELISA-based binding assay to define competition groups for the 10 murine IgG2a and 3 prioritized human IgG1 mAbs (**Tables 2.2 and 2.3**). The mAbs segregated into five competition groups: group A, Z12, Z13, and Z19; group B, Z11, Z15, Z18, and ZIKV-292; group C, Z17, ZIKV-231, and 749-A4; group D, Z14 and Z16; group E, Z20.

Protection by anti-ZIKV NS1 mAbs in immunocompetent mice. We tested the efficacy of anti-NS1 mAbs against ZIKV in immunocompetent, male and female hSTAT2 KI mice. These animals support infection because ZIKV can antagonize human STAT2 but not mouse Stat2 [39]. The hSTAT2 KI mouse model is more typical of moderate human infection and does not support the severe ZIKV disease seen with immunocompromised mice: 3-week-old infected mice have limited lethality, and fetuses from infected pregnant mice sustain high levels of ZIKV but do not develop microcephaly or fetal demise [7,39,41]. Three- to 4-week-old mice received a single 200 μg dose (~10 mg/kg) of anti-ZIKV NS1 or isotype control mAb via intraperitoneal injection concurrently with subcutaneous inoculation of ZIKV in the foot. Whereas murine mAbs Z12, Z13, Z14, Z16, and Z20 failed to diminish viral burden in the spleen or brain at 9 days post-infection (dpi), Z11, Z15, Z18, and Z17 reduced ZIKV infection in both tissues, with several animals having viral RNA levels below the limit of detection (**Figure 2.1A-B**). Human mAbs 749-A4 and ZIKV-231 conferred similar reductions in viral burden in the spleen and brain, whereas ZIKV-292 protected only in the brain (**Figure 2.1C-D**). No mAb treatment completely protected, as viral RNA

breakthrough was observed in a subset of animals.

Previous studies with some anti-WNV and anti-YFV NS1 mAbs showed that Fc effector functions were required for optimal protection [34,35]. To test for effects on protection against ZIKV, we engineered leucine (L) to alanine (A) substitutions at residues 234 and 235 (LALA) for three of the human mAbs (ZIKV-231, ZIKV-292, and 749-A4) and confirmed diminished binding to FcγRs by direct ELISA (**Figure 2.2A**). When hSTAT2 KI mice were administered the anti-NS1 mAb IgG-LALA variants and inoculated with ZIKV, we observed no protection in the brain compared to the isotype control mAb-treated mice, consistent with a contribution of Fc effector functions (**Figure 2.1D**).

For a subset of the mAbs that protected in hSTAT2 KI mice, we assessed their ability to prevent lethal ZIKV infection using a more stringent immunocompromised mouse model [39,41]. Four- to five-week-old C57BL/6J mice were administered 1 mg of anti-Ifnar1-blocking mAb and 500 μg (~25 mg/kg) of anti-ZIKV NS1 or isotype control mAb via intraperitoneal injection. The following day, mice were inoculated with ZIKV via subcutaneous injection in the foot, and lethality and weights were recorded for 21 days. Of the three murine IgG2a mAbs tested, Z17 significantly protected against ZIKV-mediated lethality and weight loss (**Figure 2.1E-F**). Although Z15 and Z18 conferred partial protection against lethality, these results did not attain statistical significance (Z15, $p = 0.052$; Z18, $p = 0.089$). Of the two human IgG1 mAbs tested in this model, both 749-A4 and ZIKV-292 prevented lethality, but only 749-A4 limited weight loss (**Figure 2.1G-H**).

Antibody protection in pregnant mice. We tested whether anti-NS1 mAbs could protect against ZIKV during pregnancy. We used hSTAT2 KI mice, in which ZIKV infection during pregnancy results in transmission to the fetal brain without fetal demise [39]. For the murine mAbs, we focused

efforts on testing Z15 (group B) and Z17 (group C), given their protection in young hSTAT2 KI mice and distinct competition groups (**Figure 2.3A-C**). We tested two human mAbs: ZIKV-292 from competition group B and 749-A4 from group C (Fig 2d-f). After mating adult male and female hSTAT2 KI mice, at embryo day (E)6.5, females were inoculated subcutaneously with ZIKV and concurrently administered 250 μg of anti-NS1 or isotype control mAb via intraperitoneal injection. Pregnant dams were euthanized on E13.5, and viral RNA levels were measured in the maternal spleen, the fetal-derived placenta, and fetal head. Despite conferring protection in non-pregnant, young hSTAT2 KI mice, murine mAb Z15 did not reduce viral burden in maternal or fetal tissues (**Figure 2.3A-C**). Administration of mAb Z17, however, markedly reduced ZIKV infection in the placenta and fetal head (**Figure 2.3B-C**). To determine whether a combination of mAbs from different competition groups could enhance protection during pregnancy, we administered pregnant mice a cocktail of Z15 (125 μg) and Z17 (125 μg) mAbs. Treatment with the mAb cocktail trended toward greater reduction in ZIKV titers in the placenta and fetal head compared to treatment with Z17 alone (51% versus 21% of samples at the limit of detection in the fetal head), although this difference did not attain statistical significance.

Treatment of pregnant dams with human mAb ZIKV-292 (group B) also reduced viral burden in the placenta and fetal head (**Figure 2.3D-F**). Group C mAb 749-A4 conferred a small yet statistically significant reduction of virus in these tissues as well. Notably, the protective effect of 749-A4 was lost when an IgG-LALA variant was used, which suggests a role for Fc effector functions in anti-NS1 antibody-mediated protection during pregnancy.

Avidity for cell surface NS1 correlates with protection. Given the Fc effector function-dependence of protection of some of our mAbs, we hypothesized that protective anti-ZIKV NS1 mAbs would recognize cell-surface forms of NS1 to enable antibody-dependent immune cell

clearance of virus-infected cells. We evaluated this idea using a flow cytometric assay with intact, ZIKV-infected cells. Murine mAbs Z11, Z15, and Z18, which protected against ZIKV in non-pregnant hSTAT2 KI mice, bound avidly to the surface of infected cells (half maximal effective concentration (EC_{50}): Z11, 2.2 ng/mL; Z15, 1.5 ng/mL; Z18, 1.5 ng/mL; **Figure 2.4A-B**, **Table 2.2**). Murine mAb Z17, which also protected *in vivo*, bound slightly less avidly than Z15 and Z18 (EC_{50} of 18.4 ng/mL) but greater than non-protective murine mAbs Z12, Z13, and Z19 (EC_{50}: Z12, 29.2 ng/mL; Z13, 105.7 ng/mL; Z19, 66.2 ng/mL). Since Fc effector function-dependent protection likely requires antibody cross-linking to low affinity Fc-γ receptors, which depends on both the strength of mAb binding to target antigens and the number of sites bound [42-46], we examined the density of mAb binding to the cell surface using the mean fluorescence intensity (MFI). Antibody binding density was substantially lower for the non-protective mAbs compared to the protective mAbs Z11, Z15, Z18, and Z17 (**Figure 2.4C**). The non-protective murine mAbs had reduced avidity and density of binding (Z14), or did not show binding to NS1 on the surface of infected cells (Z16 and Z20). The human mAbs ZIKV-231, ZIKV-292, and 749-A4 bound to NS1 on the cell surface NS1 to a similar extent as mAb Z17 (EC_{50} of 3.9, 3.4, and 14.6 ng/mL, respectively; **Figure 2.4E-F**). Despite their differential binding patterns to NS1 on the cell surface, all murine and human mAbs except for Z19 and Z21 bound strongly to solid-phase, hexameric ZIKV NS1 in an ELISA (**Figure 2.4D** and **G**).

Effector functions of anti-NS1 mAbs. To begin to understand potential Fc effector mechanisms of protection, we assessed the activity of a subset of our anti-ZIKV NS1 mAbs using *in vitro* effector function assays. To assess antibody-dependent complement deposition, we coupled beads to recombinant ZIKV NS1, added anti-NS1 mAbs, and measured complement (C3b) deposition. Among the anti-NS1 mAbs tested, Z17, ZIKV-292, and 749-A4 promoted complement (C3b)

deposition (**Figure 2.2B**). All of the mAbs tested also promoted internalization of NS1 antigen-coated beads by neutrophils or monocytes (**Figure 2.2C-D**).

Protective mAbs bind to distinct epitopes in NS1. To begin to understand the basis for differential recognition of cell surface NS1 and protection *in vivo*, we mapped the epitopes of the anti-ZIKV NS1 mAbs. We localized NS1 binding sites critical for mAb recognition using (i) alanine-scanning mutagenesis and (ii) structure-guided charge-reversal mutagenesis [47].

'Shotgun mutagenesis' [47] was performed by substituting each residue of NS1 with alanine. Pre-existing alanine residues were substituted with serine, and the invariant cysteine residues were not changed given their requirement in NS1 folding [31]. We assessed binding of anti-ZIKV NS1 mAbs to each mutant NS1 protein using a flow cytometric assay that compared staining of wild-type and mutant plasmid-transfected cells. Residues were deemed critical for mAb binding if a substitution resulted in less than 25% binding relative to that of WT NS1 but did not affect recognition by an oligoclonal pool of nine anti-NS1 mAbs. After evaluating the library of 340 mutants, we found that alanine substitution at three residues (R40, N82, and W115) within or structurally proximal to the wing domain flexible loop (residues 108-129) caused loss-of-binding of the non-protective group A mAbs, Z12 and Z13 (**Figure 2.5A**). Sequencing of the variable heavy and light chain regions revealed these two mAbs are related clonally, consistent with their shared binding patterns (**Table 2.4**). The group A mAb Z19 also showed loss-of-binding with alanine substitutions at residues R40, N82, and W115, and mutation at residue R40 resulted in diminished binding of the non-protective group E mAb Z20. The protective group C mAbs mapped to residues on the exposed loop face of the β-platform domain (residues 181-352) (**Figure 2.5B**). Human mAb ZIKV-231 mapped to residue K265 within the spaghetti loop (residues 219-272) and to residue R314 at the C-terminal tip of the β-platform domain (278-352), whereas Z17 and 749-

A4 mapped to residues exclusively at the C-terminal tip of the β-platform (*e.g.*, E289 and R338). For unclear reasons, we were unable to map the epitopes of the protective group B and non-protective group D mAbs using this approach.

A previous study identified immunodominant B cell epitopes in DENV NS1 for mice and humans [48]. Using these epitope regions as guides, we engineered charge-reversal mutants (**Table 2.5**) at solvent-exposed and adjacent residues predicted by the ZIKV NS1 atomic model [31]. We examined binding to these mutants as an alternative approach for mapping the anti-ZIKV NS1 mAbs in competition groups B (Z11, Z15, Z18, and ZIKV-292) and D (Z14). The protective group B murine mAbs mapped to residues clustered on the membrane-distal, charged surface of the wing domain: Z15: K146; Z11 and Z18: Q102; and ZIKV-292: P101 and L177/E178 (**Figure 2.5C**). The non-protective group D mAb, Z14, mapped to two residues (G305 and V307) on the membrane-facing surface of the β-platform domain (**Figure 2.5D**). This approach also identified key residues for binding of group C mAbs: Z17: T290; ZIKV-231: T293 (**Figure 2.5D** and **Table 2.5**).

Mutated residues that resulted in loss of Ab binding were mapped onto the ZIKV NS1 crystal (**Figure 2.5E**, top view; **Figure 2.5F**, side view) and secondary structures (**Figure 2.5G**). The mAb competition groups localize to distinct epitopes. The non-protective mAbs (groups A, D, and E) map to the membrane-facing surface of the dimer including the wing flexible loop and β-strand face of the β-platform. The protective mAbs (groups B and C) map to the membrane-distal, accessible surface of the dimer including the charged surface of the wing domain and the loop face of the β-platform.

2.4 Discussion

We examined the protective efficacy of newly generated mAbs targeting ZIKV NS1 *in*

vivo. We identified four murine (Z11, Z15, Z18, and Z17) and three human mAbs (ZIKV-292, ZIKV-231, and 749-A4) that conferred protection against ZIKV in non-pregnant hSTAT2 KI mice, whereas five other murine mAbs (Z12, Z13, Z14, Z16, and Z20) did not show this activity. Three of the mAbs tested (Z17, ZIKV-292, and 749-A4) also protected against lethal ZIKV challenge in immunocompromised mice and reduced viral infection the fetuses of pregnant mice. Whereas all mAbs recognize the soluble NS1 hexamer relatively equivalently, the protective and non-protective groups of antibodies differentially bind to cell-surface NS1, which is believed to be expressed as a dimer [29,49,50]. The protective mAbs bind avidly and at high site density to cell-surface NS1 and map to two accessible regions on the membrane-distal surface of the dimer: the wing domain and the loop face of the β-platform. In contrast, the non-protective mAbs bind relatively poorly to cell-surface NS1 and map to less accessible epitopes near the hydrophobic, membrane-facing surface of the NS1 dimer.

A prior study suggested that protection against lethal WNV infection by anti-NS1 mAbs correlated with recognition of NS1 on the surface of infected cells [51]. Our data suggest that avid and high-density binding to cell-surface NS1 is a determinant of protection for anti-NS1 antibodies. Structural studies suggest that dimeric NS1 interacts with the cell membrane through the hydrophobic beta-roll domain, the flexible loop, and greasy finger of the wing domain [29,31]. These regions on the cell-surface form of NS1 may be relatively inaccessible for antibody binding, which could explain why group A mAbs (Z12 and Z13; flexible loop) bound poorly and do not protect. The membrane-distal surfaces of the dimer, which should be accessible on cell-surface forms of NS1, include the charged surface of the wing domain and the loop face of the β-platform domain. These regions are recognized efficiently by group B (wing) and C (loop-face) mAbs, which protect against ZIKV infection *in vivo*.

The protective group C mAbs (Z17, ZIKV-231, and 749-A4) map to residues within the C-terminal region of the β-platform, which contains conserved sequences in flaviviruses. One epitope within the β-platform of NS1 has been described structurally. The WNV NS1-specific mAb, 22NS1, which protects against WNV challenge, contacts residues within an elongated loop that connects the fourth and fifth β-strand of the β-platform (spaghetti loop) as well C-terminal tip residues (**Figure 2.5G**) [30]. Two of our group C mAbs bind epitopes that share contact residues with 22NS1. ZIKV-231 maps to two C-terminal tip residues, which are structurally equivalent to 22NS1 epitope contacts (T293 and R314), and the third ZIKV-231 residue we identified (K265) is located within the spaghetti loop proximal to the 22NS1 epitope. We also identified two C-terminal tip epitope residues for the broadly NS1 reactive 749-A4 mAb (E289 and R314), and both of these are conserved in WNV and contacted by 22NS1. Murine mAb 9NS1, which was isolated against WNV [35], cross-reacts with all tested flavivirus NS1 proteins and also maps to conserved residues at the C-terminal tip. Thus, it is possible that other mAbs binding this C-terminal epitope could provide cross-protection against other flaviviruses, although this warrants further examination. Whereas we observed a protective effect against ZIKV following passive administration of group C mAbs, some anti-DENV NS1 antibodies that bind C-terminal epitopes (particularly residues 305-330) reportedly react with human endothelial cells, platelets, and plasminogen and are speculated to contribute to pathogenesis [52-54].

The wing domain, particularly within residues 101-130, contains immunodominant B-cell epitopes for DENV NS1 in mice and humans [48]. The group A (Z12, Z13, and Z19), group B (Z11, Z15, Z18, and ZIKV-292), and group E (Z20) mAbs map to these residues, although to distinct regions. The protective group B mAbs map to the membrane-distal, hydrophilic surface of the wing domain, whereas the non-protective group A mAbs map to the hydrophobic flexible loop

(W115) of the wing domain. A previously generated murine mAb against WNV NS1, 16NS1, also maps to residues (W118 and I122) within the flexible loop [36]. The flexible loop (residues 108-129) was disordered in the WNV and DENV NS1 crystal structures but stabilized in the ZIKV NS1 structure [31,32]. This region is believed to facilitate membrane association with the distal end of the wing domain via conserved hydrophobic residues. MAb 16NS1 protected mice against lethal WNV challenge [35], whereas Z12 and Z13 failed to inhibit ZIKV infection. Although further studies with a larger panel of mAbs that map to this particular epitope are warranted, we speculate that the flexible wing domain hydrophobic loops of ZIKV and WNV NS1 may interact differently with membranes, thereby modulating their unique antibody epitope accessibilities. Moreover, structural studies that achieve atomic-level resolution of mAb bound to NS1 may help to identify further how protective and non-protective mAbs engage NS1.

We evaluated a combination of two mouse mAbs (Z15 and Z17) during pregnancy to determine whether concurrent targeting of more than one epitope could enhance protection, as there is precedence for this approach in antiviral antibody therapies [55-57]. This combination trended toward reducing viral infection in fetal heads, although it did not attain statistical significance. We evaluated a second combination of human antibodies that bound distinct epitopes (ZIKV-292 and 749-A4) during pregnancy as well, but did not observe greater protection. In the future, additional two- or even three-antibody combinations could be tried in this model.

Passive transfer of NS1-specific mAbs can protect mice from lethal challenge with WNV, JEV, or YFV [34-36]. The mechanism of protection for many of the anti-WNV NS1 mAbs was Fc-dependent, as it was lost in mice lacking Fc-γ receptors or C1q [35]. Analogously, an anti-YFV NS1 antibody mediated antiviral protection in mice when using IgG2a, but not IgG1 isotype switch variants or cleaved $F(ab')_2$ fragments [34]. More recently, passive transfer of a single human anti-

ZIKV NS1 mAb (AA12) protected *Stat2*$^{-/-}$ mice against lethal challenge with ZIKV [37,38], although epitope mapping data was not provided. Similar to our data, protection was Fc-dependent, as determined with loss-of-function mutations in the Fc region [58]. To test Fc-dependent protection by the human mAbs, we generated Fc region LALA variants, which have reduced binding to Fc-γ receptors and complement. Although we observed loss of protection in the hSTAT2 KI mice using the Fc region LALA variants, the effect might be greater with LALA-PG or other mutations that more completely eliminate binding to Fc receptors and complement [58]. Given that ZIKV-infected cells express high levels of NS1 on the plasma membrane, NS1-specific antibodies that bind avidly and with high site density may promote clearance of infected cells via cross-linking and promoting Fc-mediated effector functions. The specific effector functions of a mAb might explain differences we observed in protection between non-pregnant and pregnant mice. Mouse mAb Z17 protects in both mouse models, whereas Z15 protects only in non-pregnant mice. Given that Z17 induces more complement deposition than Z15 in Fc effector function assays, complement-dependent cytolysis or opsonization might contribute to antibody-mediated protection of the fetus against ZIKV. Indeed, human mAbs ZIKV-292 and 749-A4, which protected in pregnancy, also promoted complement deposition. We cannot exclude the possibility that antibodies also may protect by targeting the secreted form of NS1 and blocking its potential effects on immune evasion and pathogenesis [13,18,19,26-28]. Indeed, soluble ZIKV NS1 protein may promote placental dysfunction and permeability through modulation of glycosaminoglycan expression on chorionic villi [28].

Most antibody-based therapeutic or vaccine strategies against ZIKV have focused on generating neutralizing antibodies against the viral envelope protein, which indeed protect in different animal models [40,59,60]. However, pre-existing anti-envelope protein antibodies reportedly can augment both ZIKV and DENV infection, a phenomenon termed ADE [61,62]. NS1-targeted

vaccines have been developed as an alternative to envelope protein-targeted strategies to avoid ADE because NS1 is absent from the virion. Indeed, NS1-based vaccines can protect mice against lethal YFV, TBEV, and ZIKV infections [63-67]. Whether any of these vaccine candidates can protect the developing fetus from ZIKV, however, remains to be tested. Given that several anti-NS1 mAbs that limited ZIKV infection in the placenta and fetus, NS1-targeted vaccines or antibody-based therapies might confer protection during pregnancy, without the risk of immune enhancement of homologous or heterologous flavivirus infection.

In summary, we defined a panel of anti-NS1 mAbs that limit ZIKV infection in non-pregnant and pregnant mice and established functional correlates of protection: binding to cell surface forms of NS1 and engagement of Fc receptors by mAbs. One limitation of this study is that it does not assess protection in a model of ZIKV-induced fetal demise. To achieve such extensive disease in mice requires the use of highly immunocompromised animals where ZIKV disseminates widely and replicates to high titer [39,68]. Anti-NS1 mAbs could be developed alone or in combination with anti-envelope protein antibodies (the latter possibly engineered to lack Fc interactions to avoid ADE) for prevention against ZIKV infection and congenital disease. Our studies suggest that NS1-specific antibodies recognizing antigenic sites in the charged surface of the wing domain and C-terminal end of the β-platform domain loop face optimally mediate protection *in vivo* because they are accessible in the cell-surface associated form of dimeric NS1. Vaccines targeting these epitopes may induce the most protective NS1-specific antibodies. Future studies that elucidate the atomic structures of protective mAbs bound to NS1 may refine antigen engineering strategies for rational NS1 vaccine design.

2.5 Methods

Ethics statement. All animal procedures were carried out in accordance with the

recommendations in the Guide for the Care and Use of Laboratory Animals of the National Institutes of Health. The protocols were approved by the Institutional Animal Care and Use Committee at the Washington University School of Medicine (assurance no. A3381-01). To minimize animal discomfort and suffering, injections were performed under anesthesia that was induced and maintained with ketamine hydrochloride and xylazine. All human anti-ZIKV mAbs except for 749-A4 were isolated from the blood of subject 973 [40,69], who had a history of ZIKV (African lineage strain) infection. Blood samples were collected by the Vanderbilt Clinical Trials Center following written informed consent using a protocol approved by the Vanderbilt University Medical Center Institutional Review Board. Human mAb 749-A4 was isolated after written informed consent from blood collected from an inpatient who tested positive for DENV by RT-PCR at the Hospital for Tropical Diseases [70]. The study protocol was approved by the Scientific and Ethical Committee of the Hospital for Tropical Diseases, the Oxford Tropical Research Ethical Committee, and the Riverside Ethics Committee in the United Kingdom.

Cells. Vero, HEK-293T, and C6/36 cells (all from American Type Culture Collection) were propagated in Dulbecco's modified Eagle Medium (DMEM) supplemented with 10% fetal bovine serum (FBS), 1 mM sodium pyruvate, and 10 mM HEPES, pH 7.3. Hybridoma cells were grown in Isocove's modified Eagle Medium supplemented with 20% FBS (Hyclone), 1 mM sodium pyruvate, and 100 U/mL of penicillin and streptomycin.

Viruses. The mouse-adapted variant of ZIKV strain Dakar 41525 (Senegal, 1984) has been described [39]. Virus stocks were propagated in C6/36 or Vero cells and titered by focus-forming assay [71].

Purification of NS1 domain (D)II/III protein. A ZIKV NS1 C-terminal construct was engineered, expressed, and purified essentially as described for WNV and DENV NS1 [30].

Briefly, residues 966-1148 of the ZIKV strain H/PF/2013 polyprotein (residues 172-352 of ZIKV NS1) was cloned into the NheI and NotI restriction sites of pET21a for expression in BL21 (DE3) codon plus *E.coli* cells by autoinduction [72]. Inclusion bodies (200 to 300 mg) were denatured in 7 M guanidinium hydrochloride and 30 mM β-mercapthanol for 1 h at 37°C, centrifuged for 10 min at 4°C, and diluted to 2 M guanidinium hydrocloride in 50 mM sodium acetate pH 5.2. The supernatant was filtered and refolded by rapid, serial dilution (1 mL injections, hourly) in 1 L of refolding buffer (400 mM L-arginine, 100 mM Tris-base pH 8.3, 2 mM EDTA, 0.5 mM oxidized glutathione, 5 mM reduced glutathione, and 0.2 mM phenylmethanesulfonyl fluoride) at 4°C. The recombinant protein was concentrated using a stirred cell concentrator with YM10 membrane (Millipore), centrifuged to remove aggregates, and purified on a S-75 size exclusion chromatography column equilibrated in 20 mM HEPES pH 7.4, 150 mM NaCl, and 0.01% NaN_3.

Antibody generation. (**i**) **Mouse mAbs:** Six-week-old female BALB/c mice were primed and boosted 3 weeks later with 10^6 focus forming units (FFU) of ZIKV following administration of 1 mg of an Ifnar1-blocking mAb (clone MAR1-5A3; Leinco I-401) [73]. At 6 weeks after initial infection, mice were boosted with 25 μg of recombinant ZIKV NS1 protein (Native Antigen) mixed 1:1 with Freund's Incomplete Adjuvant. Mice were given a final pre-fusion boost with 25 μg of ZIKV NS1 protein in PBS at 10 weeks after initial infection. Three days later, splenocytes were harvested and fused with P3X63 Ag8.653 myeloma cells to generate hybridomas [74]. Supernatants were screened for antibody binding to ZIKV-infected cells by flow cytometry or to recombinant ZIKV NS1 protein by ELISA. Briefly, ZIKV-infected C6/36 cells (MOI of 0.1, 3 dpi) were fixed with 4% paraformaldehyde (PFA), permeabilized in PBS, 0.1% saponin, 0.1% bovine serum albumin (BSA), and then incubated with hybridoma culture supernatants supplemented with 0.1% saponin. Anti-NS1 mAbs were detected using Alexa Fluor 647-conjugated goat anti-mouse

IgG (1:2000 dilution; Thermo Fisher). For screening by direct ELISA, recombinant ZIKV NS1 (0.4 μg/ml; Native Antigen) was immobilized onto MaxiSorp 96-well plates (Thermo Fisher) overnight at 4°C in 50 μl of sodium bicarbonate buffer, pH 9.3. Subsequently, plates were washed four times with PBS and blocked with ELISA buffer (PBS, 1% BSA, and 0.05% Tween 20) for 1 h at 37°C. Plates then were incubated with undiluted hybridoma culture supernatants for 1 h at room temperature. After washing four times with ELISA buffer, plates were incubated with biotinylated anti-mouse IgG (H + L; 1:2000 dilution; Jackson ImmunoResearch) for 30 min. Plates were washed again and incubated with streptavidin-conjugated horseradish peroxidase (1:625 dilution; Vector Laboratories) for 30 min. After a final wash series, plates were developed using 3,3',5,5'-tetramethylbenzidine substrate (Agilent). The reaction was stopped using 2 N H_2SO_4 and absorbance at 450 nm was read with a TriStar Microplate Reader (Berthold Technologies) to detect anti-NS1 antibodies. Positive hybridomas were cloned by limiting dilution, and selected mAbs were purified by a commercial source (Bio X Cell). (**ii**) **Human mAbs:** Human mAbs were generated two ways: (a) MAbs ZIKV-231 and ZIKV-292: The ZIKV-immune human donors were described previously [40,69]. Peripheral blood mononuclear cells (PBMCs) from heparinized blood were isolated using Ficoll-Histopaque and density gradient centrifugation. Ten million PBMCs were cultured in 384-well plates (Nunc) using culture medium (ClonaCell-HY medium A; StemCell Technologies) supplemented with 8 μg/mL of the Toll-like receptor (TLR) agonist CpG (phosphorothioate-modified oligodeoxynucleotide ZOEZOEZZZZZOEEZOEZZZT; Invitrogen), 3 μg/mL of Chk2 inhibitor (Sigma), 1 μg/mL of cyclosporine (Sigma), and clarified supernatants from cultures of B95.8 cells (ATCC) containing Epstein-Barr virus. After 7 days, cells from each 384-well culture plate were expanded into four 96-well culture plates (Falcon) using ClonaCell-HY medium A containing 8 μg/mL of CpG, 3 μg/mL of Chk2 inhibitor, and 10^7 irradiated

heterologous human PBMCs (Nashville Red Cross) and cultured for an additional 4 days. Supernatants were screened by ELISA for reactivity with ZIKV NS1. Hybridoma cell lines were cloned by single-cell flow cytometric sorting in a sterile FACSAria III cytometer (BD Biosciences). (b) MAb 749-A4: 749-A4 was generated from plasmablasts during acute DENV infection [70,75]. PBMCs were stained with anti-CD3 (1:20; BD Pharmingen 345766), anti-CD19 (1:50; Dako R0808), anti-CD20 (1:20; BD Pharmingen 345794), anti-CD27 (1:20; BD Pharmingen 555440), and anti-CD38 (1:20; BD Pharmingen 555462), and plasmablasts were single-cell sorted into 96-well plates containing RNase inhibitor (Promega) by gating on $CD19^{+}$, $CD3^{-}$, $CD20^{lo}$ to $CD20^{-}$, $CD27^{hi}$, and $CD38^{hi}$. RT-PCR (Qiagen). Nested PCR (Qiagen) was performed to amplify genes encoding γ-chain, λ-chain, and κ-chain with 'cocktails' of primers specific for human IgG[75]. PCR products encoding heavy and light chain genes were digested with the appropriate restriction endonuclease(s) and cloned into expression vectors for human IgG1 or Ig κ-chain or λ-chain (gift from H. Wardemann)[76]. For the expression of antibodies, plasmids encoding heavy and light chains were co-transfected into 293T cells using the polyethylenimine method [77].

Mouse experiments. Antibody protection studies were performed using hSTAT2 KI mice [39]. For non-pregnancy studies, 3- to 4-week-old male and female hSTAT2 KI mice were administered 200 μg of mAb (anti-NS1 or isotype control mAb) via intraperitoneal injection and then immediately inoculated subcutaneously in the footpad with 10^5 FFU of ZIKV in a 50 μL volume. Serum samples were obtained at 3 dpi via facial vein puncture, and tissues were harvested at 9 dpi following perfusion with 20 mL of PBS. For pregnancy studies, 8- to 16-week-old female hSTAT2 KI mice were paired with male hSTAT2 KI mice and checked each morning for a copulation plug; this day was defined as E0.5. On E6.5, plugged mice were administered 250 μg of mAb (anti-NS1

or isotype control mAb) via intraperitoneal injection and then immediately inoculated subcutaneously in the footpad with 10^6 FFU of ZIKV in a 50 µL volume. Mice were sacrificed on E13.5, and the maternal spleen, placentas, and fetal heads were collected. For antibody cocktail treatments, mice received 125 µg of each antibody.

To assess antibody-mediated protection against lethal ZIKV infection, four- to five-week-old C57BL/6J mice were administered 1 mg of anti-Ifnar1 blocking mAb (MAR1-5A3) and 500 µg of anti-NS1 or isotype control mAb via intraperitoneal injection [39]. The following day, mice were inoculated subcutaneously in the footpad with 10^3 FFU of ZIKV in a 50 µL volume. Lethality and weights were tracked for 21 days, at which point surviving mice were euthanized.

Viral burden analysis. Organs were weighed and homogenized by bead dissociation using a MagNA Lyzer (Roche) in a volume of DMEM containing 2% FBS. Viral RNA was isolated from tissue homogenates using the RNeasy Mini kit (Qiagen), per the manufacturer's instructions. ZIKV RNA levels were determined by TaqMan one-step quantitative reverse transcriptase PCR (qRT-PCR; Forward primer: TTCGGACAGCCGTTGTCCAACACAAG; Reverse primer: CCACCAATGTTCTCTTGCAGACATATTG; Probe: 56-FAM/AGCCTACCT/ZEN/TGACAAGCAGTC/3IABkFQ) [39]. To calculate FFU equivalents from RNA levels, an RNA standard curve was generated from a defined viral stock.

Antibody domain mapping and cross-reactivity analysis. Recombinant NS1 proteins (0.4 µg/mL) were immobilized onto MaxiSorp 96-well plates (Thermo Fisher) overnight in 50 µL of sodium bicarbonate buffer, pH 9.3. For mAb domain mapping, full-length ZIKV NS1 (residues 1-352) or ZIKV NS1 DII/III (residues 172-352) [35] was immobilized. For determination of cross-reactivity, ZIKV, DENV2, WNV, JEV, TBEV, or YFV NS1 proteins (all from Native Antigen) were adsorbed to wells of MaxiSorp microtiter plates overnight at 4°C. Subsequently, plates were

washed four times with PBS and blocked with ELISA buffer (PBS, 1% BSA, and 0.05% Tween 20) for 1 h at 37°C. Plates then were incubated with anti-NS1 or isotype control mAbs diluted in ELISA buffer for 1 h at room temperature. After washing four times with ELISA buffer, plates were incubated with biotinylated goat anti-human or goat anti-mouse IgG (H + L; 1:2000 dilution; Jackson ImmunoResearch) for 30 min. Plates were washed again and incubated with streptavidin-conjugated horseradish peroxidase (1:625 dilution; Vector Laboratories) for 30 min. After a final wash series, plates were developed using 3,3□,5,5□-tetramethylbenzidine substrate (Agilent). The reaction was stopped using 2 N H_2SO_4 and absorbance at 450 nm was read with a TriStar Microplate Reader (Berthold Technologies).

Antibody binding to NS1 on the cell surface. Vero cells were inoculated with ZIKV at an MOI of 1. After 24 h, the cells were washed in PBS, detached after incubation in 10 mM EDTA in PBS for 15 min at 37°C, and then washed again in chilled PBS, 4 mM EDTA, 0.4% BSA (FACS buffer). The cells then were incubated with serial dilutions (20 μg/mL to 2 pg/mL) of each anti-NS1 or an isotype control mAb for 1 h at 4°C. After washing in FACS buffer, cells were stained with Fixable Viability Dye eFluor 506 (eBioscience) and Alexa Fluor 647 conjugated to goat anti-human or anti-mouse IgG (Thermo Fisher). Cells were washed before fixing in 4% PFA in PBS for 10 min, and then processed on a MACSQuant Analyzer (Miltenyi Biotec) using FlowJo software. After gating on live cells, the percent reactivity to cell surface-expressed NS1 was determined and plotted for each dilution of mAb. The EC_{50} of binding value was calculated using a 4-parameter logistic curve.

Antibody competition ELISA. Anti-NS1 mAbs were conjugated to biotin using a sulfo-NHS-biotin kit (Thermo Scientific). MaxiSorp 96-well plates were coated with ZIKV NS1 protein, washed, and blocked as described above. Plates then were incubated with unmodified anti-NS1

mAbs at 10 μg/mL for 1 h at room temperature. Without washing, biotinylated mAbs were added to the plates at pre-optimized concentrations and incubated for 10 min at room temperature. Plates then were washed four times in PBS, 0.05% Tween 20, and incubated with streptavidin-conjugated horseradish peroxidase (1:625 dilution) for 30 min. After washing, plates were developed and absorbance was read as described above.

FcγR I ELISA. MaxiSorp 96-well plates were coated overnight with 50 μL of recombinant human FcγR I (CD64) protein (1 μg/mL; R&D Systems), washed, and blocked as described above. Serial dilutions of the anti-NS1 human antibodies (WT and LALA variants) in ELISA buffer were added to the plates and incubated for 1 h at room temperature. Subsequently, plates were washed four times and incubated with biotin-conjugated goat anti-human IgG (H + L; 1:2,000 dilution; Thermo Fisher) for 45 min. Plates then were washed and incubated with streptavidin-conjugated horseradish peroxidase (1:625 dilution) for 30 min. After a final wash series, plates were developed and absorbance was read as described above.

Alanine-scanning mutagenesis and epitope mapping. Epitope mapping was performed using alanine-scanning mutagenesis [47]. A mammalian expression vector (pFM-A1.2) was constructed to encode full-length ZIKV NS1 (strain H/PF/2013), preceded by the native signal sequence (last 25 amino acids of envelope protein) and followed in frame with a hexahistidine affinity tag. The pFM-A1.2 expression vector was subjected to site-directed mutagenesis (GENEWIZ) to generate a library of 340 total mutants. Non-alanine codons were mutated to alanine, alanine codons were mutated to serine, and cysteine codons were not changed. HEK293T cells were transfected with each mutant construct by using Lipofectamine 3000 (Thermo Fisher) and incubated at 37°C for 1 day to allow for protein expression. Cells were fixed, permeabilized, and incubated with individual mAbs or an oligoclonal cocktail of anti-NS1 mAbs (Z2, Z4, Z11, Z12, Z14, Z15, Z17, Z18, 130.99)

as a control for NS1 protein expression. Anti-NS1 mAb binding was detected using Alexa Fluor 647 conjugated to goat anti-human or goat anti-mouse IgG (1:2,000 dilution; Thermo Fisher). Flow cytometry was performed on a MACSQuant Analyzer (Miltenyi Biotec) and analyzed using FlowJo software. Based on previously published criteria [78], critical binding residues for each mAb were defined as alanine mutants with <25% reactivity relative to WT protein. Mutants with <70% binding (compared to WT) of the oligoclonal antibody pool were considered poorly expressed and excluded from further analysis. Additional structure-guided charge-reversal mutants were generated (GENEWIZ) and assessed for binding to individual mAbs or the oligoclonal cocktail. The following mAbs were mapped using the entire alanine-scanning library and all charge-reversal mutants: Z12, Z13, Z14, Z15, Z17, Z18, ZIKV-231, ZIKV-292, and 749-A4. The other mAbs (Z11, Z19, and Z20) were mapped using the mutants identified as part of epitopes for the former set of mAbs.

Antibody-dependent complement deposition. Recombinant ZIKV NS1 protein (Native Antigen) was biotinylated and coupled to red fluorescent Neutravidin beads (Life Technologies) and then incubated with serial dilutions of anti-NS1 mAbs for 2 h at 37°C to allow for binding. Freshly reconstituted guinea pig complement (Cedarlane Labs) was diluted 1:10 in veronal buffer containing 0.1% gelatin (Boston Bioproducts), which then was incubated with the antibody-bead complexes for 20 min at 37°C. After washing in 15 mM EDTA in PBS, the complexes were stained with a FITC-conjugated anti-guinea pig C3b antibody (1:100; MP Biomedicals 0855385) for 15 min at room temperature. Complement deposition was detected using an IntelliCyt iQue Screener Plus or a 3L Stratedigm S1300EXI flow cytometer, and the median fluorescent intensity of FITC was measured for all beads using FlowJo software.

Antibody-dependent neutrophil and cellular phagocytosis. Recombinant ZIKV NS1 protein

(Native Antigen) was biotinylated and conjugated to streptavidin-coated Alexa Fluor 488 beads. NS1-coated beads were incubated with serial dilutions of mAbs (5 to 0.0016 μg/mL) in cell culture medium for 2 h at 37°C. For the neutrophil phagocytosis assays, bone marrow cells from C57BL/6 mice were harvested, washed with PBS, and aliquoted into 96-well plates (5.0×10^4 cells per well). The bead-antibody complexes were added to cells and incubated for 1 h at 37°C. After washing, cells were stained with the following antibodies: CD11b APC (1:20; clone M1/70; BioLegend 101212), CD11c APC/Cy7 (1:20; clone N418; BioLegend 117324), Ly6G Pacific Blue (1:20; clone 1A8; BioLegend 127612), Ly6C BV605 (1:20; clone HK1.4; BioLegend 128036), and CD3 PE/Cy7 (1:20; clone 17A2; BioLegend 100220). Cells were fixed with 4% PFA, processed on an IntelliCyt iQue Screener Plus flow cytometer, and analyzed using FlowJo software. Neutrophils were defined as $CD3^-$ and $CD11c^-$ cells that were $Ly6C^-$, $CD11b^+$, and $Ly6G^+$. The neutrophil phagocytosis score was determined using the following calculation: (% Alexa Fluor 488^+ cells) x (geometric mean fluorescent intensity of Alexa Fluor 488^+ cells)/10,000.

For the cellular phagocytosis assays, J774A.1 (ATCC TIB-67) murine monocyte cells were incubated with the NS1-coated bead-antibody complexes for 1 h 37°C. Cells were washed in 5 mM EDTA PBS, fixed with 4% PFA, and analyzed on an IntelliCyt iQue Screener Plus or a 3L Stratedigm S1300EXI flow cytometer. The cellular phagocytic score was calculated as described for the neutrophil phagocytosis assays.

Statistical analysis. The statistical tests for each data set are indicated in the respective legends and were performed using GraphPad Prism software. Viral burden data were analyzed by a Kruskal-Wallis test with Dunn's post-test, survival analyses were performed using a Mantel-Cox log-rank test with Bonferroni correction, weight loss data were analyzed by two-way ANOVA with Dunnett's post-test, and epitope mapping data were analyzed by two-way ANOVA with

Holm-Sidak's post-test. Statistical significance was defined as $p<0.05$.

Data availability. The authors declare that all data supporting the findings of this study are available within the paper or from the corresponding author upon request. Hybridomas or purified antibodies will be made available under an MTA with Washington University or Vanderbilt University.

2.6 Acknowledgements

This study was supported by NIH grants R01 AI073755 and 75N93019C00062 and contract HHSN272201400058C and HHSN272201700060C. A.W.W. was supported by an NIH pre-doctoral training grant award (T32 5T32AI007172-38). G.R.S. was supported as a Wellcome Trust Senior Investigator (grant 095541/A/11/Z) and by the National Institute for Health Research Biomedical Research Centre Funding Scheme. We thank Rachel Nargi, Rachel Sutton, Erica Armstrong, and Robert Carnahan of Vanderbilt for preparation of recombinant human antibodies.

2.7 References

1 Gutierrez-Bugallo, G. *et al.* Vector-borne transmission and evolution of Zika virus. *Nat Ecol Evol* **3**, 561-569, doi:10.1038/s41559-019-0836-z (2019).

2 Lazear, H. M. & Diamond, M. S. Zika Virus: New Clinical Syndromes and Its Emergence in the Western Hemisphere. *J Virol* **90**, 4864-4875, doi:10.1128/jvi.00252-16 (2016).

3 Carteaux, G. *et al.* Zika Virus Associated with Meningoencephalitis. *N Engl J Med* **374**, 1595-1596, doi:10.1056/NEJMc1602964 (2016).

4 Oehler, E. *et al.* Zika virus infection complicated by Guillain-Barre syndrome--case report, French Polynesia, December 2013. *Euro Surveill* **19**, doi:10.2807/1560-7917.es2014.19.9.20720 (2014).

5 Cao-Lormeau, V. M. *et al.* Guillain-Barre Syndrome outbreak associated with Zika virus infection in French Polynesia: a case-control study. *Lancet* **387**, 1531-1539, doi:10.1016/s0140-6736(16)00562-6 (2016).

6 Brasil, P. *et al.* Zika Virus Infection in Pregnant Women in Rio de Janeiro. *New England Journal of Medicine* **375**, 2321-2334, doi:10.1056/NEJMoa1602412 (2016).

7 Miner, J. J. *et al.* Zika Virus Infection during Pregnancy in Mice Causes Placental Damage and Fetal Demise. *Cell* **165**, 1081-1091, doi:10.1016/j.cell.2016.05.008 (2016).

8 Lindenbach, B. D. & Rice, C. M. trans-Complementation of yellow fever virus NS1 reveals a role in early RNA replication. *J Virol* **71**, 9608-9617 (1997).

9 Youn, S. *et al.* Evidence for a genetic and physical interaction between nonstructural proteins NS1 and NS4B that modulates replication of West Nile virus. *J Virol* **86**, 7360-7371, doi:10.1128/jvi.00157-12 (2012).

10 Plaszczyca, A. *et al.* A novel interaction between dengue virus nonstructural protein 1 and the NS4A-2K-4B precursor is required for viral RNA replication but not for formation of the membranous replication organelle. *PLoS Pathog* **15**, e1007736, doi:10.1371/journal.ppat.1007736 (2019).

11 Winkler, G., Maxwell, S. E., Ruemmler, C. & Stollar, V. Newly synthesized dengue-2 virus nonstructural protein NS1 is a soluble protein but becomes partially hydrophobic and membrane-associated after dimerization. *Virology* **171**, 302-305, doi:10.1016/0042-6822(89)90544-8 (1989).

12 Noisakran, S. *et al.* Association of dengue virus NS1 protein with lipid rafts. *J Gen Virol* **89**, 2492-2500, doi:10.1099/vir.0.83620-0 (2008).

13 Muller, D. A. & Young, P. R. The flavivirus NS1 protein: molecular and structural biology, immunology, role in pathogenesis and application as a diagnostic biomarker. *Antiviral Res* **98**, 192-208, doi:10.1016/j.antiviral.2013.03.008 (2013).

14 Chung, K. M. *et al.* West Nile virus nonstructural protein NS1 inhibits complement activation by binding the regulatory protein factor H. *Proc Natl Acad Sci U S A* **103**, 19111-19116, doi:10.1073/pnas.0605668103 (2006).

15 Avirutnan, P. *et al.* Antagonism of the complement component C4 by flavivirus nonstructural protein NS1. *J Exp Med* **207**, 793-806, doi:10.1084/jem.20092545 (2010).

16 Avirutnan, P. *et al.* Binding of flavivirus nonstructural protein NS1 to C4b binding protein modulates complement activation. *J Immunol* **187**, 424-433, doi:10.4049/jimmunol.1100750 (2011).

17 Conde, J. N. *et al.* Inhibition of the Membrane Attack Complex by Dengue Virus NS1 through Interaction with Vitronectin and Terminal Complement Proteins. *J Virol* **90**, 9570-9581, doi:10.1128/jvi.00912-16 (2016).
18 Modhiran, N. *et al.* Dengue virus NS1 protein activates cells via Toll-like receptor 4 and disrupts endothelial cell monolayer integrity. *Sci Transl Med* **7**, 304ra142, doi:10.1126/scitranslmed.aaa3863 (2015).
19 Modhiran, N. *et al.* Dengue virus NS1 protein activates immune cells via TLR4 but not TLR2 or TLR6. *Immunol Cell Biol* **95**, 491-495, doi:10.1038/icb.2017.5 (2017).
20 Young, P. R., Hilditch, P. A., Bletchly, C. & Halloran, W. An Antigen Capture Enzyme-Linked Immunosorbent Assay Reveals High Levels of the Dengue Virus Protein NS1 in the Sera of Infected Patients. *Journal of Clinical Microbiology* **38**, 1053-1057 (2000).
21 Bosch, I. *et al.* Rapid antigen tests for dengue virus serotypes and Zika virus in patient serum. *Science Translational Medicine* **9**, eaan1589, doi:10.1126/scitranslmed.aan1589 (2017).
22 Macdonald, J. *et al.* NS1 Protein Secretion during the Acute Phase of West Nile Virus Infection. *Journal of Virology* **79**, 13924-13933, doi:10.1128/jvi.79.22.13924-13933.2005 (2005).
23 Liu, J. *et al.* Flavivirus NS1 protein in infected host sera enhances viral acquisition by mosquitoes. *Nature microbiology* **1**, 16087-16087, doi:10.1038/nmicrobiol.2016.87 (2016).
24 Liu, Y. *et al.* Evolutionary enhancement of Zika virus infectivity in Aedes aegypti mosquitoes. *Nature* **545**, 482-486, doi:10.1038/nature22365 (2017).
25 Avirutnan, P. *et al.* Secreted NS1 of dengue virus attaches to the surface of cells via interactions with heparan sulfate and chondroitin sulfate E. *PLoS Pathog* **3**, e183, doi:10.1371/journal.ppat.0030183 (2007).
26 Puerta-Guardo, H. *et al.* Flavivirus NS1 Triggers Tissue-Specific Vascular Endothelial Dysfunction Reflecting Disease Tropism. *Cell Rep* **26**, 1598-1613.e1598, doi:10.1016/j.celrep.2019.01.036 (2019).
27 Beatty, P. R. *et al.* Dengue virus NS1 triggers endothelial permeability and vascular leak that is prevented by NS1 vaccination. *Science Translational Medicine* **7**, 304ra141-304ra141, doi:10.1126/scitranslmed.aaa3787 (2015).
28 Puerta-Guardo, H. *et al.* Zika Virus Nonstructural Protein 1 Disrupts Glycosaminoglycans and Causes Permeability in Developing Human Placentas. *J Infect Dis* **221**, 313-324, doi:10.1093/infdis/jiz331 (2020).
29 Akey, D. L. *et al.* Flavivirus NS1 structures reveal surfaces for associations with membranes and the immune system. *Science* **343**, 881-885, doi:10.1126/science.1247749 (2014).
30 Edeling, M. A., Diamond, M. S. & Fremont, D. H. Structural basis of Flavivirus NS1 assembly and antibody recognition. *Proc Natl Acad Sci U S A* **111**, 4285-4290, doi:10.1073/pnas.1322036111 (2014).
31 Brown, W. C. *et al.* Extended surface for membrane association in Zika virus NS1 structure. *Nat Struct Mol Biol* **23**, 865-867, doi:10.1038/nsmb.3268 (2016).
32 Xu, X. *et al.* Contribution of intertwined loop to membrane association revealed by Zika virus full-length NS1 structure. *Embo j* **35**, 2170-2178, doi:10.15252/embj.201695290 (2016).

33 Gutsche, I. *et al.* Secreted dengue virus nonstructural protein NS1 is an atypical barrel-shaped high-density lipoprotein. *Proc Natl Acad Sci U S A* **108**, 8003-8008, doi:10.1073/pnas.1017338108 (2011).
34 Schlesinger, J. J., Foltzer, M. & Chapman, S. The Fc portion of antibody to yellow fever virus NS1 is a determinant of protection against YF encephalitis in mice. *Virology* **192**, 132-141, doi:10.1006/viro.1993.1015 (1993).
35 Chung, K. M. *et al.* Antibodies against West Nile Virus nonstructural protein NS1 prevent lethal infection through Fc gamma receptor-dependent and -independent mechanisms. *J Virol* **80**, 1340-1351, doi:10.1128/jvi.80.3.1340-1351.2006 (2006).
36 Lee, T. H. *et al.* A cross-protective mAb recognizes a novel epitope within the flavivirus NS1 protein. *Journal of General Virology* **93**, 20-26, doi:https://doi.org/10.1099/vir.0.036640-0 (2012).
37 Bailey, M. J. *et al.* Human antibodies targeting Zika virus NS1 provide protection against disease in a mouse model. *Nat Commun* **9**, 4560, doi:10.1038/s41467-018-07008-0 (2018).
38 Bailey, M. J. *et al.* Antibodies Elicited by an NS1-Based Vaccine Protect Mice against Zika Virus. *mBio* **10**, doi:10.1128/mBio.02861-18 (2019).
39 Gorman, M. J. *et al.* An Immunocompetent Mouse Model of Zika Virus Infection. *Cell Host & Microbe* **23**, 672-685.e676, doi:https://doi.org/10.1016/j.chom.2018.04.003 (2018).
40 Sapparapu, G. *et al.* Neutralizing human antibodies prevent Zika virus replication and fetal disease in mice. *Nature* **540**, 443, doi:10.1038/nature20564 (2016).
41 Lazear, H. M. *et al.* A Mouse Model of Zika Virus Pathogenesis. *Cell Host Microbe* **19**, 720-730, doi:10.1016/j.chom.2016.03.010 (2016).
42 Tang, Y. *et al.* Regulation of Antibody-Dependent Cellular Cytotoxicity by IgG Intrinsic and Apparent Affinity for Target Antigen. *The Journal of Immunology* **179**, 2815-2823, doi:10.4049/jimmunol.179.5.2815 (2007).
43 ÖHLANDLR, C., LARSSON, Å. & PERLMANN, P. Regulation of Effector Functions of Human K-Cells and Monocytes by Antigen Density of the Target Cells. *Scandinavian Journal of Immunology* **13**, 503-510, doi:10.1111/j.1365-3083.1981.tb00163.x (1981).
44 Lux, A., Yu, X., Scanlan, C. N. & Nimmerjahn, F. Impact of Immune Complex Size and Glycosylation on IgG Binding to Human FcγRs. *The Journal of Immunology* **190**, 4315-4323, doi:10.4049/jimmunol.1200501 (2013).
45 Lucisano Valim, Y. M. & Lachmann, P. J. The effect of antibody isotype and antigenic epitope density on the complement-fixing activity of immune complexes: a systematic study using chimaeric anti-NIP antibodies with human Fc regions. *Clin Exp Immunol* **84**, 1-8, doi:10.1111/j.1365-2249.1991.tb08115.x (1991).
46 Bournazos, S., DiLillo, D. J. & Ravetch, J. V. The role of Fc-FcgammaR interactions in IgG-mediated microbial neutralization. *J Exp Med* **212**, 1361-1369, doi:10.1084/jem.20151267 (2015).
47 Davidson, E. & Doranz, B. J. A high-throughput shotgun mutagenesis approach to mapping B-cell antibody epitopes. *Immunology* **143**, 13-20, doi:10.1111/imm.12323 (2014).
48 Hertz, T. *et al.* Antibody Epitopes Identified in Critical Regions of Dengue Virus Nonstructural 1 Protein in Mouse Vaccination and Natural Human Infections. *J Immunol* **198**, 4025-4035, doi:10.4049/jimmunol.1700029 (2017).
49 Crooks, A. J., Lee, J. M., Easterbrook, L. M., Timofeev, A. V. & Stephenson, J. R. The NS1 protein of tick-borne encephalitis virus forms multimeric species upon secretion from

the host cell. *J Gen Virol* **75 (Pt 12)**, 3453-3460, doi:10.1099/0022-1317-75-12-3453 (1994).
50 Pryor, M. J. & Wright, P. J. The effects of site-directed mutagenesis on the dimerization and secretion of the NS1 protein specified by dengue virus. *Virology* **194**, 769-780, doi:10.1006/viro.1993.1318 (1993).
51 Chung, K. M., Thompson, B. S., Fremont, D. H. & Diamond, M. S. Antibody Recognition of Cell Surface-Associated NS1 Triggers Fc-γ Receptor-Mediated Phagocytosis and Clearance of West Nile Virus-Infected Cells. *Journal of Virology* **81**, 9551-9555, doi:10.1128/jvi.00879-07 (2007).
52 Cheng, H. J. *et al.* Correlation between serum levels of anti-endothelial cell autoantigen and anti-dengue virus nonstructural protein 1 antibodies in dengue patients. *Am J Trop Med Hyg* **92**, 989-995, doi:10.4269/ajtmh.14-0162 (2015).
53 Chuang, Y. C., Lin, J., Lin, Y. S., Wang, S. & Yeh, T. M. Dengue Virus Nonstructural Protein 1-Induced Antibodies Cross-React with Human Plasminogen and Enhance Its Activation. *J Immunol* **196**, 1218-1226, doi:10.4049/jimmunol.1500057 (2016).
54 Cheng, H. J. *et al.* Anti-dengue virus nonstructural protein 1 antibodies recognize protein disulfide isomerase on platelets and inhibit platelet aggregation. *Mol Immunol* **47**, 398-406, doi:10.1016/j.molimm.2009.08.033 (2009).
55 Sivapalasingam, S. *et al.* Safety, pharmacokinetics, and immunogenicity of a co-formulated cocktail of three human monoclonal antibodies targeting Ebola virus glycoprotein in healthy adults: a randomised, first-in-human phase 1 study. *The Lancet Infectious Diseases* **18**, 884-893, doi:https://doi.org/10.1016/S1473-3099(18)30397-9 (2018).
56 Gilchuk, P. *et al.* Analysis of a Therapeutic Antibody Cocktail Reveals Determinants for Cooperative and Broad Ebolavirus Neutralization. *Immunity* **52**, 388-403.e312, doi:10.1016/j.immuni.2020.01.001 (2020).
57 Pal, P. *et al.* Development of a highly protective combination monoclonal antibody therapy against Chikungunya virus. *PLoS Pathog* **9**, e1003312, doi:10.1371/journal.ppat.1003312 (2013).
58 Saunders, K. O. Conceptual Approaches to Modulating Antibody Effector Functions and Circulation Half-Life. *Frontiers in Immunology* **10**, doi:10.3389/fimmu.2019.01296 (2019).
59 Zhao, H. *et al.* Structural Basis of Zika Virus-Specific Antibody Protection. *Cell* **166**, 1016-1027, doi:10.1016/j.cell.2016.07.020 (2016).
60 Fernandez, E. *et al.* Human antibodies to the dengue virus E-dimer epitope have therapeutic activity against Zika virus infection. *Nat Immunol* **18**, 1261-1269, doi:10.1038/ni.3849 (2017).
61 Bardina, S. V. *et al.* Enhancement of Zika virus pathogenesis by preexisting antiflavivirus immunity. *Science* **356**, 175-180, doi:10.1126/science.aal4365 (2017).
62 Katzelnick, L. C. *et al.* Antibody-dependent enhancement of severe dengue disease in humans. *Science*, eaan6836, doi:10.1126/science.aan6836 (2017).
63 Schlesinger, J. J., Brandriss, M. W. & Walsh, E. E. Protection against 17D yellow fever encephalitis in mice by passive transfer of monoclonal antibodies to the nonstructural glycoprotein gp48 and by active immunization with gp48. *J Immunol* **135**, 2805-2809 (1985).

64 Brault, A. C. *et al.* A Zika Vaccine Targeting NS1 Protein Protects Immunocompetent Adult Mice in a Lethal Challenge Model. *Scientific Reports* **7**, 14769, doi:10.1038/s41598-017-15039-8 (2017).
65 Jacobs, S. C., Stephenson, J. R. & Wilkinson, G. W. High-level expression of the tick-borne encephalitis virus NS1 protein by using an adenovirus-based vector: protection elicited in a murine model. *Journal of Virology* **66**, 2086-2095 (1992).
66 Liu, X. *et al.* Incorporation of NS1 and prM/M are important to confer effective protection of adenovirus-vectored Zika virus vaccine carrying E protein. *npj Vaccines* **3**, 29, doi:10.1038/s41541-018-0072-6 (2018).
67 Li, A. *et al.* A Zika virus vaccine expressing premembrane-envelope-NS1 polyprotein. *Nature Communications* **9**, 3067, doi:10.1038/s41467-018-05276-4 (2018).
68 Morrison, T. E. & Diamond, M. S. Animal Models of Zika Virus Infection, Pathogenesis, and Immunity. *Journal of virology* **91**, e00009-00017, doi:10.1128/JVI.00009-17 (2017).
69 Foy, B. D. *et al.* Probable non-vector-borne transmission of Zika virus, Colorado, USA. *Emerg Infect Dis* **17**, 880-882, doi:10.3201/eid1705.101939 (2011).
70 Dejnirattisai, W. *et al.* A new class of highly potent, broadly neutralizing antibodies isolated from viremic patients infected with dengue virus. *Nat Immunol* **16**, 170-177, doi:10.1038/ni.3058 (2015).
71 Brien, J. D., Lazear, H. M. & Diamond, M. S. Propagation, Quantification, Detection, and Storage of West Nile Virus. *Current Protocols in Microbiology* **31**, 15D.13.11-15D.13.18, doi:10.1002/9780471729259.mc15d03s31 (2013).
72 Studier, F. W. Protein production by auto-induction in high-density shaking cultures. *Protein Expression and Purification* **41**, 207-234, doi:https://doi.org/10.1016/j.pep.2005.01.016 (2005).
73 Sheehan, K. C. *et al.* Blocking monoclonal antibodies specific for mouse IFN-alpha/beta receptor subunit 1 (IFNAR-1) from mice immunized by in vivo hydrodynamic transfection. *J Interferon Cytokine Res* **26**, 804-819, doi:10.1089/jir.2006.26.804 (2006).
74 Oliphant, T. *et al.* Development of a humanized monoclonal antibody with therapeutic potential against West Nile virus. *Nat Med* **11**, 522-530, doi:10.1038/nm1240 (2005).
75 Smith, K. *et al.* Rapid generation of fully human monoclonal antibodies specific to a vaccinating antigen. *Nature Protocols* **4**, 372-384, doi:10.1038/nprot.2009.3 (2009).
76 Tiller, T. *et al.* Efficient generation of monoclonal antibodies from single human B cells by single cell RT-PCR and expression vector cloning. *Journal of immunological methods* **329**, 112-124, doi:10.1016/j.jim.2007.09.017 (2008).
77 Willis, J. R. *et al.* Redesigned HIV antibodies exhibit enhanced neutralizing potency and breadth. *J Clin Invest* **125**, 2523-2531, doi:10.1172/JCI80693 (2015).
78 Kim, A. S. *et al.* Protective antibodies against Eastern equine encephalitis virus bind to epitopes in domains A and B of the E2 glycoprotein. *Nature Microbiology* **4**, 187-197, doi:10.1038/s41564-018-0286-4 (2019).
79 Ho, I. Y. *et al.* Refined protocol for generating monoclonal antibodies from single human and murine B cells. *J Immunol Methods* **438**, 67-70, doi:10.1016/j.jim.2016.09.001 (2016).
80 Robert, X. & Gouet, P. Deciphering key features in protein structures with the new ENDscript server. *Nucleic Acids Research* **42**, W320-W324, doi:10.1093/nar/gku316 (2014).

Table 2.1 List of anti-ZIKV NS1 mAbs

mAb	Species[a]	Isotype[b]	Binding to recombinant NS1[b]	Binding to infected cells[c]
ZIKV-198	Human	IgG1	+	+
ZIKV-231	Human	IgG1	+	+
ZIKV-240	Human	IgG1	+	+
ZIKV-243	Human	IgG1	+	+
ZIKV-267	Human	IgG1	+	+
ZIKV-276	Human	IgG1	+	+
ZIKV-277	Human	IgG1	+	+
ZIKV-283	Human	IgG1	+	+
ZIKV-292	Human	IgG1	+	+
ZIKV-303	Human	IgG1	+	+
ZIKV-307	Human	IgG3	+	+
ZIKV-315	Human	IgG1	+	+
ZIKV-318	Human	IgG1	+	+
ZIKV-327	Human	IgG1	+	+
ZIKV-332	Human	IgG1	+	+
ZIKV-344	Human	IgG1	+	+
ZIKV-346	Human	IgG1	+	+
ZIKV-352	Human	IgG1	+	+
ZIKV-354	Human	IgG1	+	+
ZIKV-363	Human	IgG1	+	+
ZIKV-364	Human	IgG1	+	+
ZIKV-379	Human	IgG1	+	+
749-A4	Human	IgG1	+	+
13G3	Mouse	IgG1	+	+
33E7	Mouse	IgG1	+	+
5B8	Mouse	IgG1	+	+
7A3	Mouse	IgG1	+	+
22C8	Mouse	IgG1	+	+
22E4	Mouse	IgG1	+	+
25F8	Mouse	IgG1	+	+
3B5	Mouse	IgG1	+	+
15E4	Mouse	IgG1	+	+
22G3	Mouse	IgG1	+	+
22G10	Mouse	IgG1	+	+
34E4	Mouse	IgG1	+	+
39B6	Mouse	IgG1	+	+
4D7	Mouse	IgG1	+	+
4F3	Mouse	IgG1	+	+
8E1	Mouse	IgG1	+	+

21H10	Mouse	IgG1	+	+
19A11	Mouse	IgG1	+	+
33E8	Mouse	IgG1	+	+
5G6	Mouse	IgG1	+	+
39A6	Mouse	IgG1	+	+
39C6	Mouse	IgG1	+	+
20B7	Mouse	IgG1	+	+
Z11	Mouse	IgG2a	+	+
Z12	Mouse	IgG2a	+	+
Z13	Mouse	IgG2a	+	+
Z14	Mouse	IgG2a	+	+
Z15	Mouse	IgG2a	+	+
Z16	Mouse	IgG2a	+	+
Z17	Mouse	IgG2a	+	+
Z18	Mouse	IgG2a	+	+
Z19	Mouse	IgG2a	+	+
Z20	Mouse	IgG2a	+	+
Z21	Mouse	IgG2a	+	+
Z22	Mouse	IgG2b	+	+
Z23	Mouse	IgG2b	+	+
Z24	Mouse	IgG2b	+	+
Z25	Mouse	IgG2b	+	+
Z26	Mouse	IgG2b	+	+
Z27	Mouse	IgG2b	+	+
2H12	Mouse	IgG3	+	+
12F2	Mouse	IgG3	+	+

[a] All anti-ZIKV NS1 human mAbs except for 749-A4 were derived from donor 973 in a previously published study[40]. Prior to blood donation and B cell collection, donor 973 had been infected with an African lineage strain of ZIKV (serum neutralization IC_{50} of 798) and immunized with the YFV vaccine but had no known DENV infection. Human mAb 749-A4 was isolated from a subject with a history of DENV infection and no other known flavivirus infections.
[b] Reactivity to recombinant, soluble ZIKV NS1 and murine IgG subclass were determined by ELISA. Human IgG subclass was determined by sequencing.
[c] Reactivity to ZIKV-infected C6/36 cells was determined by flow cytometry.

Table 2.2 Characteristics of anti-ZIKV NS1 mAbs

mAb[a]	Isotype[b]	Cross-reactivity[c]	EC_{50} (ng/mL) Binding Cell Surface NS1[d]	Competition Group[e]	Binding to NS1 DII/III[f]	Domain Localization[g]	Critical Epitope Residues[g]
Z12	mIgG2a	none	29.2	A	No	Wing	R40, N82, W115
Z13	mIgG2a	none	105.7	A	No	Wing	R40, N82, W115
Z19	mIgG2a	none	66.2	A	No	Wing	N82
Z11	mIgG2a	none	2.2	B	No	Wing	Q102
Z15	mIgG2a	none	1.5	B	No	Wing	K146
Z18	mIgG2a	none	1.5	B	No	Wing	Q102
Z17	mIgG2a	none	18.4	C	Yes	β-platform	T290, R338
Z14	mIgG2a	none	1112.0	D	Yes	β-platform	G305, V307
Z16	mIgG2a	none	No binding	D	Yes		*Not identified*
Z20	mIgG2a	none	No binding	E	No	Wing	R40
ZIKV-292	hIgG1	none	3.4	B	No	Wing	P101, L177/E178
ZIKV-231	hIgG1	none	3.9	C	Yes	β-platform	K265, T293, R314
749-A4	hIgG1	W, J, D2	14.6	C	Yes	β-platform	E289, R314

[a] To generate murine mAbs, mice were inoculated and boosted with ZIKV (Dakar-MA) and then boosted with recombinant ZIKV NS1 protein. Human mAbs were isolated from subjects with a history of ZIKV (ZIKV-292 and ZIKV-231) or DENV (749-A4) infection.
[b] IgG subclass was determined by ELISA (m, murine; h, human).
[c] Cross-reactivity was determined by direct ELISA using recombinant NS1 proteins: W, WNV; J, JEV; D2, DENV2; Y, YFV; T, TBEV.
[d] EC_{50} value for binding to cell-surface NS1 was determined by flow cytometric analysis of ZIKV-infected cells, as described in **Figure 2.4**.
[e] Competition groups were determined by ELISA, as described in **Table 2.3**.
[f] Binding to recombinant ZIKV NS1 DII/III protein (amino acids 172-352) was determined by ELISA.
[g] Domain localization was determined by binding to cells transfected with WT or mutant ZIKV NS1, as described in **Figure 2.5**. Critical epitope residues were defined as mutants with <25% binding to mAb compared to WT NS1.

Table 2.3 MAb competition groups

Competition group			Second antibody													
			A			B				C			D		C/D	E
		mAb	Z12	Z13	Z19	Z11	Z15	Z18	ZIKV-292	Z17	ZIKV-231	749-A4	Z14	Z16	130.99	Z20
First antibody	A	Z12	3	1	0	103	96	94	95	95	97	90	90	99	93	74
		Z13	14	5	3	92	95	87	92	94	96	99	89	100	93	74
	B	Z15	86	82	71	4	2	0	13	90	93	100	88	92	82	70
		Z18	73	63	40	15	34	12	32	94	93	100	92	93	91	81
		ZIKV-292	112	60	71	4	5	1	1	86	96	85	93	93	97	114
	C	Z17	53	35	43	87	89	86	85	1	30	2	94	85	1	53
		ZIKV-231	87	84	70	84	83	103	94	69	40	22	92	73	96	117
		749-A4	100	82	73	103	90	80	90	72	94	7	92	73	89	92
	D	Z14	63	46	34	90	87	85	89	80	94	56	3	0	1	55

To determine mAb competition groups by ELISA, recombinant ZIKV NS1 protein was coated onto microtiter plates and incubated with the indicated first set of mAbs. Without washing, the indicated secondary set of mAbs (biotinylated) were added and after washing binding was detected using streptavidin-conjugated HRP. Values indicate percent of absorbance (OD450) signal detected relative to that obtained when the first antibody added was an irrelevant isotype control mAb.

Table 2.4 Murine mAb Variable Region Sequencing

	Heavy chain						Kappa chain				
	Gene			CDR amino acid sequence			*Gene*		CDR amino acid sequence		
mAb	*V*	*D*	*J*	CDR1	CDR2	CDR3	*V*	*J*	CDR1	CDR2	CDR3
Z12	*IGHV5*	*IGHD2*	*IGHJ2*	GFTFS**S**YG	IS**G**GGIYT	**A**TYDYYFDF	*IGKV4*	*IGKJ2*	SSVSY	GIC	QQW**X**YRVIT
Z13	*IGHV5*	*IGHD2*	*IGHJ2*	GFTFS**T**YG	IS**T**GGIYT	**T**TYDYYFDF	*IGKV4*	*IGKJ2*	SSVSY	GIC	QQW**N**YRVIT
Z11	*IGHV1*	*IGHD3*	*IGHJ3*	GYTFTGYY	INPGTGYS	ARSGAHSGSIAY					
Z15	*IGHV1*	*IGHD3*	*IGHJ3*	GFTFTNSW	IHPGGGHV	ARTVWGFAF					
Z18	*IGHV1*	*IGHD1*	*IGHJ2*	GFTFTSSW	IHPNSGIT	ARLGYYGYVRDY					

The variable regions of the indicated murine antibodies were sequenced using previously described methods [79]. Total RNA was isolated from each hybridoma and cDNA was synthesized using SuperScript IV First Strain Synthesis kit. The heavy and light (kappa) chain variable regions were amplified using allele-specific primers and submitted for Sanger sequencing. For Z12 and Z13, differences in variable region amino acid sequences are indicated in red. One residue within the kappa chain CDR3 sequence for Z12 could not be resolved from the Sanger sequencing trace files and is indicated by a red X. For Z11, Z15, and Z18, the heavy chain variable region sequences were determined to be unique, so we did not proceed with sequencing of the light chain.

Table 2.5 List of charge-reversal mutants

Mutant[a]	Z12[b]	Z13[b]	Z14[b]	Z15[b]	Z17[b]	Z18[b]	ZIKV-	ZIKV-	749-A4[b]	Oligo[c]
W50R	0.86	0.86	1.21	0.96	1.30	0.71	1.26	1.04	1.11	0.59
E51R	0.86	0.87	1.05	1.06	1.18	1.11	1.12	1.02	1.02	0.63
D52R	1.03	1.03	1.12	1.04	1.26	1.00	1.07	1.09	1.11	0.76
ED51RR	0.71	0.70	1.19	0.91	1.20	0.88	1.10	0.99	1.04	0.67
E81R	0.01	0.01	0.95	1.05	1.10	1.03	0.91	0.95	0.88	0.63
G83R	0.20	0.25	0.92	1.01	1.09	1.13	1.04	1.08	0.98	0.61
Q85E	0.96	0.93	0.90	1.10	1.14	1.14	1.06	1.06	0.95	0.61
V89R	0.93	0.87	0.85	0.99	0.99	1.09	0.85	0.93	0.94	0.66
R99E	1.05	1.06	1.01	0.96	1.00	0.94	1.02	0.91	0.99	1.05
P101K	0.97	1.01	0.91	0.85	0.87	0.69	0.78	0.01	0.81	1.04
Q102R	1.21	1.27	1.24	1.16	1.24	0.64	1.24	1.18	1.17	1.21
Q102W	1.06	1.05	1.08	0.96	1.24	0.03	1.14	1.06	1.04	0.72
D138R	0.76	0.65	0.98	1.00	1.05	1.21	1.12	1.00	0.96	0.53
K146E	1.23	1.27	1.26	0.00	1.24	1.27	1.25	1.12	1.24	1.17
K146G	1.05	0.84	1.06	0.65	1.20	0.97	0.98	0.98	0.91	0.65
K170D	0.92	0.90	1.09	1.06	1.13	1.07	1.10	1.01	1.07	0.82
E173K	1.22	1.23	1.23	1.05	1.12	1.23	1.23	1.01	1.12	1.18
D174K	1.20	1.17	1.22	1.04	1.20	1.07	1.13	0.97	1.18	1.15
ED173KK	1.04	0.96	1.10	0.99	1.10	1.01	1.04	0.71	0.98	0.92
Y175K	1.20	1.27	1.32	1.08	1.23	1.19	1.36	1.01	1.21	1.18
L177K	1.16	1.16	1.13	1.00	1.07	1.02	1.09	1.02	1.14	1.14
E178M	0.87	0.80	0.80	0.83	0.80	0.71	1.01	0.82	1.00	0.97
E178K	1.19	1.23	1.12	1.01	1.14	0.93	0.90	0.65	1.20	1.09
E178R	1.36	1.27	1.27	1.12	1.22	1.43	1.19	0.63	1.17	0.78
LE177RR	1.27	1.28	1.20	0.87	1.03	1.04	0.98	0.00	1.01	0.91
K191D	0.76	0.73	0.87	1.10	0.99	1.25	0.79	0.89	0.84	0.40
D208K	1.17	1.21	1.11	1.07	1.16	1.03	1.02	0.93	1.07	1.12
T209K	1.01	1.03	1.00	0.99	0.97	0.97	0.97	0.90	1.03	1.08
T209E	1.13	1.14	1.05	1.10	1.11	0.89	1.16	1.02	1.14	1.15
DT208RR	0.92	0.78	1.27	1.13	1.21	1.17	1.10	1.13	1.13	0.74
K227S	0.96	0.87	0.82	0.84	0.84	0.84	0.94	0.93	0.90	0.93
K227E	1.21	1.22	1.15	1.12	1.12	1.17	1.10	0.96	1.26	1.14
W232D	0.82	0.79	0.74	0.91	0.80	0.73	0.93	0.88	0.88	0.98
G235K	1.13	1.11	1.17	1.02	1.15	1.18	1.20	0.93	1.12	1.17
E237R	0.70	0.83	0.73	1.04	0.91	1.20	0.58	0.98	0.63	0.71
E238K	1.14	1.10	1.09	0.93	1.06	0.97	1.03	0.91	0.95	1.17
K245E	0.78	0.75	0.88	0.91	0.94	1.00	0.93	0.84	0.82	0.80
L251K	0.77	0.63	0.70	0.75	0.78	0.77	0.93	0.83	0.87	0.91
E258D	0.84	0.68	0.77	0.87	0.80	0.82	0.89	0.86	0.86	0.93
E258K	1.25	1.32	1.36	1.11	1.30	1.20	1.33	1.04	1.37	1.30
E289K	1.03	1.02	1.08	1.01	0.83	0.92	0.84	1.01	0.00	0.95
T290K	1.11	1.13	1.05	1.01	0.00	1.06	1.04	1.01	0.86	1.09
G292D	0.91	0.79	0.85	1.08	0.98	0.80	0.94	0.96	1.10	0.83
T293K	0.95	0.97	1.11	0.97	0.99	0.86	0.00	1.00	0.79	0.97
A303R	1.01	0.99	1.00	1.02	1.06	1.11	1.07	0.97	1.02	1.13
S304R	0.63	0.57	0.62	1.02	0.92	1.12	0.95	0.94	0.63	0.59
G305K	1.33	1.27	0.09	1.09	1.22	1.53	1.29	1.17	1.20	0.75
R306D	0.98	0.97	0.73	1.03	1.09	1.11	1.12	1.05	0.86	1.08
V307R	1.32	1.25	0.00	1.06	1.09	1.51	1.52	1.13	1.18	0.82
E309R	0.78	0.80	0.39	1.04	0.96	1.15	0.93	0.98	0.87	0.91
E309W	1.43	1.35	0.55	1.08	1.26	1.65	1.33	1.15	1.32	0.67
E310R	0.47	0.40	0.76	0.92	0.02	1.05	0.88	0.85	0.62	0.64
E315K	0.66	0.77	0.72	1.01	0.86	0.84	0.36	0.92	0.19	0.61
K326D	0.48	0.40	0.79	0.89	0.83	0.82	0.67	0.82	0.67	0.88

[a] The indicated mutants were engineered in the pFM-A1.2 expression vector for ZIKV NS1 and transfected into 293T cells, and the mAb reactivity to each mutant relative to WT NS1 was measured by flow cytometry as described in **Figure 2.5**.
[b] For each mutant, the relative mAb reactivity was normalized to the staining of an oligoclonal mAb cocktail. Critical residues were defined as those mutants with <25% binding compared to WT NS1 (red, <25%; yellow, <50%).
[c] The oligoclonal antibody pool reactivity to each mutant relative to WT NS1 is shown. Mutants with <70% binding relative to WT (orange) of the oligoclonal antibody pool were considered poorly expressed and excluded from epitope mapping analysis.

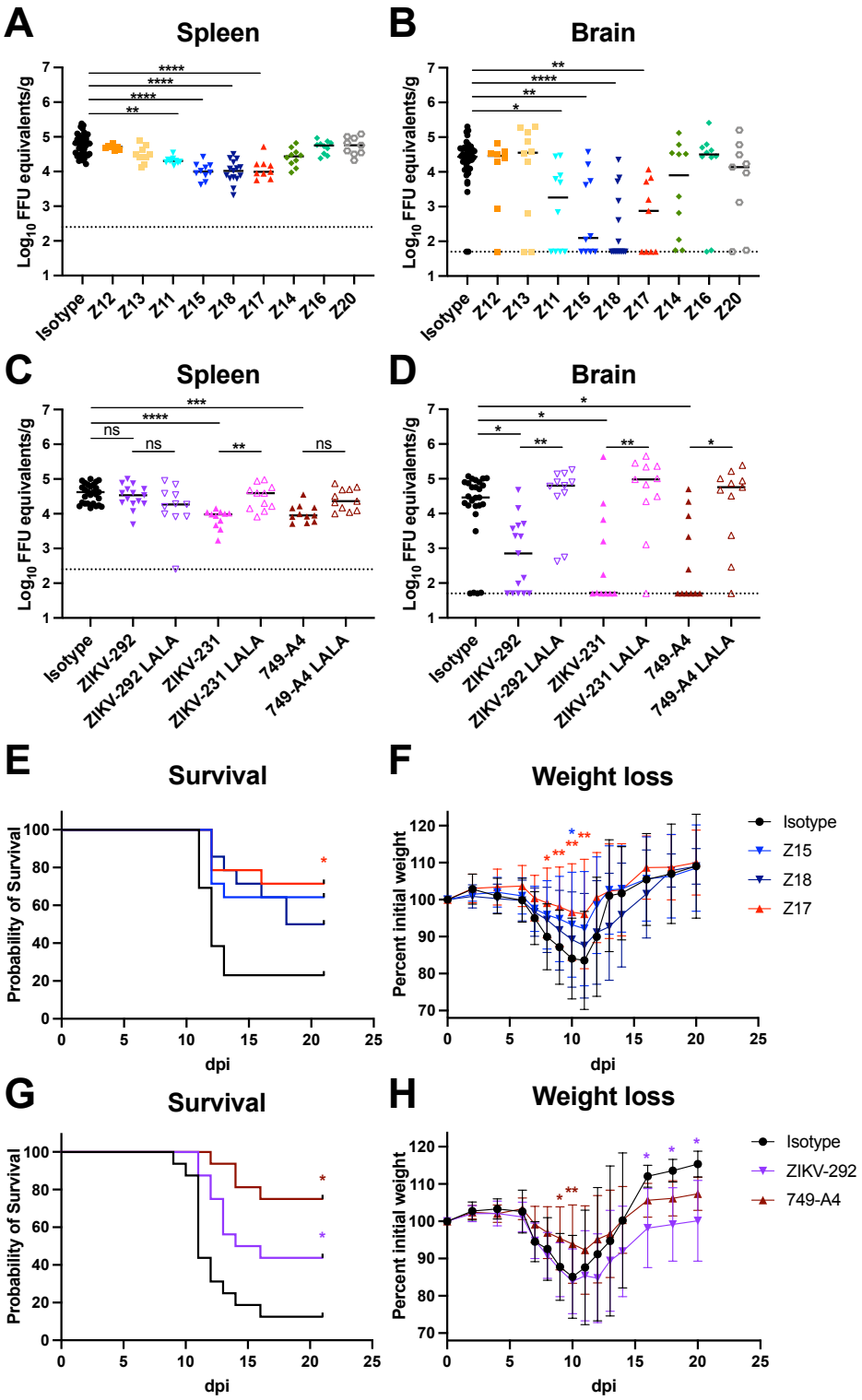

Figure 2.1. Protection by anti-ZIKV NS1 mAbs in non-pregnant mice. Three- to 4-week-old male and female hSTAT2 KI mice were administered 200 μg of the indicated murine (**A-B**) or human (**C-D**) mAbs and inoculated subcutaneously with 10^5 FFU of ZIKV. Viral burden was assessed at 9 dpi in the spleen (**A, C**) and brain (**B, D**). (**A-B**) Isotype control, n = 33; Z12, n = 8; Z13, n = 10; Z11, n = 10; Z15, n = 10; Z17, n = 9; Z18, n = 15; Z14, n = 10; Z16, n=10; Z20, n = 9. (**C-D**) Isotype control, n = 27; 749-A4, n = 11; 749-

A4 LALA, n = 11; ZIKV-231, n = 11; ZIKV-231 LALA, n = 11; ZIKV-292, n = 15; ZIKV-292 LALA, n = 11. Data are pooled from at least 2 experiments (Kruskal-Wallis one-way ANOVA with Dunn's post-test comparison between the indicated groups; *p<0.05; **p<0.01; ***p<0.001; ****p<0.0001; **A**: Z11, p = 0.002; **B**: Z11, p = 0.015; Z15, p = 0.006; Z17, p = 0.003; **C**: Isotype vs. 749-A4, p = 0.0001; ZIKV-231 vs. ZIKV-231 LALA, p = 0.004; **D**: Isotype vs. ZIKV-231, p = 0.039; Isotype vs. ZIKV-292, p = 0.012; Isotype vs. 749-A4, p = 0.013; ZIKV-231 vs. ZIKV-231 LALA, p = 0.004; ZIKV-292 vs. ZIKV-292 LALA, p = 0.003; 749-A4 vs. 749-A4 LALA, p = 0.013). Dotted lines denote the limit of detection (LOD) of the assay. (**E-H**) Four- to 5-week-old male C57BL/6J mice administered 1 mg of an anti-Ifnar1 blocking mAb and 500 μg of the indicated murine (**E-F**) or human (**G-H**) mAbs. The following day, mice were inoculated subcutaneously with ZIKV and mortality (**E, G**) and weights (**F, H**) were tracked. Data are representative of two experiments, and survival analysis was performed using the Mantel-Cox log-rank test with Bonferroni correction compared to the isotype group (**e**: isotype, n = 13; Z15, n = 14, p = 0.052; Z17, n = 14, p = 0.018; Z18, n = 14, p = 0.089; **g**: isotype, n = 16; ZIKV-292, n = 16, p = 0.026; 749-A4, n = 16, p < 0.002). In the Figure: *p<0.05, **p<0.01. Weights were analyzed by two-way ANOVA with Dunnett's post-test comparison to isotype-treated animals (*p<0.05 **F**: Z15: day 10, p = 0.037; Z17: day 8, p = 0.037; day 9, p = 0.009; day 10, p = 0.002; day 11, p = 0.006; **H**: 749-A4: day 9, p = 0.014; day 10, p = 0.005; ZIKV-292: day 16, p = 0.045; day 18, p = 0.037; day 20, p = 0.027); error bars represent the mean values +/- standard deviations (SD).

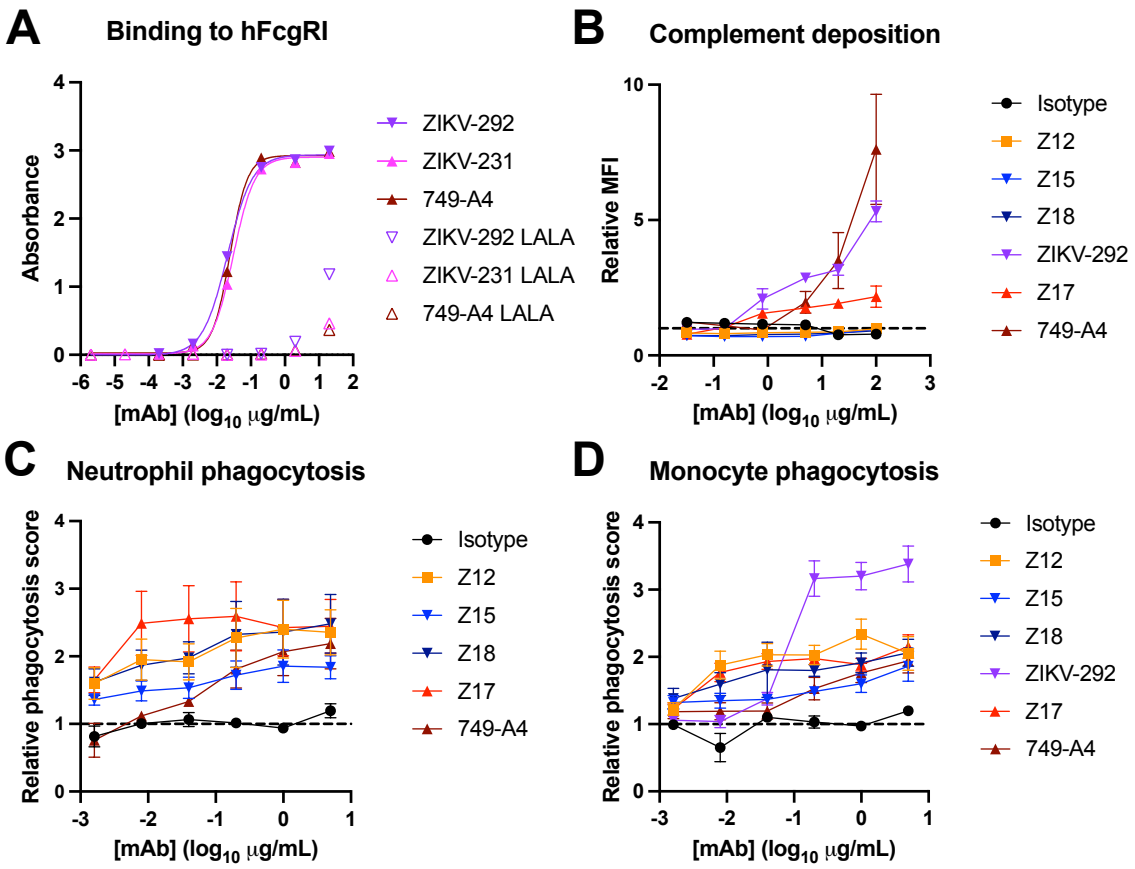

Figure 2.2. Effector functions of anti-NS1 mAbs. (**A**) Binding to hFcγRI (CD64) of wild-type and LALA variant mAbs was assessed by ELISA. Absorbance values are the average of duplicates and representative of 2 experiments. (**B**) Complement deposition assay. ZIKV NS1 protein was coupled to beads and incubated with anti-NS1 or isotype control mAb at indicated concentrations. Following incubation with complement, C3b deposition was assessed by flow cytometry (a minimum of 15,000 beads were collected). Data are presented as the mean of 2 experiments performed in duplicate or triplicate and represent the fold increase in mean fluorescent intensity (MFI) of C3b binding for anti-NS1 mAbs compared to isotype control mAb (dashed line); error bars represent SD. (**C-D**) Antibody-dependent neutrophil (**C**) and monocyte (**D**) phagocytosis of ZIKV NS1-coated fluorescent beads. The phagocytosis score was calculated as described in the Methods and is shown as the fold over the isotype control. A minimum of 7000 (**C**) or 2000 cells (**D**) were collected for each sample. Data are presented as the mean of 2 experiments performed in duplicate or triplicate; error bars represent SD.

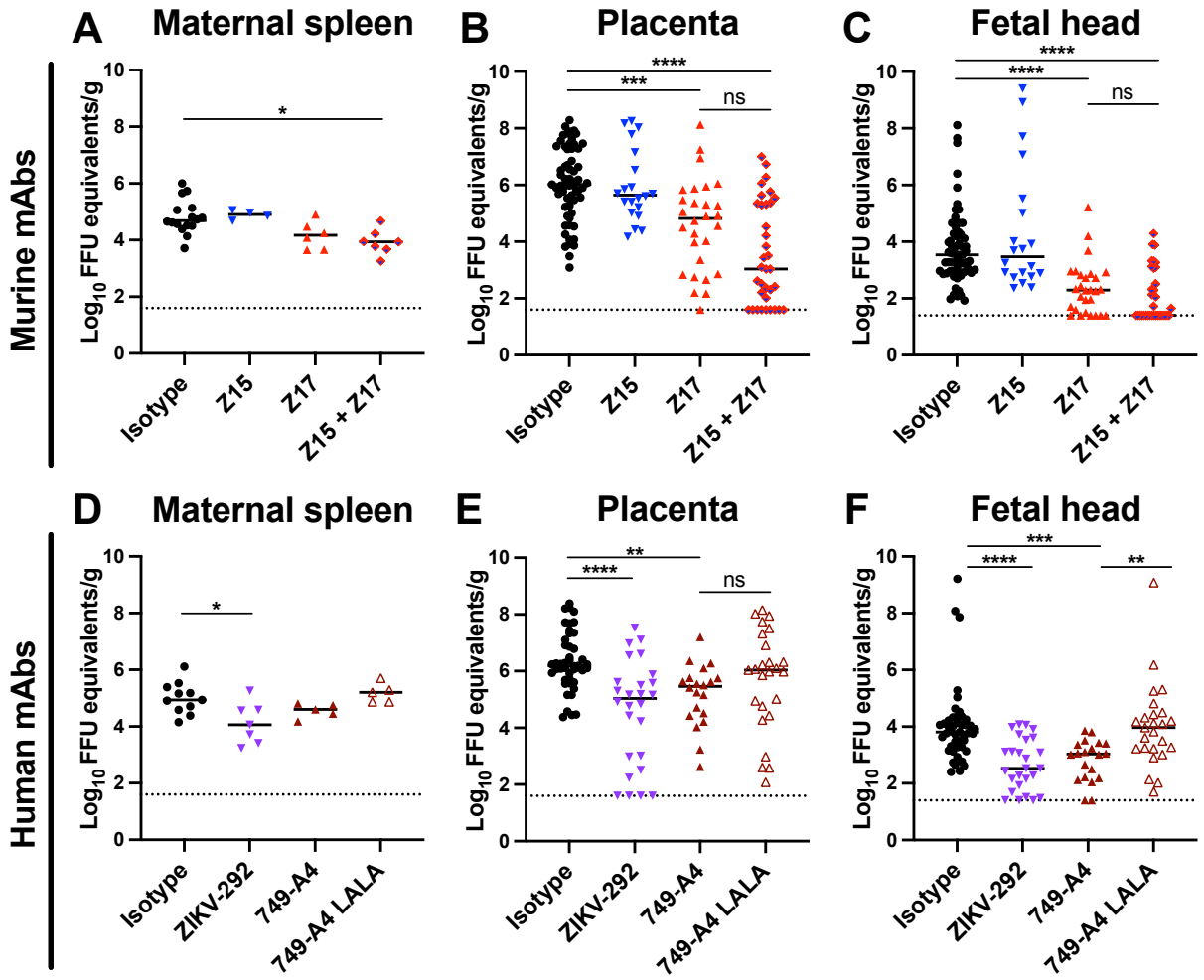

Figure 2.3. Protection by anti-ZIKV NS1 mAbs in pregnant hSTAT2 KI mice. Eight- to 16-week-old hSTAT2 KI female and male mice were mated. On E6.5, plugged females were administered 250 µg of the indicated murine (**A-C**) or human (**D-F**) mAbs and inoculated subcutaneously with 10^6 FFU of ZIKV. For experiments with antibody cocktail treatment, mice received 125 µg of each mAb. Viral burden was assessed on E13.5 in maternal spleen (**A, D**), placenta (**B, E**), and fetal head (**C, F**). Viral burden data for the maternal spleen includes mice that were plugged but did not become pregnant. For each pregnant dam, 5 placentas and fetal heads were evaluated unless the total number of fetuses was less than 5. (**A**) Isotype, n = 16; Z15, n = 4; Z17, n = 6; Z15 + Z17, n = 7. (**B-C**) Isotype, n = 61; Z15 n = 20; Z17, n = 28; Z15 + Z17, n = 35. (**D**) Isotype, n = 9; ZIKV-292, n = 4; 749-A4 and 749-A4 LALA, n = 5. (**E-F**) Isotype, n = 45; ZIKV-292, n = 26; 749-A4, n = 20; 749-A4 LALA, n = 25. Data are pooled from at least 3 experiments (Kruskal-Wallis one-way ANOVA with Dunn's post-test comparison between the indicated groups; *p<0.05; **p<0.01; ***p<0.001; ****p<0.0001; **A**: Isotype vs. Z15 + Z17, p = 0.010; **B**: Isotype vs. Z17, p = 0.0006; Isotype vs. Z15 + Z17, p < 0.0001; **C**: Isotype vs. Z17, p < 0.0001; Isotype vs. Z15 + Z17, p < 0.0001; **D**: Isotype vs. ZIKV-292, p = 0.048; **E**: Isotype vs. ZIKV-292, p < 0.0001; Isotype vs. 749-A4, p = 0.004; **F**: Isotype vs. ZIKV-292, p < 0.0001; Isotype vs. 749-A4, p = 0.0003; 749-A4 vs. 749-A4 LALA, p = 0.002). Dotted lines denote the LOD.

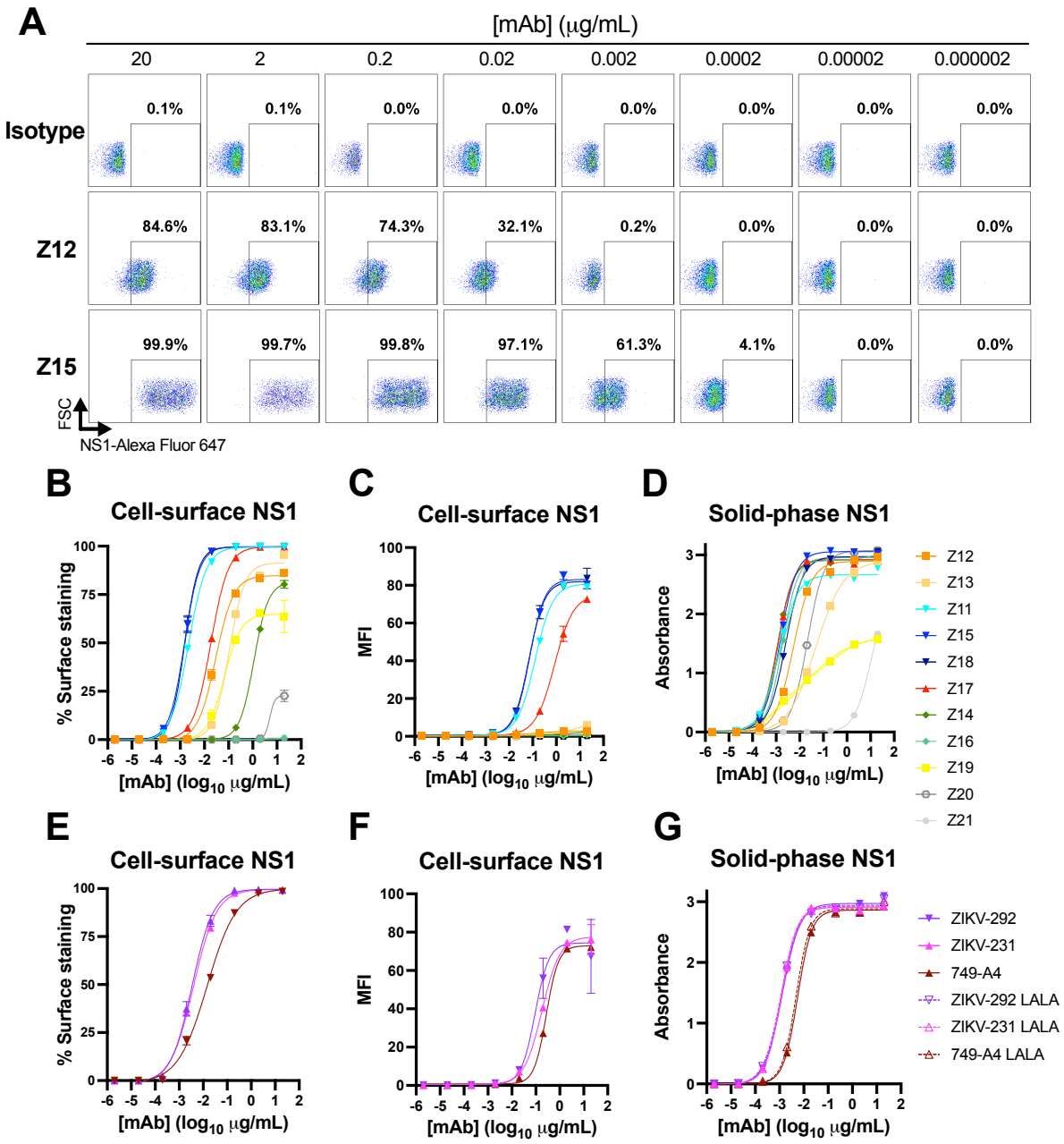

Figure 2.4. Binding properties of anti-ZIKV NS1 mAbs. Binding to NS1 by anti-NS1 mAbs. Binding to cell-surface-associated NS1 was assessed by flow cytometry following staining at 4°C of live, ZIKV-infected Vero cells with serial dilutions of murine (**A-C**) or human (**E-F**) mAbs. (**A**) Representative flow cytometry plots showing binding of anti-NS1 mAbs to NS1 on the cell surface. A minimum of 5,000 cells was collected per sample. The percentage of cells staining (**B, E**) or the mean fluorescence intensity (MFI) (**C, F**) is shown as the average of 2 replicates and is representative of 2 or 3 experiments; error bars represent the mean +/- SD. (**D, G**) Binding of mAbs to recombinant, soluble NS1 was assessed by ELISA. Absorbance values for each concentration of mAb are the average of duplicates and representative of 2 experiments. EC_{50} values for binding are reported in **Table 2.1**.

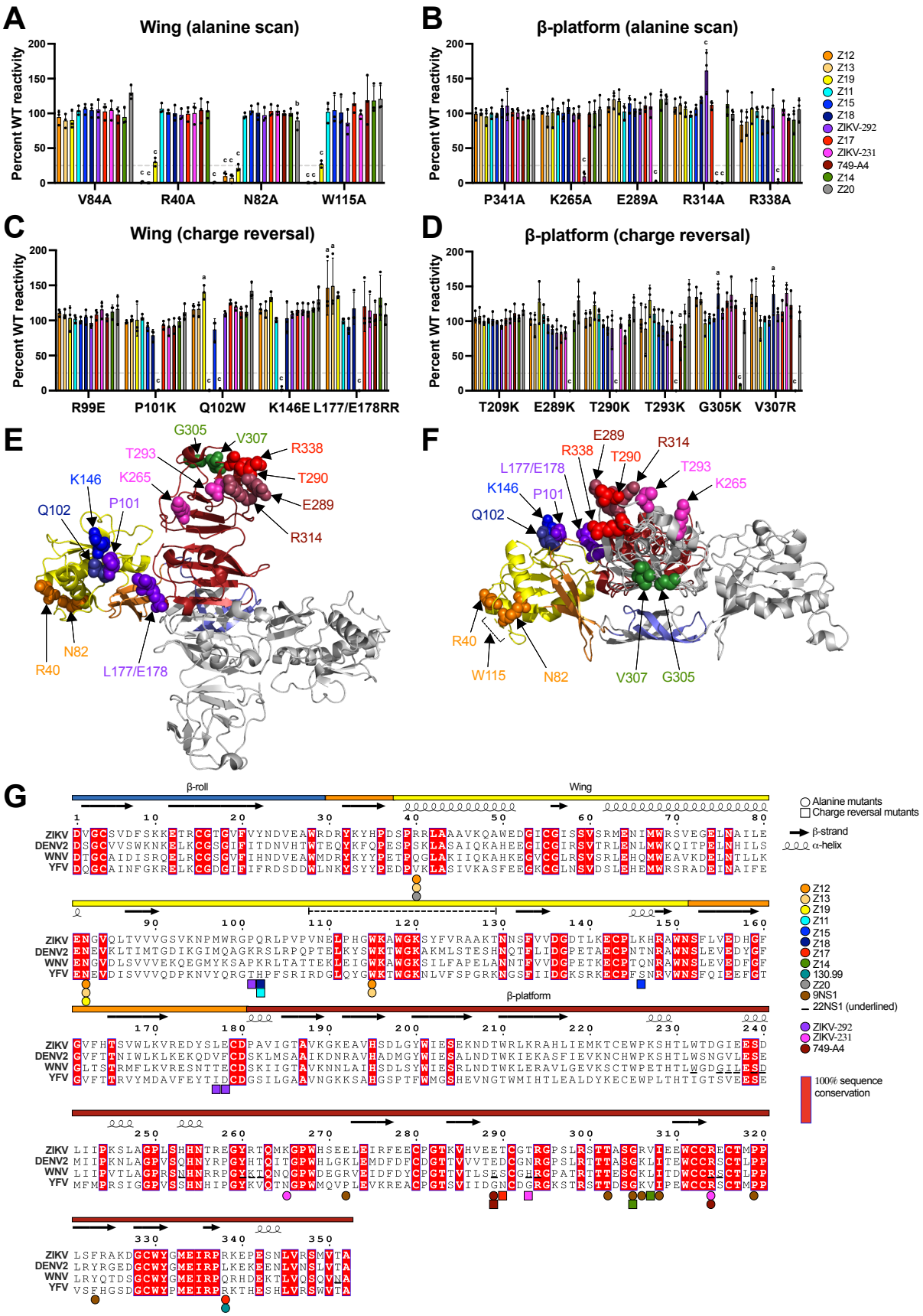
A
Wing (alanine scan)
Percent WT reactivity
V84A
R40A
N82A
W115A
B
β-platform (alanine scan)
P341A
K265A
E289A
R314A
R338A
Z12
Z13
Z19
Z11
Z15
Z18
ZIKV-292
Z17
ZIKV-231
749-A4
Z14
Z20
C
Wing (charge reversal)
R99E
P101K
Q102W
K146E L177/E178RR
D
β-platform (charge reversal)
T209K
E289K
T290K
T293K
G305K
V307R
E
G305
V307
T293
R338
T290
K146
K265
E289
Q102
P101
R314
N82
R40
L177/E178
F
E289
R338
R314
T290
L177/E178
T293
K146
K265
P101
Q102
R40
W115
N82
V307
G305
G
β-roll
Wing
β-platform
ZIKV
DENV2
WNV
YFV
Alanine mutants
Charge reversal mutants
β-strand
α-helix
Z12
Z13
Z19
Z11
Z15
Z18
Z17
Z14
130.99
Z20
9NS1
22NS1 (underlined)
ZIKV-292
ZIKV-231
749-A4
100% sequence conservation

Figure 2.5. Epitope mapping of anti-ZIKV NS1 mAbs. Critical binding residues were mapped using (**A-B**) an alanine-scanning library and (**C-D**) targeted charge-reversal mutants. 293T cells were transfected with plasmids encoding ZIKV NS1, and the mAb reactivity to each mutant relative to WT NS1 was measured by flow cytometry. For each mutant, the relative mAb reactivity was normalized to the relative reactivity of an oligoclonal staining cocktail. Critical residues were defined as those mutants with <25% binding compared to WT NS1. Data are shown for critical residues in the wing (**A, C**) and β-platform (**B, D**) domains. A minimum of ,5000 cells was collected for each sample. Data are the average of 3 experiments (error bars represent the mean +/- SD) and were analyzed by two-way ANOVA with Holm-Sidak's multiple comparison of each mutant to (**A**) V84A, (**B**) P341A, (**C**) R99E, or (**D**) T209K. Superscript letters indicate significance: a, $p<0.01$; b, $p<0.001$; c, $p<0.0001$ (Z12: LE177/178RR, $p = 0.009$; Z13: LE177/178RR, $p = 0.002$; Z18: G305K, $p = 0.007$; V307R, $p = 0.007$; Z19: Q102W, $p = 0.007$; Z20: N82A, $p = 0.0002$; 749-A4: T293K, $p = 0.0068$). (**E-F**) Mapping of critical residues for anti-NS1 mAbs onto the crystal structure of the ZIKV NS1 dimer (PDB 5K6K [http://dx.doi.org/10.2210/pdb5K6K/pdb]) in top view (**E**) or side view (**F**). Critical residues are indicated by spheres and are color-coded according to mAb panel in **A-D**. In each structure, one monomer is grey and one is color-coded by domain (blue, β-roll; yellow, wing; red, β-platform; orange, connector subdomain and greasy finger). This figure was prepared using PyMOL. (**G**) Secondary structure representation of epitopes in ZIKV NS1 as defined by alanine-scanning (circles) and charge-reversal mutagenesis (squares). Sequence alignment is shown for ZIKV (H/PF/2013), DENV2 (Thailand/16681/84), WNV (NY99), and YFV (17D); red shading indicates 100% sequence conservation. Colored bars above the alignment indicate domains: β-roll (blue, 1-29); wing (yellow, 30-180) with connector subdomain (orange); β-platform (red, 181-352). The dashed line above the alignment indicates the wing flexible loop (108-129). The corresponding contact residues of 22NS1, an anti-WNV NS1 mAb, which were determined by X-ray crystallography [30], are shown underlined in the alignment for comparison. This figure was prepared using ESPript 3.0 [80].

Chapter 3

Human monoclonal antibodies against NS1 protein protect against lethal West Nile virus infection

Alex W. Wessel, Michael P. Doyle, Taylor B. Engdahl, Jessica Rodriguez, James E. Crowe Jr., and Michael S. Diamond

.

A.W.W. performed epitope mapping, ELISA, flow cytometry, and animal studies. M.P.D. performed NS1 hybridoma screening and BLI competition studies. M.P.D. and T.B.E. generated the human anti-NS1 mAbs. M.P.D. and J.R. performed recombinant antibody generation. A.W.W. performed data analysis. J.E.C. oversaw the human subjects work. J.E.C. and M.S.D. acquired resources and directed the project. A.W.W. and M.S.D. wrote the initial manuscript draft. All other authors provided editorial comments.

3.1 Summary

Envelope protein-targeted vaccines for flaviviruses are limited by concerns of antibody-dependent enhancement (ADE) of infections. Nonstructural protein 1 (NS1) provides an alternative vaccine target that avoids this risk since this protein is absent from the virion. Beyond its intracellular role in virus replication, extracellular forms of NS1 function in immune modulation and are recognized by host-derived antibodies. The rational design of NS1-based vaccines requires an extensive understanding of the antigenic sites on NS1, especially those targeted by protective antibodies. Here, we isolated human monoclonal antibodies (mAbs) from individuals naturally infected with WNV, mapped their epitopes using structure-guided mutagenesis, and evaluated their efficacy *in vivo* against lethal WNV challenge. The most protective epitopes clustered at three antigenic sites that are exposed on cell-surface NS1: (i) the wing flexible loop, (ii) the outer, electrostatic surface of the wing, and (iii) the spaghetti loop face of the β-platform. One additional mAb mapped to the distal tip of the β-platform and conferred a lower level of protection against WNV despite not binding to NS1 on the surface of infected cells. Our study defines the modes and epitopes of protective anti-NS1 mAb antibodies following WNV infection, which informs the development of NS1-based countermeasures against flaviviruses.

3.2 Introduction

West Nile virus (WNV) is an enveloped, positive-sense RNA virus transmitted by *Culex* species mosquitos. Although the virus originally was endemic to parts of Africa, Europe, and Asia, it disseminated to North America in 1999, where it is now widely established causing thousands of human and equine infections in any given year [1]. Though most WNV infections remain subclinical, a subset of patients, principally the elderly and immunocompromised, develops life-threatening neurological disease. WNV can invade the central nervous system (CNS) and infect neurons in the brain and spinal cord, causing meningitis, encephalitis, and/or acute flaccid paralysis [2]. Surviving patients often develop long-term sequelae that can include persistent fatigue, muscle weakness, and cognitive impairment [3,4]. No approved therapeutics or vaccines exist for WNV infection in humans.

WNV is in the Flavivirus genus of the *Flaviviridae* family, which includes other clinically relevant viruses such as Japanese encephalitis (JEV), dengue (DENV), Zika (ZIKV), yellow fever (YFV), and tick-born encephalitis (TBEV) viruses. The licensed vaccines for JEV, DENV, and TBEV target the viral structural proteins and elicit neutralizing antibody responses [5,6]. The concern for possible antibody-dependent enhancement (ADE) of homologous or heterologous flavivirus infection, however, has slowed progress for E protein-targeted vaccines and antibody therapeutics, especially for DENV and ZIKV [7,8]. Alternative strategies targeting the flavivirus nonstructural protein 1 (NS1) have been proposed to avoid ADE [9-11]. NS1 is a 46-55 kilodalton glycoprotein that homodimerizes in the endoplasmic reticulum (ER) [12,13], where it acts as a scaffold to recruit viral and host factors necessary for replication [14-17]. Infected cells also express dimeric NS1 on the plasma membrane [18-20] and secrete a soluble, hexameric form of NS1 [21-25]. Secreted NS1 can be detected in circulation in infected individuals [26-28], and also binds back to the surface of infected

or uninfected cells through interactions with glycosaminoglycans and possibly other receptors [29]. Extracellular forms of NS1 can bind complement [30-33] and Toll-like receptors [34-36] to modulate or evade host immunity, and also interact with endothelial cells to regulate permeability across blood-tissue barriers [29,37-42].

The WNV NS1 dimer structure is comprised of three domains: the β-roll, wing, and β-platform (**Figure 1.6A-B**) [25,43]. The β-roll domains (residues 1-29) of two protomers intertwine and create a hydrophobic 'inner surface' that mediates interactions with lipid membranes [25]. The wing domains (residues 30-180) also contribute to this inner hydrophobic surface through two subdomains: the flexible loop (residues 108-129) and the 'greasy finger' (residues 159-163) [25,44,45]. In the hexamer (**Figure 1.6C**), these regions create a hydrophobic inner core that packs with lipid cargo [24]. The opposite 'outer surface' of the wing domain contains polar residues and is more variable in sequence among flaviviruses [45]. The β-platform domain (residues 181-352) consists largely of β-strands that face the plasma membrane in the dimeric form of NS1. The opposite face of the β-platform, termed the 'loop face', is covered by the spaghetti loop subdomain (residues 219-272), an extended loop positioned between two β-strands [25,43].

Although extracellular NS1 is believed to contribute to pathogenesis during infection, it is also immunogenic and elicits antibody responses. NS1-specific monoclonal antibodies (mAbs) have been isolated that confer protection against challenge in animal models for YFV, DENV, ZIKV, JEV, or WNV [10,11,46-50]. Protection can occur via Fc-dependent clearance of virus-infected cells [11,46,47,51,52] or Fc-independent mechanisms [9,38]. Extensive epitope mapping of ZIKV NS1-specific mAbs suggests that protective mAbs target a subset of surface-exposed regions in NS1, including the exposed spaghetti loop surface of the β-platform and the electrostatic surface of the wing domain [46]. For WNV, a previous study generated several protective NS1-specific murine

mAbs after immunization with recombinant hexameric WNV NS1 [52]. Although the epitopes for two of these protective mAbs were mapped [43,48], the breadth of epitopes in WNV NS1 that mediate protection remains largely unknown. Furthermore, no study has evaluated whether anti-NS1 human mAbs generated during natural WNV infection are similar to those induced in mice after immunization with recombinant proteins, or whether they can confer protection. These questions are important for the development of WNV NS1-based therapeutics and vaccines. Here, we generated NS1-specific mAbs from an individual naturally infected with WNV during the 2012 outbreak in Dallas, Texas. Twelve of 13 mAbs tested conferred varying degrees of protection against lethal WNV challenge in mice by limiting viral burden. Ten of the anti-WNV NS1 human mAbs that protected mice bound strongly and at high density to the surface of WNV-infected cells, whereas one non-protective mAb (WNV-100) bound poorly to the cell surface. The epitopes of mAbs that mediated protection localized principally to the surface-exposed spaghetti loop face of the β-platform domain, though one protective mAb (WNV-99) mapped to the wing flexible loop. Additionally, one mAb (WNV-97) conferred a lower level of protection despite lacking binding to cell surface-expressed NS1. As our findings suggest that human antibodies targeting specific epitopes on NS1 can protect against infection and disease, a path forward for rational design of NS1-based vaccine seems plausible.

3.3 Results

Generation of anti-WNV NS1 human monoclonal antibodies. We obtained matched serum and blood samples from 13 individuals with laboratory-confirmed, symptomatic WNV infection during the 2012 outbreak in Dallas, Texas [53,54]. We first screened sera for binding to recombinant WNV NS1 by ELISA and identified the donor with the highest serum anti-NS1 antibody titers. From this donor, we isolated B cells from the matched blood sample and generated human

hybridomas, whose supernatants were screened by ELISA for reactivity to recombinant WNV NS1 protein (**Figure 3.1**). Thirteen hybridoma clones secreting NS1-specfic monoclonal antibodies (mAbs) were recovered (**Table 3.1**), and the antibody genes were sequenced (**Table 3.2**). We analyzed the constant region sequences to determine the IgG subclass for each mAb, which revealed eleven mAbs as IgG1 and two mAbs (WNV-99 and WNV-120) as IgG3. Analysis of the variable regions confirmed that all clones expressed unique antibody molecules with different combinations of heavy and light chain genes. The variable region sequences for twelve of the mAbs were cloned into plasmids for recombinant hIgG1 expression. One mAb, WNV-106, was not cloned into an expression vector due to poor sequence recovery, although we purified this mAb from hybridoma supernatant for some studies.

We evaluated all thirteen human mAbs by ELISA for cross-reactivity with other flavivirus NS1 proteins (**Table 3.1**), including JEV, ZIKV, DENV serotype 2 (DENV2), YFV, and tick-borne encephalitis virus (TBEV). Eight mAbs were WNV-specific, whereas the other mAbs displayed varying degrees of cross-reactivity. Four mAbs bound to the closely-related (77% amino acid identity) NS1 of JEV (WNV-99, WNV-106, WNV-120, and WNV-100), and three of them bound to the more distantly-related (43% amino acid identity) NS1 of TBEV (WNV-97, WNV-99, and WNV-100). Two mAbs cross-reacted with DENV2 NS1 (55% amino acid identity) (WNV-100 and WNV-106) and one with YFV NS1 (43% amino acid identity) (WNV-106). No mAbs cross-reacted with ZIKV NS1 protein.

Epitope mapping. We used biolayer interferometry (BLI) and ELISA to define competition groups between the human mAbs and several murine mAbs that were generated previously after immunizing mice with soluble WNV NS1 (**Figure 3.2A** and **3.3A**) [47]. The mAbs segregated into four competition groups. Group A consisted of only one human mAb, WNV-120, and one murine

mAb, 8NS1. Group B also contained only one human (WNV-99) and one murine (16NS1) mAb. Group C consisted of nine human mAbs and four murine mAbs. Among these, WNV-103 showed unidirectional competition with other group C mAbs, and two group C mAbs (WNV-104 and WNV-113) demonstrated partial competition with group D mAbs. Group D contained two human mAbs, WNV-97 and WNV-100, and one murine mAb, 9NS1.

To define the epitopes in greater detail, we mapped amino acid interaction residues of the thirteen human mAbs and several of the previously published murine mAbs [47]. We identified key residues for antibody binding by assessing for loss-of-binding to engineered charge-reversal substitutions in mammalian-cell expressed WNV NS1 (strain 382-99; **Figure 3.2B** and **Table 3.1**). We prioritized solvent-exposed residues based on published NS1 structures [25,43] and previously identified epitopes in the related ZIKV NS1 [46], which shares structural similarity to WNV NS1 [44,45]. In total, we generated 102 WNV NS1 mutants, each expressing a single substitution, and compared mAb binding relative to WT WNV NS1 using a flow cytometry assay. Residues were deemed critical for mAb binding if the substitution resulted in less than 25% binding relative to WT NS1 but did not affect binding by a cocktail of five anti-NS1 human mAbs from different competition groups. We found that substitution at residues K44, N82, or G83 at the distal end of the wing domain resulted in loss-of-binding for the group A mAb WNV-120. The group A murine mAb 8NS1 mapped to proximal residues in this region (T77, K80, and G83). Substitution at L123 within the wing flexible loop resulted in reduced binding by the group B human mAb WNV-99. The murine mAb in group B, 16NS1, also mapped to adjacent residues (W118, I122, and L123) within the wing flexible loop. This latter result is consistent with previous ELISA-based peptide mapping of 16NS1 to this region [48].

The group C human mAbs mapped principally to the β-platform domain. Notwithstanding this finding, the group C mAb WNV-103 mapped to residue K141 within the wing domain. This residue lies within the outer electrostatic surface of the wing domain and is adjacent to the spaghetti loop surface of the β-platform [25,44]. Four group C human mAbs (WNV-95, WNV-96, WNV-104, and WNV-117) and one murine mAb (10NS1) mapped to residues within the spaghetti loop (residues 219-272) and loop face of the β-platform: S239, D240, R256, K261, H293, and R294. The group C murine mAb 22NS1 also has contact residues in the spaghetti loop, as determined by a crystal structure of it bound to a C-terminal fragment of WNV NS1 [43]. The group C mAbs WNV-98 and WNV-113 mapped to residues that are more C-terminal within the β-platform, although still on the spaghetti loop face (WNV-98: R314; and WNV-113: D341, E342, and K343). Two murine mAbs in this competition group, 14NS1 and 17NS1, mapped to proximal residues in this region: G295 and R314. Despite substantial effort, the epitopes for group C mAbs WNV-106 and WNV-116 were not identified using the charge-reversal substitutions. In contrast, both human mAbs and the one murine mAb in group D mapped to the distal tip of the β-platform domain (WNV-97: R339; WNV-100: L307; and 9NS1, L307).

Residues identified as key for binding were mapped onto the WNV NS1 crystal structure (**Figure 3.2C-D**). Notably, the four competition groups localized to distinct regions on the structure. Group A mAbs bound at the distal end of the wing domain, adjacent to the binding site for the group B mAbs within the wing flexible loop. Antibodies in group C localized primarily to the spaghetti loop surface of the β-platform, except for WNV-103, which mapped to the adjacent outer surface of the wing. Both regions are predicted to be exposed on the cell-surface form of NS1 [25,43]. Group D mAbs localized to the tip of the β-platform domain, at residues on or

approximating the membrane-facing β-strand surface. As such, these residues may be less accessible on the cell-surface form of NS1.

NS1 binding properties. Given that NS1 is expressed as a dimer on the cell surface and as a soluble hexamer in the extracellular space and in circulation during infection, we evaluated binding of the human and murine mAbs using two methods. First, we assessed binding to solid-phase recombinant WNV NS1 protein by ELISA. All human mAbs bound avidly (half maximal effective concentration, EC_{50}: ~1 to 5 ng/mL; **Figure 3.4A-D**). We then measured binding to NS1 expressed on the surface of intact, WNV-infected Vero cells using flow cytometry (**Figure 3.4E-H** and **Table 3.1**). The mAbs in groups A and B bound infected cells relatively similarly (EC_{50}: WNV-120: 132 ng/mL; and WNV-99: 294 ng/mL; **Figure 3.4E-F**). Within group C, WNV-95, WNV-98, and WNV-103 bound most avidly (EC_{50}: WNV-95: 15 ng/mL; WNV-98: 11 ng/mL; and WNV-103: 15 ng/mL), whereas most other group C mAb bound slightly less efficiently (EC_{50}: ~20 to 30 ng/mL; **Figure 3.4G**). One exception was WNV-116, which bound approximately 10- to 20-fold less avidly (EC_{50}: 233 ng/mL) than the other group C mAbs. The group D mAb WNV-100 (EC_{50}: 116 ng/mL) bound with similar strength as WNV-116 and the mAbs in groups A and B (**Figure 3.4H**). The group D mAb WNV-97, which mapped to a residue on the membrane-facing surface of the β-platform, failed to bind the surface of infected cells. We also compared the density of surface binding by the human mAbs using the mean fluorescence intensity (MFI; **Figure 3.4I-L**). On average, the group C mAbs bound to infected cells with the highest site density (**Figure 3.4K**), with the exception of WNV-99 in group B (**Figure 3.4J**). The mAbs in groups A and D bound at lower density to infected cells (**Figure 3.4I and L**).

For comparison, we also measured the surface binding for published anti-WNV NS1 murine mAbs (**Figure 3.3B-C**) [47]. Avidity of surface binding varied by competition group, as seen

with the human mAbs. The group C murine mAbs 10NS1, 14NS1, 17NS1, and 22NS1 all bound avidly and to a similar extent as the human mAbs in group C. Most mAbs in groups A, B, and D bound the cell surface less avidly and at lower density compared to group C. However, the group B mAb 16NS1 bound with a similar density as the group C mAbs, although with less avidity.

Protection by anti-WNV NS1 human mAbs. We next assessed the ability of anti-WNV NS1 human mAbs to protect against virus challenge in mice [55]. Four- to five-week-old C57BL/6J male mice were inoculated subcutaneously with 10^2 focus-forming units (FFU) of WNV (New York strain 382-99) and concurrently administered a single 200 μg (10 mg/kg) dose of antibody. We did not evaluate WNV-120 in group A due to its poor stability in solution or the group C mAb WNV-106 because it was not cloned successfully into an expression vector. Whereas only ~10% of mice administered an isotype control antibody (hu-CHK-152) [56] survived infection over three weeks, the NS1-specific human mAbs conferred varying degrees of protection (**Figure 3.5**). The group B mAb WNV-99 conferred ~50% protection at either a 200 or 50 μg dose (**Figure 3.5A**). The group C mAbs conferred the greatest protection, resulting in about 65% to 75% survival rates (**Figure 3.5B**). The protection was Fc-dependent for at least one mAb tested in group C, WNV-96, as demonstrated by a lack of protection using an IgG1-LALA variant that abrogates binding to most Fcγ receptors and complement [57]. The group D mAb WNV-97 trended towards conferring protection (40%), although this did not reach statistical significance (**Figure 3.5C**). The group D mAb WNV-100 did not protect against lethality.

3.4 Discussion

In this study, we show that human anti-WNV NS1 mAbs that bind with the greatest strength and site density to cell-surface-expressed NS1 confer the highest levels of protection against WNV infection. Antibody-mediated protection in mice and avid cell surface binding were

associated with epitopes on the loop face of the β-platform domain (group C), which is exposed on cell surface forms of NS1. However, one protective group C human mAb (WNV-103) mapped to the outer electrostatic surface of the wing domain, another exposed epitope on cell surface NS1. We also mapped several previously generated, protective murine mAbs (10NS1, 14NS1, 17NS1, and 22NS1) within group C to the loop face of the β-platform [47]. Our data are consistent with a recent study of anti-ZIKV NS1 mAbs, which found that protective mAbs mapped to exposed epitopes on cell surface forms of NS1, including the spaghetti loop face of the β-platform and outer surface of the wing domain [46]. Protection by anti-ZIKV NS1 mAbs was Fc-dependent, which is consistent with our data for at least one group C mAb (WNV-96). Anti-NS1 mAbs binding to cell surface NS1 may facilitate Fc-mediated clearance of WNV-infected cells, such as through phagocytosis by macrophages [52] or classical complement-mediated cytolysis [19,50]. Avid binding with high site density to infected cells may be required to cross-link bound antibodies and promote Fc effector functions [58-61].

One human (WNV-99) and one murine (16NS1) mAb in group B [47,48], which mapped to the wing flexible loop, also conferred protection. In comparison to the group C human mAbs, however, WNV-99 yielded less protection and bound less avidly to NS1 on the cell surface. Two previously generated anti-ZIKV NS1 mAbs (Z12 and Z13), which also mapped to the wing flexible loop, failed to protect against ZIKV infection and pathogenesis [46]. These mAbs, however, bound with even lower density to cell surface forms of NS1 than 16NS1 or WNV-99. Notably, the wing flexible loop is comparatively less disordered in the crystal structure for ZIKV NS1 than WNV NS1 [25,44,45]. The flexible loop structure in ZIKV NS1 forms a hydrophobic protrusion or 'spike' that is thought to facilitate association with the plasma membrane [38,44,45]. Potentially, this region is more flexible in WNV NS1 to allow for greater mAb binding to NS1 on the cell surface.

Alternatively, the angle of binding may differ between the anti-ZIKV and anti-WNV NS1 mAbs such that the plasma membrane sterically inhibits binding of some anti-ZIKV NS1 mAbs. It is also possible that substitution at the identified residues for these two mAbs might disrupt binding through allosteric rather than direct effects on contact residues. High-resolution structural studies using X-ray crystallography or cryo-electron microscopy of WNV-99 or 16NS1 Fab fragments bound to WNV NS1 may be needed to definitively characterize this epitope.

The human mAbs in groups A (WNV-120) and D (WNV-97 and WNV-100) bound less efficiently to NS1 on the cell surface than group C mAbs. Whereas WNV-97 failed to bind the surface of infected cells entirely, WNV-120 and WNV-100 bound at lower site density than group C mAbs. Based on the NS1 dimer structure, the critical binding residues for the group A mAbs span the inner and outer surfaces at the distal tip of the wing domain [25]. Potentially, the binding orientation of the mAbs may be angled toward the inner surface, leading to steric hindrance by the cell plasma membrane. Consistent with the relatively poor accessibility of their epitopes on the surface of infected cells, WNV-100 or WNV-97 conferred no or low levels of protection *in vivo*, respectively. The residual protection conferred by WNV-97, despite lacking binding to the infected cell surface, could be explained by blocking of pathogenic functions of soluble NS1, including effects on endothelial permeability [37,39,40]. Indeed, two anti-DENV NS1 mAbs mapping to this same region blocked endothelial hyperpermeability and protected mice through Fc-independent mechanisms [9,38]. Residues at the tip of the β-platform (near the epitope for WNV-97) also are critical for inducing endothelial hyperpermeability after binding by DENV NS1 [38,42]. Some group C mAbs such as 14NS1, WNV-98, or WNV-113 also might be expected to act through Fc-independent mechanisms as well, given their epitopes are proximal to the tip of the β-platform domain. Indeed, the previously generated group C murine mAb 14NS1 protected C1q-deficient or

Fcγ receptor-deficient mice [47].

Several of the anti-WNV NS1 mAbs demonstrated varying degrees of cross-reactivity with other flavivirus NS1 proteins. The group B mAbs 16NS1 and WNV-99 both bound JEV NS1 and mapped to the wing flexible loop, which contains several highly conserved residues (*e.g.*, W115, K116, W118, and G119). This region could be conserved due to its importance in association of NS1 with cell membranes [38,44,45]. All three mAbs in group D (9NS1, WNV-97, and WNV-100) bound at least one heterologous flavivirus NS1 protein. This result is consistent with the epitope location of these mAbs at the conserved regions in the tip of the β-platform domain [25,45]. At least three other previously generated, protective NS1-specific mAbs [749-A4 [46], 2B7 [38], and 1G5.3 [9]] also map to the distal tip of the β-platform and cross-react with multiple flavivirus NS1 proteins. Two of these mAbs (2B7 and 1G5.3) block DENV NS1-mediated endothelial hyperpermeability and protect against DENV pathogenesis without requiring Fc effector functions [9,38]. Thus, the tip of the β-platform might be a candidate site for immune focusing efforts to generate protective, cross-reactive mAbs against multiple flaviviruses [62-64]. Nonetheless, several reports suggest that epitopes at the tip of the β-platform of DENV NS1 (residues ~305-330) can induce autoantibodies that react with human endothelial cells, platelets, and coagulation factors [65-71]. In some mouse models, these mAbs induce thrombocytopenia, coagulopathy, and plasma leakage [70,71]. Thus, further studies are warranted to determine the safety of mAbs binding to this conserved, C-terminal region of NS1. Alternatively, targeting of other epitopes in NS1 (*e.g.*, the outer surface of wing domain or spaghetti loop) may provide protection without the risk of adverse consequences. Vaccines could be designed to focus the immune response on particular epitope locations, either through design of NS1 immunogens lacking the conserved C-terminal region or by masking these epitopes by adding additional N-linked glycans in a site-specific manner [72-75].

In summary, we isolated a panel of NS1-specific mAbs from a human subject naturally infected with WNV and defined three main epitopes associated with protection: (i) the wing flexible loop, (ii) the outer, electrostatic surface of the wing, and (iii) and the loop face of the β-platform (including the spaghetti loop and adjacent C-terminal loop face). Most protective epitopes were associated with avid binding to NS1 on the surface of infected cells, with the caveat that a subset of mAbs may confer protection without binding to the cell surface. One limitation of this study is that we only analyzed thirteen NS1-specific mAbs from one individual. A larger panel of mAbs from more human donors might enable a more extensive characterization of functionally important epitopes in WNV NS1 and provide greater resolution to structure-function analyses.

3.5 Methods

Ethics statement. (***i***) ***Animal procedures***. Animal procedures were performed in accordance with the recommendations in the Guide for the Care and Use of Laboratory Animals of the National Institutes of Health. Protocols were approved by the Institutional Animal Care and Use Committee at Washington University School of Medicine (assurance no. A3381-01). To minimize suffering during procedures, animals were anesthetized with ketamine hydrochloride and xylazine. (***ii***) ***Human subjects***. In 2014, blood samples were collected from adults with a history of symptomatic, laboratory-confirmed WNV infection during the 2012 outbreak in Dallas, Texas [54]. The study was approved by the Institutional Review Board of Vanderbilt University Medical Center, and samples were obtained by the Vanderbilt Clinical Trials Center following written informed consent from each subject.

Cell culture. BHK-21 (American Type Culture Collection (ATCC), CCL-10), C6/36 (ATCC, CRL-1660), HEK-293T (ATCC, ACS-4500), and Vero cells (ATCC, CCL-81) were propagated in Dulbecco's modified Eagle Medium (DMEM) supplemented with 10% fetal bovine serum

(FBS), 1 mM sodium pyruvate, and 10 mM HEPES, pH 7.3. Raji-DCSIGNR cells [76] were propagated in RPMI 1640 medium supplemented with 7% FBS, GlutaMAX (Invitrogen), and 100 U/mL penicillin/streptomycin (Invitrogen). DCSIGNR expression on Raji-DCSIGNR cells was confirmed using mouse anti-human DC-SIGNR/CD299 (10 μg/mL; R&D Systems, clone MAB162, 120604). Cells were maintained at the following conditions: C6/36 cells, 28°C and 5% CO_2; Raji-DCSIGNR cells, 37°C and 7% CO_2; all other cells, 37°C and 5% CO_2.

Production of infectious WNV. We generated recombinant, infectious WNV using a two-plasmid (pWN-AB and pWN-CG) infectious clone for WNV-NY99, strain 382-99 (GenBank accession no. AF196835) [77,78]. The pWN-AB and pWN-CG plasmids were purified from SURE 2 competent cells (Agilent), digested with NgoMIV and XbaI, and then treated with alkaline phosphatase. Following phenol/chloroform extraction and precipitation with ethanol, the DNA fragments were joined with T4 DNA ligase at 16°C overnight. The assembled DNA was subsequently linearized with XbaI (5 h at 37°C) and treated with proteinase K (30 min at 50°C). After purifying by phenol/chloroform extraction and ethanol precipitation, the resulting DNA was used as a template for *in vitro* transcription using the AmpliScribe T7 High Yield Transcription Kit (Lucigen). RNA product was electroporated into BHK-21 cells using a GenePulser Xcell electroporator (Bio-Rad) at 850 V, 25 mF, and infinite Ω. The P0 virus stocks were recovered within four days and propagated in C6/36 cells to generate P1 virus stocks. Titers of virus stocks were determined by focus-forming assay (FFA) using Vero cells [79].

Generation of anti-WNV NS1 human antibodies. The WNV-immune human donors were described previously [54]. Peripheral blood mononuclear cells (PBMCs) were isolated by gradient centrifugation of heparinized blood layered on Ficoll Histopaque. Subsequently, B cells from donor 876 were transformed by incubating in medium containing Epstein Barr virus (obtained

from the supernatant of B95.8 cells, ATCC), 2.5 μg/mL CpG (phosphorothioate-modified oligodeoxynucleotide ZOEZOEZZZZZOEEZOEZZZT, Life Technologies), 10 μM Chk2 inhibitor (Sigma), and 10 μg/mL cyclosporine A (Sigma). After incubating in 384-well plates for 7 days, the B cells were expanded into 4 96-well plates containing CpG, Chk2 inhibitor, and irradiated heterologous human PBMCs (to serve as feeder layers for lymphoblastoid cell clusters). After 3 days, supernatants (5 μL per well) were screened by ELISA for binding to recombinant soluble WNV NS1 protein (Native Antigen).

For wells with anti-NS1 antibody, cells were subjected to electrofusion with HMMA2.5 myeloma cells [80]. The fused cells then were cultured for 14 to 18 days in selective medium containing 100 μM hypoxanthine, 0.4 μM aminopterin, 16 μM thymidine (HAT Media Supplement, Sigma HO262) and 7 μg/mL ouabain (Sigma O3125). Hybridomas were screened by ELISA for anti-WNV NS1 antibody, and cells from positive wells were cloned by sorting live, single cells into 384-well plates using a FACSAria III cell sorter (Becton Dickinson). Cloned cells were cultured for about 14 days and screened by ELISA again for NS1-specific antibody. For purification of antibody from hybridoma clones, cells were cultured in serum-free medium (Hybridoma SFM, Life Technologies) for 21 days. Antibody in the supernatant was captured by affinity chromatography on HiTrap MabSelect SuRe columns (Life Technologies) according to the manufacturer's protocol. Antibodies subsequently were eluted from the affinity columns and concentrated using Amicon centrifugal filters (Millipore). Antibody heavy and light chain variable genes were amplified by RT–PCR from hybridoma cell RNA and Sanger sequenced. Complementary DNAs encoding antibody variable genes were synthesized and cloned into expression vectors for recombinant human IgG1, IgG1 LALA, or IgG1 LALA-PG. Recombinant antibodies were expressed in 293F cells.

Recombinant antibody purification. To generate recombinant antibodies, mRNA was isolated from hybridoma cell lines, and heavy and light chain gene sequences were amplified using 5′ RACE (Rapid Amplification of cDNA Ends). A Pacific Biosciences instrument then was used to sequence amplicon libraries. To express recombinant antibodies, heavy and light chain genes were cloned into pML or Twist plasmid expression vectors. Constructs were transfected into ExpiCHO cells using ExpiFectamine CHO reagent according to the vendor's instructions (Thermo Fisher Scientific). After 7 to 8 days, cell supernatants were harvested and clarified through 0.45 μm filters. Antibody then was purified by affinity chromatography (ÄKTA pure, Cytiva) using HiTrap MabSelect SuRe (IgG1) or Protein G (IgG3) columns (Cytiva). Eluted antibody was quenched immediately in Tris buffer and buffer-exchanged into DPBS by centrifugation or dialysis.

Epitope mapping. Epitope mapping was performed using charge-reversal mutagenesis at targeted residues in WNV NS1. A mammalian expression vector pFM-A1.2 was constructed to encode full-length WNV NS1 (strain 382-99), preceded by the cluster of differentiation 33 (CD33) signal sequence and followed in frame with a 6X histidine affinity tag. The pFM-A1.2 expression vector was subjected to site-directed mutagenesis (GenScript or GENEWIZ) to generate a library of 102 total mutants. Hydrophobic and negatively charged residues were substituted with arginine, and positively charged residues were substituted with aspartic acid or glutamic acid. In a few cases, residues were substituted with alanine. HEK293T cells were transfected with each substitution variant plasmid using Lipofectamine 3000 (Thermo Fisher) and incubated at 37°C for 1 day to allow for NS1 expression. Cells were fixed in 4% PFA in PBS for 10 min at room temperature and washed in PBS containing 2 mM EDTA and 0.2% BSA (FACS buffer). Subsequently, cells were incubated for 1 h at 4°C with individual mAbs or a cocktail of 5 anti-WNV NS1 mAbs (WNV-96, WNV-98, WNV-100, WNV-113, and WNV-116) as a control for NS1 protein expression. After

washing, cells were incubated for 30 min at 4°C in Alexa Fluor 647 conjugated to goat anti-human or goat anti-mouse IgG (1:2,000 dilution; Thermo Fisher Scientific). Flow cytometry was performed on a MACSQuant Analyzer (Miltenyi Biotec). Based on previously published criteria [46,81], critical binding residues for each mAb were defined as substitution variants with <25% reactivity relative to WT protein. Only variants with >70% reactivity (compared to WT) to the oligoclonal antibody pool were considered for epitope mapping. Critical binding residues were mapped onto the NS1 dimer structure (PDB 406D) using PyMOL software (version 2.3.4, Schrödinger).

Biolayer interferometry-based antibody competition. Competition-binding studies were performed using a FortéBio HTX biolayer interferometry instrument. HIS1K sensor tips (FortéBio lot #1907172) were soaked in wells containing recombinant WNV NS1 at 5 µg/mL diluted in kinetics buffer (Pall, lot #6090032) for 180 seconds. After a brief baseline step, a first antibody then was associated to coated sensortips at 100 µg/mL for 600 sec to achieve complete saturation. After another baseline step, tips were soaked in a second antibody at 100 µg/mL for 180 sec. Binning data were analyzed using FortéBio Data Analysis HT software (version 11.1.2.48). A buffer-only control was used to normalize all antibody binding. The competition groups were defined using a Pearson correlation analysis (embedded in Data Analysis HT software).

Antibody competition-binding ELISA. MaxiSorp 96-well microtiter plates (Nunc) were coated overnight at 4°C with 20 ng of recombinant WNV NS1 protein (Native Antigen) in 50 µL of sodium bicarbonate buffer, pH 9.3. Subsequently, plates were washed four times with PBS and blocked with ELISA buffer (PBS containing 2% BSA and 0.05% Tween-20) for 1 h at 37°C. Plates then were incubated with anti-WNV NS1 murine mAbs at 10 µg/mL for 1 h at room temperature. Without washing, anti-WNV NS1 human mAbs were added to the plates at pre-optimized

concentrations and incubated for 10 min at room temperature. Plates then were washed four times in PBS containing 0.05% Tween 20 and incubated with goat anti-human IgG conjugated to horseradish peroxidase (1:2,000 dilution; Jackson ImmunoResearch 109-035-088) for 30 min at room temperature. After washing, plates were developed using 3,3',5,5'-tetramethylbenzidine substrate (Agilent) for 5 to 10 min. The reaction was stopped using 2 N H_2SO_4 and absorbance (450 nm) was read using a TriStar Microplate Reader (Berthold Technologies).

NS1 ELISA. 50 ng of WNV, JEV, DENV2, ZIKV, YFV, or TBEV NS1 proteins (all from Native Antigen) were immobilized on MaxiSorp microtiter plates overnight at 4°C in 50 μL of sodium bicarbonate buffer, pH 9.3. Plates were washed four times with PBS and blocked with ELISA buffer by incubating for 1 h at 37°C. Subsequently, plates were incubated with mAb (anti-WNV NS1 or isotype control) diluted in ELISA buffer for 1 h at room temperature. For cross-reactivity ELISAs, plates were incubated with mAb at 1 μg/mL; for avidity studies, plates were incubated with serial dilutions of mAb as indicated in the figures. After washing four times in PBS containing 0.05% Tween-20, plates were incubated with biotinylated goat anti-human or goat anti-mouse IgG (H + L; 1:2000 dilution; Jackson ImmunoResearch) for 1 h. Plates were washed again and incubated with streptavidin-conjugated horseradish peroxidase (1:625 dilution; Vector Laboratories) for 15 min. After a final wash series, plates were developed and absorbance was read as described above. For avidity studies, the EC_{50} of binding to solid-phase NS1 was calculated using a 4-parameter logistic curve.

Binding to cell-surface NS1. Vero cells were inoculated with WNV at an MOI of 5. After 24 h, the cells were washed in PBS and detached by incubating in PBS containing 10 mM EDTA for 15 min at 37°C. The cells were washed in chilled FACS buffer and pelleted by centrifugation at 300 x g for 3 min at 4°C. Subsequently, the cells were resuspended in serial dilutions (20 μg/mL to 2

pg/mL) of mAb (anti-NS1 or isotype control) for 1 h at 4°C. After washing in FACS buffer, cells were stained with Fixable Viability Dye eFluor 506 (1:1000 dilution; eBioscience) and Alexa Fluor 647 conjugated to goat anti-human or anti-mouse IgG (1:2000 dilution; Thermo Fisher). Cells were washed again before fixing in 4% PFA in PBS for 10 min, and then processed on a MACSQuant Analyzer (Miltenyi Biotec). After gating on live cells, the percent reactivity to cell-surface-expressed NS1 was determined for each dilution of mAb. The EC_{50} of binding to cell-surface NS1 was calculated using a 4-parameter logistic curve.

Mouse experiments. Animal studies were performed using 4- to 5-week-old C57BL/6J male mice (Jackson Laboratory, 000664). Mice were inoculated by subcutaneous injection in the footpad with 10^2 FFU of WNV (New York strain 382-99) in a 50 μL volume. Concurrently, mice were administered mAb (anti-WNV NS1 or an isotype control, hCHK-152) [56] by intraperitoneal injection. Mice were euthanized after 21 days or on day 7 for assessment of virus titers in specific organs. Mice were perfused with 20 mL of PBS prior to organ harvest.

Viral burden analysis. Mouse organs were weighed and homogenized by zirconia bead dissociation using a MagNA Lyzer (Roche) in a volume of DMEM containing 2% FBS. RNA was isolated from the tissue homogenates using either the RNeasy 96 kit (Qiagen) or the MagMAX-96 Viral RNA Isolation kit (Applied Biosystems). WNV RNA levels were determined by TaqMan one-step quantitative reverse transcriptase PCR (qRT-PCR) using the following primer and probe sequences: forward primer, 5′-GGGTCAGCACGTTTGTCATTG-3′; reverse primer, 5′-TCAGCGATCTCTCCACCAAAG-3′ probe, 5′-TGCCCGACCATGGGAGAAGCTC-3′ [79]. An RNA standard curve was generated using a defined viral stock to calculate FFU equivalents from RNA levels.

Data analysis. The statistical tests for each data set are indicated in the respective legends and were performed using Prism version 8 software (GraphPad). The EC_{50} of mAb binding to solid-phase (ELISA) and cell-surface-expressed (flow cytometry) NS1 was determined by nonlinear regression using a 4-parameter logistic curve. Survival curves were analyzed by the log-rank Mantel-Cox test with a Bonferroni correction. To compare viral titers in specific organs between mAb groups, Mann-Whitney tests or one-way ANOVAs with Dunn's post-test were performed. Statistical significance was defined as $p < 0.05$. FlowJo software version 10 (Becton, Dickinson and Company) was used to analyze all flow cytometry data sets.

Data availability. All primary data will be made publicly available upon publication. Antibodies will be made available under an MTA with Vanderbilt University.

3.6 Acknowledgements

This study was supported by NIH grants R01 AI073755 and 75N93019C00062 and contract HHSN272201400058C and HHSN272201700060C. A.W.W. was supported by an NIH pre-doctoral training grant award (T32 5T32AI007172-38) and the Medical Scientist Training Program. T.C.P was supported by the Intramural Program of NIAID. We thank Rachel Nargi, Rachel Sutton, Erica Armstrong, and Robert Carnahan of Vanderbilt for help with preparation of recombinant human antibodies, and Robin Bombardi, Joe Reidy and Andrew Trivette of Vanderbilt for sequence analysis support.

3.7 References

1 Roehrig, J. T. West nile virus in the United States - a historical perspective. *Viruses* **5**, 3088-3108, doi:10.3390/v5123088 (2013).

2 Daep, C. A., Muñoz-Jordán, J. L. & Eugenin, E. A. Flaviviruses, an expanding threat in public health: focus on dengue, West Nile, and Japanese encephalitis virus. *J Neurovirol* **20**, 539-560, doi:10.1007/s13365-014-0285-z (2014).

3 Patel, H., Sander, B. & Nelder, M. P. Long-term sequelae of West Nile virus-related illness: a systematic review. *Lancet Infect Dis* **15**, 951-959, doi:10.1016/s1473-3099(15)00134-6 (2015).

4 Murray, K. O. *et al.* Survival Analysis, Long-Term Outcomes, and Percentage of Recovery up to 8 Years Post-Infection among the Houston West Nile Virus Cohort. *PLOS ONE* **9**, e102953, doi:10.1371/journal.pone.0102953 (2014).

5 Camacho, L. A. *et al.* Immunogenicity of WHO-17D and Brazilian 17DD yellow fever vaccines: a randomized trial. *Rev Saude Publica* **38**, 671-678, doi:10.1590/s0034-89102004000500009 (2004).

6 Ishikawa, T., Yamanaka, A. & Konishi, E. A review of successful flavivirus vaccines and the problems with those flaviviruses for which vaccines are not yet available. *Vaccine* **32**, 1326-1337, doi:https://doi.org/10.1016/j.vaccine.2014.01.040 (2014).

7 Shukla, R., Ramasamy, V., Shanmugam, R. K., Ahuja, R. & Khanna, N. Antibody-Dependent Enhancement: A Challenge for Developing a Safe Dengue Vaccine. *Front Cell Infect Microbiol* **10**, 572681, doi:10.3389/fcimb.2020.572681 (2020).

8 Fischer, C., de Oliveira-Filho, E. F. & Drexler, J. F. Viral emergence and immune interplay in flavivirus vaccines. *The Lancet Infectious Diseases* **20**, 15-17, doi:https://doi.org/10.1016/S1473-3099(19)30697-8 (2020).

9 Modhiran, N. *et al.* A broadly protective antibody that targets the flavivirus NS1 protein. *Science* **371**, 190-194, doi:10.1126/science.abb9425 (2021).

10 Bailey, M. J. *et al.* Antibodies Elicited by an NS1-Based Vaccine Protect Mice against Zika Virus. *mBio* **10**, doi:10.1128/mBio.02861-18 (2019).

11 Bailey, M. J. *et al.* Human antibodies targeting Zika virus NS1 provide protection against disease in a mouse model. *Nat Commun* **9**, 4560, doi:10.1038/s41467-018-07008-0 (2018).

12 Winkler, G., Maxwell, S. E., Ruemmler, C. & Stollar, V. Newly synthesized dengue-2 virus nonstructural protein NS1 is a soluble protein but becomes partially hydrophobic and membrane-associated after dimerization. *Virology* **171**, 302-305, doi:10.1016/0042-6822(89)90544-8 (1989).

13 Winkler, G., Randolph, V. B., Cleaves, G. R., Ryan, T. E. & Stollar, V. Evidence that the mature form of the flavivirus nonstructural protein NS1 is a dimer. *Virology* **162**, 187-196, doi:10.1016/0042-6822(88)90408-4 (1988).

14 Lindenbach, B. D. & Rice, C. M. trans-Complementation of yellow fever virus NS1 reveals a role in early RNA replication. *J Virol* **71**, 9608-9617 (1997).

15 Youn, S., Ambrose, R. L., Mackenzie, J. M. & Diamond, M. S. Non-structural protein-1 is required for West Nile virus replication complex formation and viral RNA synthesis. *Virology Journal* **10**, 339, doi:10.1186/1743-422X-10-339 (2013).

16 Youn, S. *et al.* Evidence for a genetic and physical interaction between nonstructural proteins NS1 and NS4B that modulates replication of West Nile virus. *J Virol* **86**, 7360-7371, doi:10.1128/jvi.00157-12 (2012).

17 Plaszczyca, A. *et al.* A novel interaction between dengue virus nonstructural protein 1 and the NS4A-2K-4B precursor is required for viral RNA replication but not for formation of the membranous replication organelle. *PLoS Pathog* **15**, e1007736, doi:10.1371/journal.ppat.1007736 (2019).
18 Noisakran, S. *et al.* Association of dengue virus NS1 protein with lipid rafts. *J Gen Virol* **89**, 2492-2500, doi:10.1099/vir.0.83620-0 (2008).
19 Schlesinger, J. J., Brandriss, M. W., Putnak, J. R. & Walsh, E. E. Cell surface expression of yellow fever virus non-structural glycoprotein NS1: consequences of interaction with antibody. *J Gen Virol* **71 (Pt 3)**, 593-599, doi:10.1099/0022-1317-71-3-593 (1990).
20 Youn, S., Cho, H., Fremont, D. H. & Diamond, M. S. A Short N-Terminal Peptide Motif on Flavivirus Nonstructural Protein NS1 Modulates Cellular Targeting and Immune Recognition. *Journal of Virology* **84**, 9516-9532, doi:10.1128/jvi.00775-10 (2010).
21 Crooks, A. J., Lee, J. M., Easterbrook, L. M., Timofeev, A. V. & Stephenson, J. R. The NS1 protein of tick-borne encephalitis virus forms multimeric species upon secretion from the host cell. *J Gen Virol* **75 (Pt 12)**, 3453-3460, doi:10.1099/0022-1317-75-12-3453 (1994).
22 Chung, K. M. & Diamond, M. S. Defining the levels of secreted non-structural protein NS1 after West Nile virus infection in cell culture and mice. *J Med Virol* **80**, 547-556, doi:10.1002/jmv.21091 (2008).
23 Flamand, M. *et al.* Dengue virus type 1 nonstructural glycoprotein NS1 is secreted from mammalian cells as a soluble hexamer in a glycosylation-dependent fashion. *J Virol* **73**, 6104-6110, doi:10.1128/jvi.73.7.6104-6110.1999 (1999).
24 Gutsche, I. *et al.* Secreted dengue virus nonstructural protein NS1 is an atypical barrel-shaped high-density lipoprotein. *Proc Natl Acad Sci U S A* **108**, 8003-8008, doi:10.1073/pnas.1017338108 (2011).
25 Akey, D. L. *et al.* Flavivirus NS1 structures reveal surfaces for associations with membranes and the immune system. *Science* **343**, 881-885, doi:10.1126/science.1247749 (2014).
26 Young, P. R., Hilditch, P. A., Bletchly, C. & Halloran, W. An Antigen Capture Enzyme-Linked Immunosorbent Assay Reveals High Levels of the Dengue Virus Protein NS1 in the Sera of Infected Patients. *Journal of Clinical Microbiology* **38**, 1053-1057 (2000).
27 Bosch, I. *et al.* Rapid antigen tests for dengue virus serotypes and Zika virus in patient serum. *Science Translational Medicine* **9**, eaan1589, doi:10.1126/scitranslmed.aan1589 (2017).
28 Macdonald, J. *et al.* NS1 Protein Secretion during the Acute Phase of West Nile Virus Infection. *Journal of Virology* **79**, 13924-13933, doi:10.1128/jvi.79.22.13924-13933.2005 (2005).
29 Avirutnan, P. *et al.* Secreted NS1 of dengue virus attaches to the surface of cells via interactions with heparan sulfate and chondroitin sulfate E. *PLoS Pathog* **3**, e183, doi:10.1371/journal.ppat.0030183 (2007).
30 Chung, K. M. *et al.* West Nile virus nonstructural protein NS1 inhibits complement activation by binding the regulatory protein factor H. *Proc Natl Acad Sci U S A* **103**, 19111-19116, doi:10.1073/pnas.0605668103 (2006).
31 Avirutnan, P. *et al.* Antagonism of the complement component C4 by flavivirus nonstructural protein NS1. *J Exp Med* **207**, 793-806, doi:10.1084/jem.20092545 (2010).

32 Avirutnan, P. *et al.* Binding of flavivirus nonstructural protein NS1 to C4b binding protein modulates complement activation. *J Immunol* **187**, 424-433, doi:10.4049/jimmunol.1100750 (2011).
33 Conde, J. N. *et al.* Inhibition of the Membrane Attack Complex by Dengue Virus NS1 through Interaction with Vitronectin and Terminal Complement Proteins. *J Virol* **90**, 9570-9581, doi:10.1128/jvi.00912-16 (2016).
34 Chao, C. H. *et al.* Dengue virus nonstructural protein 1 activates platelets via Toll-like receptor 4, leading to thrombocytopenia and hemorrhage. *PLoS Pathog* **15**, e1007625, doi:10.1371/journal.ppat.1007625 (2019).
35 Modhiran, N. *et al.* Dengue virus NS1 protein activates immune cells via TLR4 but not TLR2 or TLR6. *Immunol Cell Biol* **95**, 491-495, doi:10.1038/icb.2017.5 (2017).
36 Modhiran, N. *et al.* Dengue virus NS1 protein activates cells via Toll-like receptor 4 and disrupts endothelial cell monolayer integrity. *Sci Transl Med* **7**, 304ra142, doi:10.1126/scitranslmed.aaa3863 (2015).
37 Beatty, P. R. *et al.* Dengue virus NS1 triggers endothelial permeability and vascular leak that is prevented by NS1 vaccination. *Science Translational Medicine* **7**, 304ra141-304ra141, doi:10.1126/scitranslmed.aaa3787 (2015).
38 Biering, S. B. *et al.* Structural basis for antibody inhibition of flavivirus NS1–triggered endothelial dysfunction. *Science* **371**, 194-200, doi:10.1126/science.abc0476 (2021).
39 Puerta-Guardo, H. *et al.* Flavivirus NS1 Triggers Tissue-Specific Vascular Endothelial Dysfunction Reflecting Disease Tropism. *Cell Rep* **26**, 1598-1613.e1598, doi:10.1016/j.celrep.2019.01.036 (2019).
40 Puerta-Guardo, H., Glasner, D. R. & Harris, E. Dengue Virus NS1 Disrupts the Endothelial Glycocalyx, Leading to Hyperpermeability. *PLOS Pathogens* **12**, e1005738, doi:10.1371/journal.ppat.1005738 (2016).
41 Puerta-Guardo, H. *et al.* Zika Virus Nonstructural Protein 1 Disrupts Glycosaminoglycans and Causes Permeability in Developing Human Placentas. *J Infect Dis* **221**, 313-324, doi:10.1093/infdis/jiz331 (2020).
42 Wang, C. *et al.* Endocytosis of flavivirus NS1 is required for NS1-mediated endothelial hyperpermeability and is abolished by a single N-glycosylation site mutation. *PLoS Pathog* **15**, e1007938, doi:10.1371/journal.ppat.1007938 (2019).
43 Edeling, M. A., Diamond, M. S. & Fremont, D. H. Structural basis of Flavivirus NS1 assembly and antibody recognition. *Proc Natl Acad Sci U S A* **111**, 4285-4290, doi:10.1073/pnas.1322036111 (2014).
44 Brown, W. C. *et al.* Extended surface for membrane association in Zika virus NS1 structure. *Nat Struct Mol Biol* **23**, 865-867, doi:10.1038/nsmb.3268 (2016).
45 Xu, X. *et al.* Contribution of intertwined loop to membrane association revealed by Zika virus full-length NS1 structure. *Embo j* **35**, 2170-2178, doi:10.15252/embj.201695290 (2016).
46 Wessel, A. W. *et al.* Antibodies targeting epitopes on the cell-surface form of NS1 protect against Zika virus infection during pregnancy. *Nature Communications* **11**, 5278, doi:10.1038/s41467-020-19096-y (2020).
47 Chung, K. M. *et al.* Antibodies against West Nile Virus nonstructural protein NS1 prevent lethal infection through Fc gamma receptor-dependent and -independent mechanisms. *J Virol* **80**, 1340-1351, doi:10.1128/jvi.80.3.1340-1351.2006 (2006).

48 Lee, T. H. *et al.* A cross-protective mAb recognizes a novel epitope within the flavivirus NS1 protein. *Journal of General Virology* **93**, 20-26, doi:https://doi.org/10.1099/vir.0.036640-0 (2012).
49 Henchal, E. A., Henchal, L. S. & Schlesinger, J. J. Synergistic interactions of anti-NS1 monoclonal antibodies protect passively immunized mice from lethal challenge with dengue 2 virus. *J Gen Virol* **69 (Pt 8)**, 2101-2107, doi:10.1099/0022-1317-69-8-2101 (1988).
50 Schlesinger, J. J., Brandriss, M. W. & Walsh, E. E. Protection against 17D yellow fever encephalitis in mice by passive transfer of monoclonal antibodies to the nonstructural glycoprotein gp48 and by active immunization with gp48. *J Immunol* **135**, 2805-2809 (1985).
51 Schlesinger, J. J., Foltzer, M. & Chapman, S. The Fc portion of antibody to yellow fever virus NS1 is a determinant of protection against YF encephalitis in mice. *Virology* **192**, 132-141, doi:10.1006/viro.1993.1015 (1993).
52 Chung, K. M., Thompson, B. S., Fremont, D. H. & Diamond, M. S. Antibody Recognition of Cell Surface-Associated NS1 Triggers Fc-γ Receptor-Mediated Phagocytosis and Clearance of West Nile Virus-Infected Cells. *Journal of Virology* **81**, 9551-9555, doi:10.1128/jvi.00879-07 (2007).
53 Chung, W. M. *et al.* The 2012 West Nile encephalitis epidemic in Dallas, Texas. *Jama* **310**, 297-307, doi:10.1001/jama.2013.8267 (2013).
54 Goo, L. *et al.* A protective human monoclonal antibody targeting the West Nile virus E protein preferentially recognizes mature virions. *Nature microbiology* **4**, 71-77, doi:10.1038/s41564-018-0283-7 (2019).
55 Engle, M. J. & Diamond, M. S. Antibody prophylaxis and therapy against West Nile virus infection in wild-type and immunodeficient mice. *J Virol* **77**, 12941-12949, doi:10.1128/jvi.77.24.12941-12949.2003 (2003).
56 Pal, P. *et al.* Development of a highly protective combination monoclonal antibody therapy against Chikungunya virus. *PLoS Pathog* **9**, e1003312, doi:10.1371/journal.ppat.1003312 (2013).
57 Saunders, K. O. Conceptual Approaches to Modulating Antibody Effector Functions and Circulation Half-Life. *Frontiers in Immunology* **10**, doi:10.3389/fimmu.2019.01296 (2019).
58 Tang, Y. *et al.* Regulation of Antibody-Dependent Cellular Cytotoxicity by IgG Intrinsic and Apparent Affinity for Target Antigen. *The Journal of Immunology* **179**, 2815-2823, doi:10.4049/jimmunol.179.5.2815 (2007).
59 ÖHLANDLR, C., LARSSON, Å. & PERLMANN, P. Regulation of Effector Functions of Human K-Cells and Monocytes by Antigen Density of the Target Cells. *Scandinavian Journal of Immunology* **13**, 503-510, doi:10.1111/j.1365-3083.1981.tb00163.x (1981).
60 Lux, A., Yu, X., Scanlan, C. N. & Nimmerjahn, F. Impact of Immune Complex Size and Glycosylation on IgG Binding to Human FcγRs. *The Journal of Immunology* **190**, 4315-4323, doi:10.4049/jimmunol.1200501 (2013).
61 Lucisano Valim, Y. M. & Lachmann, P. J. The effect of antibody isotype and antigenic epitope density on the complement-fixing activity of immune complexes: a systematic study using chimaeric anti-NIP antibodies with human Fc regions. *Clin Exp Immunol* **84**, 1-8, doi:10.1111/j.1365-2249.1991.tb08115.x (1991).

62 Crill, W. *et al.* Sculpting humoral immunity through dengue vaccination to enhance protective immunity. *Frontiers in Immunology* **3**, doi:10.3389/fimmu.2012.00334 (2012).
63 Klimka, A. *et al.* Epitope-specific immunity against Staphylococcus aureus coproporphyrinogen III oxidase. *npj Vaccines* **6**, 11, doi:10.1038/s41541-020-00268-2 (2021).
64 Weidenbacher, P. A. & Kim, P. S. Protect, modify, deprotect (PMD): A strategy for creating vaccines to elicit antibodies targeting a specific epitope. *Proceedings of the National Academy of Sciences* **116**, 9947-9952, doi:10.1073/pnas.1822062116 (2019).
65 Chuang, Y. C., Lin, J., Lin, Y. S., Wang, S. & Yeh, T. M. Dengue Virus Nonstructural Protein 1-Induced Antibodies Cross-React with Human Plasminogen and Enhance Its Activation. *J Immunol* **196**, 1218-1226, doi:10.4049/jimmunol.1500057 (2016).
66 Cheng, H. J. *et al.* Correlation between serum levels of anti-endothelial cell autoantigen and anti-dengue virus nonstructural protein 1 antibodies in dengue patients. *Am J Trop Med Hyg* **92**, 989-995, doi:10.4269/ajtmh.14-0162 (2015).
67 Cheng, H. J. *et al.* Anti-dengue virus nonstructural protein 1 antibodies recognize protein disulfide isomerase on platelets and inhibit platelet aggregation. *Mol Immunol* **47**, 398-406, doi:10.1016/j.molimm.2009.08.033 (2009).
68 Cheng, H. J. *et al.* Proteomic analysis of endothelial cell autoantigens recognized by anti-dengue virus nonstructural protein 1 antibodies. *Exp Biol Med (Maywood)* **234**, 63-73, doi:10.3181/0805-rm-147 (2009).
69 Liu, I. J., Chiu, C. Y., Chen, Y. C. & Wu, H. C. Molecular mimicry of human endothelial cell antigen by autoantibodies to nonstructural protein 1 of dengue virus. *J Biol Chem* **286**, 9726-9736, doi:10.1074/jbc.M110.170993 (2011).
70 Sun, D. S. *et al.* Antiplatelet autoantibodies elicited by dengue virus non-structural protein 1 cause thrombocytopenia and mortality in mice. *J Thromb Haemost* **5**, 2291-2299, doi:10.1111/j.1538-7836.2007.02754.x (2007).
71 Sun, D. S. *et al.* Endothelial Cell Sensitization by Death Receptor Fractions of an Anti-Dengue Nonstructural Protein 1 Antibody Induced Plasma Leakage, Coagulopathy, and Mortality in Mice. *J Immunol* **195**, 2743-2753, doi:10.4049/jimmunol.1500136 (2015).
72 Duan, H. *et al.* Glycan Masking Focuses Immune Responses to the HIV-1 CD4-Binding Site and Enhances Elicitation of VRC01-Class Precursor Antibodies. *Immunity* **49**, 301-311.e305, doi:10.1016/j.immuni.2018.07.005 (2018).
73 Hariharan, V. & Kane, R. S. Glycosylation as a tool for rational vaccine design. *Biotechnology and Bioengineering* **117**, 2556-2570, doi:https://doi.org/10.1002/bit.27361 (2020).
74 Bajic, G. *et al.* Influenza Antigen Engineering Focuses Immune Responses to a Subdominant but Broadly Protective Viral Epitope. *Cell Host Microbe* **25**, 827-835.e826, doi:10.1016/j.chom.2019.04.003 (2019).
75 Eggink, D., Goff, P. H. & Palese, P. Guiding the Immune Response against Influenza Virus Hemagglutinin toward the Conserved Stalk Domain by Hyperglycosylation of the Globular Head Domain. *Journal of Virology* **88**, 699-704, doi:doi:10.1128/JVI.02608-13 (2014).
76 Davis, C. W. *et al.* West Nile Virus Discriminates between DC-SIGN and DC-SIGNR for Cellular Attachment and Infection. *Journal of Virology* **80**, 1290-1301, doi:10.1128/jvi.80.3.1290-1301.2006 (2006).

77 Kinney, R. M. *et al.* Avian virulence and thermostable replication of the North American strain of West Nile virus. *Journal of General Virology* **87**, 3611-3622, doi:https://doi.org/10.1099/vir.0.82299-0 (2006).
78 Beasley, D. W. C. *et al.* Envelope Protein Glycosylation Status Influences Mouse Neuroinvasion Phenotype of Genetic Lineage 1 West Nile Virus Strains. *Journal of Virology* **79**, 8339-8347, doi:10.1128/jvi.79.13.8339-8347.2005 (2005).
79 Brien, J. D., Lazear, H. M. & Diamond, M. S. Propagation, Quantification, Detection, and Storage of West Nile Virus. *Current Protocols in Microbiology* **31**, 15D.13.11-15D.13.18, doi:10.1002/9780471729259.mc15d03s31 (2013).
80 Yu, X., McGraw, P. A., House, F. S. & Crowe, J. E., Jr. An optimized electrofusion-based protocol for generating virus-specific human monoclonal antibodies. *J Immunol Methods* **336**, 142-151, doi:10.1016/j.jim.2008.04.008 (2008).
81 Kim, A. S. *et al.* Protective antibodies against Eastern equine encephalitis virus bind to epitopes in domains A and B of the E2 glycoprotein. *Nature Microbiology* **4**, 187-197, doi:10.1038/s41564-018-0286-4 (2019).

Table 3.1 Characteristics of anti-WNV NS1 mAbs

MAb	Isotype	Cross-reactivity	EC_{50} Binding Surface NS1	Competition Group	Domain Localization	Critical Binding Residues
WNV-120	hIgG3	J	132.3	A	Wing, distal end	K44E, N82, G83
8NS1	mIgG1		263.6	A	Wing, distal end	T77, K80, G83
WNV-99	hIgG3	J, T	294.0	B	Wing, flexible loop	L123
16NS1	mIgG2a	J	90.3	B	Wing, flexible loop	W118, I122, L123
WNV-103	hIgG1		14.5	C	Wing, outer surface	K141
WNV-95	hIgG1		15.0	C	β-ladder, spaghetti loop	K261, R294
WNV-96	hIgG1		27.4	C	β-ladder, spaghetti loop	S239, D240, K261, R294
WNV-104	hIgG1		22.1	C	β-ladder, spaghetti loop	S239, K261, H293, R294
WNV-117	hIgG1		33.3	C	β-ladder, spaghetti loop	S239, D240, K261, R294
10NS1	mIgG2a		13.3	C	β-ladder, spaghetti loop	D240, N253, R256, K261, R294
22NS1	mIgG2a	J	18.8	C	β-ladder, spaghetti loop	S239, K261
WNV-98	hIgG1		10.8	C	β-ladder, loop face	R314
14NS1	mIgG2a		13.3	C	β-ladder, loop face	G295, R314
17NS1	mIgG2a		15.9	C	β-ladder, loop face	G295, R314
WNV-113	hIgG1		33.2	C	β-ladder, loop face	D341, E342, K343
WNV-106	hIgG1	J, D2, Y	22.5	C		*Not identified*
WNV-116	hIgG1		233.0	C		*Not identified*
WNV-100	hIgG1	J, D2, T	115.6	D	β-ladder, C-terminal tip	L307
9NS1	mIgG1	J. D2, Z, Y, T	73.5	D	β-ladder, C-terminal tip	L307
WNV-97	hIgG1	T	No binding	D	β-ladder, C-terminal tip	R339

Table 3.2 Amino acid sequences of anti-WNV NS1 human mAbs		
MAb	**Heavy Chain**	**Light Chain**
WNV-95	QVQLQESGPGLVKPSQTLSLTCTVSGGSINSGAFY WSWIRQHPGKGLEWIGFIYYSGSTYYNPSLRSRV TISVDTSKNQFSLKLISVTAADTAVYYCARDRPD DPGPYFDSWGRGTLVTVSS	QSALTQPASVSGSPGQSITISCTGTSNDVGRYNSVSWY QQHPGNAPKLMIYDVSNRPSGVSNRFSGSKSGNTASL TISGLQAEDEADYYCSSYTSSSSVVFGGGTKLTVL
WNV-96	QVQLVQSGAEVKKPGASVKVSCRPSGYIFTNYYI EWVRQAPGQGLEWMGIINPSGGKTTYAQKFQGR VTMTSDTSTSTVYMELSSLRSDDTAVYYCARDG NGSDYWGQGTRVTVSS	DVQMTQSPSSLSASVGDRVTITCRASQNINNYLNWYQ QKPGRAPKLLIYATSNLESGVPSRFSGSRSGADFTLTIS SLQPEDFASYYCQQSYNAPRTFGHGTKVEIK
WNV-97	QVQLVESGGGLVQPGGSLRVSCAASGFTFSTYE MNWVRQAPGKGLEWVSYISNSGTIIYYADSVKG RFTISRDNAKNSLYLQMNSLRAEDTAIYYCGRVL RDRDVVAGPPARVWDYYYYGMDVWGQGTTVT VSS	DIVMTQSPLSLPVTPGEPASISCRSSQSLLHSSGYNCLD WYLQKPGQSPQLLIYLRSNRASGVPDRFSGSGSGTDF TLKISRVEAEDVGVYYCMQTLQTPWTFGQGTKVEIK
WNV-98	QVQLVESGGGLVKPGGSLRLSCAASGFPFTNYY MSWIRQAPGKGLEWISYITSRGDTAYYADSVKG RFTVARDNSKNSLYLQMNSLRAEDTAMYFCARG GDDYADSWGQGILVTVSS	EIVLTQSPATLPLSPGERATLSCRASQSINTNLAWYQQ KPGQAPRLLIYETSHRASAIPARFSGSGSGTDFTLKISS LEPEDLAIYYCQQYRNWPQTFGQGTRLEIK
WNV-99	QVRLVESGGGVVQPGRSLRLSCAASGFTLSSYG MHWVRQAPGKGLEWVAIISYDGSDKYYADSVK GRFTISRDNSKNTLYLQMNSLRPEDTAMYYCAK PDRSSSPFAHWGQGTLVTVSS	SYELTQPPSVSVSPGQTARITCSGDALPKQYAFWYQQ KPGQTPVVVISKDSERPSGIPERFSGSSSGTTVTLTISG VQAEDEADYYCQSADSSGIWVFGGGTKLTVL
WNV-100	QLQLQESGSGLVKPSQTLSLTCTVSGDSIGSGGFS WTWIRQPPGKGLEWIGNIYHSGGTYYNPSLKSRV TISIDNSTHFSLKLSSVTAADSAVYYCARDRGMVI KRRPWSYGLDVWGQGTTVSVSS	QSVLTQPPSASGTPGQRVTISCSGGSSNIGSNSVSWYQ HLPRTAPKLLIYSNNQRSSGVPDRFSGSKSGTSASLAIS GLQSDDEADYYCAAWDDSLHVLFGGGTKLTVL
WNV-103	EVQLVESGGGLLQPGGSLRLSCAASGFSFSRYW MHWVRQAPGKGLIWVSRINTDGSTTIYADSVKG RFTVSRDNAKNTLFLQMSRLRPEDTAVYYCARVI ASPGISYGMDVWGHGTTVTVSS	SHELTQPPSVSVSPGQTATITCSGDALPKQYAYWYQQ KSGQAPVLVIYKDTKRPSGIPERFSGSSSGTVVTLTISG VQAEDEADYYCQSADISSTYVVFAGGTKLTVL
WNV-104	QVQLVESGGGVVQPGTSLRLSCAASGFTFRSYG MHWVRQAPGKGLEWVALIWYDGSNKYYADSV KGRFTISRDNSRSTLYLQMNSLRAEDTAVYYCAR DLGEYDSLVGPLYTARLGYWGQGTLVTVSS	DIQMTQSPSSLSASVGDRVTMTCQASQDISNYLNWYQ QKPGKAPNLLIYDASNLETGVPSRFSGSGSGTDFTFTIS SLQPEDIATYYCQQYDNLPITFGQGTRLEIK
WNV-113	QITLKESGPTLVKPTQTLTVTCTFSGFSLNTNGVG VGWIRQPPGKALEWLALIYWDDVKRYRPSLESR LTITKDTSKNQVVLTMTDMDPVDTGTYYCAHRF HSRGWYTFDYWGQGTRVTVSS	SYVLTQPPSVSVAPGQTARITCGGNNIGGKNVHWYQ QKPGQAPVLVVYDDNDRPSGIPERFSGSNSGNTATLTI SRVEAGDEADFYCQVWDSNSEHVVFGGGTKLTVL
WNV-116	QMQLVESGGGVVQPGRSLRLSCVASGFNFKTYV MNWVRQAPGKGLEWVAVILSDGDNKYYADSVK GRFTISRDNSKNTLFLQMDSLRADDTAVYYCTRV PHCSTSSCYKEYYNYYMDVWGKGTTVSVSS	EIVLTQSPATLSLSPGDRATLSCRASQSLSTSLAWYQQ KPGQAPRLVIYDASNRAADIPARFSGSGSGTDFTLTIR SLEPEDFAVYYCQQRSNWPPRYTFGQGTKLEIK
WNV-117	EVQLLESGGGLVQPGGSLRLSCAASGFTFSNYAM SWVRQAPGKGLEWVSSISDRGDYTYYADSVKGR FTISRDKSRNTLYLQIKSLRAEDTAVYYCAKCWG RGSYSGIPDYWGQGTLVTVSS	DIQMTQSPSSLSASVGDRVTISCQASHDITNFLNWYQQ KPGKAPKLLIYDASNLEAGVPSRFSGSGSGTDFTFTISS LQPEDIATYYCQQYDNLFITFGQGTRLEIK
WNV-120	KVQLEESGGGWVKPGRSLRLSCGASGFRFDDYA MHWVRQVPGKGLEWVSGISWDSDGIGYADSVK GRFTISRDNAKNSLFLQMNSLRAEDTALYYCVK DKGWLIQGRFDSWGQGIRVTVSS	DIVVTQSPDSLAVSLGERVTINCKTSQSVLYTFNNQNY LAWYQQKSGQPPKLLIYWASTRESGVPDRFSGSGSGT DFTLTISRLQAEDVAVYYCQQFYISPPGTFGQGTKVEI K

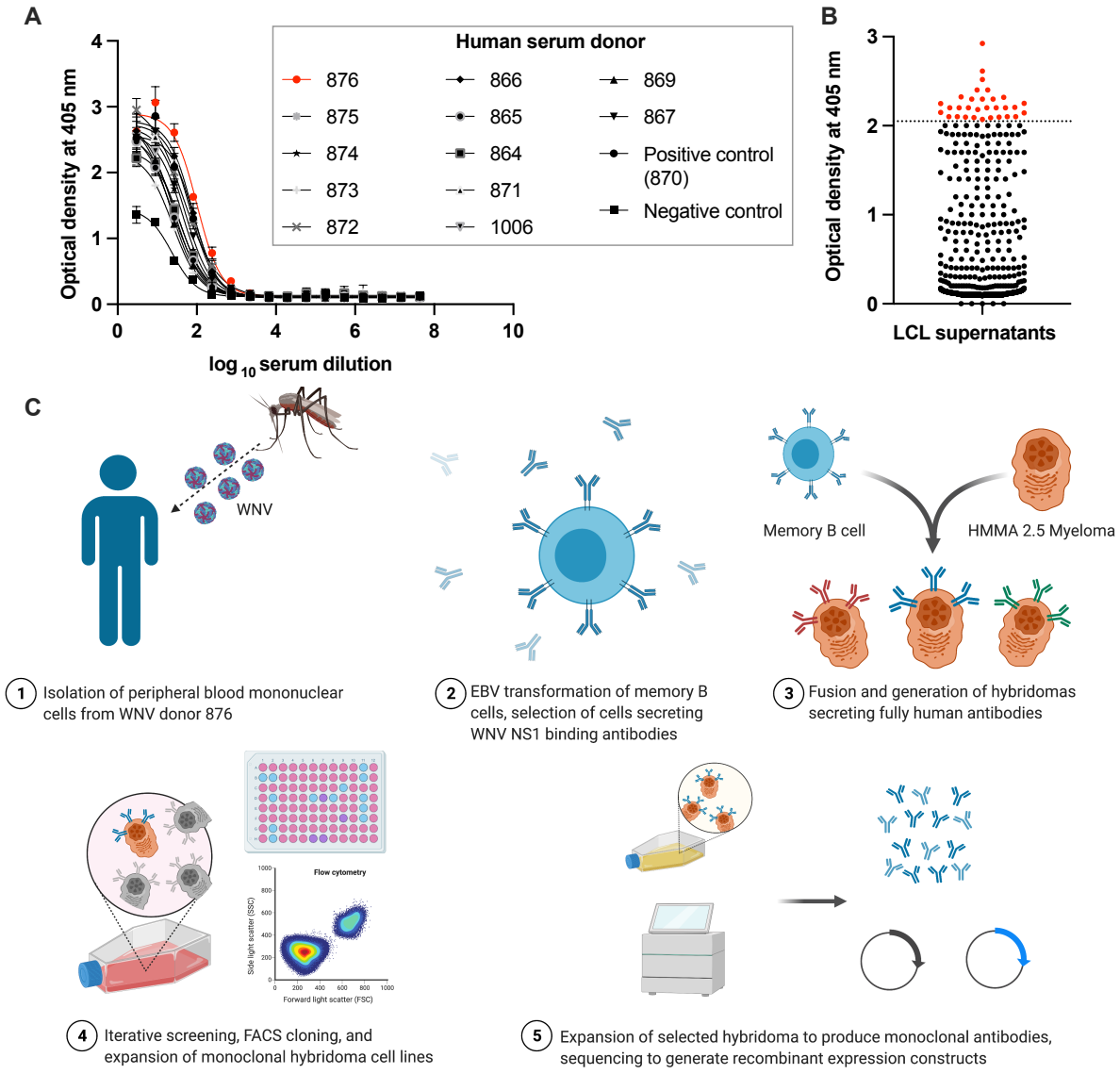

Figure 3.1. Scheme of NS1 hybridoma screen. (**A**) Analysis of human donor sera for binding to recombinant WNV NS1 by ELISA. A sample from the immune individual 876 was chosen for monoclonal antibody discovery. (**B**) Screening ELISA results of lymphoblastoid cell line (LCL) supernatants from transformed peripheral blood mononuclear cells (PBMCs). Wells highlighted in red represent LCLs chosen for electrofusion with HMMA 2.5 cells to generate hybridoma cell lines. (**C**) Full schematic of hybridoma discovery campaign design used to isolate WNV NS1-specific mAbs for further study. Panel adapted from "Monoclonal Antibodies Production" by Biorender.com (2021). Retrieved from https://app.biorender.com/biorender-templates.

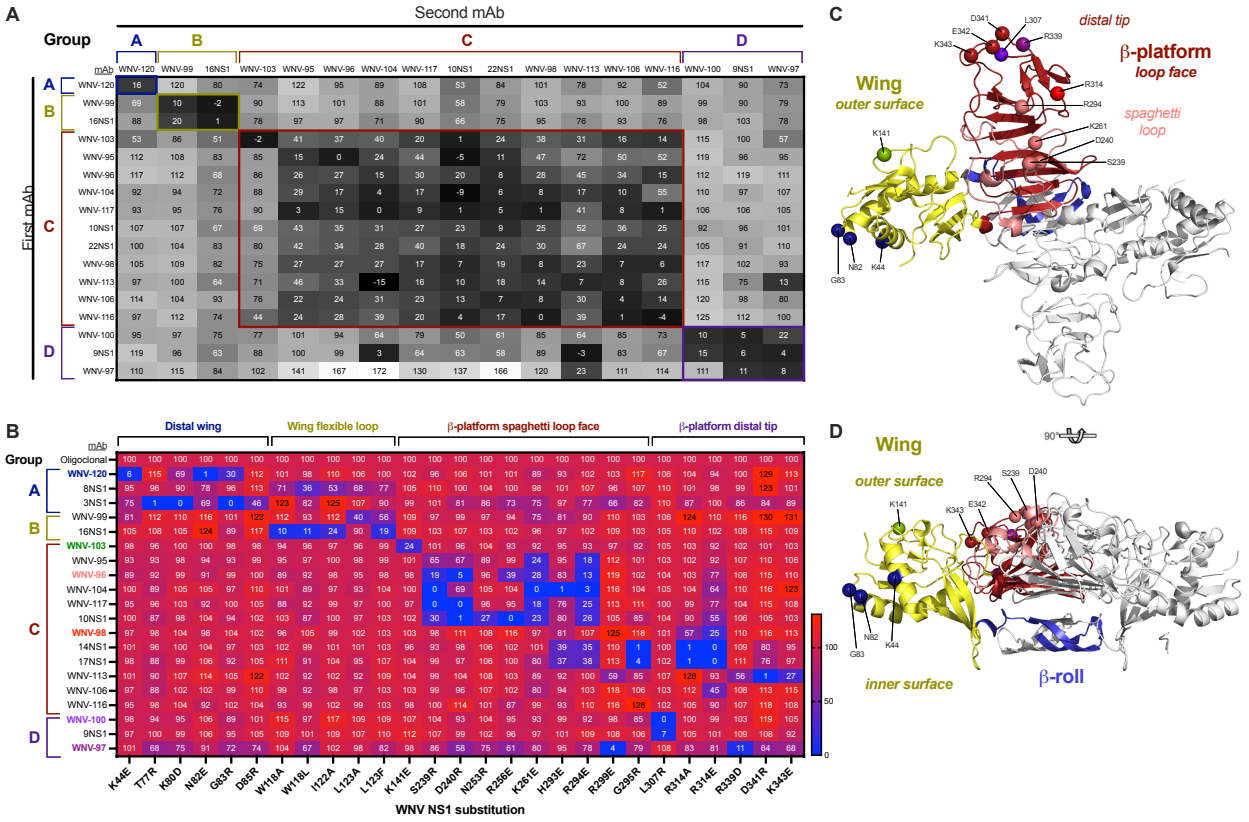

Figure 3.2. Epitope mapping. (**A**) BLI-based antibody competition for binding WNV NS1. Values represent the percent binding of the second mAb relative to its binding without a competing first mAb. Box shading indicates the degree of competition: black, strong competition (*i.e.*, minimum residual binding); gray, intermediate competition; and white, no competition. Antibodies are grouped and labeled according to their competition group. Data are representative of one experiment. (**B**) Heatmap of mAb binding to NS1 substitution variants relative to WT WNV NS1. 293T cells were transfected with plasmids encoding WNV NS1, and the mAb reactivity to each substitution variant relative to WT NS1 was measured by flow cytometry. Values represent the relative WT binding (average of two experiments), and only critical binding residues are shown (*i.e.*, residues at which substitution resulted in less than 25% binding relative to WT NS1). (**C-D**) Mapping of critical binding residues onto the WNV NS1 dimer structure (PDB 4O6D) in top view (**C**) or side view (**D**). Critical residues are indicated by spheres and are color-coded according to the mAb labels in **B**. In each structure, one monomer is gray, and one is color-coded by domain (blue, β-roll; yellow, wing; red, β-platform; and salmon, spaghetti loop). This figure was prepared using PyMOL (version 2.0, Schrödinger, LLC).

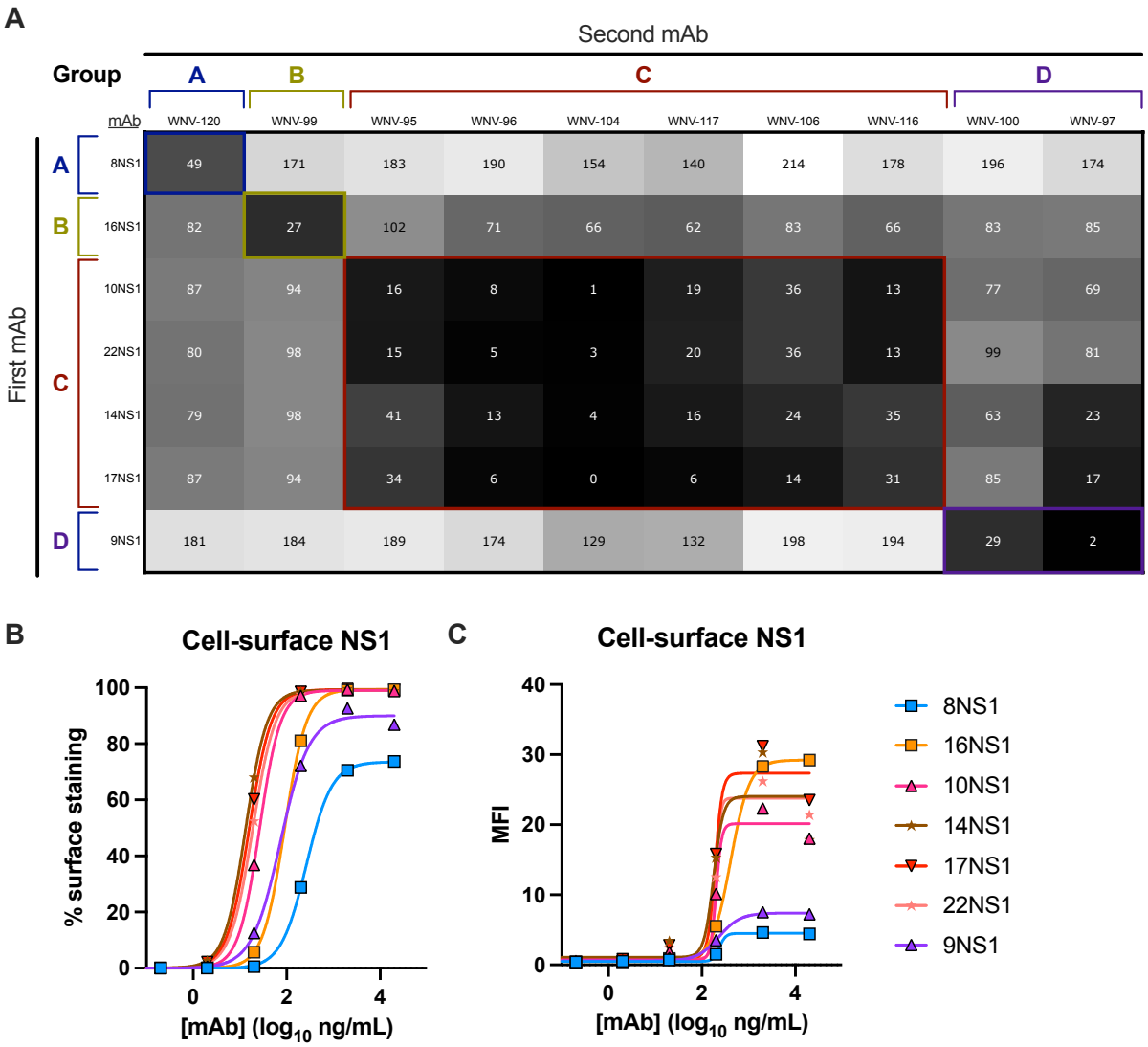

Figure 3.3. Binding properties of anti-WNV NS1 murine mAbs. (**A**) Recombinant, soluble WNV NS1 was adsorbed to plates and pre-bound to the indicated murine mAb first. Subsequently, the indicated human mAb was added, and the percent binding relative to binding in the absence of competition (*i.e.,* no first mAb) was determined by ELISA. Box values are the average of duplicates and representative of one experiment. (**B-C**) Binding to cell-surface-associated NS1 on live, WNV-infected Vero cells was assessed by flow cytometry. The percentage of cells staining (**B**) or the MFI (**C**) are from one experiment. EC_{50} values for binding to cell-surface-associated NS1 are reported in **Table 3.1**.

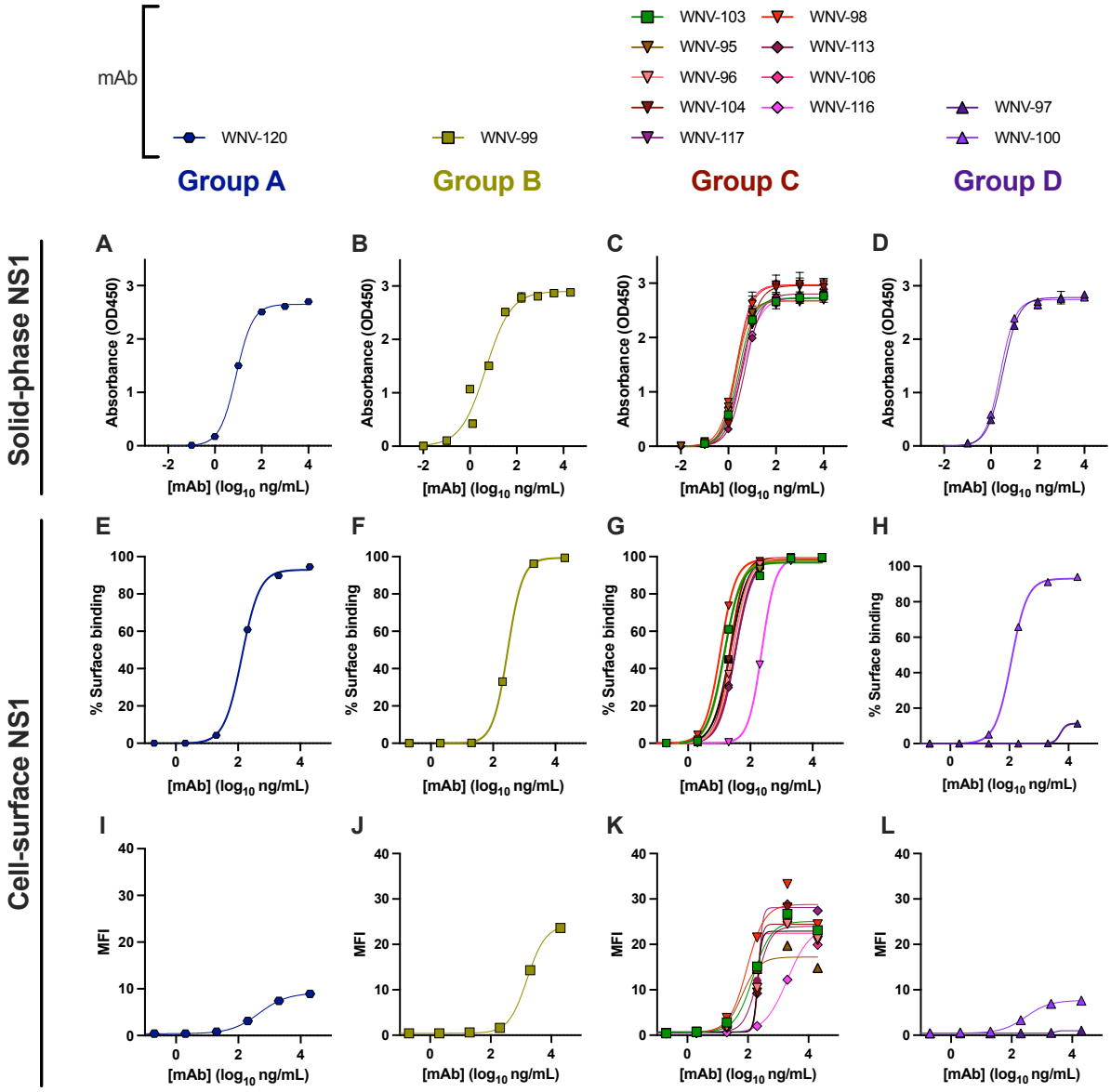

Figure 3.4. Binding properties of anti-WNV NS1 human mAbs. (**A-D**) Binding to recombinant, soluble WNV NS1 was determined by ELISA. Absorbance values are the average of duplicates and representative of two experiments. (**E-L**) Binding to cell-surface-associated NS1 on live, WNV-infected Vero cells was assessed by flow cytometry. The percentage of cells staining (**E-H**) or the mean fluorescence intensity (MFI; **I-L**) are shown for one experiment. EC_{50} values for binding to cell-surface-associated NS1 are reported in **Table 3.1**. Data are separated by antibody competition group: (**A, E, I**) group A; (**B, F, J**) group B; (**C, G, K**) group C; and (**D, H, L**) group D.

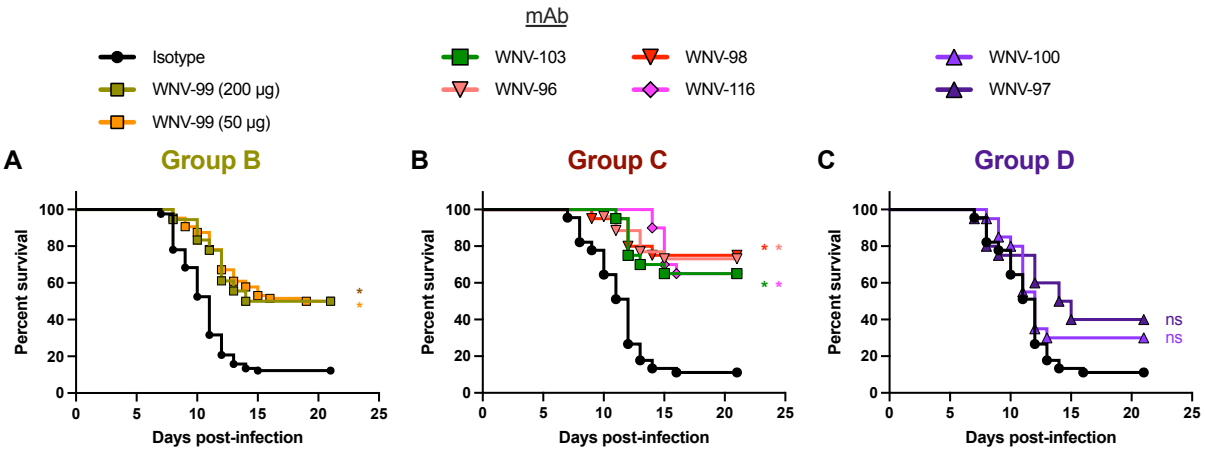

Figure 3.5. Protection against WNV challenge. (**A-C**) Survival analysis. Four- to five-week-old male C57BL/6J mice were inoculated subcutaneously with 10^2 FFU of WNV and concurrently administered an anti-WNV NS1 human mAb or an isotype control mAb. Except where indicated, mice received a 200 µg dose of mAb. (**A**) Survival for the group B mAb WNV-99 was analyzed using the log-rank Mantel-Cox test (*$p<0.05$; isotype, n = 82, 9 experiments; WNV-99 (200 µg dose), n = 18, 2 experiments; and WNV-99 (50 µg dose), n = 64, 7 experiments). (**B-C**) Survival for the mAbs in group C (**B**) and group D (**C**) were analyzed together using the log-rank Mantel-Cox test with a Bonferroni correction (*$p<0.05$; isotype, n = 45, 6 experiments; WNV-96, n = 26, 4 experiments; all other mAbs, n = 20, 2 experiments).

Chapter 4

Levels of circulating NS1 impact West Nile virus spread to the brain

This chapter is adapted from a manuscript under review at the *Journal of Virology*:

Alex W. Wessel, Kimberly A. Dowd, Scott B. Biering, Ping Zhang, Melissa A. Edeling, Christopher A. Nelson, Kristen E. Funk, Christina R. DeMaso, Robyn S. Klein, Janet L. Smith, Thu Minh Cao, Richard J. Kuhn, Daved H. Fremont, Eva Harris, Theodore C. Pierson, and Michael S. Diamond.

K.A.D. and C.R.D. generated and performed cell infectivity assays with the GFP-expressing WNV variants. P.Z. generated the WNV variants without GFP. P.Z. and A.W.W. performed virus growth curves and survival studies in mice. K.E.F prepared the mouse cortical neuron cultures. A.W.W. performed all ELISA, Western blotting, NS1 cell surface expression, intracranial inoculation, and other mouse studies. S.B.B. performed NS1 cell binding and TEER studies in HBMECs. M.A.E. generated the expression vectors for recombinant NS1. M.A.E. and C.A.N. purified the recombinant NS1 proteins. J.L.S. performed structural analysis of NS1. A.W.W. and S.B.B. performed data analysis. R.S.K., R.J.K., D.H.F., E.H., T.C.P., and M.S.D. acquired resources and directed the project. A.W.W. and M.S.D. wrote the initial manuscript draft. All other authors provided editorial comments.

4.1 Summary

Dengue (DENV) and West Nile (WNV) viruses are arthropod-transmitted flaviviruses that respectively cause systemic vascular leakage and encephalitis syndromes in humans. However, the viral factors contributing to these specific clinical disorders are not completely understood. Flavivirus nonstructural protein 1 (NS1) is required for replication, expressed on the cell surface, and secreted as a soluble glycoprotein, reaching high levels in the blood of infected individuals. Extracellular DENV and WNV NS1 interact with host proteins and cells, have immune evasion functions, and promote endothelial dysfunction in a tissue-specific manner. To characterize how differences in DENV and WNV NS1 might function in pathogenesis, we generated WNV NS1 variants with substitutions corresponding to residues found in DENV NS1. We discovered that the substitution NS1-P101K led to reduced WNV infectivity of the brain and attenuated lethality in infected mice, although the virus replicated efficiently in cell culture and peripheral organs and bound at wild-type levels to brain endothelial cells and complement components. The P101K substitution resulted in reduced NS1 antigenemia in mice, and this was associated with reduced WNV spread to the brain. As exogenous administration of NS1 protein rescued WNV brain infectivity in mice, we conclude that circulating WNV NS1 facilitates viral dissemination into the central nervous system and impacts disease outcome.

4.2 Introduction

Flaviviruses are a genera of arthropod-transmitted RNA viruses that include important human pathogens such as yellow fever (YFV), Zika (ZIKV), Dengue (DENV), West Nile (WNV), and Japanese encephalitis (JEV) viruses [1]. DENV infects up to 390 million people every year, whereas cases of WNV, ZIKV, JEV, and YFV tally in the thousands or hundreds of thousands [1,2]. Infected individuals present with a spectrum of illness and disease, ranging from febrile syndromes, hypotensive shock, liver failure, congenital malformations, meningitis, and encephalitis. For example, in severe dengue, patients develop a plasma leakage syndrome that can result in cardiovascular collapse and death. After WNV and JEV infections, some individuals progress to potentially life-threatening neuroinvasive diseases (*i.e.*, encephalitis or meningitis), in which the virus crosses the blood-brain barrier and infects neurons of the central nervous system [1]. The viral and host factors contributing to the distinct tropism and pathology caused by different flaviviruses remain poorly characterized.

Flavivirus nonstructural protein 1 (NS1) is a 46-55 kDa glycoprotein that has a required scaffold role in virus replication in the endoplasmic reticulum (ER) [3-5]. NS1 homodimerizes in the ER, traffics through the Golgi complex, and is expressed on the cell surface [6-8]. A fraction of NS1 dimers also trimerizes into soluble hexamers that are secreted [9]. Secreted NS1 accumulates in the blood of affected individuals and can be detected at particularly high levels during DENV infection (1 to 10 μg/mL) [10-12]. These extracellular forms of NS1 can interact with components of the innate immune system, such as toll-like receptors (TLRs) [13,14] and complement proteins [15-18], enabling modulation or evasion of mammalian host immunity. Secreted NS1 can also bind back to the surface of endothelial cells and promote degradation of the endothelial glycocalyx, leading to disruption of blood-tissue barriers [19-22]. Despite these many ascribed

functions, the degree to which NS1 contributes to viral pathogenesis in the host is poorly understood, as it has been challenging to uncouple the role of NS1 in flavivirus replication from its accessory functions. Mutations disrupting the function of NS1 in virus replication render it impossible to study their effects on pathogenesis.

The NS1 dimer structure has been determined for several flaviviruses and consists of three structurally conserved domains (**Figure 4.1A**): the β-roll (residues 1-29), wing (residues 30-180), and β-platform (residues 181-352) [23-26]. Hydrophobic residues within the β-roll and subdomains of the wing (flexible loop and greasy finger) form a surface for the association of the NS1 dimer with membranes and with other dimers to form the hexamer [23,24,26,27]. The opposite surfaces contain electrostatic residues that vary between flaviviruses and are exposed on the cell surface form of NS1 [23,24], providing targets for antibody recognition [27-29]. Common solvent-exposed regions lie in the C-terminal tip of the β-platform, the spaghetti loop of the β-platform (an elongated loop between consecutive β-strands), and the adjacent surface of the wing domain [27-29]. Although these surfaces are thought to mediate interactions with host proteins, the functional properties of individual domains in NS1 are still poorly characterized.

Despite highly related tertiary and quaternary structures [23], the DENV and WNV NS1 proteins display just over 50% identity and 70% similarity at the amino acid level. Moreover, the NS1 proteins of DENV and WNV exhibit functional differences. A short peptide motif at the N-terminus of NS1, which differs between DENV and WNV, targets most of WNV NS1 to the cell surface and most of DENV NS1 for secretion [30]; this explains in part the higher circulating levels of DENV compared to WNV NS1 in infected individuals [12,31]. Although DENV and WNV NS1 both can interact with complement proteins including C4 and C4b [16,17], the outcome of complement modulation differs between WNV and DENV infections [32,33], and some flavivirus-specific binding

patterns are observed (*e.g.*, WNV but not JEV NS1 binds to the alternative pathway regulator factor H) [34]. Differences in NS1-mediated regulation of endothelial blood-tissue barriers also exist. Whereas DENV NS1 can bind microvasculature and promote capillary permeability in many different tissues, WNV NS1 targets endothelial cells more specifically in the central nervous system (CNS). This pattern of NS1 binding appears to correlate with the systemic vascular effects of DENV and the neurotropism of WNV [21]. The mechanism by which NS1 triggers endothelial dysfunction is incompletely understood, particularly in terms of the residues or domains involved in cell signaling. The conserved N207 glycosylation site and other residues at the C-terminal tip of the β-platform (*e.g.*, 301 and 305) have been identified as essential for triggering endothelial hyperpermeability for DENV NS1, yet are dispensable for binding to endothelial cells [27,35]. Hydrophobic residues within the wing flexible loop (W115, W118, and G119) contribute to DENV NS1 binding to endothelial cells [24,26,27], but do not explain the tissue-specific binding patterns of different flaviviruses, as these residues are conserved between flaviviruses.

Here, to begin to define the structure-function relationships between DENV and WNV NS1, we substituted single amino acid residues in WNV NS1 for those in DENV and evaluated effects on replication and pathogenesis. We discovered that a proline to lysine substitution at residue 101 (P101K) in WNV NS1 did not affect WNV infectivity *in vitro* yet resulted in decreased lethality in mice. This phenotype with WNV NS1-P101K was associated with lower levels of virus in the brain but not in peripheral organs. The substitution did not disrupt known interactions of NS1 with brain microvasculature endothelial cells or complement proteins. Instead, the NS1-P101K substitution resulted in reduced amounts of cell-associated NS1 and less circulating NS1 in mouse serum. Exogenous administration of NS1 to mice restored brain infectivity of WNV

NS1-P101K. Our results suggest that levels of circulating WNV NS1 impact viral dissemination into the brain and disease outcome.

4.3 Results

An NS1 variant of WNV replicates efficiently *in vitro*, but is attenuated in mice. To discover residues in WNV NS1 that could be important for pathogenesis in the CNS but not for infectivity, we engineered a series of single amino acid substitutions in NS1 within the backbone of a GFP-expressing infectious cDNA clone by exchanging WNV (strain 382-99) residues with corresponding ones that were different in DENV, but conserved among all DENV serotypes [36,37]. We focused on the membrane-interacting and the exposed electrostatic surfaces of NS1 given that both are potentially involved in host interactions [23,24]. These regions included residues within the membrane-interacting surfaces of the □-roll and wing domains (including the 'greasy finger'), the flexible loop of the wing domain, and the spaghetti loop and C-terminal tip of the beta-platform domain (**Figure 4.1A**). We prioritized the following features: (i) residues with surface charge differences between WNV and DENV and (ii) regions with variable conformations between DENV and WNV NS1 based on published NS1 structures [23]. In total, we constructed 53 NS1-variant GFP-tagged viruses. Given the critical role of NS1 in virus replication [38], we first assessed infection efficiency for each variant compared to wild-type (WT) WNV by inoculating Vero cells and measuring viral yield in the supernatant after four days (**Figure 4.1B**). While the majority of the 53 variants demonstrated impaired replication, 17 replicated to similar levels as the WT virus. We selected five of these variants spanning different regions of the NS1 protein to study potential effects on viral pathogenesis without confounding effects on replication (colored bars in **Figure 4.1B**). We constructed these variants in an infectious cDNA clone without GFP to avoid

attenuation *in vivo* [39]. All five variants displayed similar replication kinetics relative to the WT control virus in multistep growth curve analyses in BHK21 cells (**Figure 4.1C**).

To determine whether the NS1 variants affected WNV pathogenesis, four- to five-week-old male C57BL/6J mice were inoculated subcutaneously with 10^2 FFU of WT or NS1-variant WNV. In this model, approximately 10% of mice survive infection over a three-week time course [40]. Infection with four of the variants (A27T, Y34F, A70Q, and S199G) resulted in similar mortality rates as the WT virus (**Figure 4.1D**). The NS1-P101K variant, however, showed greater survival as reflected both by decreased mortality rates and greater mean time to death. As the P101K substitution variant replicated efficiently *in vitro*, we hypothesized the substitution might affect an accessory function of NS1 in viral pathogenesis.

P101K substitution results in lower levels of cellular and secreted NS1. Cell surface and secreted forms of NS1 have immune evasive properties and modulate endothelial barrier permeability [13,15-17,20,21,41]. To address how a P101K substitution might affect the expression and cellular localization of NS1, Vero cells were inoculated with WNV WT or NS1-P101K. The accumulation of NS1 was measured at different times following infection in cell lysates by Western blotting using 8NS1, a monoclonal antibody (mAb) against WNV NS1. We demonstrated that 8NS1, as well as other anti-NS1 mAbs, recognize recombinant WT and P101K NS1 proteins with similar avidity by ELISA (**Figure 4.2A-F**). We also demonstrated that 8NS1 and 16NS1 recognize both proteins equally well by Western blotting (**Figure 4.2G)**. At all of the time points tested, we found that lower levels of cell-associated NS1 were apparent after infection with the P101K virus compared to the WT virus despite producing equivalent levels of cell-associated E protein (**Figure 4.3A,** *lysates*). Levels of secreted NS1 in the supernatant also were lower following infection with the NS1-P101K variant than the WT virus (**Figure 4.3A,** *supernatants*).

To determine whether the P101K substitution affects NS1 localization on the cell surface, we assayed cell surface expression of NS1 on WNV-infected Vero cells using flow cytometry (**Figure 4.3B-C**). Levels of NS1 on the cell surface, however, were not different between cells infected with the WT or NS1-P101K variant virus.

We hypothesized that the decrease in cell-associated NS1 might be due to an instability of the NS1-P101K protein. We addressed this using a cycloheximide-chase assay in which Vero cells were inoculated with virus for 20 h and then treated with cycloheximide to arrest protein translation. Levels of NS1 in cell lysates were then assessed over the chase time by Western blotting (**Figure 4.3D**). As observed in **Figure 4.3A**, the levels of NS1-P101K were lower than WT NS1 at all time points post-infection in the vehicle-treated cells. Over the course of a 12 h cycloheximide treatment, levels of both WT and P101K NS1 proteins diminished at equivalent rates (**Figure 4.3E**). This suggests that NS1-P101K is not inherently more unstable than WT NS1. Rather, the lower levels of NS1-P101K in cells are likely due to less efficient translation, folding, or oligomeric assembly in the ER.

Since lower levels of NS1-P101K were detected in the supernatant of infected cells, we measured the *in vivo* correlate, NS1 antigenemia. Four- to five-week-old male C57BL/6J mice were inoculated subcutaneously with WNV WT or NS1-P101K, and serum was collected at various days to measure NS1 levels by capture ELISA (**Figure 4.3F**). Similar to the findings *in vitro*, levels of soluble NS1 in the serum at 5 and 6 days post-infection (dpi) were lower for the NS1-P101K variant than the WT virus.

WNV NS1-P101K replicates efficiently in the periphery of mice but produces lower viral titers in the brain. Since the NS1-P101K variant virus showed reduced lethality rates in mice, we hypothesized that the virus might be restricted *in vivo*, which also could explain the differences in

NS1 antigenemia. To evaluate this hypothesis, we compared viral burden over time in different tissues after inoculation of C57BL/6J mice with 10^2 FFU of WNV WT or NS1-P101K. In the serum and spleen, viral burden levels were equivalent between the two viruses at 2, 5, or 7 dpi (**Figure 4.4A-B**). In the brain, however, titers of the NS1-P101K variant were approximately 10-fold lower at 7 dpi (**Figure 4.4C**). Nonetheless, at the time points analyzed, few mice had detectable levels of infectious virus in the spinal cord (**Figure 4.4D**), which is consistent with prior studies in mice showing WNV infects the brain before the spinal cord [42]. We next examined the kinetics of NS1-P101K spread and infection at earlier time points in greater detail by measuring viral RNA. Mice were subcutaneously inoculated with WNV, and viral RNA levels were assessed at 4, 5, or 6 dpi in peripheral organs and different regions of the brain. No differences in viral RNA were observed in the spleen or gastrointestinal tract, where WNV can infect enteric neurons (**Figure 4.4E-G**) [43]. Additionally, no substantive differences in viral RNA levels were observed in the spinal cord, olfactory bulb, or cerebellum of mice infected with WT or NS1-P101K viruses at 4, 5, and 6 dpi (**Figure 4.4H-J**). However, at 6 dpi, levels of the NS1-P101K variant were 30- to 100-fold lower than the WT virus in the brainstem and cortex (**Figure 4.4K-L**).

NS1-P101K substitution does not impair brain-intrinsic infection of WNV. Although the NS1-P101K variant virus displayed efficient replication kinetics in Vero and BHK21 cells and in the peripheral organs of mice, we questioned whether the substitution might affect replication directly in the brain. To address this question, we examined replication kinetics in neurons *in vitro* using a multi-step growth curve. Primary cortical neurons from mice were inoculated with the WNV WT or NS1-P101K, and infection over time was quantified by focus-forming assay (FFA) (**Figure 4.5A**). No differences in replication kinetics were observed between the two viruses, suggesting that the NS1-P101K substitution does not affect neuron-intrinsic replication. We also tested the

ability of the NS1-P101K variant to replicate in the brain by inoculating C57BL/6J mice by intracranial injection with WNV WT or NS1-P101K (**Figure 4.5B**). All mice infected by this route of inoculation succumbed by 8 dpi with equivalent kinetics. In a separate experiment, mice were inoculated by intracranial injection, and viral burden was measured in different brain regions at 3 and 5 dpi (**Figure 4.5C-F**). Notably, and in contrast to that observed by subcutaneous inoculation, no significant differences in infectivity of different brain regions were observed between the two viruses after intracranial inoculation. These data suggested that the WNV WT and NS1-P101K replicate efficiently and equivalently in the brain.

NS1-P101K substitution does not alter functional interactions with the endothelial barrier or complement proteins. Given the differences in brain infectivity observed with the NS1-P101K variant virus when administered via the subcutaneous and intracranial routes, we hypothesized that the substitution in NS1 might affect virus entry into the brain from circulation. Indeed, soluble NS1 from different flaviviruses differentially promotes vascular endothelial dysfunction in distinct tissues in a manner that correlates with virus tissue tropism [21]. WNV NS1 in particular binds to brain microvasculature endothelium and enhances permeability, and exogenous administration of WNV NS1 in mice induces vascular leakage in the brain but not in other organs [21]. Based on these studies, we hypothesized that the lower brain infection of the NS1-P101K variant virus after subcutaneous inoculation might be due to a failure of NS1-P101K to modulate brain endothelial cell permeability. We tested this idea first by assessing whether the P101K substitution affected the interaction of NS1 with endothelial cells. Increasing concentrations of recombinant WT or P101K NS1 protein were incubated with hCMEC/D3 cells, a human blood-brain barrier endothelial cell line, and the percentage of cells binding to NS1 was measured by flow cytometry. At all three different concentrations of NS1 (1, 5, and 10 μg/mL), the WT and P101K proteins

bound cells equivalently (**Figure 4.6A**). We also imaged and quantitated binding of NS1 (10 μg/mL) to human brain microvascular endothelial cells (HBMECs) using confocal microscopy (**Figure 4.6B-C**). No differences in cell binding were observed between the WT and P101K proteins.

We next assessed whether the NS1-P101K protein retained the ability to induce endothelial hyperpermeability of a brain vasculature-derived endothelial monolayer of HBMECs using a trans-endothelial electrical resistance (TEER) assay [20]. Recombinant WT or P101K WNV NS1 was incubated with HBMECs, and TEER was measured over time (**Figure 4.6D**). As previously observed [21], a commercially produced recombinant WNV NS1 protein caused a decrease in TEER across the cell monolayer. Similarly, recombinant, purified WT and P101K NS1 proteins that we generated induced an equivalent decrease in TEER over time. Thus, the NS1-P101K substitution did not appreciably affect the ability of NS1 to disrupt the integrity of a monolayer of brain endothelial cells.

WNV NS1 interacts with different components of the classical and alternative complement pathways [15-17]. Binding of NS1 to the complement regulatory protein factor H results in enhanced cleavage of C3b and reduced activity of the alternative pathway [15]. WNV NS1 also attenuates the classical and lectin binding mannose pathways through direct interaction with C4, C4b, and C4b-binding protein (C4BP) [16,17]. We explored whether the NS1-P101K protein differentially interacted with different complement factors by ELISA (**Figure 4.6E-G**). WT and P101K NS1 displayed similar avidity for factor H, C4, and C4b, suggesting that the P101K substitution does not disrupt these viral evasion mechanisms.

Exogenous administration of NS1 rescues infectivity in the brain of WNV NS1-P101K after subcutaneous inoculation. Since the P101K substitution did not affect interactions of NS1 with

the endothelium or complement proteins, we hypothesized that the lower levels of circulating NS1 might result in less virus translocation into the brain. To test this hypothesis, C57BL/6J mice were inoculated subcutaneously with WNV WT or NS1-P101K. At 5 dpi, mice were administered 5 μg of recombinant WNV NS1 protein by intravenous injection (**Figure 4.7A**). We chose this time point because NS1 antigenemia was reduced for the NS1-P101K variant at 5 dpi (**Figure 4.3E**), and the earliest time point for which we observed differences in brain infectivity for the NS1-P101K variant virus was one day later (**Figure 4.4K-L**). Six hours after NS1 administration, we measured levels in the serum using a capture ELISA (**Figure 4.7B**). NS1 antigenemia was increased to approximately 1,000 ng/mL (three-fold increase over WT NS1 levels and six-fold increase over NS1-P101K levels). Two days later, at 7 dpi, viral burden was assessed in the spleen and brain (**Figure 4.7C-D**). Whereas exogenous NS1 administration did not affect viral burden in the spleen for both viruses or in the brain for WT WNV, it facilitated infection in the brain for the NS1-P101K variant virus.

4.4 Discussion

DENV and WNV have distinct mechanisms of viral pathogenesis and cause disparate clinical syndromes (*e.g.*, systemic vascular leakage and encephalitis for DENV and WNV, respectively). NS1 has been implicated as a contributor to these distinct outcomes. For example, DENV NS1 binding to TLR4 on platelets and monocytes results in platelet aggregation and the production of pro-inflammatory vasoactive cytokines [14,41]. Binding of DENV NS1 to the microvasculature of the lung, liver, and other organs promotes permeability across multiple blood-tissue barriers [13,20-22,35]. Together, these data suggest that DENV NS1 may contribute to the severe vascular leakage syndrome seen in some patients. Indeed, levels of DENV NS1 correlate with disease severity [44,45]. In contrast, WNV NS1 specifically targets the brain microvasculature,

promoting permeability where the virus causes its most significant clinical disease [21]. Differences in complement consumption or generation of inflammatory mediators during DENV and WNV infection also might be explained by differences in NS1 binding to specific complement proteins [15-18]. In this study, we attempted to define potential mechanisms by which DENV and WNV NS1 mediate distinct disease outcomes by exchanging residues in WNV NS1 for those in DENV NS1 and focusing on ones that did not impact cell infectivity. We discovered that NS1-P101K substitution attenuated WNV infection in the brain without affecting virus replication, NS1 binding to endothelial cells, or NS1 interaction with complement proteins.

Exogenous addition of soluble NS1 to DENV2-infected mice worsens disease by inducing a lethal vascular leakage syndrome [20]. Other reports have shown that substitutions that alter NS1 secretion and antigenemia can impact pathogenesis. For example, a T164S substitution in DENV NS1 results in enhanced secretion of NS1 and more severe disease in AG129 mice [46]. The naturally occurring A188V substitution in ZIKV NS1 also boosts secretion and antigenemia in mice, and promotes mosquito infection during a bloodmeal [47]. However, it remains unclear how these variants alter NS1 secretion or affect viral pathogenesis. In contrast, the WNV R10N substitution (which uses the asparagine from DENV) results in enhanced secretion of WNV NS1 but attenuates the virus due to a detrimental effect on virus replication [4,30]. The R10N substitution within the β-roll domain disrupts a key association of NS1 with the viral replication complex at the ER membrane [4]. Our data suggest that the levels of circulating NS1 contribute to WNV pathogenesis by facilitating dissemination to the brain without impacting replication in peripheral organs.

Residue 101 of NS1 lies on the exposed surface of the wing domain, which is an epitope recognized by protective anti-ZIKV antibodies [28]. Only three anti-WNV NS1 antibodies (9NS1, 16NS1, and 22NS1) have been mapped previously, and none of these localize to this region [25,28,48].

All antibodies used in this study retained binding to NS1-P101K, suggesting that they do not map to this residue. The P101K substitution within WNV NS1 led to decreased accumulation of cell-associated and secreted NS1. Nonetheless, cycloheximide-chase studies revealed no obvious differences in stability between the WT and P101K proteins, suggesting a potential effect on translation efficiency or folding of NS1-P101K in the ER. Potentially, the introduction of a positively charged lysine at residue 101 of WNV NS1 alters the conformation of the wing domain and slows folding in the ER and assembly of the hexamer. Despite impacting overall levels of cell-associated NS1, the P101K substitution does not appear to interfere with the interactions of dimeric or hexameric NS1 with the plasma membrane [23,24]. Indeed, we did not observe differences in cell surface expression of NS1-P101K on WNV-infected cells or in binding of soluble NS1-P101K to the surface of endothelial cells. This is consistent with the location of residue 101 on the wing surface opposite of the greasy finger and wing flexible loop, which are thought to be the membrane interfaces [23,24,26]. Thus, we speculate that the lower levels of cell-associated and secreted NS1 reflect slowed hexamer assembly in the ER. Notably, residue 101 is conserved among neurotropic flaviviruses as a nonpolar amino acid (proline: WNV, JEV, St. Louis encephalitis virus, Murray Valley encephalitis virus, and ZIKV; glycine or valine: tick-borne encephalitis virus) [26]. In non-neurotropic flaviviruses, however, residue 101 is positively charged (lysine: DENV serotypes 1-4) or polar (threonine: YFV) [26]. We speculate that P/G101K substitutions in other neurotropic flaviviruses might similarly affect NS1 expression and/or dissemination to the CNS, though this remains to be tested.

Flavivirus NS1 can trigger endothelial dysfunction and permeability in a tissue-specific manner that reflects disease tropism [21]. After binding to endothelial cells, DENV NS1 is endocytosed and induces enzymes that degrade the endothelial glycocalyx [22,35,49]. This results in a

loss of endothelial cell barrier integrity and enhanced permeability to solutes and liquids [22,35,49]. In our cell-based experiments, the P101K substitution did not alter WNV NS1 binding to brain microvascular endothelial cells or impact TEER across endothelial monolayers. Whereas residues in the wing flexible loop mediate cell binding and those at the C-terminal tip of the β-platform contribute to endothelial hyperpermeability [27], P101 lies outside of these regions in the exposed surface of the wing domain. Instead, the lower levels of NS1-P101K in circulation may be below the threshold for causing endothelial dysfunction *in vivo*. Consistent with this idea, exogenous administration of NS1 boosted levels of circulating NS1 and rescued dissemination to the brain of mice inoculated with WNV NS1-P101K. Nonetheless, the precise mechanism remains unclear and will need to be explored. Possibilities include NS1 dose-dependent effects on blood-brain barrier permeability or interactions of soluble NS1 with E and prM proteins on virions in plasma that enhance entry and infectivity of specific endothelial cell types [50-52]. Notably, the WNV NS1-P101K variant was more attenuated in the cerebral cortex and brainstem than other brain regions. This could be explained in part by regional heterogeneity in permeability of the blood-brain barrier to different molecules [53-56]. Possibly, endothelial cells, pericytes, or neurons may respond differently throughout the brain to cytokines such as type I or type III interferons, leading to regional differences in blood-brain barrier permeability or antiviral immunity [57,58]. Alternatively, WNV NS1 could affect endothelial function more in the cortex and brainstem than other regions due to local differences in expression of NS1-binding glycosaminoglycans [19,59] or an unidentified NS1-specific protein receptor. After internalization of NS1 by endothelial cells [35], regional differences in NS1-dependent signaling also could affect infectivity and spread.

Our experiments suggest that levels of circulating NS1 during infection contribute to the neurotropism of WNV infection, at least in mice. Lower levels of NS1 in serum correlate with less

dissemination to the brain, and this phenotype is rescued by exogenous addition of NS1 protein. Based on our cell culture studies, analysis of viral RNA levels in the serum, spleen, and gastrointestinal tract, and experiments using direct intracranial virus inoculation, the P101K substitution does not appear to affect replication or viral yield of WNV. This observation that slightly lower levels of cell-associated WNV NS1 do not impact viral yield is consistent with complementation experiments using a ΔNS1 deletion virus [4,38]. Thus, small differences in NS1 expression may preferentially affect pathogenic mechanisms associated with extracellular NS1 functions rather than intracellular function in the replication complex. In summary, our study establishes a role for NS1 antigenemia in the context of flavivirus pathogenesis, which has been speculated for years based on the correlation of levels of DENV NS1 in plasma and disease pathogenesis [44].

4.5 Methods

Ethics statement. Animal procedures were carried out in accordance with the recommendations in the Guide for the Care and Use of Laboratory Animals of the National Institutes of Health. Protocols were approved by the Institutional Animal Care and Use Committee at Washington University School of Medicine (assurance no. A3381-01). To minimize suffering during procedures, animals were anesthetized with a ketamine hydrochloride and xylazine solution.

Cell culture. BHK-21 (American Type Culture Collection (ATCC), CCL-10), C6/36 (ATCC, CRL-1660), HEK-293T (ATCC, ACS-4500), and Vero cells (ATCC, CCL-81) were propagated in Dulbecco's modified Eagle Medium (DMEM) supplemented with 10% fetal bovine serum (FBS), 1 mM sodium pyruvate, and 10 mM HEPES, pH 7.3. Raji-DCSIGNR cells [60] were propagated in RPMI 1640 medium supplemented with 7% FBS. HBMECs (ScienCell Cat. No. 1000) were cultivated in endothelial cell medium (ScienCell Cat. No. 1001) supplemented with

5% FBS, endothelial cell growth supplement (ScienCell Cat. No. 1052), and penicillin/streptomycin. The hCMEC/D3 cells (Sigma Cat. No. SCC066) were propagated on collagen-coated flasks (1:20; Sigma Cat No. 08-115) in EndoGRO-MV Complete Media (Sigma Cat. No. SCME004) supplemented with 1 ng/mL of FGF-2 (Sigma Cat. No. GF003). Cells were maintained at the following conditions: C6/36 cells, 28°C and 5% CO_2; HEK-293T and Raji-DCSIGNR cells, 37°C and 7% CO_2; all other cells, 37°C and 5% CO_2.

Isolation of cortical neurons. Primary cortical neurons were prepared from embryonic day 18 mouse embryos (strain C57BL/6J) [61,62]. Pups were sacrificed by decapitation, and brains were placed in a dish containing sterile PBS. The meninges were removed using Dumont #5 forceps, and the cortices were dissected and transferred to a 15-mL conical tube containing Hibernate E media (Gibco A1247601). Cortical tissue was pelleted at 1,000 × g for 5 min, then the media was removed and replaced with digestion media containing 20 U/ml papain (Worthington Biochemical Corporation LS003126) and 2.5 U/mL DNase I (Invitrogen 18047019) dissolved in Hibernate E for 30 min at 37°C with periodic agitation. Following digestion, tissue was pelleted at 125 × g for 10 min, and the digestion media was removed and replaced with fresh Hibernate E media. Tissue was mechanically triturated using progressively smaller glass Pasteur pipettes, then centrifuged at 125 × g for 5 min. Following centrifugation, dissociated cells were resuspended in Neurobasal Plus media (Gibco 21103-049) supplemented with 2% B27 serum-free supplement (Gibco 17504044), 2 mM Glutamax (Gibco 35050061), and 100 U/mL Penicillin-Streptomycin (Gibco 15140122). After counting, 5×10^5 cells were seeded into each well of a 12-well plate that was pretreated for 1 h in poly-D-lysine (50 μg/mL; Sigma Cat No. P-6407). The cells were maintained at 37°C and 5% CO_2 for eight days, with a medium change on day four. On day +8, the cells were inoculated with WNV for analysis of virus growth kinetics as described below.

Purification of recombinant NS1 proteins. To generate recombinant NS1 protein, we cloned WNV NS1 (strain 382-99) into the mammalian expression vector pFM-1.2 [63]. We included the cluster of differentiation 33 (CD33) signal peptide sequence directly preceding the NS1 gene to enable proper targeting to the ER. Additionally, we included a 6X His tag following the NS1 sequence. A construct containing the P101K mutation was generated using site-directed mutagenesis. To generate protein, Expi293F cells were transiently transfected with the pFM-WNV-NS1 construct and after 3 days, supernatants were collected. Subsequently, NS1 was loaded on an Ni-NTA (Qiagen) column pre-equilibrated with 20 mM Tris pH 8.5, and 50mM NaCl, washed with buffer containing 10 mM then 20 mM imidazole and eluted in buffer containing 300 mM imidazole. Imidazole was removed by ultrafiltration. Alternatively, after 4 days, supernatants were collected, concentrated, and buffer exchanged into PBS, pH 6.5 and then PBS, pH 8.0, using a stirred cell concentrator loaded with a 30 kDa ultrafiltration membrane. Imidazole was added to a final concentration of 10 mM. The protein was captured on a Ni-NTA (Qiagen) column pre-equilibrated with PBS, pH 8.0 and eluted with 250 mM imidazole. The eluate was purified further using size exclusion chromatography on Superdex 200, and the NS1 protein-containing fractions were pooled.

Production of infectious WNV. ***(a) GFP-expressing WNV***. We generated infectious GFP-expressing WNV using a previously described DNA-launched WNV-NY99 (strain 382-99) molecular clone system [36,37]. In this system, a truncated WNV genome under control of a CMV promoter (from pWNV-GFP-backbone) is complemented by ligation to a DNA fragment encoding the structural genes (from pWNV-complement) using the unique BssHII and BamHI restriction sites. To construct some NS1 variants (D7N, D7S, and I8W), we performed site-directed mutagenesis on pWNV-complement, which encodes a portion of NS1 (amino acids 1-19)

downstream of the structural gene cassette and upstream of the engineered BamHI site. Alternatively, we used a three-part ligation strategy to generate the other NS1 variants. First, pWNV-GFP-backbone was truncated further by removing the sequence encoding NS1 and part of NS2. The excised NS1-NS2 fragment was cloned into pDONR221 via Gateway cloning to generate a new plasmid called pWNV-complement-NS1, which served as the template for NS1 mutagenesis. We then utilized a unique AflII restriction site in pWNV-GFP-backboneΔNS1 to complement this plasmid with pWNV-complement and the mutant variants of pWNV-complement-NS1. To produce virus using either the 2-part or 3-part ligation strategy, 1 μg of each plasmid was digested as follows: pWNV-GFP-backbone and pWNV-complement, BssHII/BamHI; pWNV-backboneΔNS1, AflII/BssHII; pWNV-complement-NS1, BamHI/AflII. The appropriate fragments were ligated with T4 DNA ligase in a total volume of 50 μL for 15 min at room temperature or 16°C overnight. The entire ligation mixture was then transfected into HEK-293T cells in 6-well plates using Lipofectamine 3000 (Life Technologies) according to manufacturer instructions. At days four and six post-transfection, virus-containing supernatants were harvested and filtered through a 0.22 μm filter. The titers of GFP-expressing WNV stocks were determined by infecting Raji-DCSIGNR cells in technical duplicates with serial two-fold dilutions of these virus-containing supernatants. Cells were incubated at 37°C for 16 to 20 h and then fixed with 2% paraformaldehyde, and the number of GFP-positive infected cells was determined by flow cytometry. The titer of each GFP virus (infectious units per mL, IU/mL) was calculated from the linear portions of the virus dilution-infectivity curve. ***(b) WNV without GFP***. We also generated recombinant, infectious WNV without GFP using a two-plasmid (pWN-AB and pWN-CG) infectious clone for WNV-NY99, strain 382-99 (GenBank accession no. AF196835) [64,65]. Using the QuikChange site-directed mutagenesis kit (Agilent), we engineered

mutations in pWN-CG to encode the following amino acid substitutions in NS1: A27T, Y34F, A70Q, P101K, and S199G. PCR primers used for site-directed mutagenesis are listed in **Table 4.1**. Following propagation in SURE 2 competent cells (Agilent), the pWN-AB and pWN-CG plasmids were purified and digested with NgoMIV and XbaI and then treated with alkaline phosphatase. The DNA fragments were purified by phenol/chloroform extraction, precipitated with ethanol, and joined with T4 DNA ligase at 16°C overnight. The assembled DNA was linearized with XbaI (5 h at 37°C), treated with proteinase K (30 min at 50°C), and then purified again by phenol/chloroform extraction and ethanol precipitation. The resulting DNA was used as a template for *in vitro* transcription using the AmpliScribe T7 High Yield Transcription Kit (Lucigen). The RNA product was electroporated into BHK21 cells using a GenePulser Xcell electroporator (Bio-Rad) at 850 V, 25 mF, and infinite Ω. The P0 virus stocks were recovered within four days and then propagated in C6/36 cells to generate P1 virus stocks. Virus stocks were titered on Vero cells by focus-forming assay (FFA) [66].

Analysis of virus growth kinetics. ***(a) Vero cells.*** We inoculated Vero cells in duplicate in 24-well plates with the GFP-expressing NS1 variants of WNV at a multiplicity of infection (MOI) of 0.01 in a final volume of 0.15 mL. After incubating for 1-2 h, the virus inoculum was removed, the cells were washed twice with PBS, and 1 mL of low-glucose DMEM (ThermoFisher 12320032) was added. Virus-containing supernatant was harvested at day +4. All supernatants were clarified by centrifugation and titered on Raji-DCSIGNR cells as described above. ***(b) BHK21 cells.*** BHK21 cells were plated one day prior to inoculation with WNV at an MOI of 0.01 for 2 h at 37°C. Supernatant was collected to confirm the inoculum virus titer, and cells were washed with PBS to remove unbound virus. After incubation of the cells at 37°C for the indicated time points, supernatant was collected and clarified by centrifugation at 300 x g for 5 min. Virus

titers were determined on Vero cells by FFA [66]. ***(c) Neurons***. For neuronal cultures, the cells were plated in 12-well plates as described above and, eight days later, were inoculated with WNV at an MOI of 0.001. Two hours post-inoculation, the medium was removed to confirm input virus titer and replaced with fresh medium. Supernatants were taken at the indicated time points, clarified by centrifugation, and titered on Vero cells by FFA [66].

Western blotting. Cellular and secreted WT and P101K NS1 were assessed by Western blotting. 3 x 10^6 Vero cells were seeded in 10-cm dishes one day prior to inoculation with the WT or NS1-P101K variant of WNV at an MOI of 5. After 1 h, the inoculum was removed, cells were washed with PBS, and fresh medium was added. At the indicated time points following infection, cell lysates were prepared in RIPA buffer (Thermo Cat. No. 89900) containing Halt Protease Inhibitor Cocktail (EDTA-free; Cat. No. 78425) and frozen at -80°C. Cell lysates were prepared similarly for cycloheximide-chase experiments (see details below). In both cases, cell lysates were thawed on ice, vortexed, and centrifuged at 18,800 x g for 10 min at 4°C to remove cellular debris. Total protein was quantitated using a Pierce bicinchoninic acid (BCA) assay (Thermo Cat. No. 23225). For each lysate sample, 10 μg of total protein was prepared in NuPAGE LDS sample buffer and reducing agent (Thermo), heated at 70°C for 10 min, and loaded into a NuPAGE 10% Bis-Tris gel (Thermo). Following polyacrylamide gel electrophoresis in NuPAGE MOPS SDS running buffer (Thermo), protein was transferred to a nitrocellulose membrane using an iBlot Gel Transfer Device (Thermo) on the manufacturer's P0 setting. The membranes were washed in PBS containing 0.05% Tween-20 (PBST) and incubated with blocking buffer (PBST containing 5% (w/v) non-fat milk) for 1 h at room temperature. The membranes were incubated overnight at 4°C with blocking buffer containing the murine anti-NS1 mAbs 8NS1 (3 μg/mL) or 16NS1 (1:1000 dilution of ascites fluid) [67] and an anti-GAPDH rabbit antibody (1:1000; clone 14C10; Cell Signaling Cat. No. 2118). The

next day, membranes were washed three times in PBST (10 min per wash) and then incubated for 1 h at room temperature in blocking buffer containing the following secondary antibodies (LI-COR): IRDye 680 donkey anti-mouse IgG and IRDye 800 donkey anti-rabbit IgG. Following three additional washes in PBST, membranes were imaged on an Odyssey infrared imager (LI-COR). To measure E protein levels in the lysates, the membranes were stained overnight at 4°C in blocking buffer containing the anti-E mAbs human E16 (hE16; 5 μg/mL) and chimeric human E60 (chE60; 5 μg/mL) [68,69]. The next day, membranes were washed in PBST and incubated for 1 h at room temperature in blocking buffer containing peroxidase-conjugated goat anti-human IgG (1:10,000; Jackson ImmunoResearch Cat. No. 109-035-088). After washing, membranes were incubated with SuperSignal West Pico Chemiluminescent Substrate (Thermo), and E protein levels were assessed after developing autoradiography film. Following image acquisition, levels of NS1 and GAPDH were quantified by densitometry using Image Studio Lite software (LI-COR). The ratio of NS1 to GAPDH was calculated at each time point for normalization, and then the fraction of NS1 remaining in the cell lysate compared to the starting amount was determined, using the time of initiation of cycloheximide treatment as the starting point.

Detection of NS1 on the cell surface. Vero cells were inoculated with the WNV WT or NS1-P101K variant at an MOI of 5. After 1 h, the inoculum was removed and replaced with fresh medium. Eighteen hours later, the cells were washed in PBS and detached by incubating in PBS containing 10 mM EDTA and 0.5% bovine serum albumin (BSA) for 20 min at 37°C. Cells then were washed in PBS containing 0.5% BSA and 2 mM EDTA (FACS buffer) and stained by incubating for 1 h on ice in FACS buffer containing an oligoclonal pool of anti-NS1 mouse mAbs (8NS1, 9NS1, 10NS1, and 17NS1; 2 μg/mL for each mAb) [67] or an isotype control antibody. After washing, cells were incubated for 30 min on ice with Fixable Viability Dye eFluor 506 (1:1000;

eBioscience) and goat anti-mouse IgG conjugated to Alexa Fluor 647 (1:2000; Thermo). Cells were washed again and fixed in PBS containing 4% PFA for 10 min, followed by washing in perm/wash buffer (PBS containing 0.1% saponin and 0.1% BSA). Cells then were incubated for 30 min on ice in perm/wash buffer containing the anti-E mAb hE16 (2 μg/mL) or an isotype control. After washing, the cells were incubated for 30 min on ice in perm/wash buffer containing goat anti-human IgG conjugated to Alex Fluor 488 (1:2000; Thermo). After a final few washes in perm/wash buffer, the cells were resuspended in FACS buffer and processed on a MACSQuant Analyzer (Miltenyi Biotec). Data was analyzed using FlowJo software by first gating on single, live cells. Within this population, the mean fluorescence intensity (MFI) of cell surface (ch17NS1) and total cellular NS1 (8NS1) for infected cells was normalized to that for non-infected cells.

Cycloheximide-chase experiments. Stability of cellular NS1 (WT and P101K) in infected cells was analyzed using a cycloheximide-chase assay. Vero cells were seeded at 5 x 10^5 cells per well in 6-well plates and incubated overnight. The next day, the cells were inoculated with the WT or NS1-P101K variants of WNV at an MOI of 1. The inoculum was removed and replaced with 1 mL of fresh medium after two hours. Twenty hours post-inoculation, protein translation was stopped by adding cycloheximide (Sigma; final concentration of 75 μg/mL) in a 0.1 mL volume. At the indicated time points following cycloheximide addition, the cells and supernatants were harvested, and cell lysates were prepared in RIPA buffer containing Halt Protease Inhibitor Cocktail as described above. Protein levels were assessed by performing SDS-PAGE and Western blotting as described above, using the anti-NS1 mAb 16NS1 (1:1000 dilution of ascites fluid).

NS1 capture ELISA. Levels of WNV NS1 in serum were determined using a previously described capture ELISA [70]. Murine anti-NS1 mAb 10NS1 (2.5 μg/well) was immobilized onto MaxiSorp 96-well plates (Thermo) overnight at 4°C in 50 μL of sodium bicarbonate buffer, pH 9.3.

Subsequently, plates were washed four times with PBS and blocked with ELISA buffer (PBS containing 2% BSA, and 0.05% Tween 20) for 1 h at 37°C. Plates then were incubated with mouse serum samples diluted in ELISA buffer for 2 h at 37°C. To generate a standard curve for NS1 quantitation, plates were incubated with serial dilutions of recombinant WNV NS1 (Native Antigen). After washing four times with ELISA buffer, plates were incubated with biotinylated 3NS1 [67] (5 μg/mL) for 1 h at room temperature. Plates were washed again and incubated with streptavidin-conjugated horseradish peroxidase (1:625 dilution; Vector Laboratories) for 30 min. After a final wash series, plates were developed using 3,3□,5,5□-tetramethylbenzidine substrate (Agilent). The reaction was stopped using 2 N H_2SO_4 and absorbance at 450 nm was read with a TriStar Microplate Reader (Berthold Technologies).

Mouse experiments. All animal studies were performed using C57BL/6J male mice (Jax Cat. No. 000664). For most experiments, 4- to 5-week-old mice were inoculated by subcutaneous injection in the footpad with 100 FFU of WT or NS1-variant WNV in a 50 μL volume. Mice were euthanized after 21 days or on the indicated days for assessment of virus titers in specific organs. For NS1 addition experiments, on day 5 post-inoculation, mice were administered 5 μg of WNV NS1-WT (strain New York 1999; Native Antigen) in a 50 μL volume by retro-orbital injection. Commercial WNV NS1 was certified to be free of endotoxin contaminants by the manufacturer. Six hours after injection, facial vein phlebotomy was performed to quantitate NS1 in serum. For intracranial infection studies, 4- to 5-week-old mice were inoculated by intracranial injection into the right cortex with 10 FFU of WT or P101K WNV in a 10 μL volume.

Viral burden analysis. Organs were weighed and homogenized by bead dissociation using a MagNA Lyzer (Roche) in a volume of PBS or DMEM containing 2% FBS. Viral RNA was isolated from the tissue homogenates and serum using the RNeasy 96 and Viral RNA Mini kits

(Qiagen), respectively. WNV RNA levels were determined by TaqMan one-step quantitative reverse transcriptase PCR (qRT-PCR) using the following primer and probe sequences: forward primer, 5'-GGGTCAGCACGTTTGTCATTG-3'; reverse primer, 5'-TCAGCGATCTCTCCACCAAAG-3'; probe, 5'-TGCCCGACCATGGGAGAAGCTC-3' [66]. To calculate FFU equivalents from RNA levels, an RNA standard curve was generated using a defined viral stock.

NS1 cell-binding assays. (a) ***hCMEC/D3 cells***. To measure binding of NS1 to the blood-brain barrier hCMEC/D3 cells, the cells were seeded in flasks one day prior to the experiment. The next day, the cells were washed in PBS containing 4 mM EDTA and detached by incubating in FACS buffer for 5-10 minutes at 37°C. After counting, 10^5 cells were aliquoted into wells of a 96-well plate, pelleted by centrifugation, and resuspended in 100 μL of DMEM containing recombinant WT or P101K NS1 (1, 5, or 10 μg/mL). The cells were incubated on ice for 1 h and then washed in FACS buffer. Subsequently, the cells were resuspended in an oligoclonal mix of murine anti-NS1 mAbs (1 μg/mL of each): 4NS1, 8NS1, 9NS1, 10NS1, 15NS1, 17NS1, and 22NS1) [67]. After incubating for 1 h on ice, the cells were washed and stained in goat anti-mouse IgG conjugated to Alexa Fluor 647 (1:2000; Thermo) and Fixable Viability Dye eFluor 506 (1:1000; eBioscience). After incubating for 30 min on ice, the cells were washed, fixed in 1% PFA in PBS, and then resuspended in FACS buffer prior to analysis on a MACSQuant Analyzer (Miltenyi Biotec). Binding data was analyzed using Flowjo software by first gating on single, live cells and then measuring the percent of cells bound to NS1. ***(b) HBMECs.*** To measure binding of WT and P101K NS1 to HBMECs [27], 10^5 cells were seeded on 0.2% gelatin-coated glass coverslips (Sigma) in 24-well plates. Cells were allowed to form a confluent monolayer for three days, with medium changes every other day. On the day of the experiment, recombinant His-tagged NS1 protein at 10

μg/mL (3 μg total protein) was added to wells and incubated for 1 h at 37°C. Subsequently, cells were incubated for 30 min at 37°C with a mouse anti-His antibody conjugated to Alexa Fluor 647 (1:200; Novus Biologicals) and nuclear stain Hoechst 33342 (1:200; Immunochemistry Cat. No. 639). Cells were washed twice in PBS and fixed in 4% formaldehyde. Coverslips were mounted onto microscope slides on a drop of ProLong Gold (Thermo Cat. No. P10144) and imaged using a Zeiss LSM 710 inverted confocal microscope (CRL Molecular Imaging Center, University of California, Berkeley).

Trans-endothelial electrical resistance (TEER) assay. As previously described [21], we used a TEER assay to measure the capacity of NS1 proteins to trigger endothelial hyperpermeability of HBMECs. 10^5 HBMECs were seeded in 300 μL of culture medium into each apical chamber of a 24-well polycarbonate membrane transwell (Corning Transwell with 0.4 μm pore size with 6.5 mm insert; Fisher Cat. No. 07-200-147). Medium (1.5 mL) was added to the basolateral chamber, and the cell monolayer was allowed to grow to confluence for three days, with daily media changes for the apical and basolateral chambers. On the day of TEER assay, NS1 protein at 5 μg/mL (1.5 μg total protein) was added to the apical chambers of the transwells. Electrical resistance values were measured in ohms (Ω) at specified timepoints using an Epithelial Volt Ohm Meter (EVOM) with "chopstick" electrodes (World Precision Instruments). Transwells without cells (medium only) or with non-treated HBMECs served as negative controls to calculate the baseline electrical resistance. Relative TEER was calculated as the ratio of resistance values according to the following formula: (Ω NS1-treated cells - Ω medium alone)/(Ω non-treated cells - Ω medium alone).

Complement factor binding ELISAs. Binding of WT and P101K NS1 proteins to complement factors (purchased from Complement Technologies) was performed by ELISA. The complement

proteins (factor H, 2.5 μg; C4 and C4b, 0.5 μg) were adsorbed to MaxiSorp 96-well plates (Thermo) overnight at 4°C in 50 μL of sodium bicarbonate buffer, pH 9.3. Subsequently, plates were washed four times with PBS and blocked with ELISA buffer (PBS containing 2% BSA, and 0.05% Tween 20) for 4 h at room temperature. Plates then were incubated with serial dilutions of recombinant WT or P101K NS1 proteins in ELISA buffer for 1.5 h. After washing, plates were incubated for 30 min with an oligoclonal cocktail of biotinylated anti-NS1 mAbs (3NS1, 8NS1, 9NS1, and 22NS1; 2 μg/mL for each mAb). After another wash series and incubation with streptavidin-conjugated horseradish peroxidase, plates were developed and read as described above.

Data analysis. The statistical tests for each data set are indicated in the respective legends and were performed using GraphPad Prism 8 software. Survival curves were analyzed by the log-rank Mantel-Cox test with a Bonferroni correction. Expression levels of WT versus P101K NS1 in flow cytometric assays were assessed by the Mann-Whitney test. To compare WNV WT and P101K in the context of NS1 antigenemia and tissue viral burden across multiple days post-infection, Mann-Whitney tests or two-way ANOVAs were performed with Sidak's post-test. Statistical significance was defined as $p < 0.05$.

Data availability. All primary data will be made publicly available upon publication.

4.6 Acknowledgements

This study was supported by NIH grants R01 AI073755 and 75N93019C00062 and contract HHSN272201400058C and HHSN272201700060C. A.W.W. was supported by an NIH pre-doctoral training grant award (T32 5T32AI007172-38) and the Medical Scientist Training Program. K.A.D., C.R.D., and T.C.P were supported by the Intramural Program of NIAID.

4.7 References

1 Daep, C. A., Muñoz-Jordán, J. L. & Eugenin, E. A. Flaviviruses, an expanding threat in public health: focus on dengue, West Nile, and Japanese encephalitis virus. *J Neurovirol* **20**, 539-560, doi:10.1007/s13365-014-0285-z (2014).

2 Bhatt, S. *et al.* The global distribution and burden of dengue. *Nature* **496**, 504-507, doi:10.1038/nature12060 (2013).

3 Lindenbach, B. D. & Rice, C. M. trans-Complementation of yellow fever virus NS1 reveals a role in early RNA replication. *J Virol* **71**, 9608-9617 (1997).

4 Youn, S. *et al.* Evidence for a genetic and physical interaction between nonstructural proteins NS1 and NS4B that modulates replication of West Nile virus. *J Virol* **86**, 7360-7371, doi:10.1128/jvi.00157-12 (2012).

5 Plaszczyca, A. *et al.* A novel interaction between dengue virus nonstructural protein 1 and the NS4A-2K-4B precursor is required for viral RNA replication but not for formation of the membranous replication organelle. *PLoS Pathog* **15**, e1007736, doi:10.1371/journal.ppat.1007736 (2019).

6 Winkler, G., Maxwell, S. E., Ruemmler, C. & Stollar, V. Newly synthesized dengue-2 virus nonstructural protein NS1 is a soluble protein but becomes partially hydrophobic and membrane-associated after dimerization. *Virology* **171**, 302-305, doi:10.1016/0042-6822(89)90544-8 (1989).

7 Winkler, G., Randolph, V. B., Cleaves, G. R., Ryan, T. E. & Stollar, V. Evidence that the mature form of the flavivirus nonstructural protein NS1 is a dimer. *Virology* **162**, 187-196, doi:10.1016/0042-6822(88)90408-4 (1988).

8 Noisakran, S. *et al.* Association of dengue virus NS1 protein with lipid rafts. *J Gen Virol* **89**, 2492-2500, doi:10.1099/vir.0.83620-0 (2008).

9 Muller, D. A. & Young, P. R. The flavivirus NS1 protein: molecular and structural biology, immunology, role in pathogenesis and application as a diagnostic biomarker. *Antiviral Res* **98**, 192-208, doi:10.1016/j.antiviral.2013.03.008 (2013).

10 Young, P. R., Hilditch, P. A., Bletchly, C. & Halloran, W. An Antigen Capture Enzyme-Linked Immunosorbent Assay Reveals High Levels of the Dengue Virus Protein NS1 in the Sera of Infected Patients. *Journal of Clinical Microbiology* **38**, 1053-1057 (2000).

11 Bosch, I. *et al.* Rapid antigen tests for dengue virus serotypes and Zika virus in patient serum. *Science Translational Medicine* **9**, eaan1589, doi:10.1126/scitranslmed.aan1589 (2017).

12 Macdonald, J. *et al.* NS1 Protein Secretion during the Acute Phase of West Nile Virus Infection. *Journal of Virology* **79**, 13924-13933, doi:10.1128/jvi.79.22.13924-13933.2005 (2005).

13 Modhiran, N. *et al.* Dengue virus NS1 protein activates cells via Toll-like receptor 4 and disrupts endothelial cell monolayer integrity. *Sci Transl Med* **7**, 304ra142, doi:10.1126/scitranslmed.aaa3863 (2015).

14 Modhiran, N. *et al.* Dengue virus NS1 protein activates immune cells via TLR4 but not TLR2 or TLR6. *Immunol Cell Biol* **95**, 491-495, doi:10.1038/icb.2017.5 (2017).

15 Chung, K. M. *et al.* West Nile virus nonstructural protein NS1 inhibits complement activation by binding the regulatory protein factor H. *Proc Natl Acad Sci U S A* **103**, 19111-19116, doi:10.1073/pnas.0605668103 (2006).

16 Avirutnan, P. *et al.* Antagonism of the complement component C4 by flavivirus nonstructural protein NS1. *J Exp Med* **207**, 793-806, doi:10.1084/jem.20092545 (2010).
17 Avirutnan, P. *et al.* Binding of flavivirus nonstructural protein NS1 to C4b binding protein modulates complement activation. *J Immunol* **187**, 424-433, doi:10.4049/jimmunol.1100750 (2011).
18 Conde, J. N. *et al.* Inhibition of the Membrane Attack Complex by Dengue Virus NS1 through Interaction with Vitronectin and Terminal Complement Proteins. *J Virol* **90**, 9570-9581, doi:10.1128/jvi.00912-16 (2016).
19 Avirutnan, P. *et al.* Secreted NS1 of dengue virus attaches to the surface of cells via interactions with heparan sulfate and chondroitin sulfate E. *PLoS Pathog* **3**, e183, doi:10.1371/journal.ppat.0030183 (2007).
20 Beatty, P. R. *et al.* Dengue virus NS1 triggers endothelial permeability and vascular leak that is prevented by NS1 vaccination. *Science Translational Medicine* **7**, 304ra141-304ra141, doi:10.1126/scitranslmed.aaa3787 (2015).
21 Puerta-Guardo, H. *et al.* Flavivirus NS1 Triggers Tissue-Specific Vascular Endothelial Dysfunction Reflecting Disease Tropism. *Cell Rep* **26**, 1598-1613.e1598, doi:10.1016/j.celrep.2019.01.036 (2019).
22 Puerta-Guardo, H., Glasner, D. R. & Harris, E. Dengue Virus NS1 Disrupts the Endothelial Glycocalyx, Leading to Hyperpermeability. *PLOS Pathogens* **12**, e1005738, doi:10.1371/journal.ppat.1005738 (2016).
23 Akey, D. L. *et al.* Flavivirus NS1 structures reveal surfaces for associations with membranes and the immune system. *Science* **343**, 881-885, doi:10.1126/science.1247749 (2014).
24 Brown, W. C. *et al.* Extended surface for membrane association in Zika virus NS1 structure. *Nat Struct Mol Biol* **23**, 865-867, doi:10.1038/nsmb.3268 (2016).
25 Edeling, M. A., Diamond, M. S. & Fremont, D. H. Structural basis of Flavivirus NS1 assembly and antibody recognition. *Proc Natl Acad Sci U S A* **111**, 4285-4290, doi:10.1073/pnas.1322036111 (2014).
26 Xu, X. *et al.* Contribution of intertwined loop to membrane association revealed by Zika virus full-length NS1 structure. *Embo j* **35**, 2170-2178, doi:10.15252/embj.201695290 (2016).
27 Biering, S. B. *et al.* Structural basis for antibody inhibition of flavivirus NS1–triggered endothelial dysfunction. *Science* **371**, 194-200, doi:10.1126/science.abc0476 (2021).
28 Wessel, A. W. *et al.* Antibodies targeting epitopes on the cell-surface form of NS1 protect against Zika virus infection during pregnancy. *Nature Communications* **11**, 5278, doi:10.1038/s41467-020-19096-y (2020).
29 Modhiran, N. *et al.* A broadly protective antibody that targets the flavivirus NS1 protein. *Science* **371**, 190-194, doi:10.1126/science.abb9425 (2021).
30 Youn, S., Cho, H., Fremont, D. H. & Diamond, M. S. A Short N-Terminal Peptide Motif on Flavivirus Nonstructural Protein NS1 Modulates Cellular Targeting and Immune Recognition. *Journal of Virology* **84**, 9516-9532, doi:10.1128/jvi.00775-10 (2010).
31 Alcon, S. *et al.* Enzyme-linked immunosorbent assay specific to Dengue virus type 1 nonstructural protein NS1 reveals circulation of the antigen in the blood during the acute phase of disease in patients experiencing primary or secondary infections. *J Clin Microbiol* **40**, 376-381, doi:10.1128/jcm.40.02.376-381.2002 (2002).

32 Mehlhop , E. & Diamond , M. S. Protective immune responses against West Nile virus are primed by distinct complement activation pathways. *Journal of Experimental Medicine* **203**, 1371-1381, doi:10.1084/jem.20052388 (2006).
33 Bokisch, V. A., Top, F. H., Russell, P. K., Dixon, F. J. & Müller-Eberhard, H. J. The Potential Pathogenic Role of Complement in Dengue Hemorrhagic Shock Syndrome. *New England Journal of Medicine* **289**, 996-1000, doi:10.1056/nejm197311082891902 (1973).
34 Krishna, V. D., Rangappa, M. & Satchidanandam, V. Virus-Specific Cytolytic Antibodies to Nonstructural Protein 1 of Japanese Encephalitis Virus Effect Reduction of Virus Output from Infected Cells. *Journal of Virology* **83**, 4766-4777, doi:10.1128/jvi.01850-08 (2009).
35 Wang, C. *et al.* Endocytosis of flavivirus NS1 is required for NS1-mediated endothelial hyperpermeability and is abolished by a single N-glycosylation site mutation. *PLoS Pathog* **15**, e1007938, doi:10.1371/journal.ppat.1007938 (2019).
36 Lin, T.-Y. *et al.* A Novel Approach for the Rapid Mutagenesis and Directed Evolution of the Structural Genes of West Nile Virus. *Journal of Virology* **86**, 3501-3512, doi:10.1128/jvi.06435-11 (2012).
37 Goo, L., VanBlargan, L. A., Dowd, K. A., Diamond, M. S. & Pierson, T. C. A single mutation in the envelope protein modulates flavivirus antigenicity, stability, and pathogenesis. *PLOS Pathogens* **13**, e1006178, doi:10.1371/journal.ppat.1006178 (2017).
38 Youn, S., Ambrose, R. L., Mackenzie, J. M. & Diamond, M. S. Non-structural protein-1 is required for West Nile virus replication complex formation and viral RNA synthesis. *Virology Journal* **10**, 339, doi:10.1186/1743-422X-10-339 (2013).
39 McGee, C. E. *et al.* Infection, dissemination, and transmission of a West Nile virus green fluorescent protein infectious clone by Culex pipiens quinquefasciatus mosquitoes. *Vector Borne Zoonotic Dis* **10**, 267-274, doi:10.1089/vbz.2009.0067 (2010).
40 Engle, M. J. & Diamond, M. S. Antibody prophylaxis and therapy against West Nile virus infection in wild-type and immunodeficient mice. *J Virol* **77**, 12941-12949, doi:10.1128/jvi.77.24.12941-12949.2003 (2003).
41 Chao, C. H. *et al.* Dengue virus nonstructural protein 1 activates platelets via Toll-like receptor 4, leading to thrombocytopenia and hemorrhage. *PLoS Pathog* **15**, e1007625, doi:10.1371/journal.ppat.1007625 (2019).
42 Shrestha, B. & Diamond, M. S. Role of CD8+ T cells in control of West Nile virus infection. *J Virol* **78**, 8312-8321, doi:10.1128/jvi.78.15.8312-8321.2004 (2004).
43 White, J. P. *et al.* Intestinal Dysmotility Syndromes following Systemic Infection by Flaviviruses. *Cell* **175**, 1198-1212.e1112, doi:10.1016/j.cell.2018.08.069 (2018).
44 Libraty, D. H. *et al.* High Circulating Levels of the Dengue Virus Nonstructural Protein NS1 Early in Dengue Illness Correlate with the Development of Dengue Hemorrhagic Fever. *The Journal of Infectious Diseases* **186**, 1165-1168, doi:10.1086/343813 (2002).
45 Avirutnan, P. *et al.* Vascular leakage in severe dengue virus infections: a potential role for the nonstructural viral protein NS1 and complement. *J Infect Dis* **193**, 1078-1088, doi:10.1086/500949 (2006).
46 Chan, K. W. K. *et al.* A T164S mutation in the dengue virus NS1 protein is associated with greater disease severity in mice. *Science Translational Medicine* **11**, eaat7726, doi:10.1126/scitranslmed.aat7726 (2019).
47 Han, G.-Z. A Single Substitution Changes Zika Virus Infectivity in Mosquitoes. *Trends in Microbiology* **25**, 603-605, doi:10.1016/j.tim.2017.05.014 (2017).

48 Lee, T. H. *et al.* A cross-protective mAb recognizes a novel epitope within the flavivirus NS1 protein. *Journal of General Virology* **93**, 20-26, doi:https://doi.org/10.1099/vir.0.036640-0 (2012).
49 Puerta-Guardo, H. *et al.* Zika Virus Nonstructural Protein 1 Disrupts Glycosaminoglycans and Causes Permeability in Developing Human Placentas. *J Infect Dis* **221**, 313-324, doi:10.1093/infdis/jiz331 (2020).
50 Scaturro, P., Cortese, M., Chatel-Chaix, L., Fischl, W. & Bartenschlager, R. Dengue Virus Non-structural Protein 1 Modulates Infectious Particle Production via Interaction with the Structural Proteins. *PLOS Pathogens* **11**, e1005277, doi:10.1371/journal.ppat.1005277 (2015).
51 Blitvich, B. J., Mackenzie, J. S., Coelen, R. J., Howard, M. J. & Hall, R. A. A novel complex formed between the flavivirus E and NS1 proteins: analysis of its structure and function. *Arch Virol* **140**, 145-156, doi:10.1007/bf01309729 (1995).
52 Alcon-LePoder, S. *et al.* The secreted form of dengue virus nonstructural protein NS1 is endocytosed by hepatocytes and accumulates in late endosomes: implications for viral infectivity. *J Virol* **79**, 11403-11411, doi:10.1128/jvi.79.17.11403-11411.2005 (2005).
53 Villaseñor, R. *et al.* Region-specific permeability of the blood-brain barrier upon pericyte loss. *J Cereb Blood Flow Metab* **37**, 3683-3694, doi:10.1177/0271678x17697340 (2017).
54 Banks, W. A., Clever, C. M. & Farrell, C. L. Partial saturation and regional variation in the blood-to-brain transport of leptin in normal weight mice. *Am J Physiol Endocrinol Metab* **278**, E1158-1165, doi:10.1152/ajpendo.2000.278.6.E1158 (2000).
55 Banks, W. A. & Kastin, A. J. Differential permeability of the blood-brain barrier to two pancreatic peptides: insulin and amylin. *Peptides* **19**, 883-889, doi:10.1016/s0196-9781(98)00018-7 (1998).
56 Moinuddin, A., Morley, J. E. & Banks, W. A. Regional variations in the transport of interleukin-1alpha across the blood-brain barrier in ICR and aging SAMP8 mice. *Neuroimmunomodulation* **8**, 165-170, doi:10.1159/000054814 (2000).
57 Daniels, B. P. *et al.* Regional astrocyte IFN signaling restricts pathogenesis during neurotropic viral infection. *J Clin Invest* **127**, 843-856, doi:10.1172/jci88720 (2017).
58 Cho, H. *et al.* Differential innate immune response programs in neuronal subtypes determine susceptibility to infection in the brain by positive-stranded RNA viruses. *Nature Medicine* **19**, 458-464, doi:10.1038/nm.3108 (2013).
59 Modhiran, N. *et al.* Dual targeting of dengue virus virions and NS1 protein with the heparan sulfate mimic PG545. *Antiviral Res* **168**, 121-127, doi:10.1016/j.antiviral.2019.05.004 (2019).
60 Davis, C. W. *et al.* West Nile Virus Discriminates between DC-SIGN and DC-SIGNR for Cellular Attachment and Infection. *Journal of Virology* **80**, 1290-1301, doi:10.1128/jvi.80.3.1290-1301.2006 (2006).
61 Funk, K. E. & Lotz, S. K. Assessing the Expression of Major Histocompatibility Complex Class I on Primary Murine Hippocampal Neurons by Flow Cytometry. *J Vis Exp*, doi:10.3791/61436 (2020).
62 Funk, K. E., Mirbaha, H., Jiang, H., Holtzman, D. M. & Diamond, M. I. Distinct Therapeutic Mechanisms of Tau Antibodies: Promoting Microglial Clearance Versus Blocking Neuronal Uptake. *J Biol Chem* **290**, 21652-21662, doi:10.1074/jbc.M115.657924 (2015).

63 Mancia, F. *et al.* Optimization of protein production in mammalian cells with a coexpressed fluorescent marker. *Structure* **12**, 1355-1360, doi:10.1016/j.str.2004.06.012 (2004).
64 Kinney, R. M. *et al.* Avian virulence and thermostable replication of the North American strain of West Nile virus. *Journal of General Virology* **87**, 3611-3622, doi:https://doi.org/10.1099/vir.0.82299-0 (2006).
65 Beasley, D. W. C. *et al.* Envelope Protein Glycosylation Status Influences Mouse Neuroinvasion Phenotype of Genetic Lineage 1 West Nile Virus Strains. *Journal of Virology* **79**, 8339-8347, doi:10.1128/jvi.79.13.8339-8347.2005 (2005).
66 Brien, J. D., Lazear, H. M. & Diamond, M. S. Propagation, Quantification, Detection, and Storage of West Nile Virus. *Current Protocols in Microbiology* **31**, 15D.13.11-15D.13.18, doi:10.1002/9780471729259.mc15d03s31 (2013).
67 Chung, K. M. *et al.* Antibodies against West Nile Virus nonstructural protein NS1 prevent lethal infection through Fc gamma receptor-dependent and -independent mechanisms. *J Virol* **80**, 1340-1351, doi:10.1128/jvi.80.3.1340-1351.2006 (2006).
68 Nybakken, G. E. *et al.* Structural basis of West Nile virus neutralization by a therapeutic antibody. *Nature* **437**, 764-769, doi:10.1038/nature03956 (2005).
69 Oliphant, T. *et al.* Development of a humanized monoclonal antibody with therapeutic potential against West Nile virus. *Nat Med* **11**, 522-530, doi:10.1038/nm1240 (2005).
70 Chung, K. M. & Diamond, M. S. Defining the levels of secreted non-structural protein NS1 after West Nile virus infection in cell culture and mice. *J Med Virol* **80**, 547-556, doi:10.1002/jmv.21091 (2008).

Table 4.1 List of mutagenesis primers		
Mutant	**Primer**	**Sequence**
A27T	Forward	TACACAATGATGTGGAGACTTGGATGGACCGGTAC
Y34F	Forward	GATGGACCGGTACAAGTTTTACCCTGAAACGCCAC
A70Q	Forward	CTGGAGCATCAAATGTGGGAACAGGTGAAGGACGAGCTGAACAC
P101K	Forward	GGGAATGTACAAGTCAGCAAAGAAACGCCTCACCGCCACCA
S199G	Forward	GCGATCCACAGTGACCTGGGCTATTGGATTGAAAGCAG
A27T	Reverse	GTACCGGTCCATCCAAGTCTCCACATCATTGTGTA
Y34F	Reverse	GTGGCGTTTCAGGGTAAAACTTGTACCGGTCCATC
A70Q	Reverse	GTGTTCAGCTCGTCCTTCACCTGTTCCCACATTTGATGCTCCAG
P101K	Reverse	TGGTGGCGGTGAGGCGTTTCTTTGCTGACTTGTACATTCCC
S199G	Reverse	CTGCTTTCAATCCAATAGCCCAGGTCACTGTGGATCGC

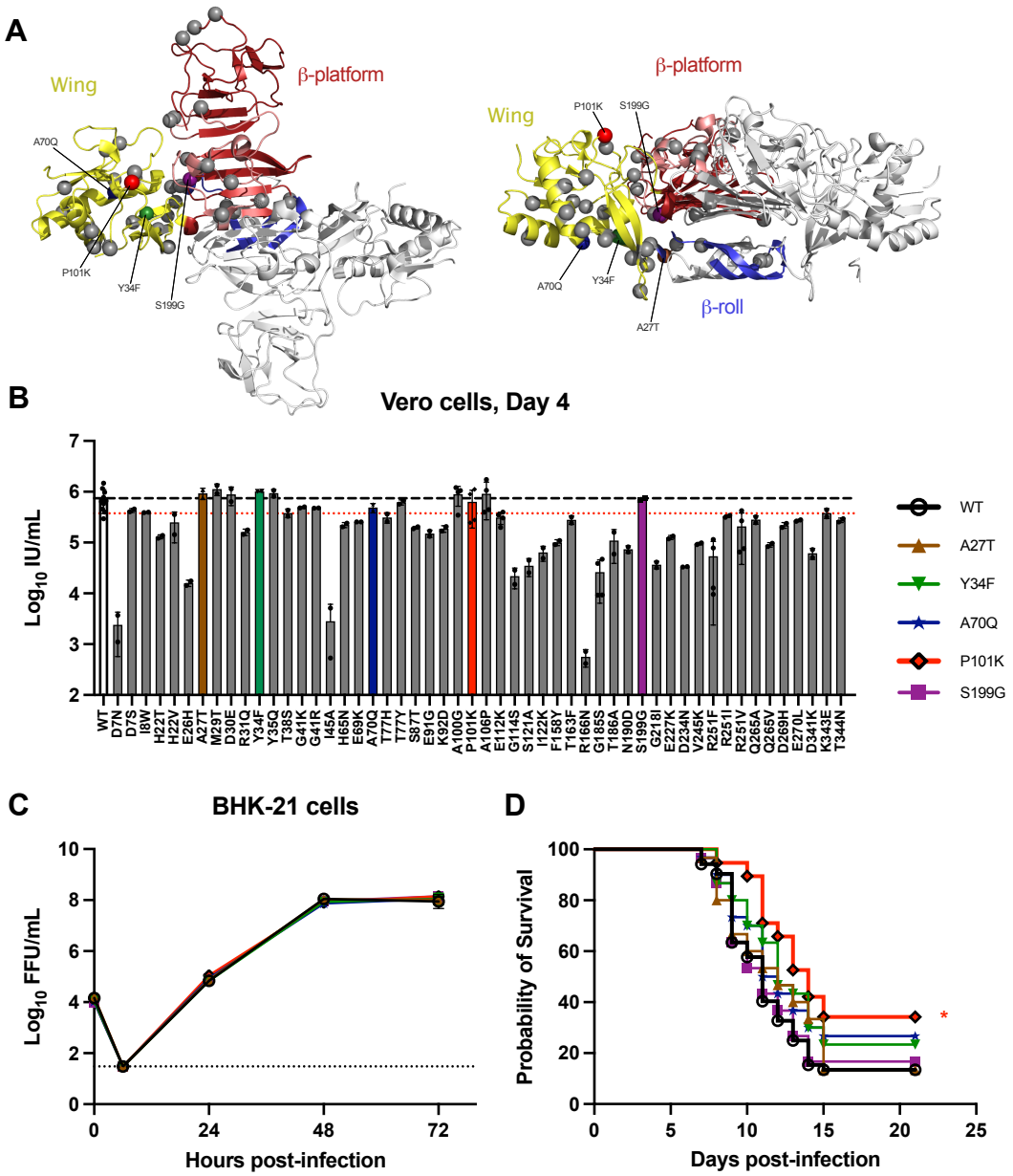

Figure 4.1. The NS1-P101K variant of WNV replicates efficiently *in vitro* but is attenuated in mice. (**A**) Structural representation of the WNV NS1 dimer (PDB 4O6D), with one monomer colored by domain: blue, β-roll; yellow, wing; red, β-platform. The second monomer is colored silver in each dimer. Substitution variants that were generated in the GFP-expressing WNV infectious clone are represented by gray or colored spheres. This figure was prepared using PyMOL software (Version 1.2r3pre, Schrödinger, LLC). (**B-C**) WNV replication kinetics *in vitro*. (**B**) Vero cells were inoculated with GFP-expressing WNV NS1 variants at an MOI of 0.01. Four days post-inoculation, virus in the supernatant was titered on Raji-DCSIGNR cells (IU/mL, infectious units per mL). Each dot represents an independent experiment (n = 10 for WT, n = 2-4 for each NS1 variant). Bar height, mean values; error bars, standard deviation (SD). Black dashed line represents the mean titer of WT virus; red dotted line represents one SD from the WT mean. (**C**) BHK-21 cells were inoculated with five selected WNV NS1 variants (without GFP; colored bars in **B**) at an MOI of 0.01. Virus in the supernatant was titered at the indicated time points by focus-forming assay (FFA). Data are pooled from two experiments performed in duplicate; error bars, SD. (**D**) Survival analysis.

Four- to five-week-old male C57BL/6J mice were inoculated with 10^2 FFU of the same WNV NS1 variants as in **C**. Survival was analyzed by the log-rank Mantel-Cox test with a Bonferroni correction (*$p<0.05$; WT, n = 52, two experiments; P101K, n = 38, three experiments; all other variants, n = 30, two experiments).

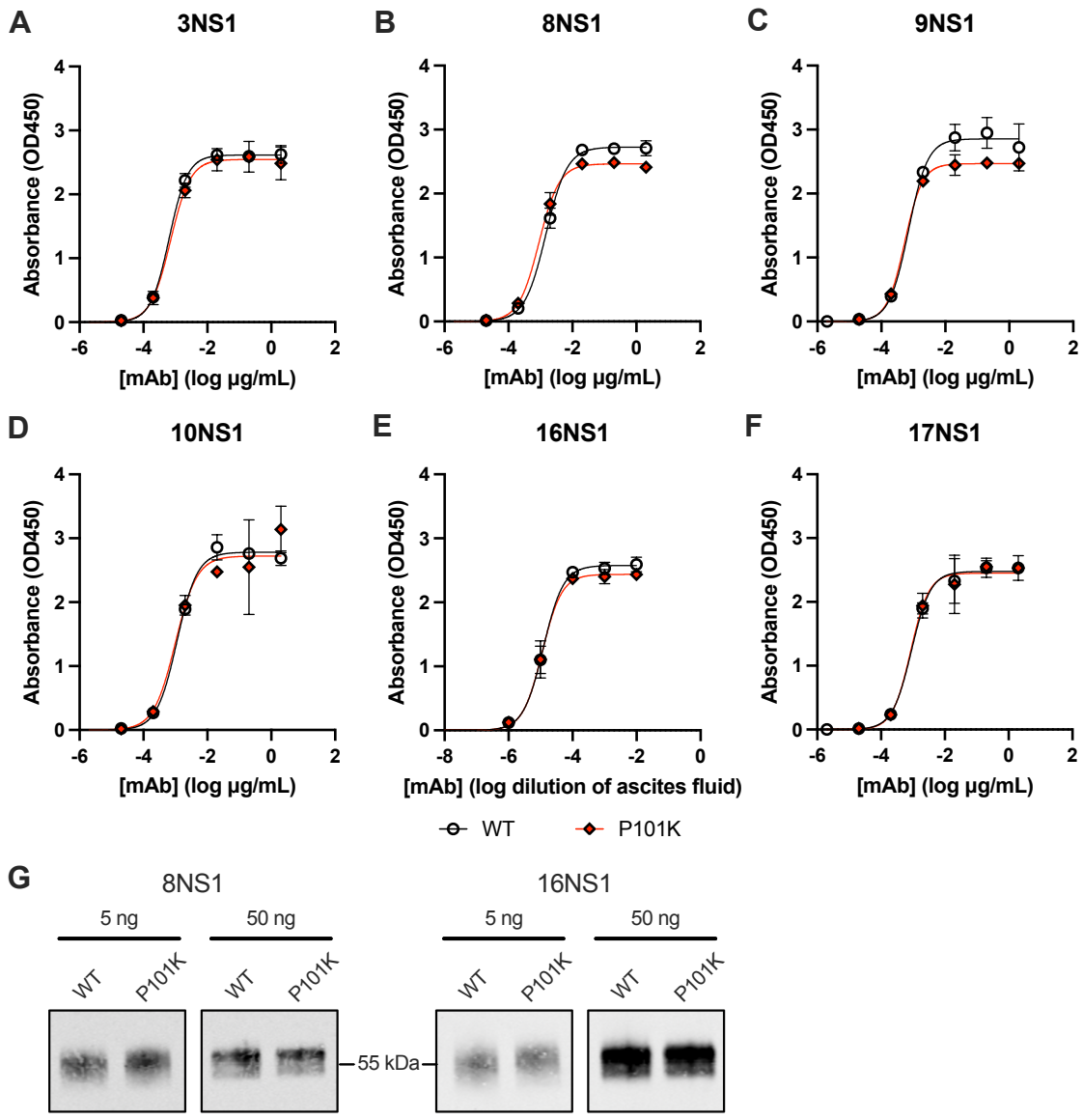

Figure 4.2. Anti-NS1 mouse mAbs retain binding to NS1-P101K protein. (**A-F**) Avidity of binding to recombinant WT and P101K protein was determined by direct ELISA for the following anti-NS1 mouse mAbs: (**A**) 3NS1, (**B**) 8NS1, (**C**) 9NS1, (**D**) 10NS1, (**E**) 16NS1, and (**F**) 17NS1. (**G**) Binding of anti-NS1 mouse mAbs 8NS1 (left) and 16NS1 (right) to boiled and reduced recombinant WT and P101K NS1 proteins (5 or 50 ng per lane) was performed by Western blotting.

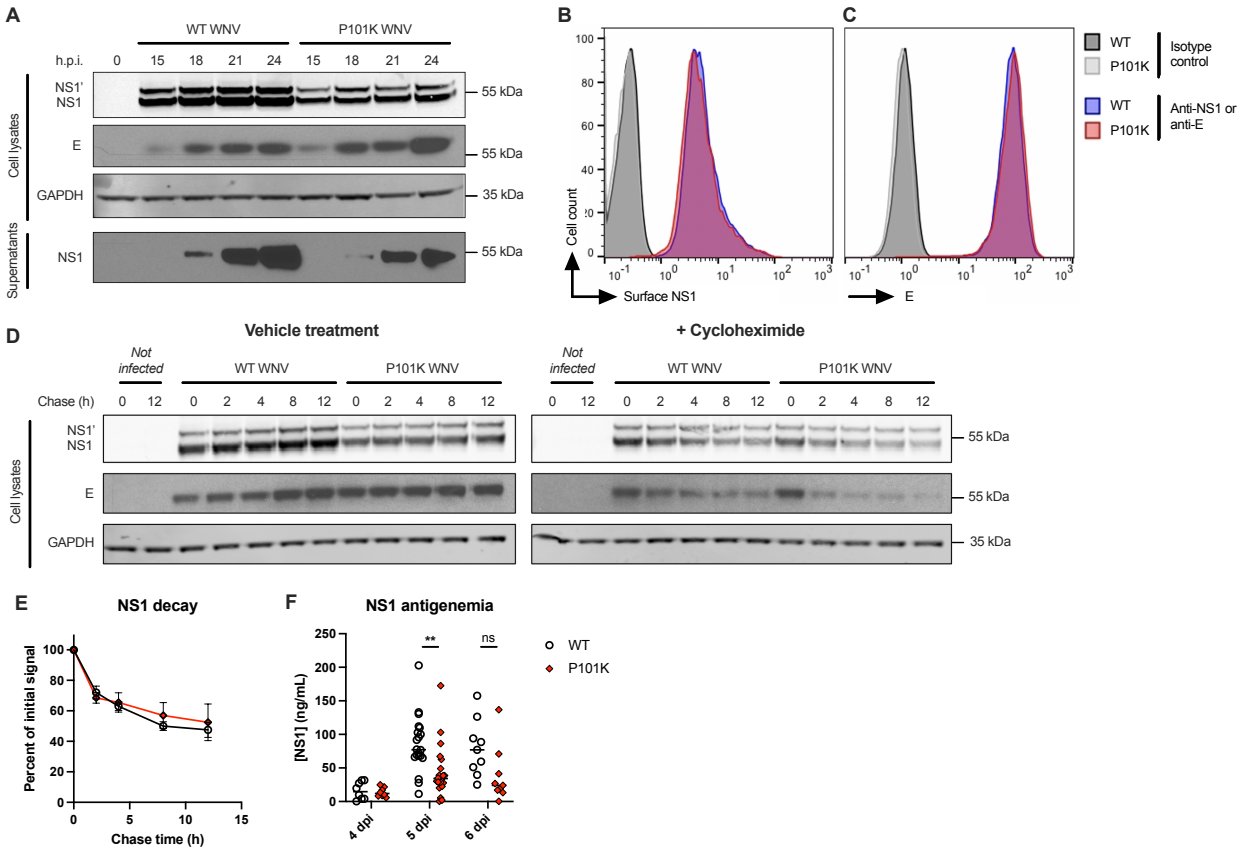

Figure 4.3. NS1-P101K substitution results in lower levels of cellular and secreted NS1. (**A**) Cellular and secreted levels of NS1. Vero cells were inoculated with the WT and NS1-P101K variant of WNV at an MOI of 5. Cell lysates and supernatants were harvested at the indicated time points, and protein levels were assessed by Western blotting using the following antibodies: anti-NS1 (8NS1), anti-E (hE16 and chE60), and anti-GAPDH. Images are representative of three experiments. (**B-C**) Cell surface NS1. Vero cells were inoculated with WNV as in **A** for 18 h and then analyzed by flow cytometry. Representative histograms are shown for cell surface staining with an oligoclonal mix of anti-NS1 mAbs (8NS1, 9NS1, 10NS1, and 17NS1) (**B**) and intracellular staining with an anti-E mAb (hE16) (**C**). Surface and intracellular staining with isotype control mAbs are shown. Data are representative of two experiments performed in duplicate. (**D**) Stability of cellular NS1. Vero cells were inoculated with WNV at an MOI of 1 for 20 h and then treated with cycloheximide (0 h chase time point). Cell lysates were harvested at the indicated chase time points, and protein levels were assessed by Western blotting using anti-NS1 16NS1, anti-E hE16, and anti-GAPDH antibodies. Images are representative of two experiments. (**E**) Densitometry analysis of **D**. Data represent the fraction of NS1 (normalized to GAPDH) remaining over time compared to the initiation of cycloheximide treatment. Densitometry was performed for two experiments; error bars, SD. (**F**) NS1 antigenemia. Four- to five-week-old male C57BL/6J mice were inoculated subcutaneously with 10^2 FFU of the WNV WT or NS1-P101K. On the indicated days post-infection, serum was collected and NS1 levels were determined by capture ELISA. Data are from at least two experiments per time point (two-way ANOVA with Sidak's post-test: **p<0.01; day +4: WT, n = 8 and P101K, n = 8; day +5: WT, n = 20 and P101K, n = 21; day +6: WT, n = 9 and P101K, n = 9).

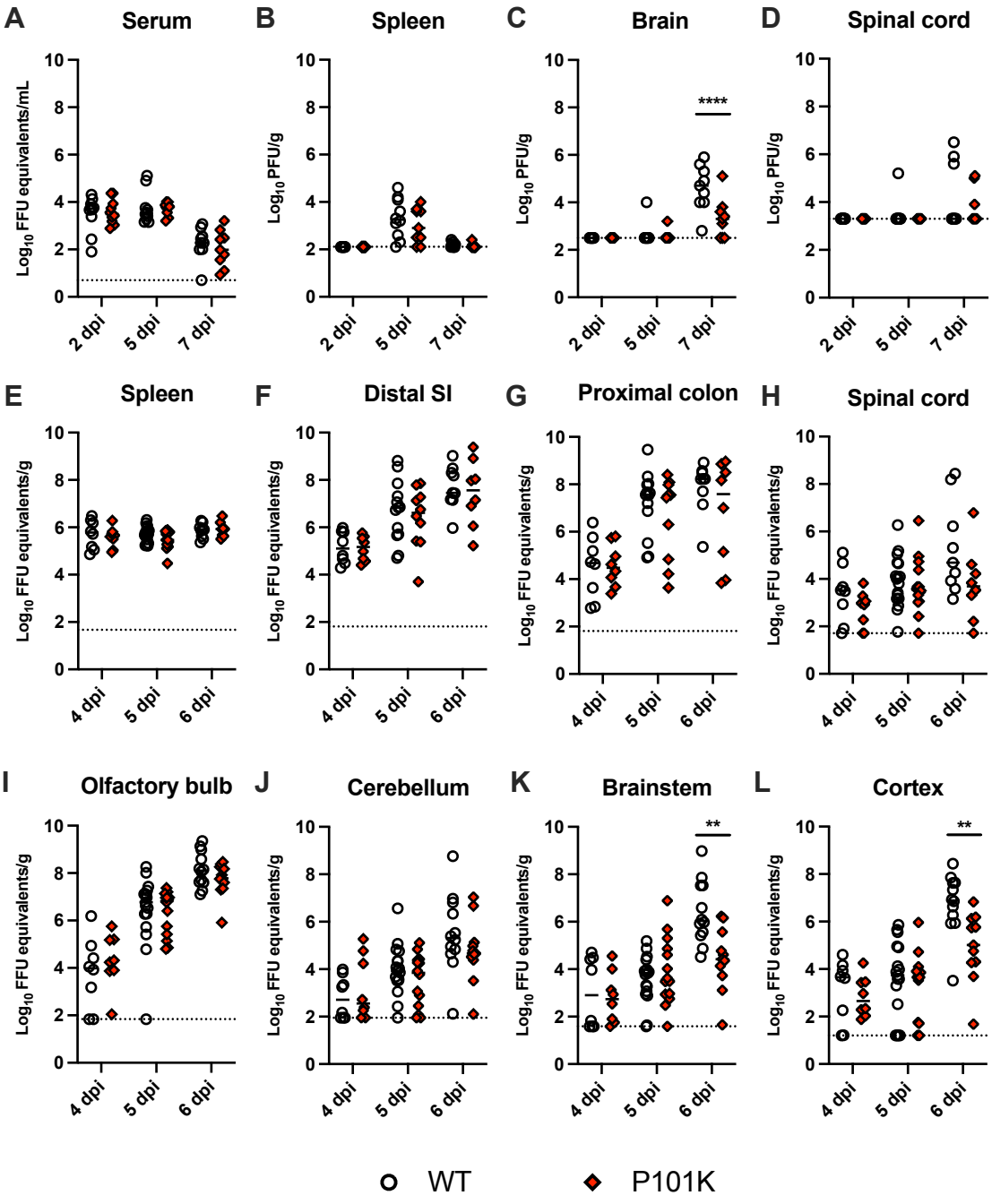

Figure 4.4. WNV NS1-P101K replicates efficiently in peripheral organs of mice but produces lower titers in the brain. (**A-D**) Four- to five-week-old male C57BL/7J mice were inoculated subcutaneously with 10^2 FFU of WNV WT or NS1-P101K. On the indicated days post-infection, viral titers were determined by RT-qPCR in serum (**A**) and by plaque assay in the (**B**) spleen, (**C**) brain, and (**D**) spinal cord. Data are from two experiments per time point (two-way ANOVA with Sidak's post-test: ****p<0.0001; Day +2: WT, n = 10 and P101K, n = 10; Day +5: WT, n = 10 and P101K, n = 9; Day +7: WT, n = 9 and P101K, n = 9). (**E-L**) Mice were inoculated with 10^2 FFU of WNV as in **A-D**, and viral RNA levels were determined by RT-qPCR in the following tissues: (**E**) spleen, (**F**) distal small intestine (SI), (**G**) proximal colon, (**H**) spinal cord, (**I**) olfactory bulb, (**J**) cerebellum, (**K**) brainstem, and (**L**) cerebral cortex. Data are from at least two experiments per time point (two-way ANOVA with post-test: **p<0.01; Day +4: WT, n

= 8 and P101K, n = 8; Day +5: WT, n = 13 (**E**-**H**) or 17 (**I**-**L**) and P101K, n = 10 (**E**-**H**) or 14 (**I**-**L**); Day +6: WT, n = 9 (**E**-**H**) or 12 (**I**-**L)** and P101K, n = 8 (**E**-**H**) or 11 (**I**-**L**)).

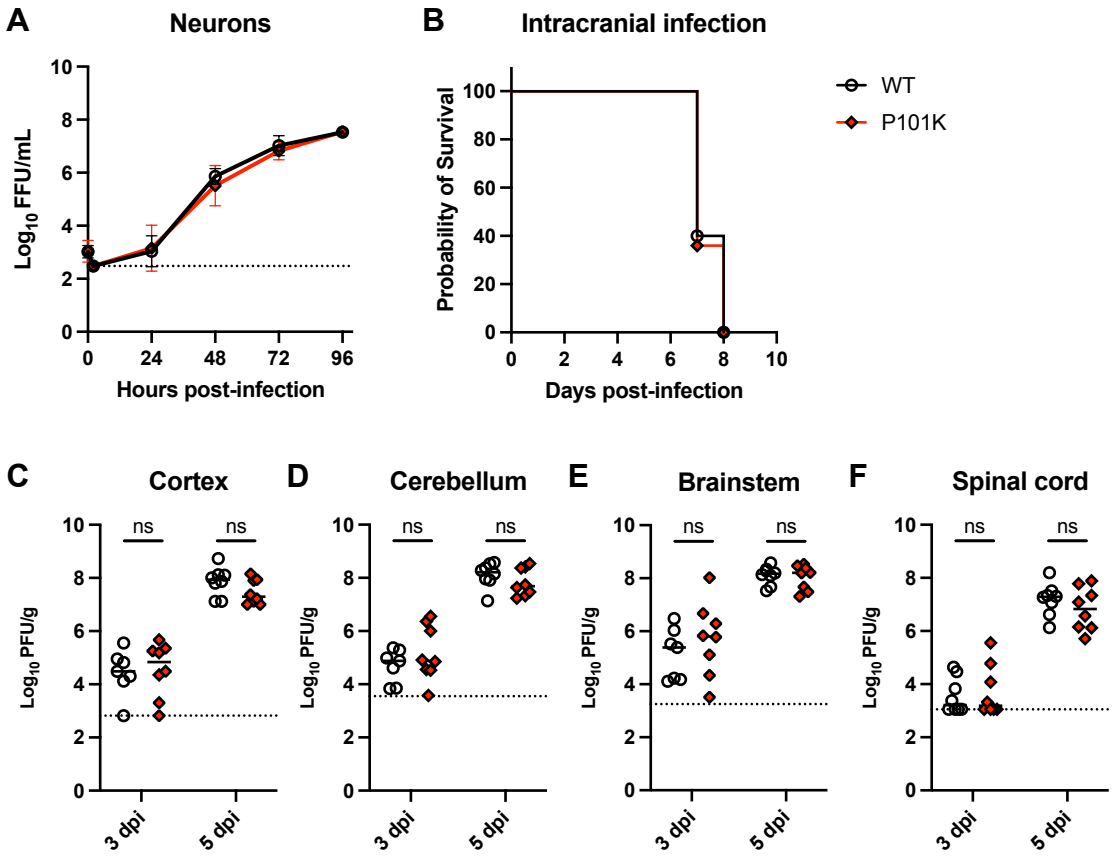

Figure 4.5. WNV NS1-P101K replicates efficiently in neurons *in vitro* and *in vivo*. (**A**) WNV replication kinetics in neurons. Primary murine cortical neurons were inoculated with the WNV WT or NS1-P101K at an MOI of 0.001. Virus in the supernatant was titered at the indicated time points by focus-forming assay (FFA). Data include two experiments performed in duplicate; error bars, SD. (**B**) Survival analysis following intracranial infection. Four- to five-week-old male C57BL/6J mice were inoculated via intracranial injection with 10^1 FFU of the WNV WT or NS1-P101K. Data are from two experiments and were analyzed by the log-rank Mantel-Cox test (WT, n = 25; P101K, n = 25). (**C-F**) Mice were inoculated via intracranial injection with WNV as in **B,** and viral burden was measured by plaque assay on the indicated days post-infection in the following tissues: (**C**) cerebral cortex, (**D**) cerebellum, (**E**) brainstem, and (**F**) spinal cord. Data are from two experiments (two-way ANOVA with Sidak's post-test: Day +3: WT, n = 7 and P101K, n = 8; Day +5: WT, n = 8 and P101K, n = 8).

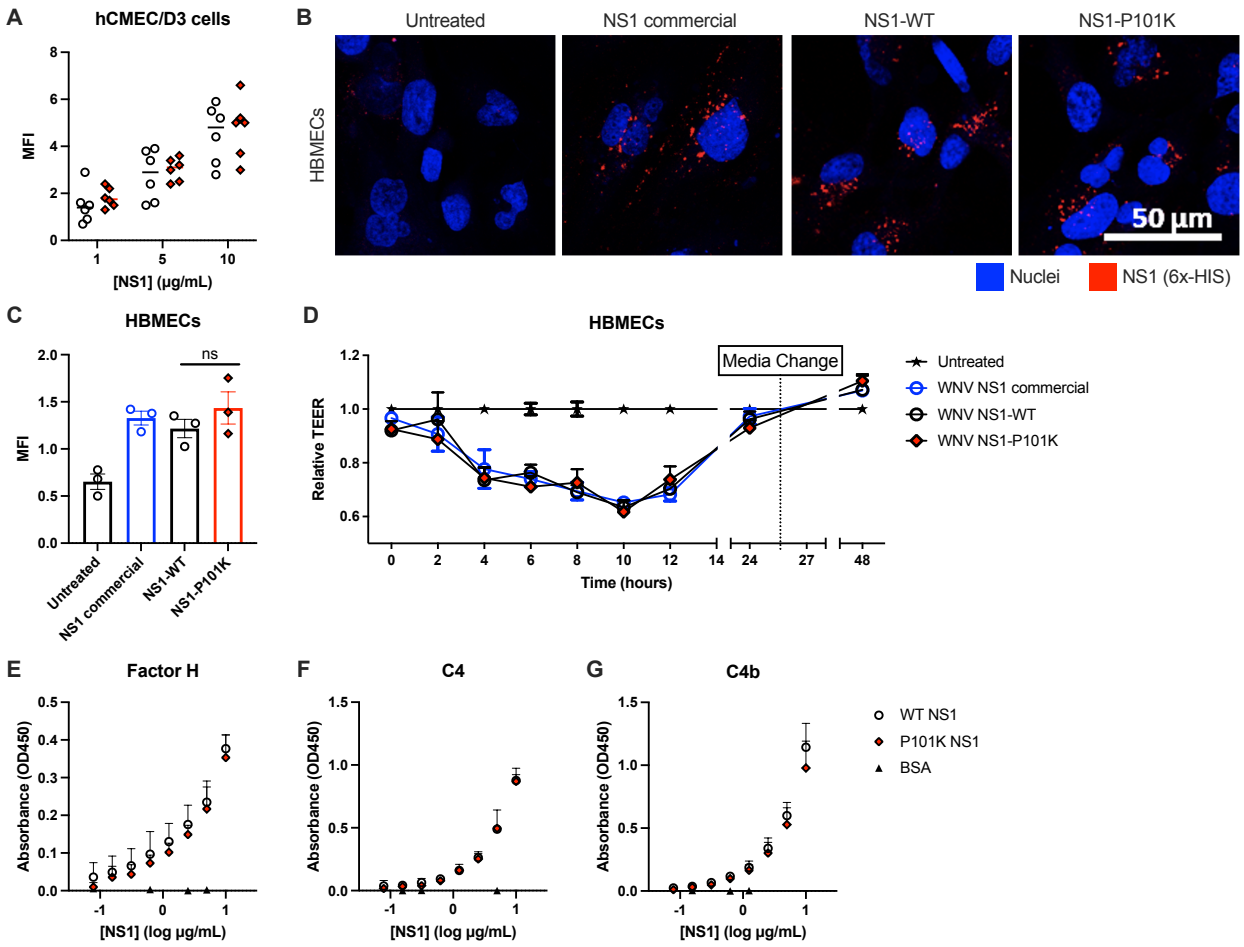

Figure 4.6. NS1-P101K substitution does not affect NS1 binding to endothelial cells or complement factors. (**A-C**) NS1 binding to endothelial cells. (**A**) Recombinant WT or P101K NS1 at the indicated concentrations was incubated with hCMEC/D3 cells and detected by flow cytometry using a cocktail of anti-NS1 mAbs. Data are from three experiments performed in triplicate. (**B**) Recombinant WT or P101K NS1 (10 μg/mL) was incubated with HBMECs for 1 h and then imaged by immunofluorescence microscopy. Representative images from three experiments are shown (scale bars, 50 μm). (**C**) Quantitation of **B**. (**D**) HBMEC permeability measured by trans-endothelial electrical resistance (TEER) assay at the indicated time points after the addition of WT or P101K WNV NS1. Commercially purchased WNV NS1 (Native Antigen) served for comparison. Relative TEER was calculated as the ratio of resistance values according to the following formula: (Ω NS1-treated cells - Ω medium alone)/(Ω non-treated cells - Ω medium alone). Data are pooled from two experiments performed in triplicate. (**E-G**) NS1 binding to complement proteins by direct ELISA: (**E**) factor H, (**F**) C4, and (**G**) C4b. Data are pooled from two experiments performed in duplicate; error bars, SD.

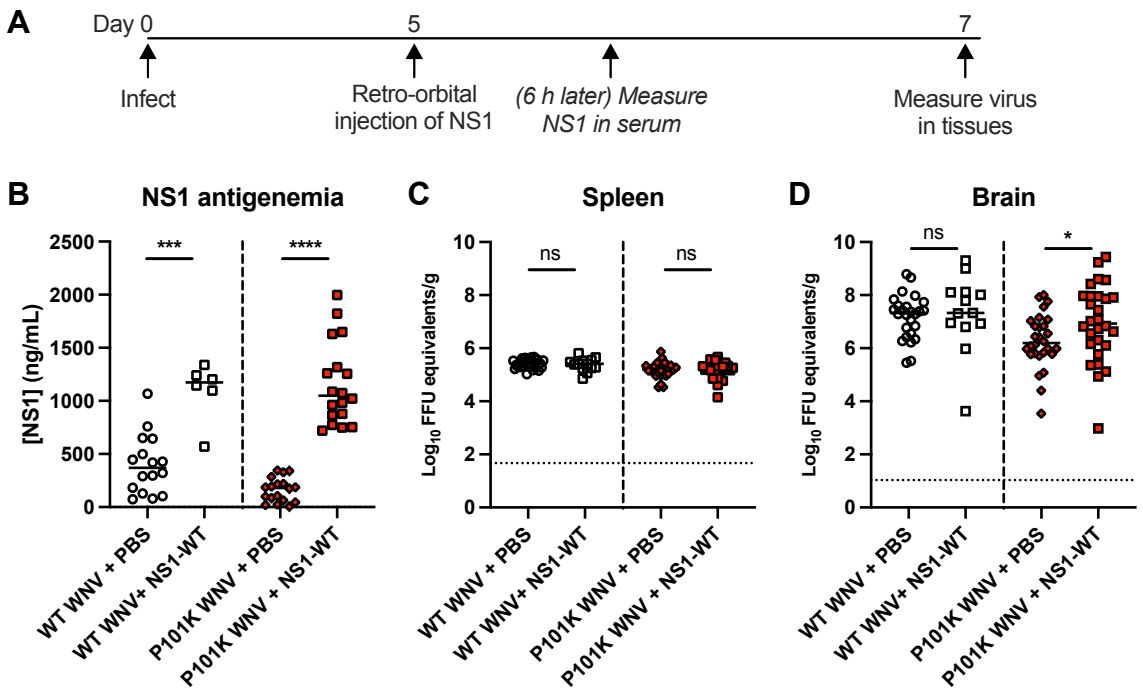

Figure 4.7. Exogenous administration of soluble NS1 rescues the infectivity of WNV NS1-P101K in the brain. (**A**) Experimental outline. Four- to five-week-old male C57BL/6J mice were inoculated subcutaneously with 10^2 FFU of WNV WT or NS1-P101K. At 5 dpi, mice were administered 5 µg of WNV NS1-WT protein by retro-orbital injection. (**B**) Six hours after injection, mice were bled to measure NS1 levels in serum by capture ELISA. (**C**-**D**) Two days later (at 7 dpi), viral RNA levels were determined by RT-qPCR in the (**C**) spleen and (**D**) brain. Data were analyzed by Mann-Whitney test between the indicated groups. **B:** two experiments (***$p<0.001$; ****$p<0.0001$; WT, n = 16; WT + NS1-WT, n = 6; P101K, n = 18; P101K + NS1-WT, n = 18); **C** and **D:** four experiments (*$p<0.05$; WT, n = 26; WT + NS1-WT, n = 13; P101K, n = 28; P101K + NS1-WT, n = 28).

Chapter 5

Conclusions and Future Directions

5.1 Summary and Future Directions

In these studies, we examined the protective efficacy of murine and human mAbs targeting NS1 in animal models for ZIKV and WNV. Although the NS1 proteins of these viruses retain only ~50% amino acid identity, our epitope mapping studies revealed common features. In particular, protective mAbs against ZIKV or WNV NS1 predominantly mapped to similar epitopes on the respective NS1 protein structures: i) the loop face of the β-platform domain and ii) the electrostatic outer face of the wing domain. Notably, these regions lie on the outer face of the NS1 dimer which is predicted to be accessible in the cell surface form of NS1[1,2]. Given that virtually all flaviviruses express NS1 on the surface of infected cells[3-6], these epitopes may represent a common target of protective mAbs against flaviviruses. Most likely, protective mAbs binding these epitopes promote clearance of infected cells through Fc effector functions, such as complement-dependent cytotoxicity[7] or phagocytosis[8]. Indeed, studies using Fc-variant mAbs (*e.g.*, LALA or LALA-PG) suggested that NS1-specific human mAbs for ZIKV and WNV tended to protect through Fc-dependent mechanisms. This is consistent with prior reports of protection associated with Fc receptor engagement for murine mAbs against WNV NS1[9] and other human mAbs against ZIKV NS1[10].

Recent reports demonstrate that some NS1-specific mAbs confer protection against DENV through Fc-independent mechanisms[11,12]. In particular, two mAbs engaging the tip of the β-platform conferred protection against lethal DENV challenge and prevented NS1-dependent endothelial hyperpermeability[11,12]. Structural analysis for one of these mAbs suggested that it prevented binding of soluble DENV NS1 to endothelial cells through steric hindrance of the wing flexible loop[12]. Additionally, this mAb directly contacted residues at the tip of the β-platform that are critical for NS1-dependent endothelial permeability following binding. Vascular dysfunction

and plasma leakage are hallmarks of clinical DENV infection, and disease severity correlates with the levels of soluble NS1 in blood[13,14]. Thus, blocking of binding of soluble NS1 and limiting endothelial hyperpermeability possibly represents one mechanism of antibody-based protection against DENV. The relevance of this mechanism to other flaviviruses that express lower levels of secreted NS1, such as WNV or ZIKV, remains unclear. One recent study identified an NS1-specific human mAb that conferred partial Fc-independent protection against ZIKV in neonatal mice; however, its epitope was not precisely mapped[15]. In our studies using limited panels of mAbs, we did not identify mAbs with robust Fc-independent protection. However, one human mAb (WNV-97) against WNV NS1 and one murine mAb (Z14) against ZIKV NS1 trended toward low levels of protection despite no or poor binding to cell surface NS1. Notably, WNV-97 and Z14 mapped to the tip of the β-platform at similar positions as the contact residues for the protective mAbs against DENV NS1[12]. Since WNV-97 and Z14 bind poorly to the surface and therefore likely cannot promote clearance of virus-infected cells, they possibly contribute to protection by blocking effects of soluble NS1. Indeed, soluble ZIKV and WNV NS1 proteins can promote hyperpermeability at blood-tissue barriers[16,17]. Furthermore, our studies with WNV NS1-P101K suggest that circulating soluble NS1 plays a role in WNV dissemination to the brain. Soluble ZIKV and WNV NS1 also may mediate pathogenesis through other unidentified mechanisms which potentially could be blocked by antibody binding.

We identified mAbs mapping to the wing flexible loop of NS1 for both ZIKV (Z12 and Z13) and WNV (WNV-99 and 16NS1[18]). Whereas WNV-99 and the previously generated 16NS1[18] conferred protection against lethal WNV challenge, Z12 and Z13 failed to protect hSTAT2 KI mice against ZIKV. Notably, WNV-99 and 16NS1 bound avidly to cell surface NS1 and with considerable site density. Z12 and Z13 bound with comparatively much lower site density. Avid

binding with high site density to infected cells may be required to cross-link bound antibodies and promote efficient Fc effector functions[19-22]. Although these mAbs mapped to similar residues, structural differences in the flexible loops of ZIKV and WNV may explain the differential protection *in vivo*. The flexible loop was disordered in the WNV NS1 dimer structure{Akey, 2014 #19}. In contrast, the ZIKV NS1 dimer structure revealed the flexible loop to form a hydrophobic 'spike' oriented toward the inner face of the dimer[1,2,23]. This orientation suggests that the flexible loop could be less accessible in the cell surface form of ZIKV NS1. Alternatively, Z12 and Z13 may bind the flexible loop at different angles than WNV-99 or 16NS1, such that they are orientated toward the membrane. Structural studies that achieve atomic-level resolution of mAb bound to NS1 may help to elucidate differences in how WNV-99, 16NS1, Z12, and Z13 engage NS1.

Although our studies mostly assessed protection by individual NS1-specific mAbs, the combination of two murine mAbs (Z15 and Z17) trended toward enhanced protection against ZIKV in the placenta and fetal heads of pregnant mice. These antibodies mapped to distinct regions of NS1 that were associated with protection for ZIKV and WNV, namely the outer surface of the wing domain and the loop face of the β-platform domain. Additionally, mAbs targeting the wing flexible loop in this study and in a previous study{Lee, 2012 #72}{Chung, 2006 #70} conferred protection against lethal WNV challenge. Future studies could assess combinations of two or more mAbs from distinct competition groups. Though mAbs like Z14 and WNV-97 conferred limited protection (likely due to poor binding to cell surface NS1), co-administration of these mAbs with other surface-binding mAbs could potentially provide synergistic protection. Compared to mAbs and vaccines targeting the flavivirus structural proteins, NS1-targeted mAbs and vaccines tend to confer lower levels of protection in animal models. NS1 mAbs or vaccines also could be combined with strategies targeting the structural proteins to provide potentially synergistic antiviral

responses.

Various reports suggest that epitopes at the tip of the β-platform of DENV NS1 (residues ~305-330) can induce autoantibodies that react with human endothelial cells, platelets, and coagulation factors[24-30]. These mAbs are speculated to contribute to pathogenesis, and indeed can induce thrombocytopenia, coagulopathy, and plasma leakage in some mouse models[29,30]. While these findings have only been shown for mAbs generated from DENV NS1 immunization, the C-terminal region of flavivirus NS1 displays considerable sequence conservation. We identified several protective mAbs mapping to epitopes that overlapped with this cross-reactive C-terminal region (*e.g.,* Z17, ZIKV-231, 749-A4, WNV-98, 14NS1[9], and 17NS1[9]). Though these mAbs conferred protection in our animal models, further studies are warranted to determine the safety of mAbs and vaccines targeting this region of NS1. Alternatively, vaccine immunogens could be designed to focus the immune response on other protective epitopes (*e.g.*, the outer surface of the wing domain or spaghetti loop). This could be accomplished by designing NS1 immunogens lacking the cross-reactive C-terminal region[31,32] or by masking these epitopes by attachment of N-linked glycans in a site-specific manner[33-36].

For murine and human mAbs against ZIKV or WNV, the most commonly targeted regions were the loop face of the β-platform and outer face of the wing domain. This is consistent with peptide microarray mapping studies using DENV-immune sera, which suggest that these are immunodominant antibody epitopes for DENV NS1[37]. Indeed, the NS1 dimer structures for DENV, WNV, and ZIKV and C-terminal domain structures for JEV and YFV all adopt similar folding and domain organization[1,2,23,38-40]. Future studies looking at larger panels of NS1-specific mAbs potentially could hasten epitope mapping by prioritizing assessment of these immunodominant regions, especially since these epitope regions tend to be associated with

protection.

In summary, we defined panels of mAbs against the NS1 proteins of ZIKV and WNV that conferred protection in multiple animal models for these viruses. We identified two epitopes associated with protection against ZIKV and WNV: (i) the electrostatic outer surface of the wing domain and (ii) the loop face of the β-platform domain. These epitopes facilitated avid binding at high site density to cell surface NS1 and engagement of Fc receptors. Importantly, these studies suggest that vaccine immunogens could be designed to target protective epitopes while avoiding adverse risks associated with the cross-reactive C-terminal region of NS1. Future studies that elucidate the atomic structures of protective mAbs bound to NS1 may refine antigen engineering strategies for rational NS1 vaccine design. A major limitation of our studies is that we assessed limited panels of mAbs against ZIKV and WNV and did not address the role of Fc for all protective mAbs. Future studies could perform more extensive epitope mapping on larger panels of NS1-specific mAbs to fully understand the breadth of epitopes associated with protection against flaviviruses.

5.2 Concluding remarks

Flaviviruses continue to disseminate geographically and to emerge and re-emerge, causing epidemics that threaten public health. Although successful vaccines exist for some flaviviruses, the concern for antibody-dependent enhancement of disease hampers the design of vaccines targeting the structural proteins. NS1-targeted approaches offer a promising alternative and demonstrate success in animal models. These studies can serve as a resource for the continued development of NS1-targeted antibodies and vaccines, providing insight into the rational design of immunogens that could focus immune responses on protective epitopes while avoiding potentially pathogenic responses.

5.3 References

1 Xu, X. *et al.* Contribution of intertwined loop to membrane association revealed by Zika virus full-length NS1 structure. *Embo j* **35**, 2170-2178, doi:10.15252/embj.201695290 (2016).

2 Brown, W. C. *et al.* Extended surface for membrane association in Zika virus NS1 structure. *Nat Struct Mol Biol* **23**, 865-867, doi:10.1038/nsmb.3268 (2016).

3 Youn, S., Cho, H., Fremont, D. H. & Diamond, M. S. A Short N-Terminal Peptide Motif on Flavivirus Nonstructural Protein NS1 Modulates Cellular Targeting and Immune Recognition. *Journal of Virology* **84**, 9516-9532, doi:10.1128/jvi.00775-10 (2010).

4 Schlesinger, J. J., Brandriss, M. W., Putnak, J. R. & Walsh, E. E. Cell surface expression of yellow fever virus non-structural glycoprotein NS1: consequences of interaction with antibody. *J Gen Virol* **71 (Pt 3)**, 593-599, doi:10.1099/0022-1317-71-3-593 (1990).

5 Flamand, M., Deubel, V. & Girard, M. Expression and secretion of japanese encephalitis virus nonstructural protein NS1 by insect cells using a recombinant baculovirus. *Virology* **191**, 826-836, doi:https://doi.org/10.1016/0042-6822(92)90258-Q (1992).

6 Winkler, G., Randolph, V. B., Cleaves, G. R., Ryan, T. E. & Stollar, V. Evidence that the mature form of the flavivirus nonstructural protein NS1 is a dimer. *Virology* **162**, 187-196, doi:10.1016/0042-6822(88)90408-4 (1988).

7 Schlesinger, J. J., Foltzer, M. & Chapman, S. The Fc portion of antibody to yellow fever virus NS1 is a determinant of protection against YF encephalitis in mice. *Virology* **192**, 132-141, doi:10.1006/viro.1993.1015 (1993).

8 Chung, K. M., Thompson, B. S., Fremont, D. H. & Diamond, M. S. Antibody Recognition of Cell Surface-Associated NS1 Triggers Fc-γ Receptor-Mediated Phagocytosis and Clearance of West Nile Virus-Infected Cells. *Journal of Virology* **81**, 9551-9555, doi:10.1128/jvi.00879-07 (2007).

9 Chung, K. M. *et al.* Antibodies against West Nile Virus nonstructural protein NS1 prevent lethal infection through Fc gamma receptor-dependent and -independent mechanisms. *J Virol* **80**, 1340-1351, doi:10.1128/jvi.80.3.1340-1351.2006 (2006).

10 Bailey, M. J. *et al.* Human antibodies targeting Zika virus NS1 provide protection against disease in a mouse model. *Nat Commun* **9**, 4560, doi:10.1038/s41467-018-07008-0 (2018).

11 Modhiran, N. *et al.* A broadly protective antibody that targets the flavivirus NS1 protein. *Science* **371**, 190-194, doi:10.1126/science.abb9425 (2021).

12 Biering, S. B. *et al.* Structural basis for antibody inhibition of flavivirus NS1–triggered endothelial dysfunction. *Science* **371**, 194-200, doi:10.1126/science.abc0476 (2021).

13 Libraty, D. H. *et al.* High Circulating Levels of the Dengue Virus Nonstructural Protein NS1 Early in Dengue Illness Correlate with the Development of Dengue Hemorrhagic Fever. *The Journal of Infectious Diseases* **186**, 1165-1168, doi:10.1086/343813 (2002).

14 Avirutnan, P. *et al.* Vascular leakage in severe dengue virus infections: a potential role for the nonstructural viral protein NS1 and complement. *J Infect Dis* **193**, 1078-1088, doi:10.1086/500949 (2006).

15 Yu, L. *et al.* Monoclonal Antibodies against Zika Virus NS1 Protein Confer Protection via Fcγ Receptor-Dependent and -Independent Pathways. *mBio* **12**, doi:10.1128/mBio.03179-20 (2021).

16 Puerta-Guardo, H. *et al.* Zika Virus Nonstructural Protein 1 Disrupts Glycosaminoglycans and Causes Permeability in Developing Human Placentas. *J Infect Dis* **221**, 313-324, doi:10.1093/infdis/jiz331 (2020).
17 Puerta-Guardo, H. *et al.* Flavivirus NS1 Triggers Tissue-Specific Vascular Endothelial Dysfunction Reflecting Disease Tropism. *Cell Rep* **26**, 1598-1613.e1598, doi:10.1016/j.celrep.2019.01.036 (2019).
18 Lee, T. H. *et al.* A cross-protective mAb recognizes a novel epitope within the flavivirus NS1 protein. *Journal of General Virology* **93**, 20-26, doi:https://doi.org/10.1099/vir.0.036640-0 (2012).
19 Tang, Y. *et al.* Regulation of Antibody-Dependent Cellular Cytotoxicity by IgG Intrinsic and Apparent Affinity for Target Antigen. *The Journal of Immunology* **179**, 2815-2823, doi:10.4049/jimmunol.179.5.2815 (2007).
20 ÖHLANDLR, C., LARSSON, Å. & PERLMANN, P. Regulation of Effector Functions of Human K-Cells and Monocytes by Antigen Density of the Target Cells. *Scandinavian Journal of Immunology* **13**, 503-510, doi:10.1111/j.1365-3083.1981.tb00163.x (1981).
21 Lux, A., Yu, X., Scanlan, C. N. & Nimmerjahn, F. Impact of Immune Complex Size and Glycosylation on IgG Binding to Human FcγRs. *The Journal of Immunology* **190**, 4315-4323, doi:10.4049/jimmunol.1200501 (2013).
22 Lucisano Valim, Y. M. & Lachmann, P. J. The effect of antibody isotype and antigenic epitope density on the complement-fixing activity of immune complexes: a systematic study using chimaeric anti-NIP antibodies with human Fc regions. *Clin Exp Immunol* **84**, 1-8, doi:10.1111/j.1365-2249.1991.tb08115.x (1991).
23 Akey, D. L. *et al.* Flavivirus NS1 structures reveal surfaces for associations with membranes and the immune system. *Science* **343**, 881-885, doi:10.1126/science.1247749 (2014).
24 Chuang, Y. C., Lin, J., Lin, Y. S., Wang, S. & Yeh, T. M. Dengue Virus Nonstructural Protein 1-Induced Antibodies Cross-React with Human Plasminogen and Enhance Its Activation. *J Immunol* **196**, 1218-1226, doi:10.4049/jimmunol.1500057 (2016).
25 Cheng, H. J. *et al.* Correlation between serum levels of anti-endothelial cell autoantigen and anti-dengue virus nonstructural protein 1 antibodies in dengue patients. *Am J Trop Med Hyg* **92**, 989-995, doi:10.4269/ajtmh.14-0162 (2015).
26 Cheng, H. J. *et al.* Anti-dengue virus nonstructural protein 1 antibodies recognize protein disulfide isomerase on platelets and inhibit platelet aggregation. *Mol Immunol* **47**, 398-406, doi:10.1016/j.molimm.2009.08.033 (2009).
27 Cheng, H. J. *et al.* Proteomic analysis of endothelial cell autoantigens recognized by anti-dengue virus nonstructural protein 1 antibodies. *Exp Biol Med (Maywood)* **234**, 63-73, doi:10.3181/0805-rm-147 (2009).
28 Liu, I. J., Chiu, C. Y., Chen, Y. C. & Wu, H. C. Molecular mimicry of human endothelial cell antigen by autoantibodies to nonstructural protein 1 of dengue virus. *J Biol Chem* **286**, 9726-9736, doi:10.1074/jbc.M110.170993 (2011).
29 Sun, D. S. *et al.* Antiplatelet autoantibodies elicited by dengue virus non-structural protein 1 cause thrombocytopenia and mortality in mice. *J Thromb Haemost* **5**, 2291-2299, doi:10.1111/j.1538-7836.2007.02754.x (2007).
30 Sun, D. S. *et al.* Endothelial Cell Sensitization by Death Receptor Fractions of an Anti-Dengue Nonstructural Protein 1 Antibody Induced Plasma Leakage, Coagulopathy, and Mortality in Mice. *J Immunol* **195**, 2743-2753, doi:10.4049/jimmunol.1500136 (2015).

31 Lai, Y. C. *et al.* Antibodies Against Modified NS1 Wing Domain Peptide Protect Against Dengue Virus Infection. *Sci Rep* **7**, 6975, doi:10.1038/s41598-017-07308-3 (2017).
32 Volpina, O. M. *et al.* A synthetic peptide based on the NS1 non-structural protein of tick-borne encephalitis virus induces a protective immune response against fatal encephalitis in an experimental animal model. *Virus Research* **112**, 95-99, doi:https://doi.org/10.1016/j.virusres.2005.03.026 (2005).
33 Duan, H. *et al.* Glycan Masking Focuses Immune Responses to the HIV-1 CD4-Binding Site and Enhances Elicitation of VRC01-Class Precursor Antibodies. *Immunity* **49**, 301-311.e305, doi:10.1016/j.immuni.2018.07.005 (2018).
34 Hariharan, V. & Kane, R. S. Glycosylation as a tool for rational vaccine design. *Biotechnology and Bioengineering* **117**, 2556-2570, doi:https://doi.org/10.1002/bit.27361 (2020).
35 Bajic, G. *et al.* Influenza Antigen Engineering Focuses Immune Responses to a Subdominant but Broadly Protective Viral Epitope. *Cell Host Microbe* **25**, 827-835.e826, doi:10.1016/j.chom.2019.04.003 (2019).
36 Eggink, D., Goff, P. H. & Palese, P. Guiding the Immune Response against Influenza Virus Hemagglutinin toward the Conserved Stalk Domain by Hyperglycosylation of the Globular Head Domain. *Journal of Virology* **88**, 699-704, doi:doi:10.1128/JVI.02608-13 (2014).
37 Hertz, T. *et al.* Antibody Epitopes Identified in Critical Regions of Dengue Virus Nonstructural 1 Protein in Mouse Vaccination and Natural Human Infections. *J Immunol* **198**, 4025-4035, doi:10.4049/jimmunol.1700029 (2017).
38 Edeling, M. A., Diamond, M. S. & Fremont, D. H. Structural basis of Flavivirus NS1 assembly and antibody recognition. *Proc Natl Acad Sci U S A* **111**, 4285-4290, doi:10.1073/pnas.1322036111 (2014).
39 Poonsiri, T. *et al.* Structural Study of the C-Terminal Domain of Nonstructural Protein 1 from Japanese Encephalitis Virus. *J Virol* **92**, doi:10.1128/jvi.01868-17 (2018).
40 Wang, H. *et al.* Crystal structure of the C-terminal fragment of NS1 protein from yellow fever virus. *Sci China Life Sci* **60**, 1403-1406, doi:10.1007/s11427-017-9238-8 (2017).